MC/60

VOLUME II

A DESIGN OF THE EUROPEAN 300 GeV RESEARCH FACILITIES

CHAPTERS 2 - 16

GENEVA - 2 DECEMBER, 1970

A DESIGN OF THE EUROPEAN 300 GeV RESEARCH FACILITIES

Chapters 2 - 16

Index

Chapter 2

THE MACHINE LATTICE

2.1 General Description

The lattice is of separated-function type and FODO configuration. Six long straight sections created by simply omitting bending magnets from the lattice provide space for injection, ejection and r.f. It is designed in such a way that the full complement of magnets need not be installed initially if one wishes to make provision for later superconducting conversion. The radius of the machine, 1100 m, is more than adequate to accommodate the machine of 300 GeV peak energy which is the aim of the eight year programme and which is matched to its financial provisions.

In the following sections we discuss the way in which the present separated-function, missing-magnet lattice design has been developed and optimized and present more detailed information on the lattice structure, insertions, dynamics and aperture assumptions. Table 2.1 lists the principal lattice parameters.

2.2 Separated Function v. Combined Function

In the 1964 Design Report[2.1] a lattice was proposed which was very similar to that of the existing CERN PS. The magnets were of combined-function type, i.e. their hyperbolic poles formed a field which provided both focusing and bending forces. The horizontally focusing (F) magnets and defocusing (D) magnets had identical apertures and the normal period, repeated 216 times around the ring, had the configuration FOFDOD. The phase advance per period, μ, was close to 45° and the ring was subdivided into twelve identical superperiods separated by Collins insertions.

Later, in 1968, a more unusual lattice was proposed in the Design Report of the American 200/400 GeV Project[2.2]. This employed magnets of separated-function type, the bending being provided by simple dipole magnets, the focusing by relatively few quadrupole magnets. In a separated-function machine the bending magnets are able to run at a field of 1.8 T, about 50% higher than combined-function magnets, and although extra space must be found for quadrupoles these, in a machine of this radius, represent only 10% of the circumference.

Clearly such a machine would have a smaller radius for a given energy. What was not obvious to us was whether savings on radius dependent costs (tunnel and r.f.) would be offset

Table 2.1

Lattice and Orbit Parameters

		A	B	C	
Maximum momentum		200	300	400	GeV/c
Maximum bending field		1.8	1.8	1.8	T
Magnetic bending radius		370.6	555.9	741.2	m
Mean radius		1100	1100	1100	m
Injection momentum		10	10	10	GeV/c
Injection field		0.090	0.060	0.045	T
Number of bending magnets per normal period		4	6	8	
Quadrupole gradient for Q = 28.75	F	8.456	12.68	16.91	T/m
	D	12.05	18.08	24.10	T/m
Quadrupole gradient for Q = 27.75	F	8.23	12.34	16.45	T/m
	D	11.73	17.60	23.46	T/m
Nominal length of F quadrupole				3.799	m
Nominal length of D quadrupole				2.650	m
Nominal length of bending magnet				6.017	m
Length of inter-magnet gap				0.6	m
Length of short straight section				2.304	m
Free length in empty semiperiod				28.782	m
Length of period				63.994	m
Structure of a period				FODO	
Number of periods	(N)			108	
Number of superperiods	(S)			6	
Nominal working point	(Q)			27.75	
Total transition energy/rest energy	(γ_{tr})			24.6	
Phase advance/period	(μ)			92.5	^{o}
Maximum β value in F quadrupole	($\hat{\beta}_H$)			108.4	m
Maximum β value in D quadrupole	($\hat{\beta}_V$)			110.2	m
Minimum β value in D quadrupole	($\check{\beta}_H$)			17.8	m
Minimum β value in F quadrupole	($\check{\beta}_V$)			18.0	m
Maximum of momentum compaction function	($\hat{\alpha}_p$)			4.9	m
Minimum of momentum compaction function	($\check{\alpha}_p$)			-0.2	m

by the increased stored energy of the more compact separated-function machine.

We therefore made a careful comparison of fully optimized combined and separated-function machines designed to meet identical specifications and with the same assumptions about apertures and free space. The machine designs were costed using unit price figures for components derived from recent experience with the CERN Intersecting Storage Rings project and other machines and the costs were calculated using computer programmes developed by staff of the Karlsruhe laboratory[2.3], who also carried out the calculations.

The result of this study (reported in more detail in Ref. (2.4)) was that the separated and combined-function costs turned out to be the same within 1%, an agreement which is surprising when one considers the uncertainty in estimating the costs.

In spite of there being no difference in cost, the separated-function design was selected for further study because it allowed more flexibility and simplicity in many aspects of the machine design. This decision later proved to be a happy one since it allowed us to contemplate the construction of the machine on the Meyrin site and to exploit the missing-magnet philosophy.

2.3 Missing Magnet Concept

The idea of a machine whose energy can be increased during its life to match the needs of the physics programme is not new. For many of its early years the CERN PS ran at reduced energy to take advantage of a higher repetition rate which at that time was more important to the experimental programme than a high proton energy. It is interesting to speculate whether during those years a physical limitation to 15 GeV would have been a handicap. In the NAL Design Study it was also proposed that the machine would operate initially at 200 GeV, less than half the capability of the bending magnets. Only later would the missing power supplies and cooling capacity be added to give a useful repetition rate at 400 GeV. In 1967 a group at LRL, Berkeley, first proposed another type of extendible energy machine[2.5] which has since come to be known as the "missing magnet" concept. In one of their proposals they suggested that at first only half the bending magnets should be installed to give 200 GeV, then by later adding the remainder evenly around the ring the energy would rise to 400 GeV.

Of these two kinds of extendible energy machines the missing-magnet scheme seems more appropriate to our needs since it allows the option of filling the spaces not with conventional magnets but superconducting magnets should they prove both feasible and economic. There are, of course, other ways of adding superconducting magnets which apply to any machine but this option has the virtue that it exploits new technology to give higher energies while making maximum use of existing capital equipment. Yet another advantage of the missing-magnet concept is that it allows the choice of completing the machine with either three quarters or the full set of conventional magnets depending upon how successful we are in obtaining low bids for the machine components.

2.3.1 The three missing-magnet stages with conventional magnets

The three missing-magnet stages we propose for the machine equipped with conventional magnets are as follows:

Table 2.2

Stage	Energy (GeV)	Magnets per semi-period*
A	200	2
B	300	3
C	400	4

Stage A (200 GeV) is the machine with only half the bending magnets installed. This machine could be completed in about five years and would leave open the option of filling the remaining half of the machine with superconducting magnets. These by themselves would raise the energy to above 500 GeV (assuming a field of 4.5 T) or 700 GeV if both superconducting and conventional magnets were powered together.

Should it become clear later in the construction period that there seemed no reasonable hope of using superconducting magnets in the lattice and the physics interest made the extra 100 GeV important one could decide to order and install a third magnet in each semi-period (Stage B). The decision would be taken in the third year of the construction period so that the date of completion of either stage would not be delayed beyond the limit already set by the expenditure profile. Stage B, being more expensive than Stage A, would be completed about a year later, i.e. towards the end of the sixth year. The remaining two years of the Programme would be devoted to completing and equipping the North Experimental Area. Stage B, 300 GeV, is the nominal design matched to the Programme budget. It is not possible within the budget to fill the whole of the 2.2 km diameter ring with magnets unless magnet prices or those of other components turn out to be less than we have estimated. However, in the event that bids prove lower than estimates, a fourth magnet per semi-period could be installed giving Stage C, 400 GeV.

2.3.2 Geometry

In each of the 216 semi-periods of the proposed machine there is room between adjacent quadrupoles for four 6 m long conventional magnets. In Fig. 2.1 can be seen the normal semi-period with four magnets (Stage C) and, dotted, with two magnets (Stage A). In changing from A to C only a slight realignment of the outer pair of magnets is needed. The sagittal distance $x \simeq R\,(\pi/N)^2/16 = 5.8$ cm.

---

* The circumference of the machine is divided into 216 semi-periods nearly all of which contain bending magnets.

An alternative modification is to insert only one of the missing magnets (Stage B). If the quadrupoles and equipment in their adjacent straight sections are not to be realigned, the third magnet must be placed midway between the other two to preserve the centre of bend. If it is thought necessary to place it off centre in order to leave the maximum free space for a later addition, this can be done by displacing radially the D quadrupoles and B2 magnets in the normal periods by 3.2 cm.

It is unfortunately not possible to remove or add magnets in only some of the periods of the machine once it is built as this alters the whole curvature of the superperiod and displacements necessary become much greater than the bore of the tunnel. However, the lattice does include special semi-periods which contain less than the normal complement of magnets even in Stage C and form the long straight section insertions where bulky equipment is located. The arrangement of these special semi-periods must be fixed before the tunnel is excavated and their bending strength must be augmented in the same 2/3/4 ratio as the normal semi-periods.

2.3.3 Superconducting conversion procedure

Re-equipping a completed machine of this size with superconducting magnets would be a long procedure lasting more than a year. During this time experiments would stop. Nearly 1000 conventional magnets would have to be removed from the ring tunnel and replaced by superconducting magnets. Inherent in the missing-magnet concept is the idea that this shut-down may be avoided. Given intelligent provision for their installation, the missing superconducting magnets can be wheeled in in multiples of six during the normal shut-down periods, installed in position but left dead. Once they are all there and tested, both superconducting and conventional magnets would be moved a few centimetres to their new positions and realigned. This might take as little as a month. The superconducting machine would then be ready for commissioning. Should any unforeseen operational difficulty be experienced it is even possible to return to the old alignment positions and run the machine as before.

As far as one can predict, it will not be easy to construct a superconducting magnet whose aperture has a very high aspect ratio. It may also be an advantage to reduce the number of individual cryostats. For these reasons we have proposed that the missing magnets should be the two adjacent B3 magnets which lie near the centre of the semi-period and not the outer pair B1 and B2.

The final conversion to a fully superconducting machine would, of course, require a long interruption in the operation of the machine but at a time when one would have considerable experience of the problems of manufacturing and operating pulsed superconducting magnets. The remaining conventional magnets and quadrupoles would all be replaced. This would offer an energy above 1000 GeV at 4.5 Tesla.

2.3.4 Quadrupole strength

The strength of the quadrupoles is sufficient for Stage C. If in the third year it is

decided to complete the machine at Stage A to leave space for superconducting magnets, an estimate will then be made of the extra quadrupole strength needed to cover the superconducting option and, if there is still time, quadrupole length will be increased. Failing this an additional quadrupole could be placed beside the existing one. In order to make room for this, B1 and B2 could be moved somewhat closer together. The space for the superconducting magnets would then be somewhat shorter. This kind of manipulation of the lattice elements can also be carried out even after the machine has run. It involves only a small radial and azimuthal adjustment to the location of B1 and B2.

2.4 The Normal Period

The 108 focusing periods of the lattice are identical and have a FODO configuration. They each contain two quadrupoles (F and D) followed by equal drift lengths (O). In 90 of the periods each of the drift lengths contains a full complement of bending magnets. These are the normal periods. Figure 2.2 shows the arrangement of magnets in a normal period together with the betatron amplitude and the phase advance in both horizontal and vertical planes. Also shown are the beam envelopes at a point in the lattice where they are largest. The orbit functions are not significantly different for the A, B and C stages.

The FODO configuration has been chosen because it requires the least amount of focusing strength and hence, in a separated-function machine, results in the smallest radius. Another advantage of the FODO configuration is that the betatron amplitude is very different at the F and D quadrupoles so that correcting elements in the short straight section following the quadrupoles act almost independently on the horizontal and vertical dynamics. The large value of β_{max}, naturally occurring in the normal period, makes it unnecessary to use a special focusing insertion to inflate β at the ejection septum where a large β contributes to a high ejection efficiency.

A consequence of the large β_{max}/β_{min} ratio is that the width and height of the beam vary considerably throughout the period and at least two bending magnet types, B1 and B2, are required if aperture and stored energy are not to be wasted. B1 close to the F quadrupole has a large horizontal aperture and a narrow gap. B2 close to the D quadrupole has an almost square aperture. The two missing magnets, B3, have yet another aperture specification. The sequence of magnets B1, B3, B3, B2 in the FD semi-period is reversed in the DF semi-period. This variety of magnet types will of course add to the development cost but the saving in stored energy and overall capital cost is considerable.

The F and D quadrupoles are also different in aperture since the beam is very wide and flat in F and circular in D. Their lengths are chosen to give Q = 28.75 at peak energy. We have assumed a field at the edge of the beam of 1.06 T and 0.636 T in F and D respectively at 400 GeV. The currents of the F and D quadrupoles will be controlled independently to follow the bending magnet excitation and to allow Q to be varied during the cycle.

The 0.6 m gap between magnets is sufficient only for a vacuum connection to be made and to leave room for the flat coil overhangs. All correction and diagnostic equipment together with special quadrupoles, sextupoles and dipoles for ejection will be placed in the short straight section, 2.3 m long, following each quadrupole. Even in the special periods this space will be reserved for these components.

2.5 Long Straight Section Insertions

The machine is divided into six identical superperiods. Each superperiod is composed of fifteen normal periods and a sequence of three special periods which form the long straight section insertion[2.6]. Some or all of the bending magnets are omitted from the special periods to make room for the bulky components of the machine but the regular spacing of quadrupoles is preserved throughout the superperiod.

Of the six long straight sections spaced equidistantly around the ring, four will be occupied by equipment. One straight section is assigned to an ejection system feeding a beam to the West Experimental Area, a second is allocated to the injection system for the input beam from the CPS, a third section to an ejection system feeding the North Experimental Area, and the fourth to the r.f. accelerating system. The other two are reserved for future developments, perhaps to house more r.f. equipment needed if superconducting magnets are added to the machine or perhaps to provide an injection point for a fast cycling synchrotron to boost the intensity should this later be thought desirable.

In a later Section we shall see that the superperiodicity (S = 6) gives rise to a pattern of stop bands which determine the working point Q. A smaller number of insertions would cause this pattern to shrink and it would be hard to find a Q value sufficiently far from a stop band. The superperiodicity of six also places the injection and ejection paths in good alignment with the existing ejected beam from the CPS and with the West Area.

The sequence of special periods in the insertion is shown in Fig. 2.3 for the full (Stage C) machine. The pattern is determined by the design of the ejection and r.f. systems. In the r.f. straight section the three empty semi-periods near the centre of the insertion provide enough space for the three cavities. In the straight sections reserved for ejection each empty semi-period will contain one of the three septa which form the ejection channel. On either side of the empty semi-periods are special semi-periods where kickers for fast ejection and beam scrapers will be placed. These contain, even in Stage C, less than the normal complement of magnets. Figure 2.4 shows the arrangement of magnets in the special semi-periods at the A, B and C Stages. In order to maintain the 2/3/4 ratio in the development of bending strength through the three stages an additional magnet type B4 is required. This is simply a three-quarter length version of B2. It is not needed in Stage C.

In earlier machine designs the regular focusing structure was interrupted at an insertion and the beam was carried across a long drift space by special quadrupole magnets at each end

of the drift space. These quadrupoles had to be specially designed, manufactured and powered. They also introduced a set of stop bands due to the superperiodicity in focusing. The solution which we have adopted is much simpler and the quadrupoles which lie in the ejection region do not seem to make the design of the ejection system more difficult.

Inevitably either kind of insertion will cause the momentum compaction function, α_p, to beat around the ring so that its peak excursion is almost twice as large as it would be in a homogeneous machine (Fig. 2.5). This, however, can be turned to our advantage. α_p is small in the neighbourhood of the insertion itself and the beam does not fill the horizontal aperture of the magnets. This provides valuable space for the injected and ejected beam paths. Another useful feature is that beam losses can be localised in a few regions where α_p is maximum and where special precautions may be taken against radiation damage.

2.6 Aperture Requirements

The beam size at injection and transition is calculated by adding the amplitude of betatron oscillations for a given emittance, the expected amplitude of closed-orbit distortion and, in the horizontal plane, the allowance for the momentum spread. The random errors which will cause closed-orbit distortion are listed in Table 2.3 together with their individual contributions to the uncorrected closed-orbit amplitude.

Table 2.3

Random error	Tolerance (r.m.s.)	Distortion amplitude (mm) horizontal	vertical
Misalignment of quadrupoles	0.15 mm	14.4	14.6
Field errors ($\Delta B/B$)	0.5×10^{-3}	20.4	
Median plante tilt	0.2 mrad		8.4
Stray vertical field	0.28 G	20.2	
Stray horizontal field	0.11 G		8.2
r.m.s. sum of components		32.1	18.7

These contributions and their r.m.s. sum are computed at the 98% confidence level. There is only a 2% probability that they will be exceeded. This procedure for estimating the closed-orbit allowance is similar to that which was adopted in the 1964 Design Report following a detailed examination of measurements of closed-orbit amplitudes in the CPS. In the 1964 Design Report, however, apertures were calculated by combining the uncorrected closed-orbit allowance with the full design emittance of the injected beam. This resulted in apertures which we now consider to be too large. Since 1964 the correction of closed-orbit distortion by cybernetic techniques has been successfully applied to the CPS and other accelerators. It does not now seem unreasonable to determine apertures by combining the design emittance, not with the uncorrected closed-orbit amplitude, but with the amplitude

after correction has been applied. This saves a large fraction, about 30%, of the magnet aperture and reduces the cost of the magnets and their power supply considerably.

Figure 2.5 shows how we expect the correction of closed-orbit distortion to be progressively applied and acceptance to improve during the development of the machine. The "staircases" mark the boundary between the allowance for closed-orbit distortion and the allowance for betatron oscillations. The upper diagram shows the breakdown of apertures at injection at a point in the lattice where β_V is maximum, the centre of a D quadrupole. The lower staircase shows the breakdown in the horizontal plane at a place where both β_H and α_p are maximum, the centre of an F quadrupole. The beam injected from the CPS will have a large momentum spread. This considerably simplifies the problem of debunching the CPS beam once it is injected into the main ring. The momentum spread becomes even larger at transition and it is at transition that the maximum horizontal aperture is needed. The first three steps of the staircase for the horizontal plane refer to injection and the last step refers to transition.

In the first step we see the breakdown before systematic correction is applied. There is just room for a pencil beam to circulate. Correction will then be applied and acceptance will improve until, in the final step, the closed-orbit distortion amplitude assumed is 5 mm in the vertical plane and 10 mm in the horizontal plane. This is the residual amplitude we expect after full correction has been applied (Chapter 9). The acceptance of the machine will then be 3.4 π mm. mradians in the vertical plane at injection ($E\beta\gamma$ = 36 π mm. milliradians) and 3.05 π mm.milliradians in the horizontal plane at transition ($E\beta\gamma$ = 75 π mm. milliradians). These design acceptances are considered to be sufficient for the full beam of 10^{13} ppp from the improved CPS. The momentum spread assumed in the horizontal plane (± 3% at injection) is that we expect from the improved CPS and close to the maximum which can be held in the buckets of the r.f. accelerating system.

In Fig. 2.2 the horizontal and vertical envelopes of the beam corresponding to the last step in each case are plotted through a complete period in which α_p is maximum. The semi-apertures required by the beam in each of the magnets (Table 2.4) are determined by this profile.

Table 2.4

	Semi-apertures required by the beam (mm)	
	H	V
Q_F	62.6	10.1
Q_D	26.8	24.5
B1	60.3	13.3
B2 and B4	33.5	23.8
B3	50.8	20.0

We have assumed that B3 will have an aperture which is large enough to accommodate the beam in either of the two central magnet locations in the semi-period. If it is decided later to complete the machine with only one B3 magnet per semi-period a small reduction in the aperture of B3 could be made.

The special magnets B4 which have the same aperture as B2 but which are shorter are not placed in the usual B2 position. Fortunately, because they are only needed in special periods where α_p is small, their horizontal aperture is nevertheless sufficient.

The emittance and magnet apertures determine the intensity at which the space charge Q shift becomes serious. For a Q shift of about 0.25 at 10 GeV/c and assuming a bunch factor after injection from the CPS of 0.02, the incoherent space-charge limit is 5.6×10^{13} ppp and the coherent space-charge limit is 8.8×10^{13} ppp. Clearly these limits are comfortably above the design intensity of the machine.

The vertical aperture of the machine would not have been smaller had we intended to use an 8 GeV fast cycling booster as an injector rather than the CPS. The large momentum spread of the debunched CPS beam does demand an extra 10 mm horizontal aperture but horizontal aperture is a comparatively cheap commodity and it can be argued that this extra 10 mm is necessary in any case for the slow ejection system.

2.7 Choice of Periodicity and Phase Advance

Given the radius and assumptions about aperture requirements and straight section length there remain two free parameters in the lattice design, namely N, the number of periods and μ, the phase advance per period. Choice of these parameters affects not only the apertures and hence magnet system costs, but has an influence on orbit parameters like β_{max} and α_p, and can also determine the ease of ejection.

In choosing these parameters it was first established by designing a number of lattices that there was a very flat cost optimum in phase advance between $\mu = 70^\circ$ and 100° and in periodicity of between 90 and 130.

Increasing the periodicity, N, reduces α_p and increases γ_{tr}. Both of these tendencies are desirable from the point of view of transfer from the CPS since acceptance of the main ring is limited at transition by the large momentum spread. Increasing N also had a general tendency to reduce apertures and stored energy.

On the other hand, a large number of periods imply a small β_{max} and a short distance between quadrupoles, features which hamper efficient slow ejection. The lattices with higher N contain more magnet units and also tend to demand higher field from the bending magnets since a larger proportion of the ring must be devoted to focusing magnets.

Fortunately, a small range of periodicities which includes N = 108 and 114 seemed to satisfy these constraints and finally N = 108 was chosen since it was in this narrow range, it lay in the cost optimum and it was a number with many factors, an important consideration for the location of correcting elements.

A phase advance close to 90° was thought desirable since it simplified many of the correction procedures, notably closed-orbit correction. The quantization of Q dictated by structure resonances (Section 2.8) lead eventually to two alternative Q values being chosen, 28.75 ($\mu = 95.8^{\circ}$) and 27.75 ($\mu = 92.5^{\circ}$).

2.8 Choice of Working Point

It can be shown that stop bands occur at Q values given by

$$kQ = nS \quad \text{or} \quad nN$$

where: k, the order of the stop band is 1, 2, 3 or 4
n is any integer.

For a superperiodicity S = 6 this leads to the pattern of stop bands shown in Fig. 2.6. There is a strong tendency to choose a Q close to the centre of the diagram and remote from the k = 1 stop bands. This minimises $\hat{\alpha}_p$. At the same time it is wise to avoid the k = 2 stop band at Q = 27 and the higher order stop bands, k = 3 and k = 4, should not cut the integer square in which the working point is located. This leaves only 26.25 and 27.75 as desirable working points. Since Q is in general driven downwards by space charge we prefer 27.75 and have chosen this as the nominal working point.

The only stop band in the vicinity which is associated with the periodicity, N is the fourth order stop band, 4Q = N at Q = 27.0. This can be driven by systematic errors in the field of the quadrupoles. We have calculated its width assuming that the error in the quadrupole field, $\Delta k/k$, is the specified value of $\pm 2 \times 10^{-3}$ at the edge of the beam. The estimated width is $\Delta Q = 0.03$ and therefore we conclude that the stop band is sufficiently weak and remote from the nominal working point.

It is clearly an advantage of the separated-function lattice that the nominal Q can be moved to an adjacent integer square by programming the quadrupole currents should experience with the machine suggest that this is desirable. The most attractive alternative working point seems to be 28.75 since the k = 4 stop band just below it, may well prove to be very weak indeed. It can only be driven by octupoles of superperiodicity six which in our homogeneous lattice do not exist to a first order. We therefore intend to ensure that the quadrupoles can drive Q to 28.75 even at the peak machine energy and in Table 2.1 quote parameters for both working points.

Finally, we should point out that the machine will, in practice, be tuned so that there is a small difference between Q_V and Q_H.

2.9 Conclusions

The lattice presented in this report is consistent with the other machine parameters and embodies several features, separated-function magnets, the missing-magnet concept, an insertion for high efficiency ejection and apertures which are minimized by closed-orbit correction; features which stem from advances in accelerator design since the 1964 Design Report was written.

Many lattices, this is the forty-seventh, were considered during the work leading up to this report and it would be surprising if during the final engineering design of the machine further improvements and modifications were not incorporated in the lattice. Even as this report is written such improvements are being considered.

References

(2.1) CERN/563, Vol. I and II, November 1964.

(2.2) National Accelerator Laboratory, Design Report, July 1968.

(2.3) F. Arendt, MCOST-BSG-Notiz 69/26 - Karlsruhe.

(2.4) J.B. Adams and E.J.N. Wilson, Nucl. Inst. and Meth., 87 (1970), pp. 157-180.

(2.5) A.A. Garren, G.R. Lambertson, E.J. Lofgren and L. Smith, Nucl. Inst. and Meth., 54 (1967), pp. 223-228.

(2.6) A. Laisné and J. Parain, Proc. VII Int. Acc. Conf. (Yerevan, 1969).

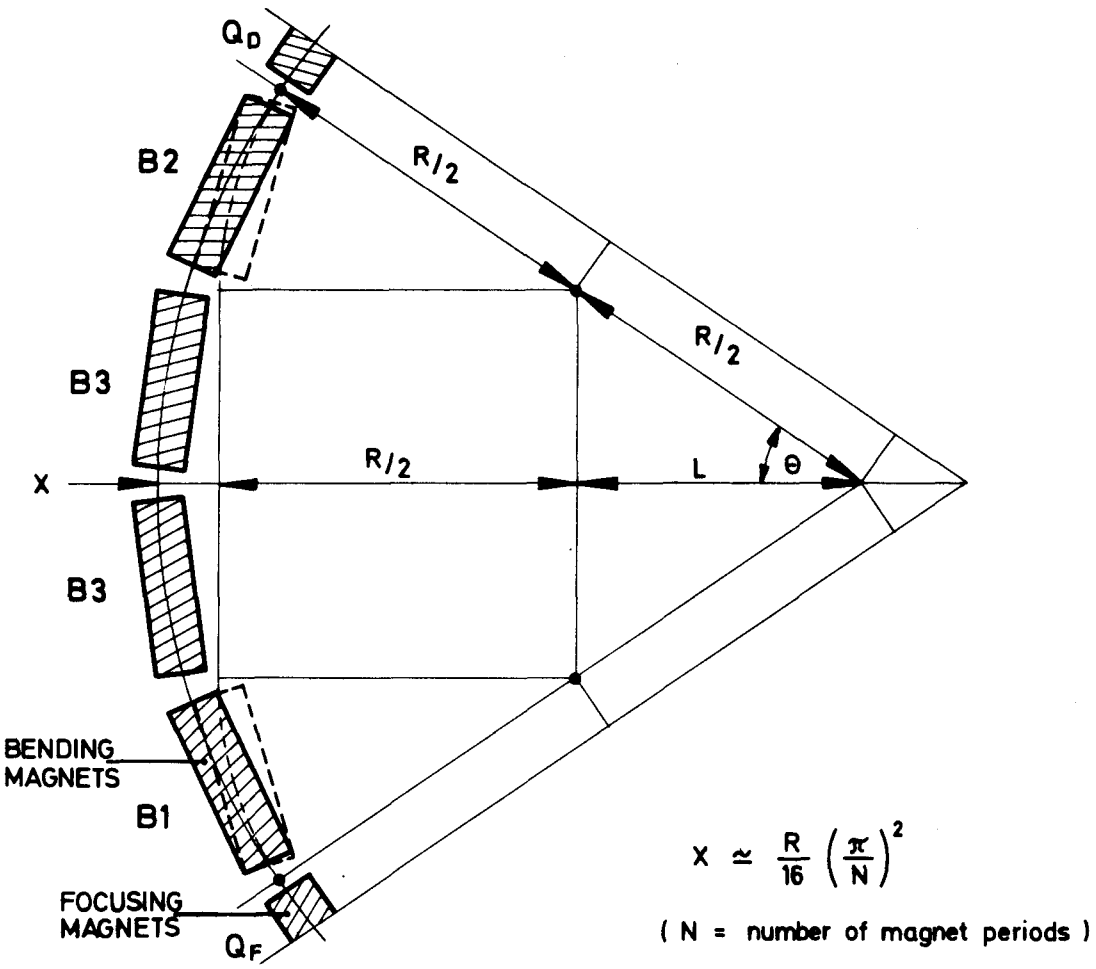

Fig. 2.1 Missing magnet geometry (one half period)

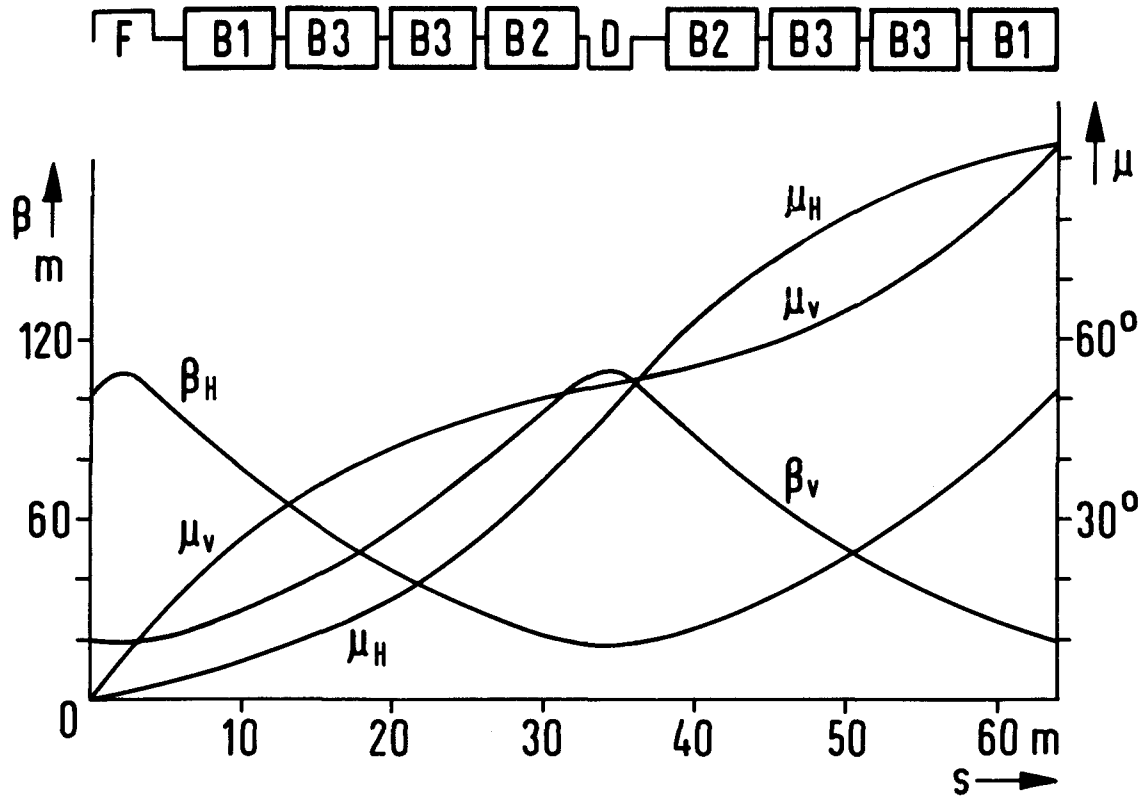

a) Lattice functions in a period

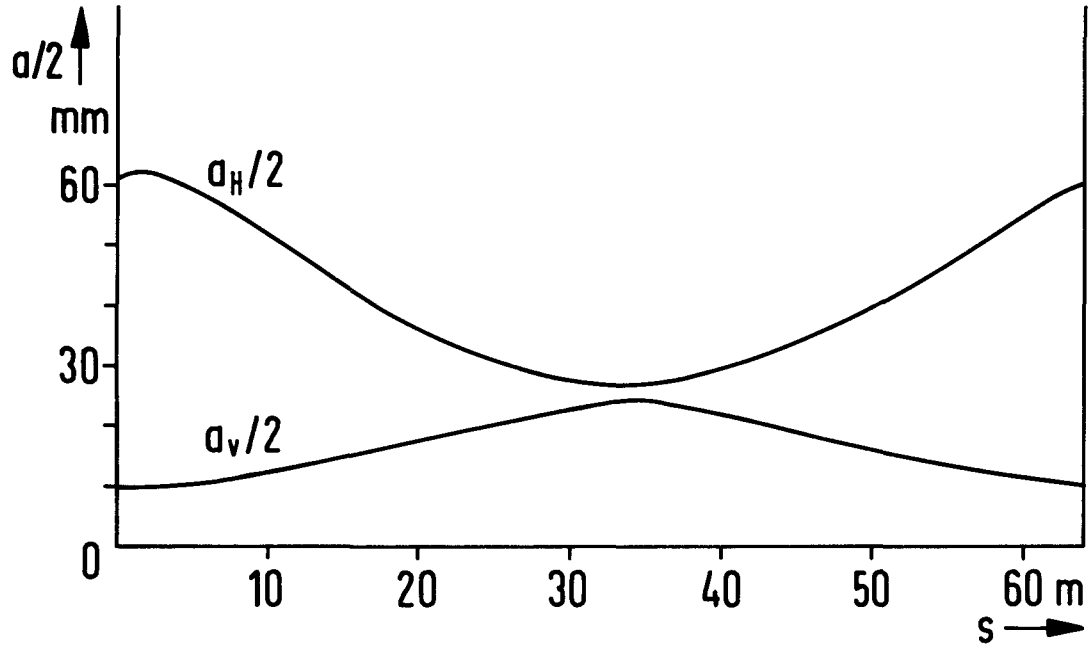

b) Semi-apertures in period with $\alpha_{p,max}$

Fig. 2.2

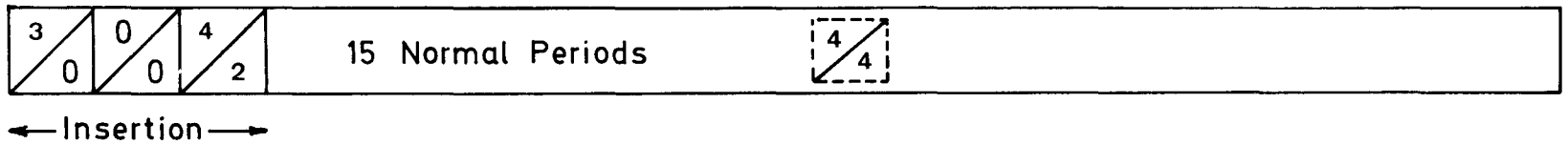

a) Composition of the Superperiod

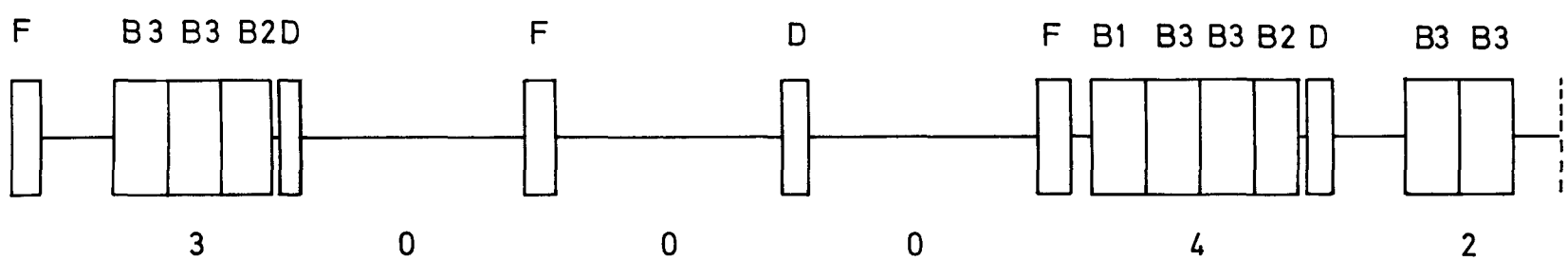

b) The insertion (Stage C)

Fig. 2.3

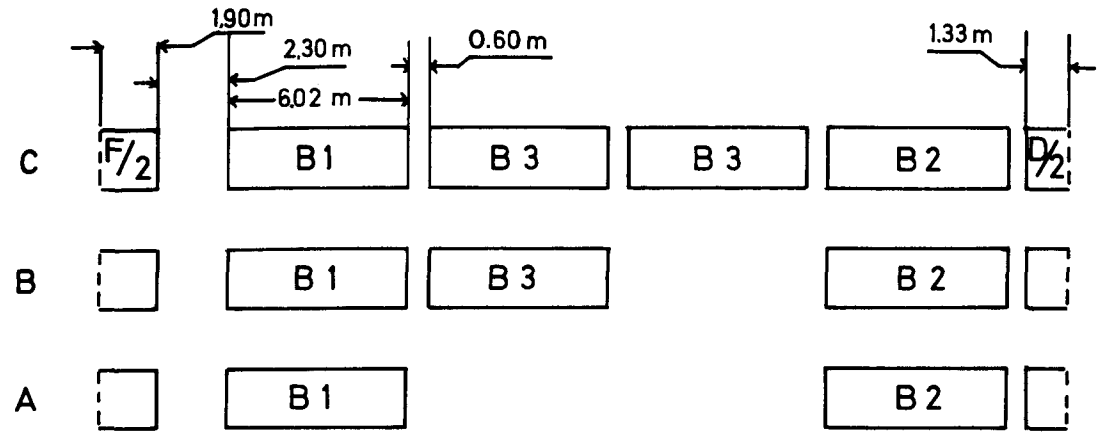

a) Normal semiperiod

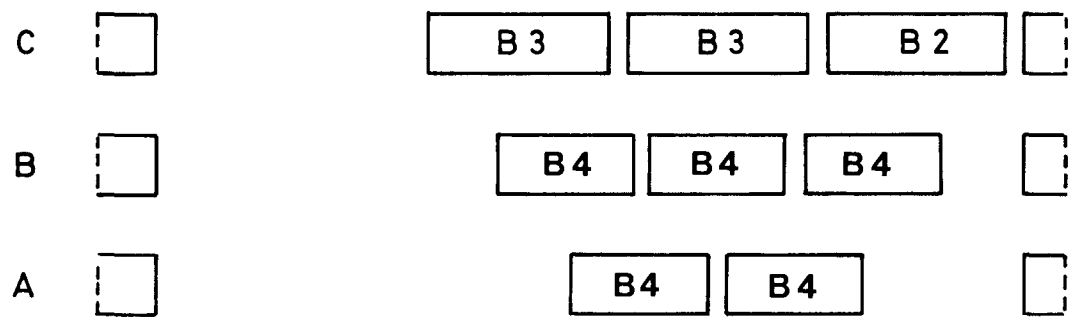

b) Special semiperiod (3 magnets in C)

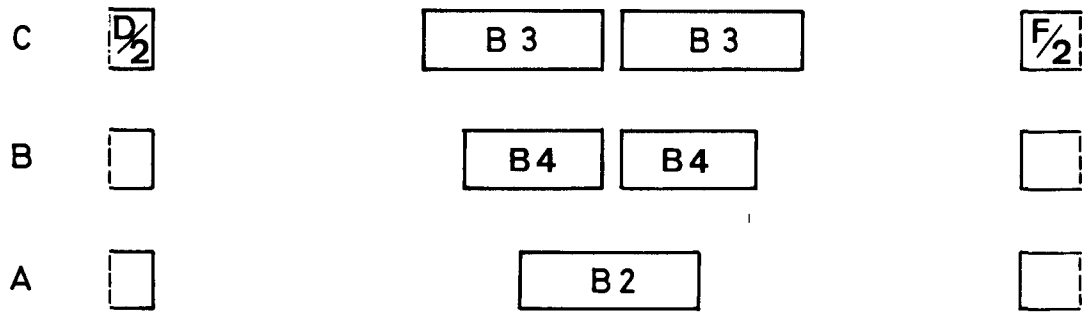

c) Special semiperiod (2 magnets in C)

Fig. 2.4 Normal and special semiperiods

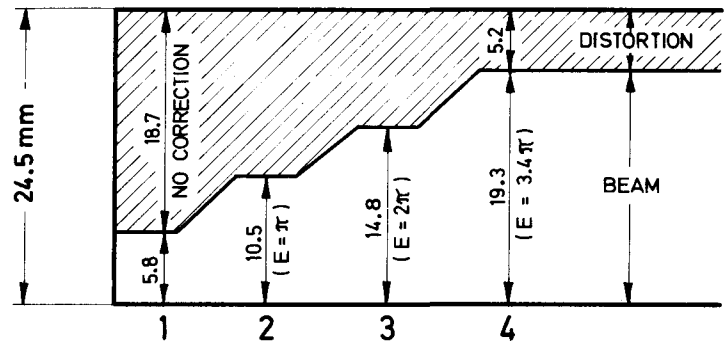

a) Vertical

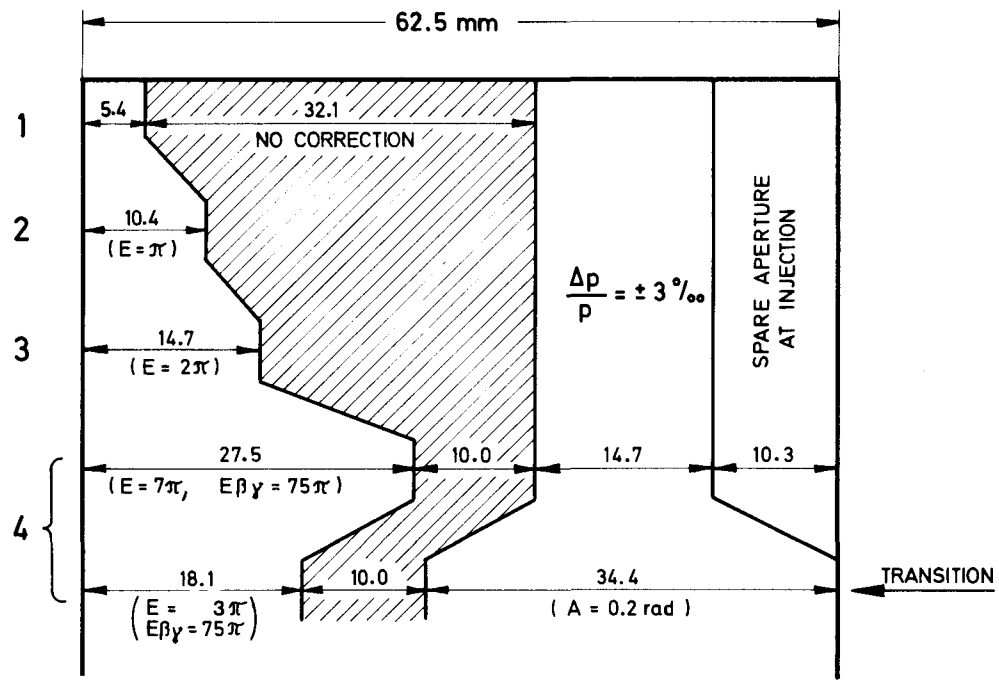

b) Horizontal

Fig. 2.5 Breakdown of semi-apertures for 10 GeV/c at β_{max} and $\alpha_{p_{max}}$

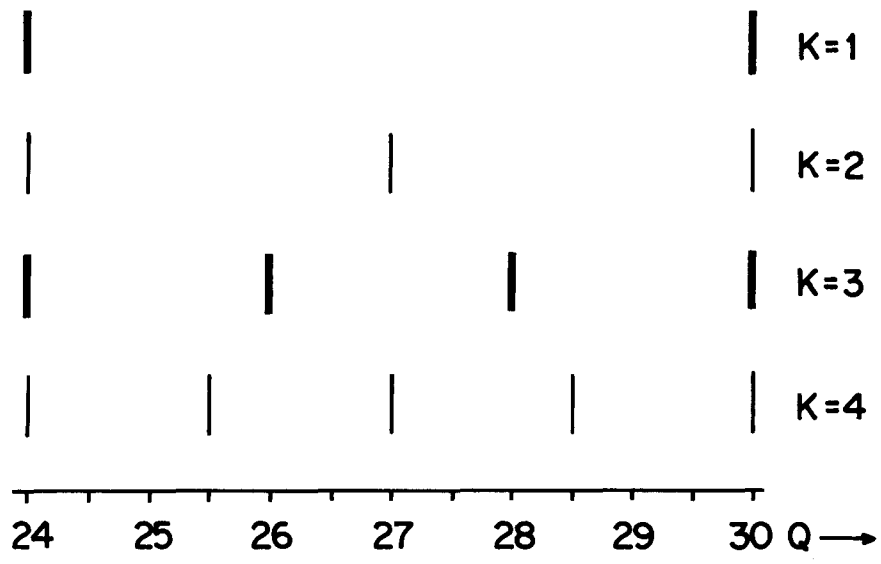

Fig. 2.6 Structure stopbands S = 6

Chapter 3

THE INJECTION SYSTEM

3.1 Introduction

The CERN Proton Synchrotron (CPS) is foreseen as injector for the main ring[3.1]. For the shorter main ring cycle times (Stages A and B) one filling cycle would alternate with a 25 GeV cycle for physics. At Stage C two 25 GeV cycles could be inserted between filling cycles.

At present CPS intensities ($\sim 2\ 10^{12}$ p/p) the CPS beam could simply be ejected with the existing fast kicker system, be transferred into the main ring and, after debunching, be trapped and accelerated by the 180 MHz r.f. system of the main ring. At these intensities there are comfortable margins with respect to main ring betatron and momentum acceptances, as well as for space-charge and self-bunching limits.

To improve the uniformity of the azimuthal distribution in the main ring, a bunch by bunch transfer scheme has been studied and will be tested. Several solutions to this problem are discussed in Subsection 3.2.2. We expect that even at 10^{13} p/p a beam transferred with this technique would be acceptable for the main ring.

Another possibility, discussed in Subsection 3.2.3, is a continuous transfer based on a very thin electrostatic septum in the CPS. This septum would "peel off" the CPS beam during eleven revolutions. In this case the horizontal emittance is reduced. As there is now no need to leave gaps in the beam for kicker rise and fall times, the longitudinal transformation of the 10 MHz CPS bunches into 180 MHz bunches can in this case be made partly or fully in the CPS, resulting in a smaller longitudinal bunch area in the main ring.

Since the main ring parameters chosen are compatible with all transfer schemes described here, no immediate need exists for the selection of one particular scheme. Thus they can be further explored theoretically and experimentally and their merits compared. The selection has a bearing on the minimum requirements for the main ring acceptances.

If one has to fix now a value of the horizontal main ring aperture, one should base this value on bunch by bunch transfer. If a decision to use continuous transfer could be made in time, a smaller aperture could be considered from the injection point of view.

Beam behaviour in the main ring also depends on the transfer scheme. We devote Section 3.3 to a study of debunching, trapping and passage through main ring transition.

All these considerations apply to single pulsing of the CPS. However, they do not exclude double pulsing at a later date, though this would require a main ring r.f. holding system (unless the main r.f. system could be used), doubling the speed of continuous transfer and modification of the main ring inflector.

The first part of the existing CPS - ISR transfer line (TT2) can also be used for transfer to the main ring. The additional line, which needs to be built, has a total length of about 800 m, and represents the most costly item of the injection system. We therefore present in Section 3.4 a first layout with cost figures.

3.2 CPS ejection modes

3.2.1 General description

The ejection modes considered in more detail are (i) bunch by bunch ejection and (ii) continuous ejection. Single (or double) pulse ejection of the whole CPS beam, while being operational to-day, is not attractive since at higher intensities r.f. beam loading and debunching problems would arise in the main ring[3.2-4].

The equidistant placing of the 20 CPS bunches around the main ring requires repetitive pulsing of the CPS kickers. For this we propose in Subsection 3.2.2 a system which is fast enough to avoid premature debunching of the bunches already transferred.

If one fills the main ring longitudinal phase space by simply letting the twenty bunches drift until they overlap, the resulting momentum spread fits well into the momentum acceptance of the main ring (see Subsection 3.3.2). If so desired, the momentum spread can be reduced by a debuncher cavity in the main ring[3.5], which can be added at any stage. In order to avoid self-bunching of the beam with reduced $\Delta p/p$ a reduction of the coupling impedance of the main ring r.f. cavity would then probably be required at 10^{13} p/p.

In the case of continuous ejection, the beam is more uniform in the longitudinal direction, thus leading to a suitable azimuthal distribution in the main ring. Depending on the r.f. treatment in the CPS the transferred beam is bunched at 10 MHz, fully debunched or already prebunched at 180 MHz (see Subsection 3.3.3). To facilitate inflection into the main ring, only single turn filling, i.e., ejection in eleven revolutions, is considered.

3.2.2 Bunch by bunch ejection using fast kicker magnets

Repetitive pulsing of a kicker magnet in rapid sequence as required for a fast kicker can be achieved in two ways:

i) Multiple use of one system (4 or 5 modules). This can be envisaged if the present recharging time can be reduced sufficiently. It is the preferred solution and described below under a).

ii) Single use of several systems of known design. This is the alternative solution in case any major difficulties occur with the first scheme, b).

a) Transfer in 1 ms of 20 bunches equally spaced around the main ring (Fig. 3.1)

Brückner has proposed a method[3.6] which achieves the fast recharging by the use of a second high voltage thyratron connecting the kicker pulse forming network (PFN 1) to another high voltage storage line (PFN 2) which is long compared to PFN 1.

Reproducible recharging of PFN 1 requires that the time for all 20 pulses is less than twice the propagation time of PFN 2. The time T_s between two pulses is determined by the deionizing times of the thyratrons Th 1 and Th 2 (about 20 μs each). Adding ∿ 10 μs for the charging process itself, one arrives at ∿ 50 μs for the interval between pulses, i.e., at ∿ 1 ms for the whole transfer.

The fastest conceivable transfer could take place in one main ring revolution and would require to kick every eleventh bunch, i.e. one pulse every μs (t_s). In order to adjust the interval between bunches to the time given by the recharging method, t_s may be multiplied by any integer which has no factor in common with 20. The many possibilities obtained in this way result from the choice of R_{MR} = 1100 m. T_s = 100 μs is about the permissible limit if one wants to preserve the option for a debunching system[3.5] in the main ring. Otherwise one could relax T_s to about 0.5 ms.

As the requirements on rise and fall times and constancy of the flat top of the kicker pulse are more stringent for bunch by bunch transfer than for targeting (or many-bunch transfer into the ISR), it is essential to prove the feasibility of this system by a model. We propose to order such a model as soon as possible.

b) Alternative solutions

If one cannot rely on fast recharging, it is advantageous to reduce the number of pulses. This can be done by ejecting pairs of bunches simultaneously, so that only ten pulses are required. Only five will need to have a short rise-time if every other pair of bunches is ejected first.

The fast kicker modules planned for ejection at 28 GeV/c could then be divided into three groups, each ejecting two bunches at 10 GeV/c. Two more such groups would be added in order to eject the first five pairs of bunches, and the remaining five pairs of bunches could then be extracted by kickers of much reduced rise-time specification. Again R_{MR} = 1100 m is convenient in this case.

Other schemes can be thought of, but the above should suffice as a feasibility demonstration.

3.2.3 Continuous ejection

Consider an increasing closed orbit bump of half a betatron wave length. An electrostatic septum placed at the maximum excursion will then peel off the beam unwinding it like a spiral (see Fig. 3.2).

In order to achieve a constant intensity for eleven revolutions the bump amplitude, d(t), has to be properly programmed. A computation made for a Gaussian phase plane density of the internal beam and a frequency $Q_H = 6.42$ leads to a function d(t) shown in Fig. 3.3. The maximum displacement of the fast bump can be achieved with deflections of 1 mrad.

The emittance of the ejected beam decreases during the process due to the higher density of the core (see Fig. 3.4).

Defining the emittance of the ejected beam as an average over-all particles:

$$E_H = 2\left[\beta\,\overline{(x' - x_0')^2} + \beta^{-1}\,\overline{(x - x_0)^2}\right], \qquad (3.1)$$

where β and (x_0, x_0') refer to the transfer line, E_H is a minimum for a given group of particles when

$$x_0 = \bar{x},\ x_0' = \bar{x}' \qquad \text{and} \qquad \beta = \left[\overline{(x - x_0)^2}/\overline{(x' - x_0')^2}\right]^{\frac{1}{2}}.$$

A reasonable assumption is that β will be constant during the process, whereas (x_0, x_0') could be adjusted in time by the additional programmable dipole. With β matched to the beginning of the process, a constant emittance with an area of one third of that of the CPS can be obtained.

In order to minimize the losses and the performance requirements for the electrostatic deflector the CPS amplitude function is increased locally to 90 m. With an emittance $E_H = 6\,\pi\,10^{-6}$ rad m, the horizontal beam diameter is about 50 mm and the necessary septum deflection 0.6 mrad. An electrostatic deflector 0.8 m long, with less than 100 kV/cm is adequate and already exists at the CPS. With the present septum thickness (0.1 mm) losses are expected to be less than 5 %.

There exists a possibility to improve this scheme by modifying even more the focusing properties of the CPS until one reaches the integer resonance. This would be a fast version of the slow ejection[3.7] which has been in use for several years. The septum requirements are eased by the reduced divergence of the beam, and the increased radial size of the outgoing beam reduces the loss on the septum. The advantage is that one should have smaller and more stable emittances. On the other hand, it would be more difficult to maintain a constant intensity during the spill. The beam should be debunched before ejection in order to stay within the momentum acceptance of the resonance. First numerical results concerning spill duration, beam emittance and permissible momentum bite are encouraging, but to confirm the performance a further six to nine months of theoretical and experimental work is required.

Most of the hardware needed for continuous ejection is already in operation. The only extra pieces of equipment are the programmable dipoles. Their characteristics are summarized in Table 3.1.

Table 3.1

Characteristics of Dipoles used for Continuous Ejection

Magnet aperture w × h	150 mm × 54 mm
length	0.5 m
inductance	1.75 μH
Number of turns	4
Peak flux density	0.085 T
Peak current	0.93 kA
Peak voltage	10 kV
Stored magnetic energy	21 Ws
High voltage supply	resonant type

3.2.4 Comparison of phase-space volume resulting from these modes

Estimates of the phase space volume of the beam transferred are given in Table 3.2

Table 3.2

Expected Main Ring Beam Emittances (in units of 10^{-6} rad m) and Main Ring Bunch Areas (in rad) at 10 GeV/c and 10^{13} p/p

Quantity / Transfer scheme	$E_H\beta\gamma$	E_H	$E_V\beta\gamma$	E_V	A
Bunch by bunch	75π	7π	36π	3.4π	0.18
Bunch by bunch and main ring debuncher (3.6)	75π	7π	36π	3.4π	0.08
Continuous ejection	25π	2.3π	36π	3.4π	0.08

The beam to be transferred from the PSB into the CPS (at 1.463 GeV/c) will have:

$$E_H\beta\gamma \approx 50\pi\ 10^{-6} \text{ rad m} \qquad E_V\beta\gamma \approx 20\pi\ 10^{-6} \text{ rad m} .$$

Some blow-up will occur up to 10 GeV/c, as was measured recently (3.8) with 1.6×10^{12} p/p. Extrapolating the blow-up towards 10^{13} p/p is difficult (3.9). The main ring vertical acceptance of $3.4\pi\ 10^{-6}$ rad m corresponds to $(E_V\beta\gamma)_{max} = 36\pi\ 10^{-6}$ rad m and is compatible with a blow-up of $\Delta E\beta\gamma \approx 10\pi\ 10^{-6}$ rad m in the CPS and an additional blow-up of twenty percent in the transfer from the CPS. Using similar blow-up assumptions for the horizontal plane leads

to the emittance values given in Table 3.2 for bunch by bunch transfer*. In case of continuous ejection, a reduction of E_H by a factor three is assumed (see Subsection 3.2.3). If so desired, the H and V phase planes could be exchanged in the transfer (see Subsection 3.4.3).

In longitudinal phase space, we expect a bunch area of 0.01 rad at transfer from the PSB. A blow-up of 2 may occur when passing transition and another factor 2 may be found due to the instabilities above transition*. We thus assume a CPS bunch area of

$$A = \pi \, \Delta(\beta\gamma) \, \phi_{rf} = 0.04 \text{ rad}$$

at 10 GeV/c and 10^{13} p/p and arrive at the main ring values listed in Table 3.2.

For transfer with simple "debunching" in the main ring, the main ring bunch area is given by the energy spread of the CPS bunches (see Subsection 3.3.2). For schemes with debunching (and possibly prebunching at 180 MHz in the CPS, see Subsection 3.3.3) we assume a blow-up of two for the total debunching and rebunching process. When using a debuncher** in the main ring[3.5] the coupling impedance of the 180 MHz r.f. structure would be lowered to preserve the self-bunching limit in spite of a lower $\Delta p/p$.

3.3 Debunching and trapping

3.3.1 Relevant parameters

a) General remarks

As the two machines have different radii, and the r.f. systems work at different frequencies, we have to debunch the beam and rebunch it before acceleration can start in the main ring. One may think of:

i) debunching and rebunching in the main ring,

ii) debunching in the CPS and rebunching in the main ring,

iii) debunching and rebunching in the CPS.

Bunch by bunch transfer schemes by means of kickers need gaps in the CPS beam, and therefore require debunching and rebunching to be done in the main ring. Multiturn ejection can probably work with any of the three debunching schemes. Resonant ejection requires a small momentum spread and therefore debunching in the CPS.

b) Bunch area limitations in the main ring

The resulting bunch area in the main ring must not be too large because of two kinds of bottlenecks.

---

* Should this blow-up factor prove optimistic, continuous ejection could be used to reduce phase space volume.

** Using a sinusoidal debuncher voltage, the beam can be "smeared out" over about 70% of the circumference at injection. This figure may be improved, if one is willing for instance to add some higher voltage harmonics[3.5].

Firstly, the bunches must be smaller than the main ring buckets. The bucket area has two minima, one at $\gamma_{tr}\sqrt{3}$, and another near injection.

Secondly, horizontal aperture will limit the permissible bunch area, as momentum oscillations contribute to the beam width. Two limitations are important: at transition, where the momentum oscillations have their maximum, and at injection, where the betatron oscillations are large.

For the lattice adopted, the maximum permissible bunch area is determined by aperture limitation at transition.

Table 3.3

Horizontal Main Ring Half-apertures for $\beta_H = \hat{\beta}_H$, $\alpha_p = \hat{\alpha}_p$

Parameters used:		
$\hat{\beta}_H$ = 108.4 m		f_{rf} = 182.5 MHz
$\hat{\alpha}_p$ = 4.90 m		ϕ_s = 45°
γ_{tr} = 24.6		g_0 = 4.5
$\dot{p}$ = 165 GeV/c/s		N = 10^{13} p/p
Half-aperture (HA) available		62.5 mm
Values computed:	at injection	at transition
Allowance for closed orbit	10 mm	10 mm
HA occupied by betatron oscill.	27.5 mm	18.1 mm
HA occupied by momentum oscill.*	14.7 mm	34.4 mm
Corresponding momentum spread $\Delta p/p$	$\pm 3 \times 10^{-3}$	$\pm 7 \times 10^{-3}$
Maximum acceptable bunch area A_{tr} from Eq. (3.2)		0.2
Space charge parameter(3.10) $\eta_0(0)$ for A_{tr} = 0.2		0.015
Half width of non-adiabatic region(3.10)		T = 1.84 ms Δ_γ = 0.29

* Linear addition of betatron and momentum oscillation amplitudes assumes that a lossfree passage through transition is required. One may relax aperture requirements if one is willing to lose the tail of the distribution.

c) Main ring apertures at injection and transition

The aperture situation is summarized in Table 3.3 under the assumption of a normalized emittance of $E_H \beta\gamma = 75\pi\ 10^{-6}$ rad m.

The half-aperture required at transition to accommodate momentum spread is given by[3.10]:

$$\Delta r_{tr} = \alpha_p \frac{\Delta p}{p}_{tr} = \left\{ \alpha_p \frac{0.465}{\beta} \left(\frac{A}{\gamma}\right)^{\frac{1}{2}} \left[\frac{\gamma \cot^2 \phi_s}{f_{rf}} \frac{d(\beta\gamma)}{dt}\right]^{\frac{1}{6}} \right\}_{tr} . \qquad (3.2)$$

The bunch area $A_{tr} = 0.2$ as determined by the transition aperture is slightly smaller than the r.f. "bucket" area $A_{rf} \simeq 0.24$. By special means (e.g. by a fast Q-jump), it seems possible to reduce Δr_{tr} (Eq. 3.2) by about 15%. Matching of A_{tr} to A_{rf} appears then possible.

3.3.2 Debunching and rebunching in the main ring

The proposed bunch by bunch ejection scheme (see Subsection 3.2.1) injects 20 × 1 CPS bunches spaced equidistantly around the main ring. The simplest way to "debunch" them is to let the beam drift until bunches overlap due to momentum spread.

Table 3.4 gives the momentum acceptance, $\Delta p/p$, and the corresponding debunching time, t.

The maximum acceptable bunch area being limited at transition, the values of Table 3.4 are computed assuming invariance of $A = A_{tr} = 0.2$. To relate the maximum momentum spread of the debunched beam at injection to the bunch area, we use:

$$\frac{\Delta p}{p} = \pm \frac{A}{4\pi\beta\gamma} . \qquad (3.3)$$

The debunching time is given by:

$$t = \frac{1}{n\, f_{rev} \left(\frac{\Delta p}{p}\right) |\eta|} , \qquad (3.4)$$

where n is 20 for the 20 × 1 bunch mode. Here t is twice the time after which bunches just touch. $\Delta p/p$ is the momentum spread before capture. After capture (adiabatic or high trapping), the r.f. voltage will be further increased and $\Delta p/p$ will rise to about 3×10^{-3} at the beginning of acceleration.

Table 3.4 shows the expected momentum spread of the improved CPS for bunch by bunch transfer. For $A = 0.04$ rad, the figure of $\Delta p/p = 1.3 \times 10^{-3}$ implies that one would lower the CPS r.f. voltage to reduce the momentum spread, leaving gaps 75 ns wide for kicker rise and fall times. The momentum spread could still be reduced in the main ring by a debunching system[3.5]. But this is only necessary if an unexpected effect increases the momentum spread beyond 1.5×10^{-3}.

Table 3.4

Main Ring Beam Properties of 10 GeV/c Transfer for N = 10^{13} p/p

Parameters used:	
$f_{rev} = \beta c/2\pi R = 43.4$ kHz	$\beta\gamma = \gamma = 10.7$
n = 20 (20 × 1 bunch mode)	$h_{MR} = 4224$
$\eta = \lvert 1/\gamma_{tr}^2 - 1/\gamma^2 \rvert = 0.0071$	$Z/h^* = 1$ kΩ
Values computed:	
Peak acceptable momentum spread*	$\Delta p/p = \pm 1.5 \times 10^{-3}$
Expected CPS momentum spread for bunch by bunch ejection	$\Delta p/p = \pm 1.3 \times 10^{-3}$
Debunching time for $\Delta p/p = \pm 1.4 \times 10^{-3}$	$t = 115$ ms
Bunch area required to avoid self-bunching	$A \geq 0.13$ rad
Corresponding momentum spread*	$\Delta p/p \geq \pm 10^{-3}$

* Before trapping.

Table 3.4 was arrived at assuming an ideal machine. If longitudinal or transverse blow-up occurs between injection and transition, the acceptable bunch area and therefore the momentum acceptance decrease and debunching times become longer.

During the debunching - rebunching process, interaction between the beam and the cavities or other coupling impedances may cause problems. Beam-induced voltages may prevent the beam from debunching, or may cause self-bunching at an unwanted frequency. Debunching in the presence of a coupling impedance resonating at a frequency much higher than the bunch frequency is an unsolved theoretical problem. We use a self-bunching criterion[3.11,12] which establishes the condition under which a coasting beam of circulating current I_0 is stable against self-bunching. Experiments indicate[3.4] that the criterion gives reasonable results for a bunched beam, if I_0 stands for the average current.

The debunching criterion can be rewritten in the following convenient form[3.13]:

$$A \geq \left[\frac{64\pi}{0.7} \frac{\beta\gamma}{|\eta|} \frac{|Z|/h^*}{Z_0} \frac{Nr_p}{R}\right]^{\frac{1}{2}} , \qquad (3.5)$$

where h^* is the undesired harmonic number, $|Z|$ and Z_0 denote the impedances of the cavities and of free space, r_p the classical proton radius, R is the radius of the machine, N the number of particles and A is the bunch area after (ideal) trapping.

The resulting value $A \geq 0.13$ is safely below the bottleneck $A_{tr} = 0.2$.

3.3.3 Debunching and rebunching in the CPS

As stated in Subsection 3.3.1, these methods are applicable only with continuous transfer.

a) Debunching

Debunching in the CPS will give a small momentum spread and thereby ease continuous ejection. The minimum $\Delta p/p$ obtainable at 10 GeV/c by adiabatic debunching is, according to Equation 3.3:

$$\frac{\Delta p}{p} = \pm 0.3 \times 10^{-3} \quad \text{for} \quad A = 0.04 \text{ rad} .$$

Three debunching methods can be envisaged:

i) adiabatic r.f. voltage reduction

ii) 90° bunch rotation

iii) phase jump to the unstable fixed point followed by bunch rotation.

Method i) may suffer from the presence of coupling impedances in the CPS[3.14,15]. The advantage of ii) is that the r.f. system can work at a relatively high voltage level so that beam loading is less critical. However, the minimum $\Delta p/p$ is larger than the adiabatic figure. Moreover, non-linearities may cause either blow-up in longitudinal phase space or loss. Method iii), already in use in the CPS, is subject to similar limitations as method ii).

The best procedure for debunching will result from a compromise between:

i) final momentum spread

ii) self-bunching and beam loading

iii) longitudinal blow-up (or particle losses)

iv) debunching times.

b) Prebunching at 180 MHz

Prebunching of the beam at 180 MHz in the CPS would ease r.f. trapping in the main ring. However, this could create beam loading problems especially if one has to work with low voltages in the main ring.

The amount of bunching which can be performed already in the CPS is limited by the value of $\Delta p/p$ tolerable for the ejection process.

For comparison, Table 3.5 shows results for two different bunch shapes and three different bunch areas.

Table 3.5

180 MHz Prebunching in CPS at 10 GeV/c

Bunch length \ A in rad		0.08	0.04	0.02
± 180° bunches	180 MHz CPS r.f. voltage	96 kV	24 kV	25 kV
	$\Delta p/p$ at transfer	$\pm 0.92 \times 10^{-3}$	$\pm 0.46 \times 10^{-3}$	$\pm 0.23 \times 10^{-3}$
	Main ring voltage for matched buckets	400 kV	100 kV	25 kV
± 100° bunches	180 MHz CPS r.f. voltage	375 kV	94 kV	23.5 kV
	$\Delta p/p$ at transfer	$\pm 1.37 \times 10^{-3}$	$\pm 0.68 \times 10^{-3}$	$\pm 0.34 \times 10^{-3}$
	Main ring voltage for matched buckets	1500 kV	400 kV	100 kV
	Required main ring voltage during 90° rotation	2500 kV	1300 kV	630 kV

c) Capture of 180 MHz bunches in the main ring

The straightforward way to capture the CPS 180 MHz bunches is to inject them into matched buckets.

The voltage V_{MR} required for matching is related to the CPS voltage V_{CPS} by:

$$V_{MR} = \frac{|\eta|_{MR}}{|\eta|_{CPS}} \frac{R_{MR}}{R_{CPS}} V_{CPS} \approx 4.3\, V_{CPS} \qquad (3.6)$$

These voltages also shown in Table 3.5 may turn out to be uncomfortably low. One can then foresee to inject CPS bunches into unmatched buckets (higher r.f. voltage), perform a 90° rotation in phase space, and then match by a fast increase of the r.f. voltage[3.16] (last line of Table 3.5). Tolerances for these beam gymnastics, precise dilution factors, etc., are still under study.

3.4 Transfer line

3.4.1 General description

After ejection from CPS SS 16, the beam travels along the existing CPS-ISR transfer line TT2 and branches off after 300 m (about 2 m downstream from the switch of TT2 and TT2a) towards the main ring. From this point onwards a new transfer line has to be designed. For injection into a main ring of 1100 m radius, the following characteristics of this line have been worked out:

Table 3.6

Characteristics of the Transfer Line

Total length (up to middle of main ring long SS)	810 mm
Horizontal bending angle with TT2	+ 11°
Horizontal bending angle with main ring long SS	- 3.5°
Difference in level of floor TT2 and main ring	32.4 m
Vertical bending angles	± 3° to 4°
Crossing of St. Genis road	- 20 m

In addition to the existing section, 5, on Fig. 3.5, the transfer line will consist of four sections with different functions:

1: the branching off from TT2, including the total horizontal bend of 11° (length about 45 m);

2: the matching to the transfer line lattice (about 50 m);

3: the long distance transfer, including the vertical bends at both ends and a system exchanging the two transverse phase planes (about 715 m);

4: inflection into the main ring.

3.4.2 Branching off from TT2

Without removing nor changing any active element in TT2, a branching off behind quadrupole QF 333 (or QF 335) is possible. A bending magnet installed close behind QF 333 with a bending angle of about 3.5° will deflect the beam clear of the following quadrupole QD 334. The beam stopper upstream of QD 334 which cannot be cleared may be shifted to the next straight section between QD 334 and QF 335.

Subsequently, two FODO periods of the TT2 lattice will be installed into which the other required bending magnets are inserted. Their exact positions will depend on α_p.

3.4.3 Lattice for the long distance transfer

It is proposed to use for this section of the transfer line the FODO lattice of the main ring, having a period length of 64 m and a phase advance per period of 92.5°. Thus a total of only 22 quadrupoles (11 QD + 11 QF) with a strength of $k\ell = 0.045\ m^{-1}$ and a bore radius of 60 mm are required for this section. The choice of this lattice has the advantage that an extra betatron matching to the main ring is avoided.

The vertical bends are inserted near the beginning and the end of this section, such that the vertical α_p is zero after the beam travels again horizontally.

In case of a continuous CPS ejection (where the horizontal emittances may be smaller than the vertical ones, see Subsection 3.2.3), an exchange of the phase planes might be desirable. This can be done inserting three skew quadrupoles of the same type and strength into the line at distances of one period length. For our lattice with $\mu \approx 90°$ and with positions of the skew quadrupoles where $\beta_h = \beta_V = \beta$ (which is not a necessary condition) the required strength is only $1/f = 1/\beta \approx 0.02\ m^{-1}$.

3.4.4 Betatron matching

In order to match the TT2 lattice to the main ring lattice, an extra section of about 50 m length is foreseen. A series of quadrupoles, possibly in doublet or triplet arrangement, have to be installed. The aperture and strength requirements may differ from those for the long distance transfer section.

3.4.5 Inflection into the main ring

A horizontal inflection scheme as shown in Fig. 3.6 is proposed. It requires a septum magnet of modest characteristics (1 ms flat top if pulsed, septum thickness 8 mm, gap height 30 mm, $B \approx 0.8$ T for about 3 m total length) and a full aperture kicker system for a bending angle of 2.8 mrad. Two different supplies for the kicker magnet have been considered (Fig. 3.6a and b), one which gives within a minimum time of 1 ms twenty half sine pulses of 2 μs length (for bunch by bunch CPS ejection), and a second one which gives a single pulse with flat top length of 23 μs and fall time of about 0.5 μs (for continuous ejection). The characteristics of this system, which does not appear to present particular difficulties are summarized in Table 3.7. The magnet would be basically of the Serpukhov type[3.17].

The kicker position is a compromise between a position further downstream, requiring less kick strength, and a position further upstream, requiring less aperture in the D quadrupole. With the septum magnet and kicker magnet positions shown in Fig. 3.6, the injected beam will just stay in the "good" field region of the D quadrupole, if the local closed orbit is controlled suitably.

Table 3.7

Characteristics of Main Ring Injection Kicker System

Magnet aperture w × h	41 mm × 48 mm
length	1 m
inductance	1.5 μH
Number of turns	1
Peak density	0.12 T
Peak current	4.5 kA
Peak voltage	11 kV
Stored magnetic energy	15 Ws

Bunch by bunch transfer:
Half sine wave excitation by means of a concentrated capacitor of 0.25 μF and a pulser 11 kV/4.5 kA (one thyratron CX 1140), recharged from a C-L-C-R battery for 20 × 1 pulses supplied by a stabilized d.c. power supply 11 kV/100 mA.

Continuous transfer:
Excitation from a 25 μs storage line 34 kV/4.5 kA/3.75 Ω, charged from a resonant supply of existing design; fall time with thyratron clipper: 0.5 μs.

3.4.6 Utilization of elements of TT2a

This line, which transports the 28 GeV CPS beam from TT2 into the West Hall, will consist of 25 F quadrupoles, 25 D quadrupoles, 26 horizontal and 10 vertical bending magnets of the ISR transfer standard series. In the case that this line will be shut down and the elements become available, the new transfer line can probably be built with these elements. However, the quadrupoles have to be operated at less than a quarter of their nominal power, if one keeps the lattice as proposed above.

Taking also into account partial utilization of the existing power supplies and the vacuum system, a total of about 2 MSF could be saved.

3.5 Conclusions

We confirm that the CPS appears to fulfil the requirements for an injector for the main ring. Either bunch by bunch or continuous transfer can be used. The continuous transfer potentially provides extra insurance, should an unexpected beam blow-up occur when raising the CPS intensity from 2×10^{12} to 10^{13} p/p or in the main ring between injection and transition where the main ring is aperture limited.

To permit the choice between the two ejection modes, we recommend to:

i) study experimentally at the CPS the influence of the kicker pulse properties on the resulting beam emittances, to order and test the model for fast recharging,

ii) develop and install in the CPS the required hardware for the continuous ejection and so complement the theoretical work experimentally.

The choice of R_{MR} = 1100 m offers the two most attractive possibilities of transfer scheme (Section 3.2). With this radius, in the case of bunch by bunch transfer by means of kickers, the choice of possible intervals between two kicker pulses is wide enough to be considered as independent of the as yet unknown pulsing period of the CPS ejection kicker (see Subsection 3.2.2).

The transfer momentum of 10 GeV/c is a compromise between the necessity to provide large enough r.f. buckets and the requirements to debunch the beam at main ring injection. A high transition energy is useful to improve the horizontal aperture limitation with large bunches and to provide large enough buckets at $\gamma_{tr} \sqrt{3}$. $\gamma_{tr} \approx 25$ is a compromise between these requirements and the desire to have long enough straight sections for ejection at top energy.

The main ring acceptance looks just sufficient even for bunch by bunch transfer at 10^{13} p/p, as it should be if the main ring is not to be overdesigned.

The main ring inflector design depends on the transfer scheme chosen. One expects that this choice can be made before the design has to be frozen.

Preferably, the sum of one CPS filling cycle and one CPS experimental physics cycle should match the main ring cycle (3.0 to 4 s).

3.6 Budget and time schedule

Table 3.8

Preliminary Cost Estimates

Item	MSF
CPS ejection system including models (0.6 MSF)	2.0
CPS-Main Ring transfer system	
Magnets, lenses, their supports, cables, power supplies	2.7
Main ring injection magnet system (septum, kicker)	1.2
Local controls (including cables), beam observation and display	0.5
Vacuum system*	
Installation (plus material)	0.5
Miscellaneous	0.5
Buildings*	
Tunnel*	
* included elsewhere TOTAL	7.4

The cost of the ejection system will evidently depend on the choice to be made and the quoted figure is therefore necessarily rough.

The cost estimate for the transfer line is for a d.c. powered system. The quadrupoles and bending magnets are laminated. It will be studied if a pulsed system is cheaper. Use of magnets, power supplies and vacuum components of the TT2a line would reduce this cost by about 2 MSF.

No cost figures for a CPS 180 MHz r.f. prebunching system nor for double pulsing the CPS are given.

Table 3.9

Time Schedule

Models for CPS ejection system:	
components ordered	early 1971
start feasibility test	late 1971
Final system:	
start construction	early 1973
complete	mid 1975

References

(3.1) The alternative 300 GeV programme, CERN/963.

(3.2) O. Barbalat, W. Hardt and K.H. Reich, The improved CPS as injector for the 300 GeV synchrotron, CERN/MPS-SI/DL/70-8.

(3.3) D. Möhl, W. Schnell, A. Sørenssen and C. Zettler, The feasibility of using the PS as an injector for "Project B", RF problems, CERN/MPS-DL/70-6.

(3.4) Y. Baconnier et al., Debunching in the presence of high-freqeency cavities, MPS/DL/Note 70-14 (MC/33).

(3.5) W. Hardt and D. Möhl, Debunching in "Project B", MC-34.

(3.6) A. Brückner, A proposal for 20 × 1 or 10 × 2 bunch ejection from the CPS to the 300 GeV machine based on a new fast charging system, MPS-SI/Note 300/INJ/2.

(3.7) H.G. Hereward, The possibility of resonant extraction from the CPS, AR/Int. GS/61-5.

(3.8) E. Brouzet, C. Johnson and P. Lefèvre, Mesures des dimensions verticales du faisceau du PS, MPS/DL-Note 70-21.

(3.9) C. Bovet et al., Evolution of proton density between ion source and ISR, CERN/MPS-SI/Int. DL/70-7.

(3.10) A. Sørenssen, The effect of strong longitudinal space-charge forces at transition, MPS/Int. MU/EP 67-2.

(3.11) A. Sessler and V. Vaccaro, Longitudinal instabilities of azimuthally uniform beams in circular vacuum chambers with walls of arbitrary electrical properties, CERN 67-2.

(3.12) E. Keil and W. Schnell, Concerning longitudinal stability in the ISR, CERN/ISR-TH-RF/69-48.

(3.13) D. Möhl, A. Sørenssen and C. Zettler, How to inject into which lattice, MC-41.

(3.14) H.G. Hereward, Effects of cavities on debunching, rough estimates for the CPS, CERN/MPS/DL 69-7.

(3.15) A. Sørenssen, What sort of coupling impedances are tolerable in the future CPS, MPS/DL/70-1.

(3.16) See for example H.H. Umstätter, Data on longitudinal phase space matching for beam transfer from the booster into the PS at 800 MeV, MPS/SR/Note 69-20 Rev.

(3.17) P.G. Innocenti, B. Kuiper, A. Messina and H. Riege, On the design of a "fast kicker" magnet, PS/FES/70-3.

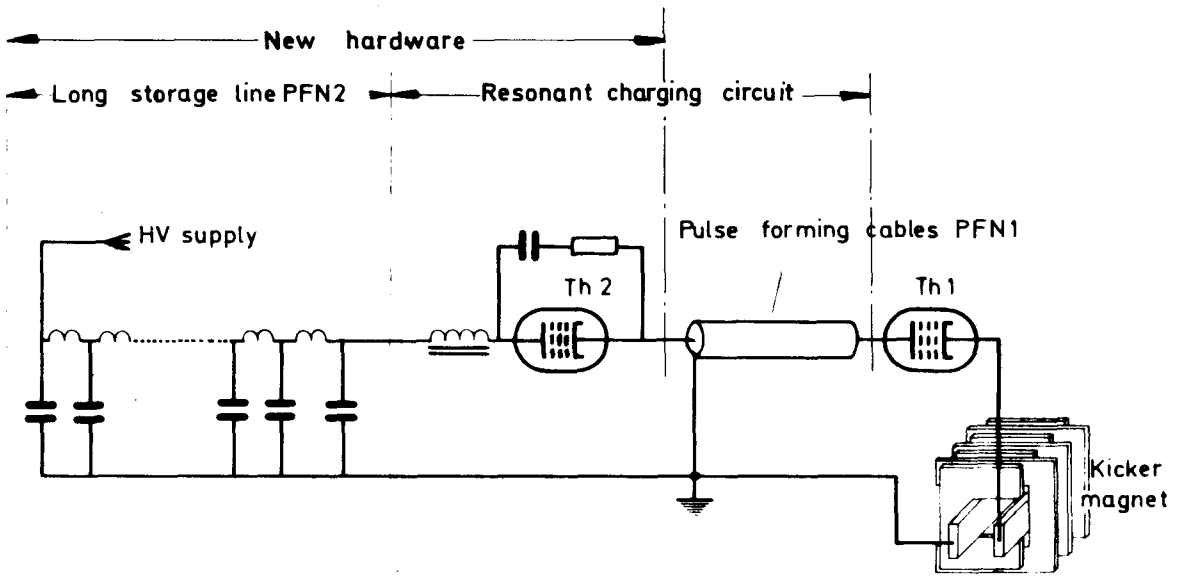

Fig. 3.1 Proposal for fast recharging of PFN 1

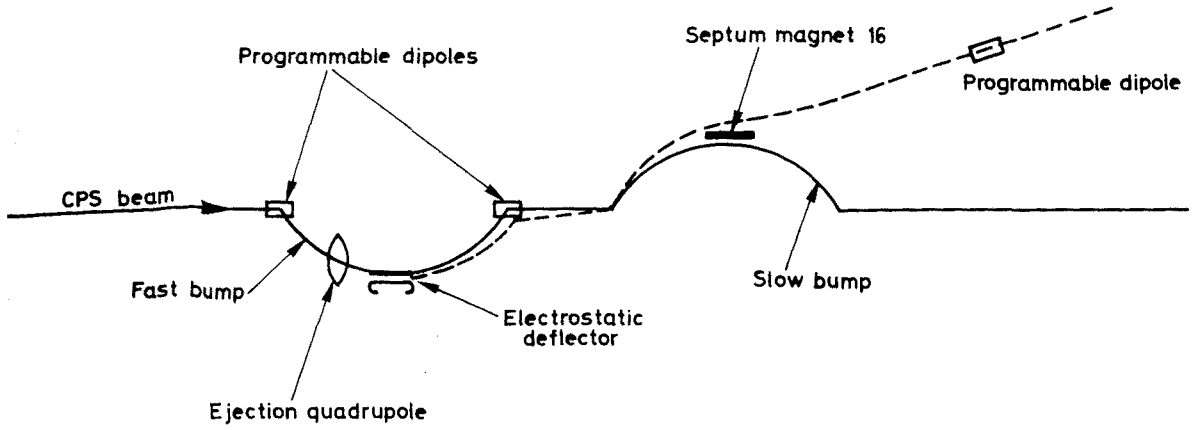

Fig. 3.2 Continuous ejection (schematic)

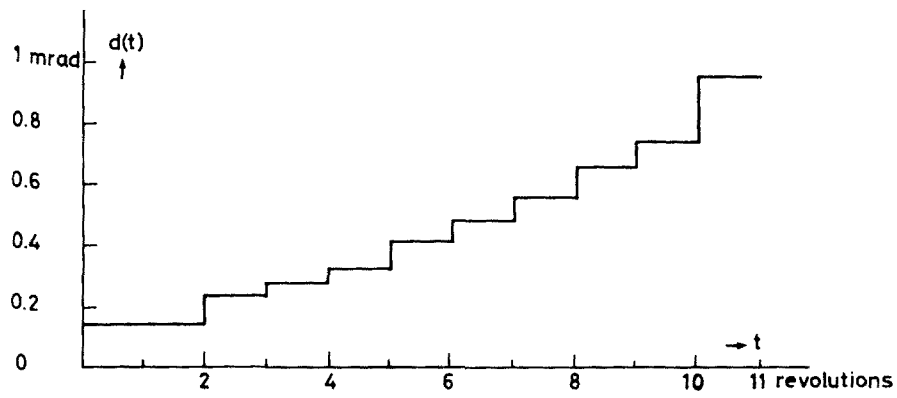

Fig. 3.3 Computed amplitude of fast bump

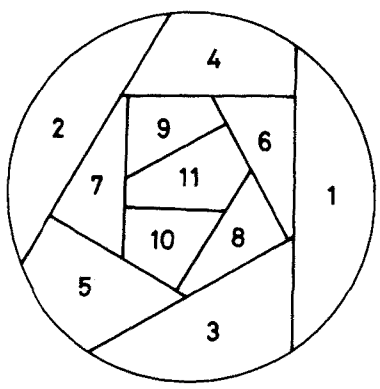

Fig. 3.4 Eleven-turn continuous ejection in the horizontal phase plane

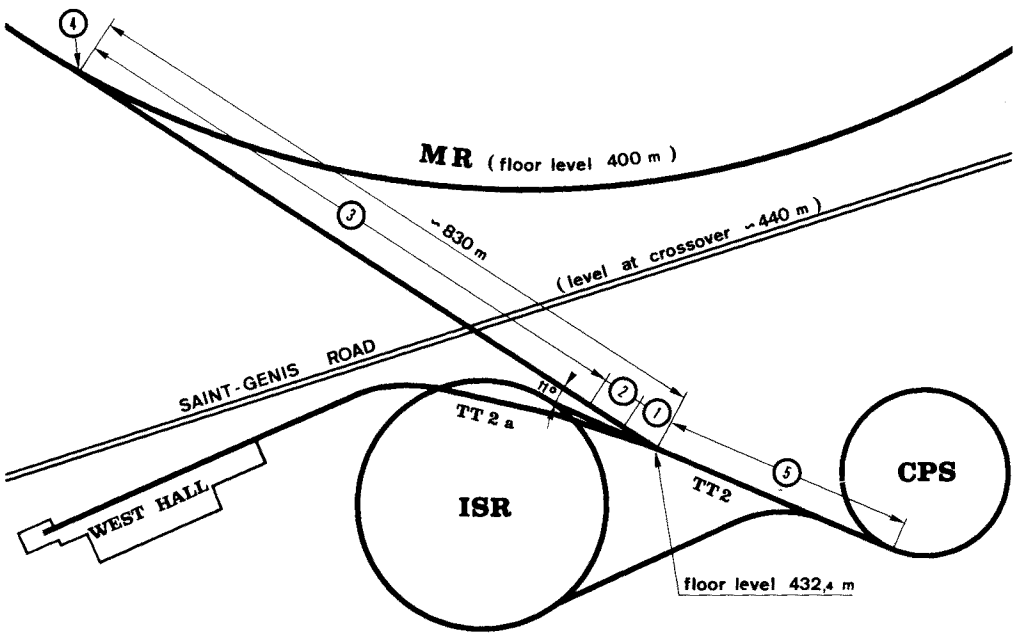

① Branching off section (~45m) ② Matching section (~50m)

③ Long distance transfer section (~735 m) ④ Injection into MR in long SS 1 .

⑤ Part of the existing CPS - ISR transfer line TT 2 .

Fig. 3.5 CPS-MR transfer line (schematic)

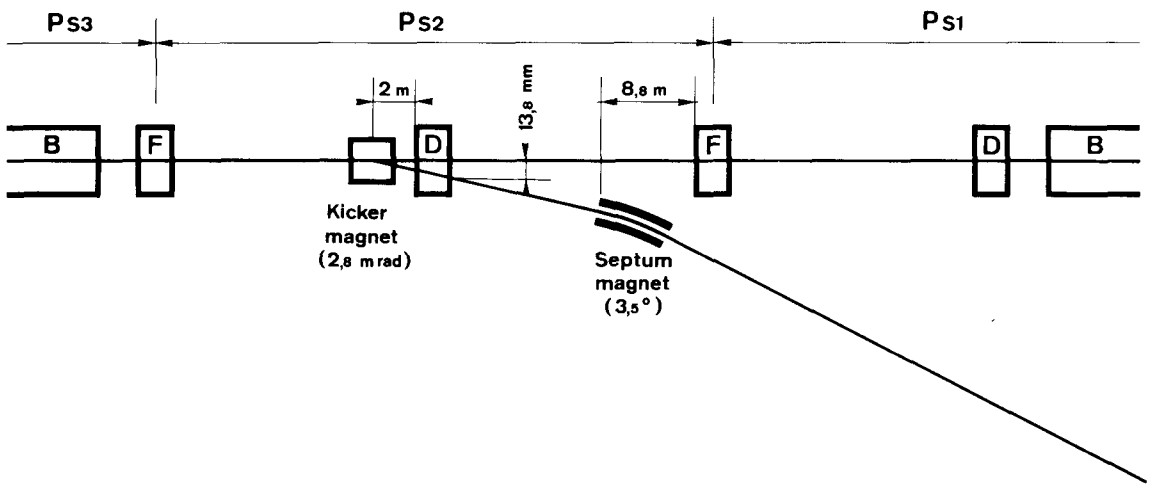

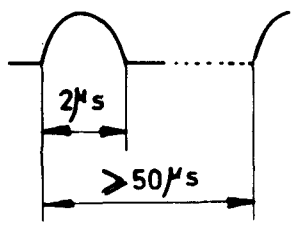

a) Kicker excitation cycle for bunch by bunch transfer

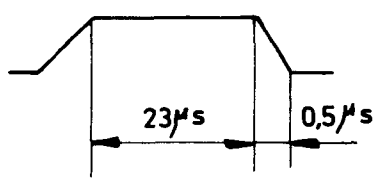

b) Repeated twenty times, and continuous transfer

Fig. 3.6 Horizontal inflection (Schematic)

Chapter 4

THE MAGNET SYSTEM

4.1 General Layout of the Magnet System

The main magnet system of the 300 GeV proton synchrotron consists of dipoles, which have the function of bending the protons along a closed path, and quadrupoles, which exert a focusing action to maintain them within the vacuum chamber aperture. A number of small correcting magnets are regularly interspersed between the main magnet elements.

Quadrupoles of two different types, designated as Q_F and Q_D have been selected for exerting the focusing action in the horizontal and vertical planes, respectively, because their required apertures are very different. There are 108 quadrupoles of each type, which alternate in regular succession at equal distances all along the machine, thus forming 108 focusing periods.

The number of dipoles placed within each focusing period depends on the final energy of the machine; in the "regular" periods there are 4, 6 and 8 dipoles for Stages A, B and C, respectively. There are also some "special" periods in which part or all of the dipoles are omitted, to allow space for injection and ejection equipment, accelerating stations and other apparatus. The main magnet system is thus subdivided in 6 equal sectors, each containing 15 normal periods and 3 special ones.

The required apertures for the dipoles depend on their positions in the focusing period. In order to limit the number of different magnets, which has a consequence on tooling requirements and on flexibility, it is appropriate to have only 3 types of normal dipoles, all of equal length. Two, called B1 and B2, have cross-sections which fit as closely as possible the local aperture requirements in the vicinity of the Q_F and Q_D quadrupoles respectively; the third, called B3, suits practically any position between the other two. For the special periods, a 3/4 length version of magnet B2, called B4 , is necessary in Stages A and B of machine development. No B3 magnets are required in Stage A.

As a consequence of the above choices the number of magnets of each type required at each stage of machine development is given in Table 4.1. The table shows also the length of each magnet, the peak field in the dipoles and the peak gradient in the quadrupoles. The quoted lengths are the magnetic equivalent lengths at the required peak excitation: the steel core lengths will be either equal to the said values or slightly smaller, depending

on the end pole taper.

The numbers and strengths of the different correcting magnets are discussed in Chapters 8 and 9.

Table 4.1

Composition of the Main Magnet System

	Q_F	Q_D	B1	B2	B3	B4
Length (m)	3.799	2.650	6.017	6.017	6.017	4.512
Field (T)			1.8	1.8	1.8	1.8
Gradient (T/m)	16.91	24.10				
Number for Stage A	108	108	186	192	-	12
" " Stage B	108	108	186	186	186	30
" " Stage C	108	108	186	192	396	-

4.2 Design of the Dipole Magnets

4.2.1 Shapes and apertures

The purity of a dipole field is best ensured by a magnet configuration in which the cross-section is symmetrical with respect to a vertical axis: such a magnet appears typically as having two symmetrical windings around the poles and a return yoke with equal sides. In a particular case of this configuration, the whole region surrounding the useful aperture may be occupied by conductors, which thus form a frame inside the gap itself: this magnet is called in this report a "window frame" (WF) magnet, while the name of "H-magnet" is reserved to designate the symmetrical dipole in which the coils are flat pancakes around the poles.

Both these shapes of magnets were considered for the machine dipoles. In fixing their vertical apertures it was assumed that the H-magnet core would be made in one block and that coils and vacuum chamber would be inserted through the gap between the poles, while the WF magnet, whose coils must have bent-up ends to clear the beam passage, would have a core split into two halves. Therefore, some extra gap height is left in the H-magnet for inserting the vacuum chamber and to allow for its subsequent deflection under vacuum. The clearance is different for the magnets of the 3 types on account of the different aspect ratio of the vacuum chamber.

An additional constraint in fixing the gap heights is imposed by the necessity of having the gap heights in the 3 types of magnets in the ratios of even integers in order to be able to power them in series, i.e. to satisfy their ampereturn requirements with the same current but different number of turns.

Table 4.2 shows the maximum beam heights and the selected gap heights for the 3 types of magnets of each shape and the corresponding number of turns.

The horizontal aperture, intended as the radial width of the "good field" region in the horizontal symmetry plane, is the same for H and WF magnets and is obtained for each type of magnet by adding to the maximum beam width the sagitta of the curved beam orbit over the total length of the magnet unit, which is assumed to be straight to simplify the construction (see Section 4.4). In dipoles B1 and B2, the orbit sagitta during Stage A operation of the machine has to be taken into account, while in dipole B3 only the smaller value, corresponding to Stage B, occurs. In B4 the sagitta is smaller than in B2, because of its shorter length, but the same horizontal aperture has been assumed in the two versions because the possible difference of 5 mm does not justify the expense for special tools.

The horizontal apertures of the dipoles are also shown in Table 4.2.

Table 4.2

Dipole Apertures and Numbers of Turns

	B1	B2	B3
Beam height (mm)	26.6	47.6	40.0
H magnet gap height (mm)	36.6	54.9	50.3
H magnet coil turns	16	24	22
WF magnet gap height (mm)	33.44	54.34	45.98
WF magnet coil turns	16	26	22
Beam width (mm)	120.6	67.0	101.6
Maximum sagitta (mm)	12.1	12.1	8.1
Horizontal aperture (mm)	132.7	79.1	109.7

4.2.2 Basic assumptions and limitations

Once the gap heights and the horizontal apertures have been selected, the dimensioning of the dipoles depends essentially on two elements: the pole width to obtain the required "good field" aperture over the operating range of field values and the space needed by the excitation coils.

The problem of detailed pole design is somewhat different for H and WF magnets because in the former the field shape in the required aperture depends practically on the pole profile alone, while in the latter the influence of the conductors inside the gap has also to be taken into account. For the coils, however, the optimum r.m.s. current density is not very different in the two cases. On account of the compact shape of the cross-section this optimum density is higher than for conventional C-shaped combined function magnets and is

further increased if the interest rates during the time over which the running expenses are capitalized are taken into account. For the present design study a peak current density of 6.65 A/mm^2 has been assumed. With the typical magnet cycles for full energy operations in the different stages, this corresponds to an r.m.s. density of 4.2 A/mm^2, which is slightly on the high side of the very flat optimum, which can be estimated at present. These values should obviously be revised by the time when the design will be finalized.

For pole profile designs the "good field" region in the dipoles is defined as the region over which the relative field error due to a sextupole component does not exceed $5 \cdot 10^{-4}$ and the additional gradient, due to all other components, is limited by the expression $\left|\frac{B'}{B}\right| \leq 0.01\ m^{-1}$. The sextupole limit is deduced from slow ejection requirements, taking into account the further contribution of end effects (the total sextupole tolerance should be less than 10^{-3}); the gradient limit corresponds to betatron stability limits for systematic gradient errors.

In order to dimension the return yoke, it was assumed that the ampereturns lost in the yoke at maximum field should not exceed 4% of the useful ampereturns. This value is an arbitrary assumption, suggested by experience: the larger the losses in iron the more stringent the requirements on magnet manufacturing uniformity for a given tolerable r.m.s. field spread (see Section 4.4). In the computation of field patterns at high fields it is assumed that the magnet cores are made out of decarburized steel sheet having similar characteristics to those of the ISR steel (Fig. 4.4) and stacked with a packing factor of at least 96%. In the design of the coils, after consideration of the test voltages involved and consultation with manufacturers, maximum clearances of 0.65 mm for conductor insulation and 3 mm for ground insulation were assumed. Taking into account commercial tolerances on conductor dimensions and straightness and practical tolerances on the moulds, these assumptions in coil dimensioning should ensure that an adequate insulation thickness will exist everywhere in the coils (0.5 mm on conductor and 2 mm to ground).

Cooling water passages inside the coil conductor were designed to limit the temperature rise to 15°C under a differential pressure of 4 atm.

4.2.3 Dimensioning of cores and coils

On the basis of the criteria and assumptions exposed in Subsection 4.2.2, preliminary designs have been produced for H and WF magnets of the three types.

The cross-sections of the H magnets are shown in Fig. 4.1 and their main characteristics are given in Table 4.3. The coils of the magnets B2 and B3 consist of two pancakes only, one on each pole; this is the simplest and cheapest solution for coil making and mounting. Although the coil width turns out to be about 25% larger than that which would be adopted if double pancakes were used, the space for coil ends is the same, because the smaller width of the individual conductors permits a smaller bending radius of the inner turn, and stays well below the available half-gap between cores. In each pancake, there are 2 water circuits in

parallel, with inlets at the ends and outlets in the middle. For magnet B1, 4 pancakes have to be adopted because of the limit imposed by the small gap height through which the pancakes must pass. These 4 pancakes are hydraulically in parallel, with water inlets outside and outlets inside.

The blank weight has been computed assuming a 10 mm margin all around the finished lamination. The quoted inductance is the maximum value, which corresponds to medium field levels (infinite steel permeability).

The cross-sections of the WF magnets are shown in Fig. 4.2 and their main characteristics are given in Table 4.4.

In the B1 type, because of the small gap height, the two conductors inside the gap have their axes in the median plane: therefore, complete symmetry between top and bottom halves of the winding is not maintained at the ends. In types B2 and B3, on the contrary, the conductors inside the gap are symmetrically paired with respect to the median plane. In all cases, however, the design does not include separate upper and lower coils but just one common winding, with several water circuits in parallel and a common insulation to ground. A different design (Mk 2), in which each coil would have only 2 water circuits, with input at the ends and output in the middle, would increase the steel weight by 7% and the stored energy by 10%.

The positions of the conductors in the gap has been chosen so that the copper of the innermost conductor is at 30 mm from the edge of the useful aperture. This decision will ensure the required field quality without imposing conductor position tolerances which are unacceptable to industrial coilmakers. Detailed computations have shown that in magnet B2 a vertical shift of the two inner conductors together by 0.3 mm produces at 30 mm distance from the copper a radial field component of $2 \cdot 10^{-4}$ times the vertical field. The same effect is produced by a radial displacement of the two conductors by 1 mm with respect to each other.

A symmetrical vertical displacement of the same two conductors by 0.5 mm with respect to the median plane creates at 30 mm a gradient to field ratio of 0.006 m^{-1}.

4.2.4 Expected field patterns and performance at high fields

The preliminary designs of all types of H and WF dipoles shown in Figs. 4.1 and 4.2 have been based on computer studies performed by means of the bidimensional programs MARE and TRIM. These studies indicate that field variations and gradients can be kept within the prescribed limits inside the whole useful aperture up to a field of 1.8 T with both dipole shapes. A full optimization of the pole profile has not been possible in the limited time available and, therefore, it is not possible to say exactly up to what field limit an acceptable field pattern can be maintained in each individual case. This is particularly important for the WF dipoles, where the range of useful field levels depends on the position

Table 4.3

Main Characteristics of H Dipoles

Magnet type		B1	B2	B3	B4
Peak field	(T)	1.8	1.8	1.8	1.8
Core characteristics					
Unit length	(m)	6.017	6.017	6.017	4.512
Gap height	(mm)	36.6	54.9	50.3	54.9
Useful width	(mm)	132.7	79.1	109.7	79.2
Packing factor		0.96	0.96	0.96	0.96
Lamination height	(mm)	493	489	493	489
Lamination width	(mm)	838	988	1016	988
Core weight	(ton)	16.6	19.3	20.8	14.1
Blank weight	(ton)	20.1	23.4	24.3	17.5
Coil characteristics					
Copper weight	(ton)	0.99	1.54	1.40	1.23
Number of turns		16	24	22	24
Number of pancakes		4	2	2	2
Conductor of dimensions	(mm^2)	23.9×24.5	43×14.25	40×15.3	43×14.25
Cooling hole dimensions	(mm)	ø= 10	25×4	20×5	25×4
Number of water circuits		4	4	4	4
Pressure drop (max.)	(atm)	4	4	4	4
Temperature rise (max.)	(^{o}C)	15	15	15	15
Coil end width	(mm)	185	235	235	235
Excitation characteristics					
Peak ampereturns		54'500	81'900	75'000	81'900
Peak current	(A)	3'410	3'410	3'410	3'410
Peak current density	(A/mm^2)	6.65	6.65	6.65	6.65
r.m.s. current density	(A/mm^2)	4.2	4.2	4.2	4.2
Peak stored energy	(kJ)	83	137	130	102.5
Losses	(kW)	34.5	52.5	48.5	41
Maximum inductance	(mH)	15.7	25.9	24.7	19.4
Resistance	(mΩ)	7.4	11.2	10.2	8.8

Table 4.4

Main Characteristics of WF dipoles (Mk 1)

Magnet type		B1	B2	B3	B4
Peak field	(T)	1.8	1.8	1.8	1.8
Core characteristics					
Unit length	(m)	6.017	6.017	6.017	4.512
Gap height	(mm)	33.44	54.34	45.98	54.34
Useful width	(mm)	132.7	79.1	109.7	79.2
Packing factor		0.96	0.96	0.96	0.96
Lamination height	(mm)	480	500	480	500
Lamination width	(mm)	840	850	840	850
Core weight	(ton)	16.7	17.0	16.4	12.8
Blank weight	(ton)	20.2	21.2	20.2	15.9
Coil characteristics					
Copper weight	(ton)	0.85	1.38	1.17	1.06
Number of turns		16	26	22	26
Number of pancakes		1	1	1	1
Conductor dimensions	(mm^2)	22.5×26.0	22.5×26.0	18.7×29.5	22.5×26.0
Cooling hole dimensions	(mm)	12	12	10	12
Number of water circuits		4	6	5	5
Pressure drop (max.)	(atm)	4	4	4	4
Temperature rise (max.)	(^{o}C)	15	15	15	15
Excitation characteristics					
Peak ampereturns		48'600	80'600	68'200	80'600
Peak current	(A)	3'100	3'100	3'100	3'100
Peak current density	(A/mm^2)	6.66	6.66	6.66	6.66
r.m.s. current density	(A/mm^2)	4.2	4.2	4.2	4.2
Peak stored energy	(kJ)	78	120	105	90
Losses	(kW)	31	50	42	38
Maximum inductance	(mH)	16.2	25.0	21.8	18.7
Resistance	(mΩ)	8.0	13.0	11.0	10.0

and angle of the pole taper as well as on the ratio of ampereturns in the gap to total ampereturns; the combination of these variables for which the maximum is reached is a function of the ratio of gap height to gap width and therefore is different for each type of magnet.

It can already be said, however, that the WF dipoles can meet the tolerances on field pattern at least up to a field level of 2 T while in the H dipoles the corresponding limit is 1.8 T. In the H dipole the field drop at the edge of the horizontal aperture at 2 T is twice the tolerated value. It is interesting to notice that in optimized WF magnets the field tends to increase radially at high fields, while in H magnets it tends to decrease.

The influence of end effects on the overall dependence of bending strength on radial position has been studied by using the results of measurements on magnets of the two shapes. This influence appears to go in the same direction as the deterioration of the bidimensional field distribution, but is relatively weak (20 to 30% of the total effect) in 6 m long magnets.

4.3 Design of the Quadrupoles

4.3.1 Shapes and apertures

A magnet with complete quadrupolar symmetry, i.e. with symmetry axes at 45°, is best for creating a pure quadrupole field inside an inscribed circular aperture, since the first higher component compatible with its symmetry is a dodecapole. With the proposed machine parameters, this shape is very well suited for the D quadrupoles (Q_D) in which the beam has almost equal vertical and radial dimensions, but would be very wasteful for the F quadrupoles (Q_F), in which the beam width is more than 6 times the beam height.

The F quadrupoles, therefore, are given an "elliptical" aperture, in the sense that they create the required quadrupole field only in a region which fits the flat beam shape as closely as possible. With this configuration, many more harmonic field components, starting from the octupole one, may be present and, therefore, saturation effects and end effects must be more closely watched.

In both cases the basic pole profile is hyperbolic, but different portions of the hyperbola are preserved and ad-hoc compensations for the missing parts are introduced. The quadrupole apertures, which can be defined by giving the radii of the inscribed circles to the pole hyperbolae must accommodate the necessary vacuum chambers. The chambers have been assumed to be circular and elliptical respectively and with such inner dimensions that, under vacuum, a radial free space corresponding to the momentum spread is still available at maximum beam height. The total of vacuum chamber wall thickness and clearance to the poles has been assumed to be at least 2 mm in Q_D (circular chamber) and 3 mm in Q_F (elliptical chamber).

An additional constraint in fixing the quadrupole apertures comes from the wish to excite them in series, in order to reduce the tracking problems of the power supplies. With the chosen maximum gradients only minor adjustments are necessary to fit conveniently small numbers of turns per pole.

Table 4.5 shows the maximum beam dimensions, the selected inscribed radii, the gradients and the smallest possible number of turns for Q_D and Q_F and, for Q_F, the semi-axes of the elliptical vacuum chamber (external contour).

4.3.2 Dimensioning of cores and coils

In determining the dimensions of the quadrupole cores and of their windings, similar assumptions to those of the dipole design were made, taking into account, however, that the quadrupoles must perform satisfactorily up to 400 GeV at least, although their optimum operation corresponds to Stage B. It was requested that the relative variation of gradient inside the useful aperture would not exceed $2 \cdot 10^{-3}$ over the whole range of excitation. The drop of ampereturns in the magnetic circuit was kept below 2% to maintain the proportionality between gradients in Q_F and Q_D. The peak current density was raised to 8.8 A/mm^2 for 400 GeV operation, which corresponds to 6.5 A/mm^2 at 300 GeV so that at this operating level the r.m.s. density is 4.1 A/mm^2. The insulation thickness was slightly reduced on account of the lower voltages involved.

For reasons of economy in punching and assembling the laminations, it seems desirable to have the cores split in two halves, rather than in 4 quadrants; the coils have then to be introduced between the two poles of each half core.

Two designs have been considered: one in which the coils are mounted on the poles in such a position as to be shielded against radiation; and another in which the coils reach the symmetry planes and are therefore exposed. In the first case the necessary clearance for mounting the coils one after the other is easily obtained, in the second the coils have to be so shaped as to fit together into the gap between poles. The second design is somewhat more compact and leads to 10% higher useful gradients, but, besides exposing the insulation, is also more critical from the point of view of coil dimensions and positions.

The increase in useful gradient is of special importance for the F quadrupoles, in which the field pattern at the edge of the horizontal aperture deteriorates at gradients above 18.5 T/m, while the D quadrupoles can be used up to 29 T/m.

Further study is being devoted to this design in order to assess its possible performance and to determine the required tolerances. The present proposal, however, is based on the shielded-coil design, which is shown in Fig. 4.3. The main characteristics of the proposed quadrupoles are listed in Table 4.5a.

Table 4.5a

Main Characteristics of the Quadrupoles

Quadrupole type		Q_F	Q_D
Peak gradient	(T/m)	16.91	24.10
Gradient at Stage B	(T/m)	12.68	18.08
Unit length	(m)	3.799	2.650
Half beam height	(mm)	10.1	24.5
Half beam width	(mm)	62.6	26.8
Radius of inscribed circle	(mm)	31	29
Semi-axes of inscribed ellipse	(mm)	{ 14.6 65.6	
Packing factor		0.96	0.96
Lamination height	(mm)	380	430
Lamination width	(mm)	540	430
Core weight	(ton)	3.8	2.5
Blank weight	(ton)	6.6	4.2
Loss of ampereturns at 400 GeV	(%)	< 2	< 2
Number of turns per pole		4	5
Peak current at Stage B	(A)	1210	1210
Peak current density at Stage B	(A/mm^2)	6.5	6.5
r.m.s. current density at Stage B	(A/mm^2)	4.1	4.1
Stored energy at Stage B	(kJ)	3.8	3.0
Losses at Stage B	(kW)	7.2	6.4
Copper weight	(kg)	225	200
Conductor dimensions	(mm^2)	14.5×14.5	14.5×14.5
Cooling hole diameter	(mm)	5	5
Pressure drop	(atm)	4	4
Temperature rise (Stage B)	(^oC)	8	10
Temperature rise (Stage C)	(^oC)	14.2	17.8

Table 4.5b

Alternative Parameters for Q_F with Enlarged Aperture

Quadrupole type		Q_{F_p}	Q_{F_e}
Peak gradient	(T/m)	16.91	16.91
Gradient at Stage B	(T/m)	12.68	12.68
Unit length	(m)	3.799	3.799
Half beam height	(mm)	10.1	10.1
Half beam width	(mm)	62.6	62.6
Radius of inscribed circle	(mm)	44	44
Packing factor		0.96	0.96
Lamination height	(mm)	480	520
Lamination width	(mm)	630	700
Core weight	(ton)	4.8	6.6
Loss of ampereturns at 400 GeV	(%)	< 2	< 2
Number of turns per pole		8	8
Peak current at Stage B	(A)	1210	1210
Peak current density at Stage B	(A/mm^2)	6.5	6.5
r.m.s. current density at Stage B	(A/mm^2)	4.1	4.1
Stored energy at Stage B	(kJ)	10.8	9.2
Losses at Stage B	(kW)	14.6	14.6
Copper weight	(kg)	460	460
Conductor dimensions	(mm^2)	14.6×16.7	14.6×16.7
Cooling hole diameter	(mm)	8	8
Pressure drop	(atm)	4	4
Temperature rise (Stage B)	(^oC)	10	10

Note: Q_{F_p} = protected coils (coils in double pancake)

Q_{F_e} = exposed coils (coils in single layer)

The very small gap height of the F quadrupoles imposes extremely tight tolerances on the gap profile: an error of 6 µm/cm on the rate of variation of the gap height would produce an error of $2 \cdot 10^{-3}$ in gradient at the edge of the radial aperture. Should such tight tolerances not be achievable, it would be necessary to increase the radius of the inscribed circle and, consequently, the size of the quadrupoles, the stored energy and the power dissipation. Table 4.5b shows possible parameters for F quadrupoles with $\sqrt{2}$ times larger radius. Alternatively, other methods of quadrupole manufacturing, such as the insertion of truncated coils into a fully punched monolithic core and their subsequent interconnection, as used in the PS booster quadrupoles, could be considered.

4.4 Core Construction

4.4.1 Steel properties

All magnet cores are stacks of insulated steel laminations. A laminated structure is necessary in order to avoid excessive eddy currents during pulsed excitation, which would distort the field pattern in the magnet gap. The upper limit to lamination thickness imposed by eddy current considerations, however, is higher than the maximum thickness for precision punching, which is between 1 and 1.5 mm.

The magnetic properties of the steel sheet influence the field distribution mainly at high fields, where certain regions of the core approach saturation, and at low fields, where the contribution of the steel coercivity to the field in the gap is not negligible. In order to maintain a satisfactory field distribution in the gap over the widest possible range of excitation value, a high permeability at high fields and a low coercivity are required. For both of these properties, also the uniformity over the whole delivery is important, for the sake of field uniformity along the proton orbits.

The best saturation characteristics are obtained in low-carbon steel sheet with low impurity content: when decarburized in open coils in a controlled atmosphere and then subjected to a grain-growing treatment consisting of reductions and special anneals, this material has also a low coercivity. Silicon steel sheet, which may be satisfactory from the point of view of coercivity, has a lower saturation limit.

Considerable experience has been acquired by several European steelmakers in the production of this material, with reproducible magnetic characteristics and at rather low cost, during the construction of the CERN Intersecting Storage Rings (ISR). On the basis of similar experience, decarburized steel sheet has also been adopted for the magnets of the NAL accelerator.

Systematic magnetic measurements during the production of 10'000 ton steel sheet for the ISR have given the following results:

Magnetizing field (oersted)	Magnetic induction (gauss)	
	average	spread (95% of samples)
0.5	2'000	± 700
15	15'520	± 180
300	20'350	± 100

The coercivity had an average value of 0.63 Oe, with a spread of ± 0.1 Oe on 95% of the samples and ± 0.15 Oe on all samples. A typical magnetization curve is shown in Fig. 4.4.

If the spread in average coercivity from magnet to magnet would be equal to the spread in coercivity from ingot to ingot, namely ± 0.1 Oe, the spread in field value at an injection field of 0.060 T (corresponding to Stage B) could be as high as 0.4%. Even higher values of field spread could result, at high fields, from the spread in permeability as measured on the ingot samples. Therefore, it would be desirable for each magnet to contain sheets from different ingots, different annealing loads and different heats. Coercivity and permeability measurements on steel sheet samples during production could orient a moderate mixing, without requiring full scale storage or shuffling, and would permit steps to be taken to prevent any systematic drift of the average values of these characteristics in the course of production.

The steel sheet could be insulated at the rolling mill by phosphatization or other surface treatment. Since the final anneal for grain growth is performed in coils, the steel can be delivered to the coremaker either in the form of coils or as bundles of flat sheets cut to size.

Success in achieving grain orientation of decarburized steel during the grain growth process has been reported recently by Japanese steelmakers. This process does not change the ultimate saturation limit, but raises the permeability in the preferred direction by an appreciable amount, in the region up to 2 T.[4.1] It is proposed to investigate with European steelmakers the possibility of applying this method and its financial implications.

4.4.2 Punching and assembling

For laminations of comparable sizes to those of the dipoles, good quality profiles have been obtained by punching 1.5 mm thick sheets of decarburized steel in two operations, the second one being reserved to shearing the pole profiles and the reference surfaces. In addition to reducing the forces in the profile cutting stage, the two-step punching process has the advantage of freeing most of the internal stresses in the steel sheet before finalizing the profile. If the steel sheet is flat and sufficiently stress-free, it is possible that the same results may be obtained by a single punching operation, using a thinner steel sheet. For the NAL magnets, 1 mm thick sheet is punched in this way.

An idea of the punching tolerances in the present design can be obtained by considering that, in the B1 dipoles, an error of 0.02 mm in gap height would create a field error of $5 \cdot 10^{-4}$. In the F quadrupoles, the tolerance on gradient variation at edge of the radial aperture requires the systematic error in the slope of the pole profile to be kept below 3 µm/cm at that position.

As a result of the previous considerations, 1 mm thick sheet is assumed to be punched in one operation for the dipole laminations, but in two operations for the quadrupoles, which have more critical profiles.

After punching, deburring of the profile on an automatic machine could be done on one side of the lamination only, thus preserving the insulation layer on the other side.

The laminations could be stacked using as reference selected external surfaces, in the case of the H dipoles, or the poles and the mating surfaces in the case of the quadrupoles and of the WF dipoles. It is proposed to make the dipole cores in straight stacks, having the full magnet length. Present experience of European manufacturers would make them prefer to stack shorter elements, which should be assembled afterwards on a common girder. In this case the sagitta of the curved orbit in each block would be smaller and the radial aperture could be reduced if both the core assembly and the coils were given an appropriate curvature, which should be such as to cope with the different stages of machine operation. However, the use of long girders and the complexity of the structure would probably make this solution too expensive. In view of the length of the cores, stacking should probably be done horizontally, but the stacking jig could be somewhat tilted, to ensure automatic positioning of the laminations.

It is important to achieve a good uniformity in stacking in order to avoid excessive fluctuations of the magnetic field from magnet to magnet at high field levels. For a drop of magnetomotive force of 4% in the steel, a 1% difference in packing factor would produce a 0.4% difference in field, because of the rapid variation of permeability with induction at high fields. These differences in field are of the same order of magnitude as those which could be produced by the spread in steel permeability values at high fields, but cannot be reduced by steel mixing. Excessive closed orbit distortions at high fields could, however, be avoided by measuring the bending power (integral of the field) of each magnet at maximum field and distributing at least a certain number of magnets around the ring, according to the results.

The stacks will be welded between thick end plates to form full cores, in the H dipole structure, or half-cores, in the WF dipole and quadrupole structure. The technique of welding the stack to machined angle-irons, as developed at NAL, could be used for the half-cores, while for the H cores simple straps would probably be sufficient. The half-cores of the WF dipoles and of the quadrupoles would be welded together only after mounting the coils and the vacuum chamber.

4.5 Coil Construction

The basic assumptions in coil design and the dimensions of the hollow conductors have been given in Sections 4.2 and 4.3. For the conductors, copper is preferable to aluminium, because the increase in size and cost of the cores which would be necessary to locate aluminium coils of equal electrical resistance would outweigh the saving in conductor cost. Moreover, aluminium coils would require a double number of pancakes in H magnets B2 and B3 and an extension of coil ends in B1. Hollow copper conductors are generally not available in lengths corresponding to more than 200 kg billet and therefore for most of the coils brazed joints will be needed, but the technique of watertight brazes is now so well mastered in the electromechanical industry that no difficulties are anticipated.

Dry insulating tape (e.g. glass-samica-glass) will be wound on the conductor to form the interturn insulation. With the conductor size and the bending radii foreseen in the H dipole coils, automatic taping will be possible during the coil winding process. In the case of the WF dipoles and of the quadrupoles, automatic pretaping of the ends would not seem appropriate, if the ends of the coils were to be bent sharply against the end faces of the cores. The pancakes will be insulated to ground with a layer of similar tape followed by other layers of glass or polyester tape for mechanical strength. They will then be impregnated in a mould under vacuum with a suitable thermosetting resin and cured at the appropriate temperature.

The choice of the impregnating resin is important from the point of view of radiation damage. According to the figures given in Chapter 11, the maximum yearly dose received by magnet coils in the quiet regions of the machine is $5 \cdot 10^7$ rad, but in the hottest part of the ejection regions the yearly dose may reach $5 \cdot 10^9$ rad. The radiation resistance of the best epoxy resins currently used in coil impregnation in European industry is around $5 \cdot 10^9$ rad, but glass reinforced resin systems can withstand at least twice this value.

These epoxy resins would make most of the magnets completely safe against radiation damage and only for very few, immediately downstream the ejection system, would it be worth considering the use of very special new composites which require a modification of insulating techniques.

In practice it is expected that operation at the highest intensity will only occur when very high ejection efficiency will have been obtained. If the doses received by the most exposed components are regularly monitored, it will be possible to replace the critical ones before failure occurs. In the worst situation this replacement will be needed after some years.

In the H dipoles, the upper coils would be introduced through the gap on a hairpin sledge with imbedded hydraulic jacks which would then lift them into position. They could be kept there by means of inflatable stainless steel bags, which apply a lateral thrust.

The bottom coils could in turn be introduced on the hairpin sledge and then lowered into position by withdrawing the sledge, which would be fitted with a wedge-shaped tail for the purpose. The final location of the coils with respect to the sides and to each other could also make use of inflatable stainless steel bags filled with oil and maintained under pressure by an oleo-pneumatic system. The same location could be used for the quadrupole coils.

Although it seems preferable to have an elastic location, in order to let the coils expand and contract freely, the possibility of glueing them into position, which is especially important for WF dipoles, should also be investigated. In this case pre-heating of the conductors to prestress them with respect to the core, as adopted at NAL, could be considered.

4.6 Selection of Magnet Parameters

Considerable effort has been put by representatives of several European laboratories into a detailed study of H and WF dipoles, in order to assess their characteristics and their relative merits. Several different designs have been made and the preferred ones for each shape have been presented in Section 4.2 of this Chapter. The WF dipoles require less steel and have a smaller stored energy than the H dipoles. The difference is more marked for the dipoles with a higher gap.

For Stage B of the machine, the gross steel weight is 10% lower and the stored energy is 13% lower using WF dipoles than using H dipoles. WF dipoles also maintain the required field distribution over the whole aperture up to 10% higher fields. On the other hand, their cores are split in two halves and therefore a double number of individual laminations have to be handled and stacked, even if two laminations are punched simultaneously from a single sheet. A double number of stacking tools is also needed. The two half cores have to be individually welded and suitable structural elements (e.g. angle irons) have to be used in this process in order to prevent distortions.

The ends of the WF dipole coils are bent upwards so that the space they occupy in the gap between magnets may be a little shorter (possible gain 10 cm at each end). However, these coils are more laborious to wind and to insulate than the flat pancakes of the H dipoles and have to be manufactured to tighter geometrical tolerances, at least as far as the conductors adjacent to the gap are concerned. Errors in the position of these conductors may distort the field pattern at the edge of the aperture and also contribute radial field components in that region.

The coils and the vacuum chamber have to be mounted before the two half cores are welded together. This may facilitate coil mounting and certainly permits the vacuum chamber to be prestressed between the poles, but makes magnet assembling an integral part of the core manufacturing process. The achievement of the required tolerances on the gap height depends on the correct assembly of the two half cores.

From the point of view of radiation damage to the insulation, the long sides of the coils of the WF dipoles are more exposed than those of the H dipoles. According to the indications of Chapter 11, the dose received may be double. The importance of this consideration depends, of course, on the absolute amount of beam losses in the machine.

The technology of WF dipoles has been considerably developed at NAL, where this type of magnet has been selected for the accelerator. There, all technological problems have been solved and the production is progressing very fast. However, it is doubtful whether the same methods of organizing the construction, splitting its different operations, instructing the contractors, sharing the responsibility for production and undertaking directly some of the manufacturing work could be applied in the proposed European project.

Although three firms in Europe are actually producing some of the coils for the NAL accelerator, the H-type construction presents at the moment the smallest number of unknowns for European industry. This state of affairs is reflected in the present reluctance of European manufacturers to give relative cost estimates for the two solutions: in the most complete one received during the studies, the WF version appears to be substantially (about 20%) more expensive than the H one, despite the reduced steel weight.

The extra labour cost involved in the split-core manufacture has been recognized at NAL too and suggestions have been put forward recently[4.2] to the effect of achieving the same window frame geometry by inserting non-impregnated flat coils into a monolithic core and impregnating the whole system after having bent up the coil ends.

This suggestion is an interesting indication of the possibilities of further evolution in the field, although its intrinsic difficulties may partly upset its economic advantage.

Since with the present estimates of ejection efficiency the lifetime of the coil insulation in the two regions of the machine where the highest doses would be reached can be expected to be of at least two years, a higher exposure of the coils to radiation damage only involves the replacement of a few magnets at more frequent but nevertheless tolerable intervals in the WF solution.

Therefore, it is clear that the problem of the choice between H and WF dipoles is essentially one of technology and overall economy. It is suggested that full scale prototype studies could be started at the earliest possible time after project approval, in collaboration with several European industries, to obtain a better knowledge of the real manufacturing problems and of their economic implications. A final decision could then be taken on the basis of competitive tenders for the two solutions, or other intermediate ones. It must be borne in mind, of course, that the exploitation of the higher field potentialities of the WF magnet would also have economic implications.

At the moment, the H dipoles seem to provide the safest and most economical solution. Therefore, the overall characteristics of the magnet system given in Table 4.6, the cost estimates in the following section, together with parameters given in other Chapters, are based on the use of H dipoles.

Table 4.6

Overall Characteristics of the Main Magnet System

Dipoles (H shape)

		Stage A	Stage B	Stage C
Number of B1 dipoles		186	186	186
Number of B2 dipoles		192	186	192
Number of B3 dipoles		0	186	396
Number of B4 dipoles		12	30	0
Peak field	(T)	1.8	1.8	1.8
Gross steel weight	(ton)	8'400	13'100	17'800
Copper bar weight	(ton)	495	768	1'034
Resistance (without cables)	(Ω)	3.65	5.68	7.67
Maximum inductance	(H)	8.0	12.9	17.7
Peak current	(A)	3'410	3'410	3'410
Stored energy	(MJ)	42.9	68.1	93.1
Dissipation	(MW)	17	26.4	35.7

Quadrupoles

		Q_F	Q_D
Number of elements		108	108
Gradient at 400 GeV	(T/m)	16.91	24.10
Gradient at 300 GeV	(T/m)	12.68	18.08
Gross steel weight	(ton)	720	460
Copper bar weight	(ton)	24.4	21.6
Resistance (without cables)	(Ω)	1.34	1.18
Maximum inductance	(H)	0.56	0.45
Current at 300 GeV	(A)	1'210	1'210
Stored energy at 300 GeV	(MJ)	0.41	0.33
Dissipation for Stage B	(MW)	0.78	0.69
Current at 400 GeV	(A)	$\leq$ 1'650	$\leq$ 1'650

4.7 Cost Estimates

Tentative cost estimates for the main magnet system are shown in Table 4.7. These estimates are based on the most favourable prices obtained from European manufacturers in regular tendering in 1967 for a project of smaller, but comparable scale. Material and labour costs have been increased in the proportion of the average European indices. However, an extreme simplification of the coremaking process has been assumed for the H dipoles, as explained in Section 4.4, relying on the inherent symmetry and rigidity of the H laminations.

A similar simplification could by no means be assumed in the case of the quadrupoles, where unusually tight tolerances for cores made in two elements are required. Since the material cost is only a small fraction of the manufacturing cost, an increase of the quadrupole dimensions to ease manufacturing tolerances would not have a great influence on the quadrupole budget estimates. The cost of the power supply would be affected more seriously.

Table 4.7

Tentative Cost Estimates

H dipoles	Stage A	Stage B
Steel sheet and plate	10.05 MF	15.70 MF
Coremaking	12.15 MF	18.20 MF
Copper bar	6.95 MF	10.70 MF
Coilmaking and mounting	7.20 MF	10.90 MF
Accessories	2.75 MF	4.10 MF
Total	39.10 MF	59.60 MF
Quadrupoles		
Steel sheet and plate	1.40 MF	
Coremaking	7.60 MF	
Copper bar	0.65 MF	
Coilmaking	2.30 MF	
Assembling and accessories	1.45 MF	
Total	13.40 MF	
Watercooled cables (installed)		
For all magnets in series	4.00 MF	
For all lenses in series	1.50 MF	
Total	5.50 MF	
Models and instrumentation	3.50 MF	

References

(4.1) T. Doke et al., Nucl. Instr. and Meth. 83 (1970), pp. 300-308.

(4.2) Reardon and Sheldon - TM 246.

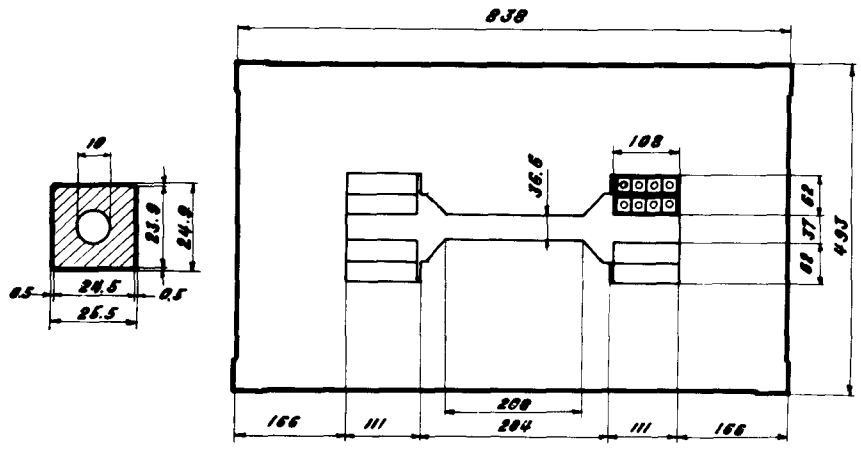

Magnet B1

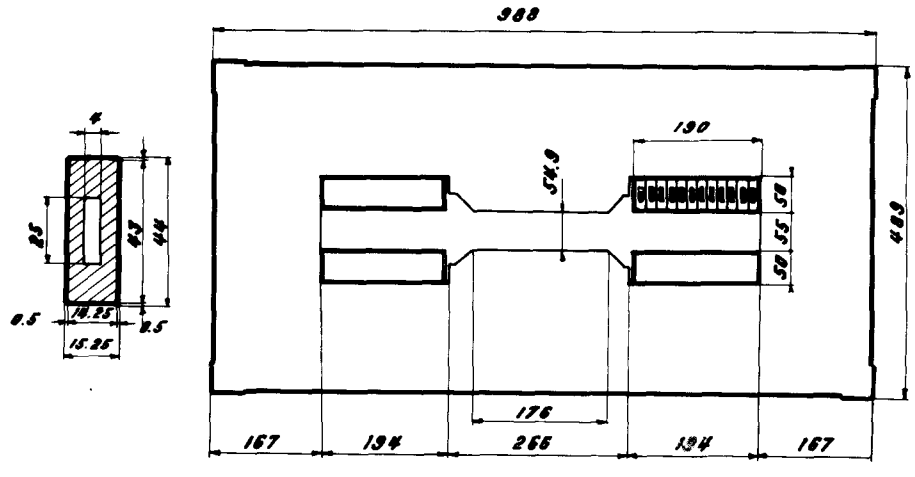

Magnet B2

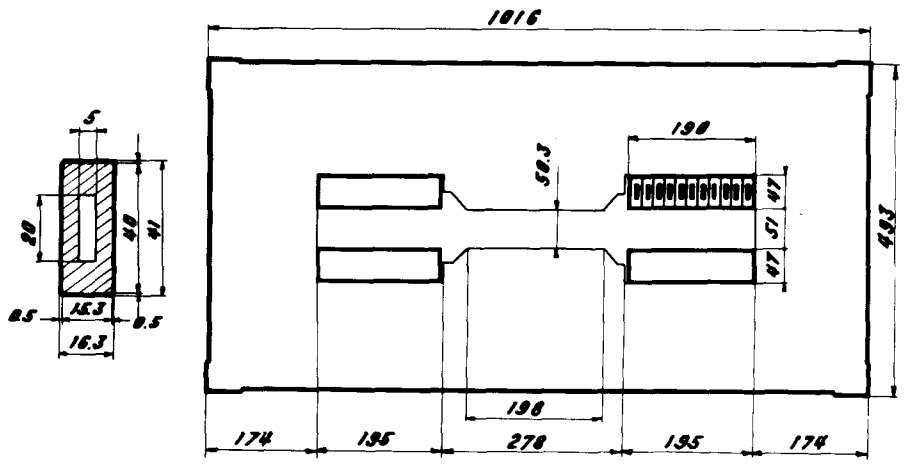

Magnet B3

Fig. 4.1 "H" magnets

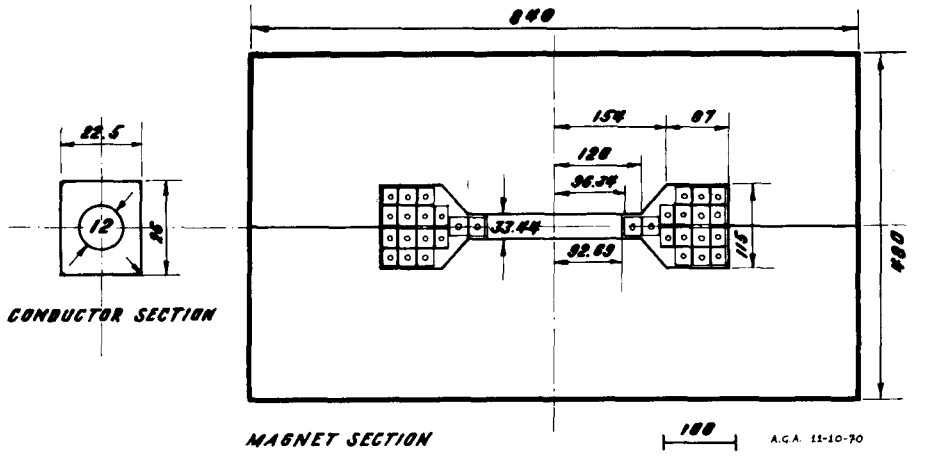

Magnet B1 (Mk1)

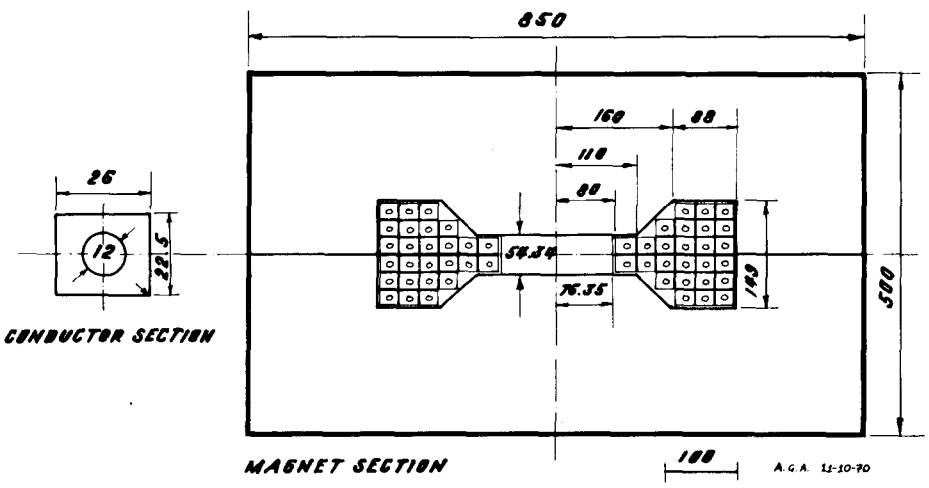

Magnet B2 and B4 (Mk1)

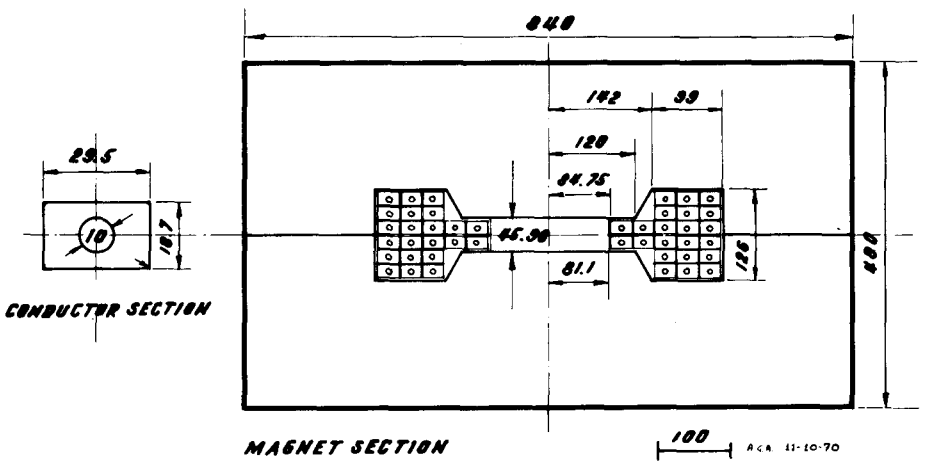

Magnet B3 (Mk1)

Fig. 4.2 "Window frame" magnets

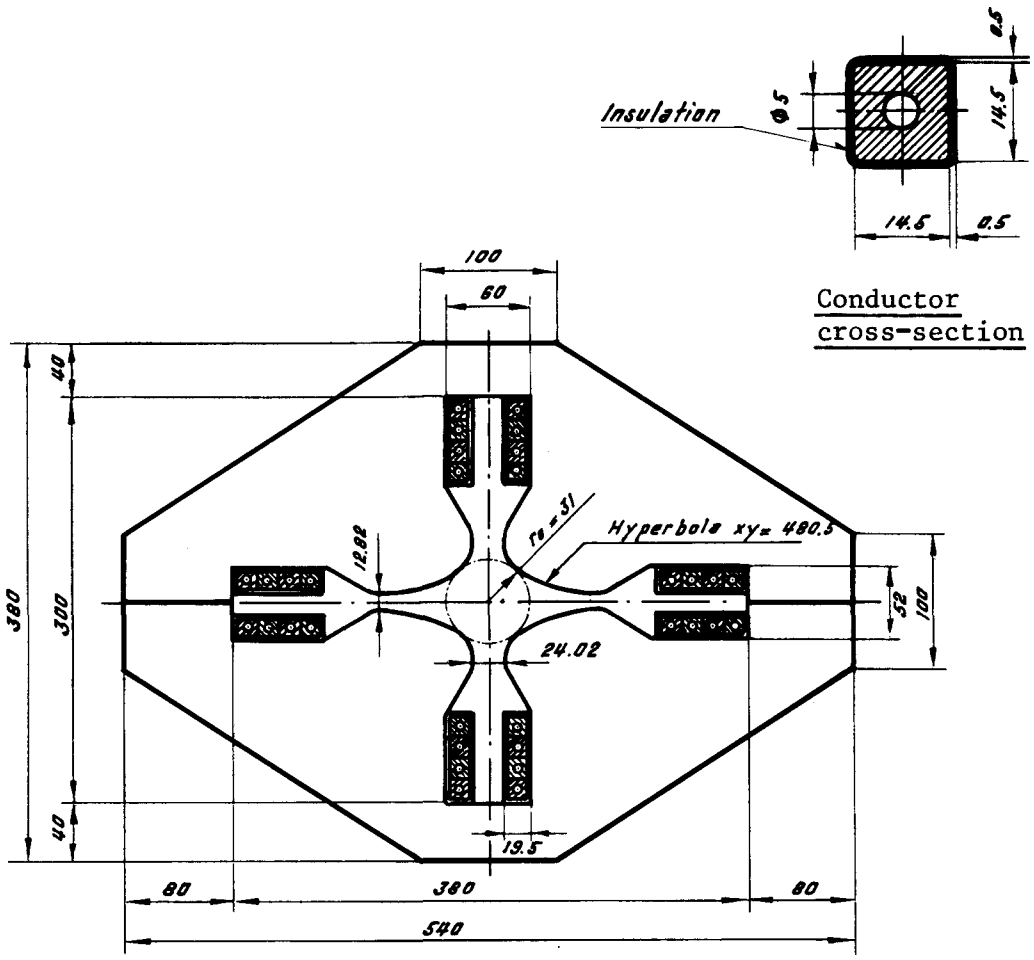

F - Quadrupole

50 mm

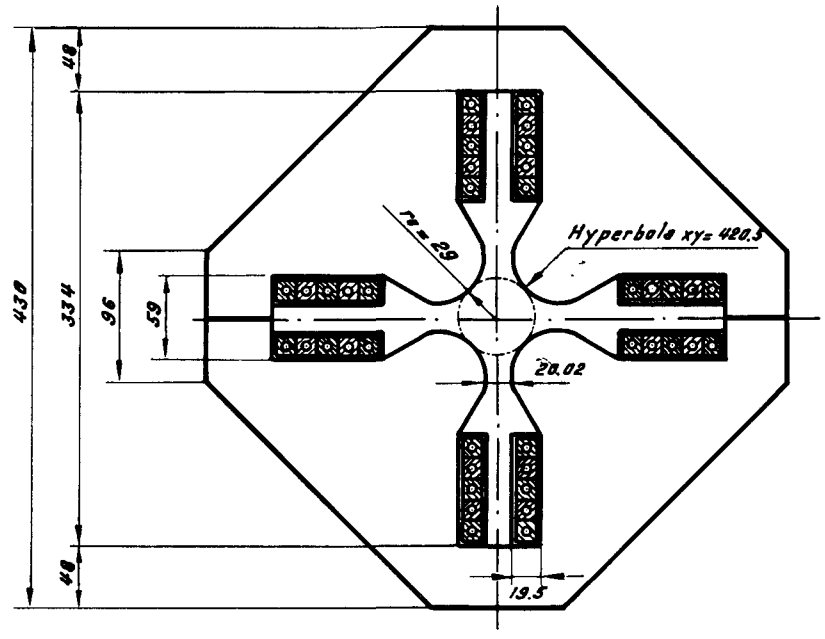

D - Quadrupole

Fig. 4.3

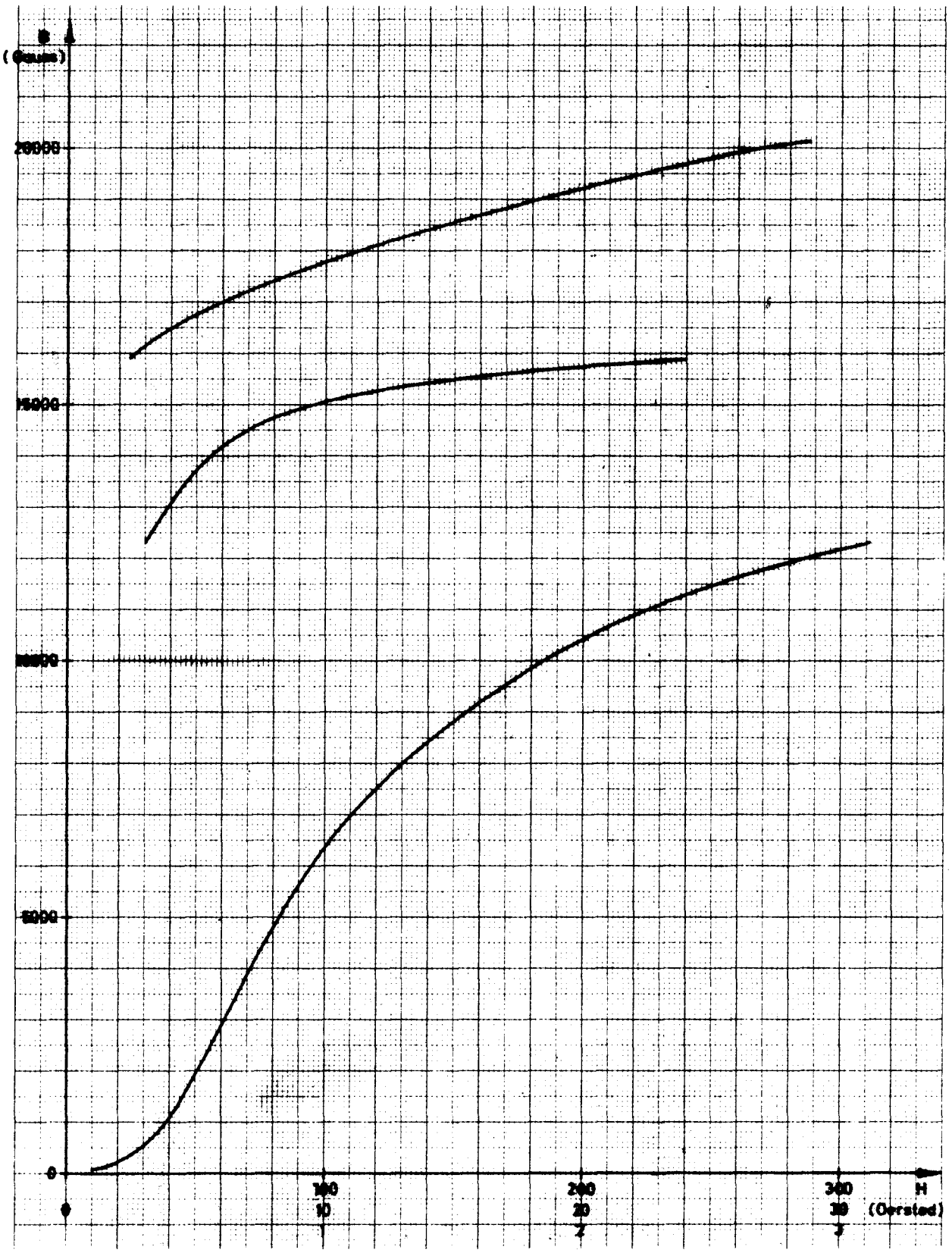

Fig. 4.4 Normal magnetization curve for a typical decarburized steel

Chapter 5

THE MAGNET POWER SUPPLIES

5.1 Acceleration Cycles

The power supply design is based on producing the following nominal accelerator cycles at Stage A, B and C. Table 5.1 gives the values for single flat-top operation.

Table 5.1

Nominal Cycles

	Stage A	Stage B	Stage C
Injection, s	0.2	0.2	0.2
Front porch	0.15	0.15	0.15
Rise (+ "round-off")	1.18	1.98	3.32
Flat-top	0.7	0.7	0.7
Decay (+ "round-off")	0.87	1.19	1.44
Rest	0.1	0.1	0.1
Total	3.2	4.32	5.91

At values below the peak energy of each stage longer flat-tops will be available, the limit being set by the maximum dissipation of the magnet coils. For instance, the 400 GeV cycle can have a 250 GeV platform of indefinite length - the cycle being increased by the platform duration.

5.2 Magnet Excitation Accuracy Requirements

The a.c. terminals of the magnet power supply will be subjected to the following incoming EHT transmission system disturbances;

Voltage -	Slow changes (> 10 minutes)	± 7%
	Fast changes (> 5 ms)	± 0.15%
	Intermediate changes (> 10 s)	± 0.3%
	Voltage asymmetry	0.5%
	Frequency	50 Hz ± 0.2%

The pulse to pulse magnet current tolerances ($\Delta I/I$) specified below must be achieved, with respect to a given i (t) profile reference in the presence of these "mains" borne disturbances.

	Bending	Quadrupole (referred to bending system)
Injection	$\pm 3 \times 10^{-4}$	$\pm 10^{-3}$
Rise + Front Porch	$\pm 5 \times 10^{-3}$	$\pm 10^{-3}$
Flat-top	$\pm 10^{-4}$	$\pm 10^{-4}$

In addition, $\dot{B}$ during front porch and rise must not exceed:

for Stage A operation 1.6 Tesla/s
Stage B " 1.07 "
Stage C " 0.8 "

The peak to peak ripple voltage must not exceed:

Injection	25%	of the instantaneous magnet voltage
Rise + Front Porch	5%	
Flat-top	1%	

5.3 Magnet Power Supply

The conventional method of powering large accelerator pulsed magnet systems has previously been achieved by using a motor alternator set in combination with a multi-phase convertor plant for the ac/dc conversion. In this specialized accelerator application the motor-alternator set is used as a buffer between the public supply and the magnet, permitting a cyclic kinetic-energy exchange between the motor-alternator set and magnet, while maintaining virtually constant power input from the "mains" supply.

As can be seen from Fig. 5.1 the pulse power profile contains sharp power changes at entry and exit from flat-top. The resultant torque changes and reversals excite the vibratory characteristics of the coupled shaft-system and cause impact forces on the stator and complex stress patterns in windings, fastenings and other appendages. Most accelerator laboratories using large motor-alternator sets for pulsed magnet power supplies have experienced MG set failures, some more serious than others, hence the evidence shows that pulse duties represent a severe hazard to satisfactory performance of such rotary machine systems.

The only really practical alternative is to attempt to take the pulse power directly from the public system.

5.3.1 Static power supply

Four main conditions must be satisfied in order to extract large pulses of power from the public supply network.

(i) The installed generating capacity of the network must be very large in comparison with the peak pulse power so that the pulse power contribution from individual generators will be low.

(ii) The dynamic distribution of the pulse in the network must be as uniform as possible.

(iii) The connection of the pulse load must be made at an electrically strong point in the public network.

(iv) The pulse-induced voltage and phase angle fluctuations at the point of "common-coupling" with the public network must be small.

Other conditions also apply, for example harmonic penetration, equivalent frequency and so on, but they are essentially subservient to the main criteria detailed above.

Voltage fluctuation is predominantly associated with the reactive component of the pulse load. It can therefore be minimized by a controlled form of power factor correction at the laboratory busbars. Phase angle fluctuation is dependent only on the magnitude of the pulse current and the intervening system reactance. Equivalent frequency change due to transmission angle change can be reduced by increasing the time period of the most severe load changes - entry and exit from flat-top. Harmonic current penetration of the public network can be minimized by using a multi-phase convertor plant (Ø 24).

All of the other aspects previously mentioned are functions of the public power system characteristics. It will therefore be understood that since the pulse energy is supplied and absorbed by the public generation groups the magnet power supply is not in fact static. The reactive compensation equipment installed for power factor correction at the laboratory busbars is, however, composed of static devices. We therefore use the term static power supply to distinguish it from the conventional MG set which it supplants.

5.3.2 Reactive compensation

The reactive compensator will comprise a 3 phase unit connected to the 18 kV magnet busbar of the main electrical substation rated to produce a variable nett reactive power from 0 to 69 MVAr. It is not necessary to define the actual form of the device now, this will be done at the design stage based on one of the methods described in Ref. 5.1.

The resultant maximum pulse-induced voltage and phase angle fluctuations are given in Table 5.2 and are based on the 225 kV transmission line proposals described in Chapter 15 (electricity supply to site).

Table 5.2

Voltage and Phase Angle Fluctuation (peak/peak envelope)

	CERN II (225 kV bus)		GENISSIAT (EDF)	
	Voltage	Phase Angle	Voltage	Phase Angle
Stage A	1.1%	4.45°	0.226%	1.43°
Stage B	1.137%	4.54°	0.235%	1.46°
Stage C	1.177%	4.65°	0.247%	1.49°

These values represent reasonable fluctuation levels at both CERN II and Génissiat. The CERN II 225 kV pulse load busbar is, of course, electrically separated from the 225 kV CERN II general-load busbar.

5.3.3 Magnet convertor plant

In order to reduce both magnet voltage to ground and delay line mode characteristics the series connected magnet ring is supplied at 12 points. Consequently under uniform convertor firing conditions the magnet voltage is symmetrically distributed with respect to earth around the ring. One of the 12 groups of series connected magnet will be earthed at mid-point.

These 12 convertor stations are located in pairs at six points on the ring circumference (Fig. 5.2).

Each convertor station consists of four bridge rectifier groups, producing a 24 phase output. Each station is also equipped with "by-pass" rectifiers in order to produce, particularly at or near peak current, the required total magnet voltage with minimum control angles and hence minimum harmonic current content and reactive compensation requirements. In addition each station will incorporate a passive and dynamic filter to fulfil the magnet voltage ripple tolerance.

During the early portion of the current rise the convertor groups are controlled in order to limit $\dot{B}$ to the prescribed value. Thereafter the rectifier firing angle is reduced to the minimum value consistent with stable control.

A smooth entry into flat-top is achieved by sequentially advancing the firing angles of each rectifier station until successive by-pass occurs, leaving only the minimum number of stations in circuit to supply the flat-top constant current.

The commencement of the decay period of the magnet excitation normally corresponds to the sharpest power change in the pulse cycle. Consequently, this is smoothed or "rounded off" by sequentially advancing the convertor stations into inversion during a period of ≈200 ms.

Subsequently full inversion is maintained limited only by invertor safety angle considerations. The resultant power profile during decay thus causes less shock impact on the public system - additionally the equivalent frequency change, due to transmission angle change, is also reduced.

The rest period is dictated by the recovery time (from full inversion) of the magnet servo-control. Approximately 100 ms is required for this.

5.3.4 Quadrupole magnets

One main quadrupole rectifier station will feed the F and D quadrupoles in series. In addition a small correcting supply will be provided to give fine adjustment (max. 6%) of the difference between F and D excitation. This arrangement costs less than two separate F and D systems, mainly because of savings in d.c. cabling.

A further small rectifier group may be required to provide precise regulation during the injection and front porch periods.

The time constant of the quadrupole circuit is small ($\simeq$ 0.3 s), hence it would serve little purpose to have the quadrupole convertor set work in the inversion region. The best choice therefore, from the point of view of economy and minimum power fluctuation, is a mixed diode-thyristor rectifier system.

5.3.5 Plant ratings

On the basis of the pulse repetition rates given in Table 5.1 we compute the pulse load characteristics and the required convertor and reactive compensator plant ratings for 200, 300 and 400 GeV operation.

It would be extremely uneconomic and impractical to make the initial purchase of the main power supply items (i.e. for bending magnets) for other than the 400 GeV operational level, consequently the power supply equipment (bending and quadrupoles) will be installed at the following ratings:

Convertors (Bending)	78 MVA
Convertors (Quadrupoles)	7.2
Power Transformers	80
Reactive Compensation	- 69 MVAr.

Table 5.3

	Stage A	Stage B	Stage C
Bending Magnets			
Voltage, kV	33.7	34.4	35.3
Current (peak), kA	3.41	3.41	3.41
Current (rms), kA	2.27	2.22	2.26
Power (peak), MW	111	113	116
Losses (I^2_{rms} R_m), MW	19	28	39.3
Reactive compensation, MVAr	-62	-63	-65
Nett load (rms), MVA	54	63	73
Quadrupole Magnets			
Voltage, kV	3.3	4.7	6.1
Current (peak), A	807	1210	1650
Current (rms), A	530	790	1120
Power (peak),MW	2.7	5.7	10
Reactive compensation, MVAr	-2	-3	-4
Nett load (rms), MVA	1.7	3.7	6.7
Plant Ratings			
Convertors (bending), MVA	65	72	78
Convertors (quadrupoles), MVA	1.9	4	7.2
Power Transformer, MVA	55.7	66.7	79.7
Reactive compensator, MVAr	-64	-66	-69

5.3.6 A.C. Harmonic filter

The shunt capacitors of the reactive compensation plant will be combined with harmonic filters, mainly in order to suppress interference between the different rectifier stations.

5.4 Controls

5.4.1 Bending magnet supply control

Because of the flexibility needed in generating many different types of magnet current cycles and the complication involved in the differing sequential voltage changes required at the 12 convertor stations, it is intended to have 12 reference programmes generated by a computer equipped with digital to analogue convertors.

During most of the rise time the rectifier output voltage is the important parameter to be considered. However, during the injection and debunching platform as well as during flat-top the current is the controlled quantity. During decay the convertor voltage is controlled subject to considerations of invertor safety angle.

It is therefore proposed that the computer generates 12 voltage reference waveforms (including control signals for the by-pass thyristors) and provides, in addition, a separate current reference input for one selected station. For this last station (which will normally never be by-passed) the voltage waveform will serve only as "feedforward" quantity and so reduce the error of the current feedback loop. In addition, the voltage output from this rectifier and the output current will be monitored by the computer so that corrections can be applied to the various references between pulses in order to obtain the required voltage distribution between stations and output current waveshape. The latter would hardly be obtainable through current feedback alone because of the low loop gain available at the frequencies present in the current programme.

The necessary suppression of mains voltage fluctuations will be easily achieved with the required precision through the voltage regulation alone. The current regulation will mainly be required to reduce the influence of magnet resistance changes on injection and flat-top currents.

5.4.2 Quadrupole supply control

The regulation system of the quadrupole power supplies will be similar to that of the bending magnets. The bending magnet current will be used as a reference in order to improve the tracking precision. Corrections may, of course, have to be added for the different saturation characteristics of magnets, F lenses and D lenses. The use of field and gradient pickup coils mounted in the reference magnets and lenses and giving signals proportional to the Q errors might also be considered.

5.4.3 Reactive power compensation control

If a "switched step" form of reactive power compensation is chosen, the control of the steps can be satisfactorily achieved by the same computer that generates the magnet programmes, since the reactive component of the a.c. current is a sufficiently well defined function of the magnet current programme.

5.4.4 Other controls

Nearly all other controls and status signals will be transferred between the equipment buildings and the control centre by means of the multiplex system (see Chapter 9).

The only exception will be a few hard-wired interlock circuits needed for the main circuit breakers, short circuit switches etc.

5.5 Parameter List

5.5.1 Bending Magnets

	Stage A	Stage B	Stage C
Magnet inductance, max., H	8.	12.9	17.7
Magnet winding resistance, Ω	3.65	5.68	7.67
Cable resistance, Ω	0.37	0.37	0.37
Magnet voltage, kV	33.7	34.4	35.3
Magnet current, peak, kA	3.41	3.41	3.41
RMS, kA	2.27	2.22	2.26
I^2R, MW	19	28	39.3
Pulse cycle time, s	3.2	4.32	5.91
Peak power, MW	111	113	116
Nett compensation, MVAr	-62	-63	-65
Nett load (rms), MVA	54	63	73

5.5.2 Quadrupole Magnets (F + D)

Magnet inductance, max. H	1.0	1.0	1.0
Magnet resistance, Ω	2.5	2.5	2.5
Cable resistance, Ω	0.9	0.9	0.9
Maximum voltage, kV	3.3	4.7	6.1
Maximum current, A	807	1210	1650
RMS current, A	530	790	1120
I^2R, MW	1.0	2.1	4.3
Peak power, MW	2.7	5.7	10.0
Compensation, MVAr	-2	-3	-4
Nett load (rms), MVA	1.7	3.7	6.7

5.5.3 Load on public electricity supply

RMS load on EDF, MVA	55.7	66.7	79.7
Mean power from EDF, MW	25	35.5	50

5.6 Summary of Costs

Reactive compensator and a.c. harmonic filter	5.2 MSF
18 kV distribution to convertor stations	0.75 "
Convertor stations for bending magnet system	14.6 "
Convertor plant for quadrupole system	1.5 "
Magnet current control system	in control group budget
TOTAL magnet power supply cost	22.05 MSF

References

(5.1) Dwek, M.G., Eggleton, M.N. and Fox, J.A., "Direct Supply of a Large Pulsed Load from the e.h.v. Transmission Network", Proc. I.E.E., Vol. 117, No. 5, May 1970.

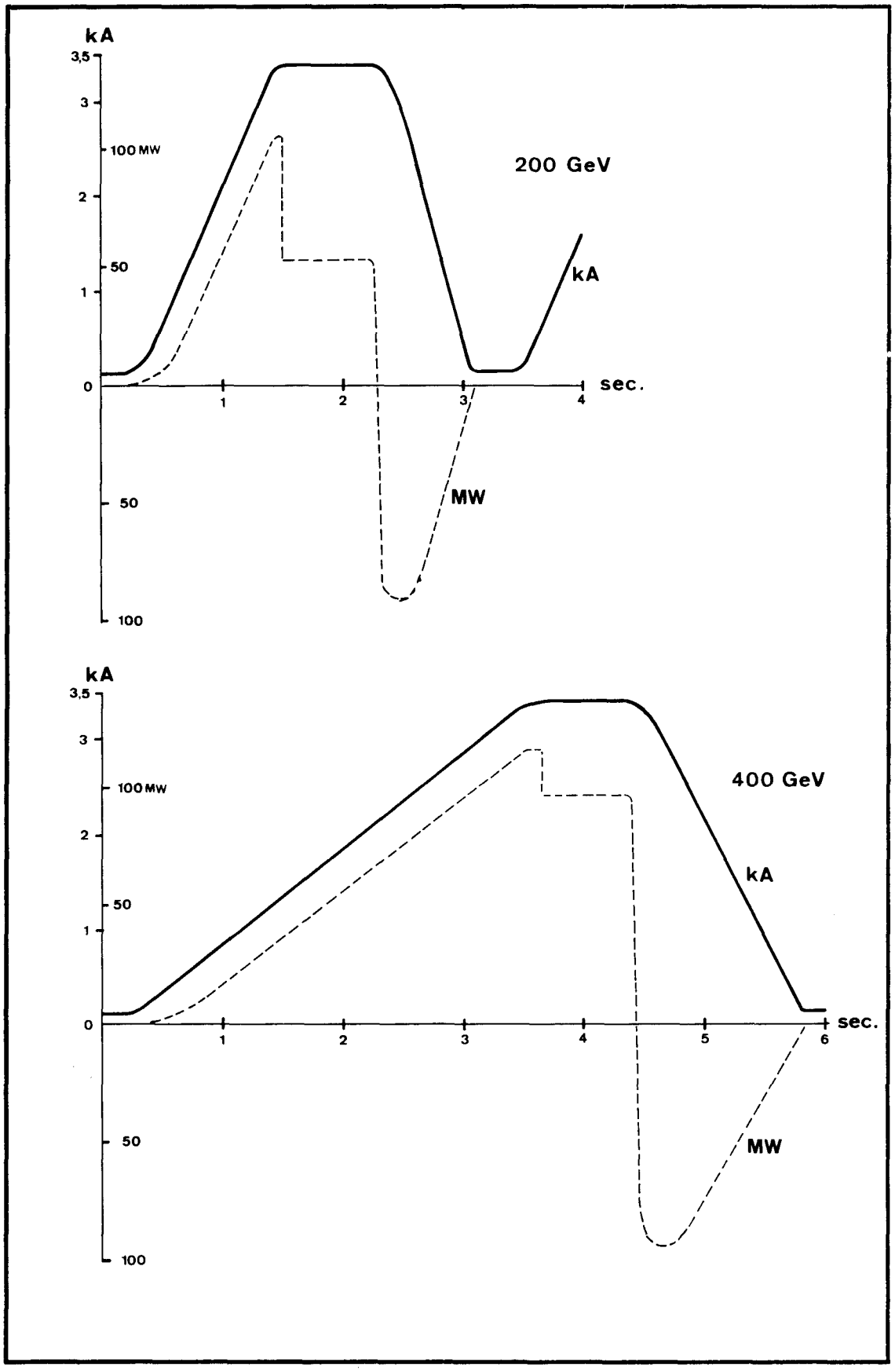

Fig. 5.1 Pulse power profiles

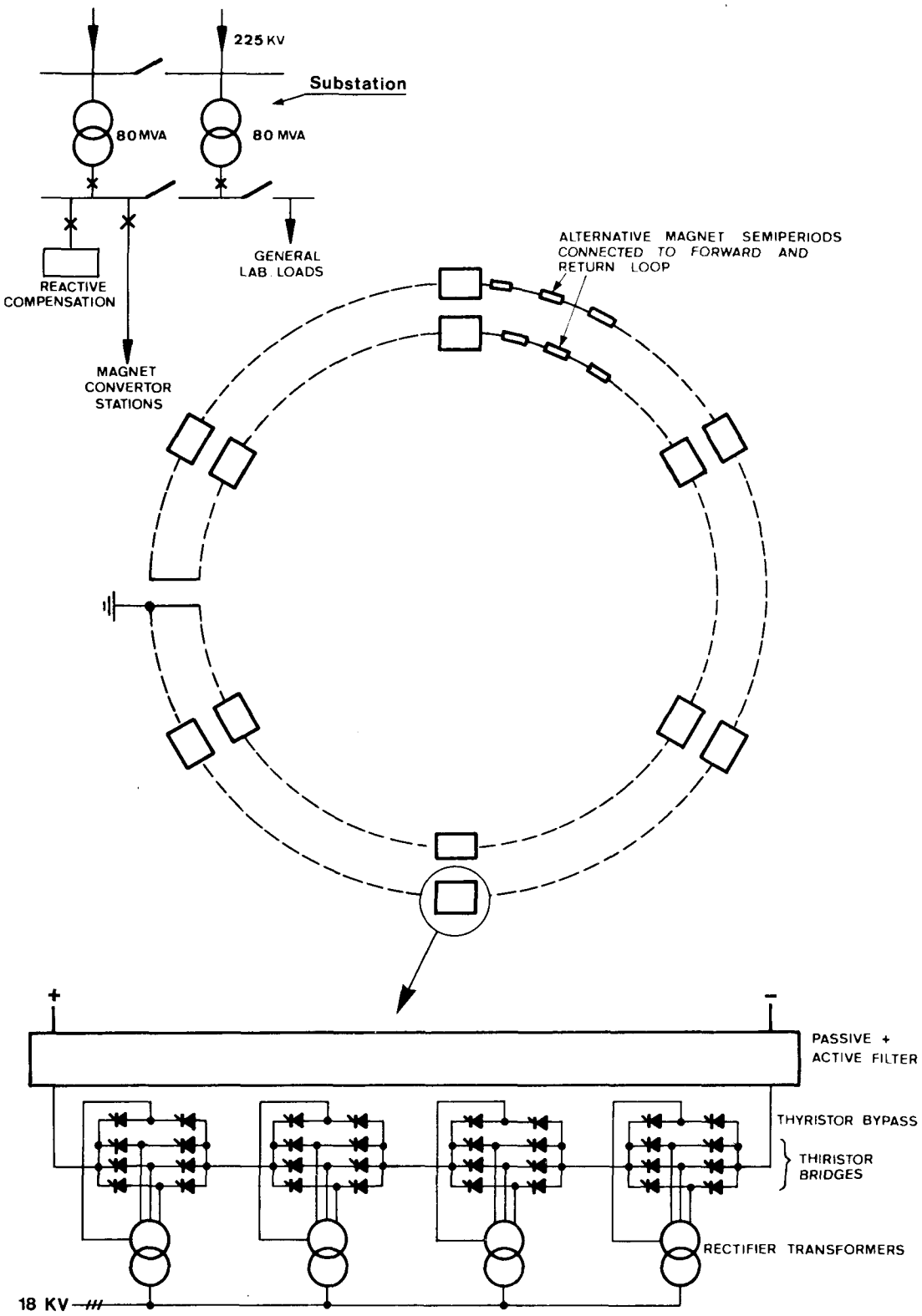

Fig. 5.2 Magnet power supply layout

Chapter 6

THE ACCELERATION SYSTEM

6.1 Introduction

The r.f. accelerating system has to provide for a minimum total peak accelerating voltage per turn, V, which is given by two conditions. Firstly, the bucket area (longitudinal phase space), at injection and later on, must be large enough to accommodate the energy spread of the injector. Secondly, sufficient energy gain of the particles per turn must be available to obtain a reasonable short accelerating time.

For both conditions the stable phase angle ϕ_s plays a very important role. The smaller the value of ϕ_s, the larger the bucket area becomes, but the accelerating time increases also. This is probably illustrated best by the following two equations:

Bucket area
$$A = \alpha(\phi_s)\left(eV \frac{\gamma}{|\eta|} \frac{128}{h \pi E_0} \right)^{\frac{1}{2}} \tag{6.1}$$

Accelerating rate
$$\dot{p} = \sin \phi_s \frac{eVc}{2\pi R} \tag{6.2}$$

where:

A = bucket area in units of $\Delta(\beta\gamma)\phi_{rf}$

ϕ_s = synchronous phase angle (measured from zero crossing of the accelerating wave)

$\alpha(\phi_s)$ = moving bucket factor

γ = energy to rest energy ratio

η = $\frac{1}{\gamma^2} - \frac{1}{\gamma_t^2}$; $\gamma_t = \gamma$ at transition

h = harmonic number

E_0 = rest energy

c = velocity of light

R = average machine radius.

At injection ϕ_s is zero ($\dot{p} = 0$) and, once transfer and transition energy are chosen, the free parameters which determine the bucket area are only the voltage and the harmonic number which in turn determines the frequency. In practice these two parameters are not completely free since they determine Q_s, the number of phase oscillations per turn, which must be kept small.

$$Q_s = \frac{\sqrt{\cos \phi_s}}{\beta} \sqrt{\frac{|\eta|}{\gamma} \frac{heV}{2\pi E_0}} \qquad (6.3)$$

must be less than 0.2 and preferably even less than 0.1 if the accelerating gaps are not distributed symmetrically around the ring[6.1]. This certainly presents a strong argument for having a frequency as low as possible, a fact which will be taken into account in the next section. For a given choice of harmonic number, Equations 6.1 and 6.3 give us the lower and upper limits for the accelerating voltage. These voltage boundaries are directly affected by ϕ_s as soon as acceleration starts and tend to diverge towards the end of the accelerating cycle. ϕ_s must only be increased slowly after injection during the so-called front porch. This subject will be dealt with in detail in Section 6.6. If ϕ_s were to increase up to values in the vicinity of 90°, a small amplitude disturbance of the accelerating voltage would be harmful. For this reason ϕ_s should not exceed a certain maximum. We propose the somewhat conservative value of $\phi_s = 45°$ corresponding to a safety factor $\simeq \sqrt{2}$ in voltage. Hence the boundary conditions of choice of voltage are determined throughout the cycle and the accelerating voltage can be chosen within them. To keep within the boundaries, voltage as well as ϕ_s, can, or must, be programmed.

6.2 Choice of Frequency

The choice of frequency is influenced by a number of factors, some of which are technical and some of which are concerned with beam dynamics. We shall now give a survey of the most important of all the relevant arguments.

First of all, it can be said generally for all r.f. systems that have been proposed so far, that their shunt impedance per unit length tends to increase with increasing frequency, i.e. for an accelerating structure occupying a given length along the particle orbit, the r.f. power required to generate a given accelerating voltage tends to decrease with increasing frequency. Another advantage of a higher frequency is reduced filling and discharge times due to a smaller energy storage. This is a fact which might be important for the phase jump at transition as well as for various phase correcting procedures.

Factors against the choice of a high frequency are the already mentioned ratio of bucket area to number of phase oscillations per turn; the necessity of a minimum aperture which decreases with increasing frequency, possibly higher losses in the cavities, and lastly the availability of suitable hardware. High frequency systems tend to consist of many small units and therefore yield a complex system, and it is not easy to find large power generators for high frequencies.

Another important consideration not taken into account above is the necessary bandwidth, as the accelerating system which must be chosen depends very much on the relative frequency swing and therefore restrictions might be imposed on the choice of the accelerating frequencies by available technology.

Fortunately, the frequency variation during acceleration is rather small since all injection energies considered are high. The relative frequency swing is given by

$$\frac{\Delta f}{f} = 1 - \beta_i \qquad (6.4)$$

where β_i denotes the particle velocity at injection. At 8 GeV injection energy (which would be the transfer energy for a later fast cycling booster synchrotron) one finds $\Delta f/f = 0.55\%$ and for the proposed transfer at 10 GeV/c from the PS, $\Delta f/f = 0.44\%$. We propose a system compatible with booster or CPS which, in all cases, will provide for the necessary bucket areas and accelerating rates.

This small bandwidth permits us, as we will see later, to use untuned wideband systems and to reject ferrite or mechanically tuned cavities.

6.3 Acceleration Parameters

In Table 6.1 we list those machine parameters which are of importance for the r.f. accelerating system.

Table 6.1

Injection momentum	10 GeV/c
$\gamma_{transition}$	24.6
Maximum possible bunch area at transition, A_t, with fast Q-jump	0.24 rad
Maximum synchronous phase angle	45°
Average circulating beam current for 10^{13} p.p.p.	70 mA
Maximum bending field	1.8 T

A_t, which is given by the available horizontal aperture, sets the lower limit for the size of the bucket area which is to be maintained by the r.f. accelerating voltage all over the cycle. There are two "bottle necks" which require special consideration; the already mentioned problems near injection and a minimum in bucket area around $\sqrt{3}\ \gamma_{tr}$ for V = const. We now consider these two cases in Table 6.2.

Table 6.2

	$\alpha(\phi_s)$	$(V/h)_{A=0.24}$	$(V.h)_{Q_s=0.05}$	h_{max}	$F_{rf\ max}$
Injection	1	876.5	22×10^9	5000	216
$\sqrt{3}\ \gamma_{tr}$	0.175	1120	805×10^9	26800	1250
		volts	volts		MHz

Equations 6.1 and 6.3 determine V/h for A = 0.24 and V.h for Q_s = 0.05. These quantities then define a maximum value of h. The highest possible r.f. frequency for a conservative Q_s value of 0.05 appears to be around 200 MHz. We have chosen a harmonic number of 4224 which yields an r.f. frequency of 183 MHz. With this harmonic number we get the voltage boundaries:

Table 6.3

	Injection	$\sqrt{3}\ \gamma_{tr}$
V_{min} for A = 0.24	3.7 MV	4.7 MV
V_{max} for Q_s = 0.05	5.2 MV	(190 MV)

For high accelerating rates modulation of V over the cycle will be necessary in order to reduce the r.f. voltage near injection to values below 5.2 MV.

6.4 Choice of Travelling Wave Structure

A survey of possible methods of r.f. acceleration is given in page 117 of Reference (6.2). We have adopted an untuned, wide band, travelling wave system. Compared with the conventional solution of servo-tuned resonant cavities - such as ferrite cavities - our system offers the following advantages:

(a) total absence of tuning equipment (ferrite, saturation, ferrite-cooling), with the associated cost and complexity;

(b) absence of any equipment other than passive metal structures in the accelerator tunnel;

(c) the possibility of concentrating the total r.f. power in a few large power sources located in a surface building, leading to economy and simplicity;

(d) the feature that the accelerating structure and the power source are separated by a matched transmission line, making it possible to add or change power sources at any time in order to cope with increasing beam intensity or repetition rate;

(e) the peculiar property of our structure to convert power loss into beam power at increasing beam intensities, leading to an increase of efficiency with increasing beam load.

Points (d) and (e) are particularly valuable for an accelerator of expandable intensity and energy.

The travelling wave system will now be discussed in detail. In such a system the accelerated particles are in nearly continuous interaction with an accelerating wave. A particle would experience a maximum energy gain if it rode on the crest of the accelerating wave all the time, in other words, the velocity of the phase of the r.f. wave should equal the velocity of the particles. The phase velocity v_p is given by

$$v_p = 2\pi \frac{f}{\xi} \tag{6.5}$$

where f = r.f. frequency, ξ = phase shift per unit guide length. Only if $\xi = 2\pi/d$ = const. (where d is the distance between two bunches) will all bunches be in the same phase with the r.f. wave. On the other hand, the propagation speed of energy, the so-called group velocity v_g, is given by

$$v_g = 2\pi \frac{df}{d\xi} \tag{6.6}$$

and cannot be made equal to infinity. In a periodically loaded waveguide v_p and v_g are independent variables, v_p is chosen so as to equal one particular particle velocity and by v_g the phase slip between particles and wave per unit guide length as a function of particle velocity variation will be given. If we linearize Equation 6.6 we may write after a few manipulations.

$$L\,\Delta\xi = \frac{L}{|v_g|}\,\omega_0 \left(\frac{\beta}{\beta_0} - 1\right) = \tau \tag{6.7}$$

where:

L = interaction length

ω_0 = r.f. angular frequency for which $\tau = 0$

β_0 = particle velocity for which $\tau = 0$.

Assuming that the phase angle between the centre of the bunch and the wave equals ϕ (measured from zero crossing of the wave) right in the middle of the structure, the angles at each end are $(\phi - \tau/2)$ and $(\phi + \tau/2)$ and the equation for the energy gain of a particle becomes

$$U = \int_{Z=-L/2}^{+L/2} E_m(z) \sin\left(\phi + \tau \frac{z}{L}\right) dz \;; \tag{6.8}$$

$E_m(z)$ is the amplitude of the electric field in z direction and is a function of z due to losses of r.f. power in the structure and to beam load. For a guide length which is small compared to the attenuation length z_0 (which is defined as the length along which the power flow would be reduced to a factor 1/e), and for a negligible beam load we may assume that E_m is constant all over the length L and obtain

$$|U| = L\, E_m \sin\phi \, \frac{\sin\frac{\tau}{2}}{\frac{\tau}{2}} \qquad (6.9)$$

$$\text{for } L << z_0 = \frac{v_g Q}{\omega}$$

where ϕ may stand for ϕ_s.

To calculate the circuit impedance, V^2/P, we take $\sin\phi = 1$ and introduce $\sin\phi_s$ again in acceleration parameter computation. This impedance is defined by the square of the total voltage seen by a particle along one structure divided by the r.f. power, P:

$$P = W\, v_g \,, \qquad (6.10)$$

where W = energy stored per unit length in travelling wave structure.

Combining Equations 6.9 and 6.10 yields

$$\frac{V^2}{P} = \frac{E_m^2}{W}\,\frac{L^2}{v_g}\,\frac{\sin^2\frac{\tau}{2}}{(\tau/2)^2} = \frac{R}{Q}\,\frac{\omega}{v_g}\,L^2\,\frac{\sin^2\frac{\tau}{2}}{(\tau/2)^2} \,. \qquad (6.11)$$

E_m^2/W is a quantity which equals the product of the angular frequency ω and the familiar term R/Q whose meaning is given by

$$\frac{R}{Q} = \frac{2 \cdot \text{characteristic impedance}}{\text{unit length}} \text{ of the structure.}$$

The characteristic impedance, which for instance can be expressed by $\sqrt{L/C}$ for the low-frequency circuit, is determined by the dimensions and geometrical configurations of the circuit and can be obtained by model measurements as it is independent of frequency and losses. Therefore R/Q is proportional to frequency since the number of cells per unit length is proportional to frequency. For a given r.f. power and a given frequency the energy gained by a particle is proportional to the interaction length along the beam, as long as $\tau \approx 0$ and both losses and beam load are small. On the other hand $|\tau|$ increases with length for a given β/β_0. This effect can be used to accommodate the modulation for the energy gain of the particles without modulating the r.f. power sources a great deal (see Table 6.3). For this reason β_0 should be close to unity so that the full energy gain is available during the steep rise of the magnetic field, whereas the downward modulation near injection is adjusted by proper choice of v_g and L.

It follows from Equation 6.11 that the accelerating structure should have as high a value of R/Q as possible. The first possible choice that comes to mind is, of course, the

usual disc-loaded guide. A typical value of R/Q for this structure is about 250 Ω/m at 180 MHz. There are, however, several other structures which exhibit substantially higher R/Q values than the disc-loaded structure. The ones that seem to be most interesting for our purpose belong to a group of bar-loaded structures which have become known under names such as jungle-gym, wire-loaded, or cross-bar structures. These structures consist of circular or square guides which are periodically loaded with transverse bars. The bars may be single or double with or without drift tubes. Measurements of bar-loaded structures have been carried out at CERN[6.3] yielding R/Q-values up to 600 Ω/m by adding drift tubes. As the ratio of R/Q-values to the corresponding v_g values is nearly constant with varying drift tube length an appropriate choice can be made to match the modulation requirements at injection.

6.5 Beam Loading

Without beam loading the output power of the accelerating guide very nearly equals the input power. However, the presence of beam loading modifies the spatial distribution of electric field along the guide so that the output power can be quite different from the input power. The change of input power required to restore the average accelerating field to its desired value does not necessarily equal the beam power, in fact, it may even be negative under certain circumstances. When the phase velocity equals the particle velocity, the average beam-induced electric field in the guide is 180° out of phase with the beam and of purely decelerating nature. The angle is leading with a purely decelerating field when the frequency is below the centre value and lagging when the frequency is above. The beam-induced field $E_{b(z)}$ is described by[6.4]

$$E_b(z) = \frac{J_{rf}}{4} \frac{R}{Q} \frac{\omega}{v_g} \left(- \frac{\sin(\Delta\xi . z)}{\Delta\xi} + j \frac{1 - \cos(\Delta\xi . z)}{\Delta\xi} \right) \tag{6.12}$$

J_{rf} = a.c. beam current.

Integration of Equation 6.12 yields the beam-induced voltage per structure

$$\underline{V}_b = \frac{J_{rf}}{4} \frac{R}{Q} \frac{\omega}{v_g} L^2 \left(- \frac{1 - \cos\tau}{\tau^2} + j \frac{\tau - \sin\tau}{\tau^2} \right) \tag{6.13}$$

The total equivalent accelerating voltage of amplitude V_t and phase ϕ_t with respect to the beam is the sum of $\underline{V}_b$ and the r.f. driven voltage $\underline{V}_{rf}$. For symmetric bunches we may write $\phi_t = \pi/2 - |\phi_s|$; ϕ_t is negative below transition and positive above, as the accelerating peak of the r.f. voltage has a lagging phase angle with respect to the beam below transition and vice versa, hence

$$\underline{V}_t = V_t (\cos\phi_t + j \sin\phi_t) \tag{6.14}$$

Fig. 6.1 shows the vector diagram for all these voltages with respect to the beam phase.

In order to compensate for the beam loading the r.f. input has to be adjusted so as to make $\underline{V}_t$ equal in amplitude and phase to the desired acceleration voltage. If we subtract $\underline{V}_b$ from $\underline{V}_t$ we will obtain the required r.f. voltage $\underline{V}_{rf}$

$$\underline{V}_{rf} = V_t\left[\left(\cos\phi_t + \frac{P_b}{P_t}\frac{1}{4\cos\phi_t}\right) + j\left(\sin\phi_t + \frac{P_b}{P_t}\frac{1}{4\cos\phi_t}\,\mathrm{tg}\,\phi_b\right)\right] \qquad (6.15)$$

$$\text{with } \mathrm{tg}\,\phi_b = -\frac{\tau - \sin\tau}{1-\cos\tau}$$

$$\text{and beam power } P_b = V_t\, J_{rf}\,\frac{\cos\phi_t}{2}\,.$$

P_t stands for the power which is necessary to obtain V_t without beam loading

$$P_t = \frac{V_t^2}{(V^2/P)} \quad \text{with } (V^2/P) \text{ from (6.11)}$$

The amplitude V_{rf} is given by the root mean square of the real the and the imaginary part of Equation 6.15 and together with $P_{rf}/P_t = (V_{rf}/V_t)^2$ we obtain the amount of the required r.f. power P_{rf} with beam loading:

$$P_{rf} = P_t\left\{\left(\frac{P_b}{P_t}\frac{\sqrt{1+\mathrm{tg}^2\phi_b}}{4\cos\phi_t}\right)^2 + \frac{P_b}{P_t}\frac{1}{2}\left(1+\mathrm{tg}\,\phi_b\,\mathrm{tg}\,\phi_t\right) + 1\right\} \qquad (6.16)$$

During most of the accelerating time τ tends to be negligibly small and ϕ_t equals $45°$, then:

$$P_{rf} = P_t\left\{\left(\frac{P_b}{P_t}\right)^2\frac{1}{8} + \frac{P_b}{P_t}\frac{1}{2} + 1\right\} \qquad (6.16a)$$

The phase angle of the driven r.f. voltage is given by:

$$\tan\phi_{rf} = \frac{2\sin 2\phi_t - P_b/P_t\,\mathrm{tg}\,\phi_b}{2\cos 2\phi_t + 2 + P_b/P_t} \qquad (6.17)$$

and with $\tau = 0$; $\phi_t = 45°$

$$\tan\phi_{rf} = \frac{1}{1 + 0.5\,P_b/P_t} \qquad (6.17a)$$

The second term in Equation 6.16 needs particular consideration because it is affected by the signs of two transcendental functions. If ϕ_b and ϕ_t are properly chosen the weight of this term can be reduced quite considerably, it might even vanish for certain conditions ($|\phi_b - \phi_t| = \pi/2$), or become negative ($|\phi_b - \phi_t| < \pi/2$). The least which can be said is that the phase jump at transition does not cause any abrupt change of beam loading conditions if ϕ_b equals π, which is the case for a phase slip $\tau = 0$. Therefore β_0 in

Equation 6.7 should be made equal to β at transition, which means that a dispersion curve for the structure must be chosen which yields $\xi d = 2\pi$ for the r.f. frequency at transition (d = bunch distance). If this is done τ will be negative for all frequencies below transition and positive above, without any difference whether a forward or a backward wave structure is chosen. One realizes easily by checking with Fig. 6.1 that beam loading has a flat maximum around $\tau \approx 0$. The required r.f. power for this region is given by Equation 6.16a for our maximum $|\phi_s| = \pi/4$. Another fact is worth mentioning, namely that shortly after injection a phase difference of less than $\pi/2$ between $\underline{V}_b$ and $\underline{V}_t$ is possible and therefore a reduction rather than an increase in r.f. power is required for increasing beam load during this part of the cycle.

The phase angle of the driven r.f. voltage is not equal to ϕ_t and a function of the beam loading as expressed by Equations 6.17 and 6.17a. However, a probe right at the middle of the tank measures the phase of $\underline{V}_t$ which can be compared with the phase of the beam and the r.f. phase can be controlled normally.

The beam induced voltage does not only affect the r.f. power balance, but at high intensities it is likely to produce some other effects. There is the problem of self-bunching of the beam at any of the harmonic numbers that fall within the passband. This effect would occur during injection when the r.f. voltage is not yet switched on and it could prevent debunching for slow ejection (see Chapters 3 and 12).

Another disturbance may appear by coherent longitudinal instabilities due to the fields in the wake of the bunches which affect the subsequent bunches via the interaction with the r.f. structure. These instabilities may lead to bunch blow up at high intensity. For the passband a fairly general antidote seems to be the use of a feedback system which counteracts the r.f. potential induced by the bunch oscillations. More study is needed before we can decide whether this or possibly other cures need to be applied.

Parasitic resonances outside of the passband or higher passbands would also make an interaction possible and will therefore be suppressed, for instance, by resistive loading of the structure via a highpass device and tapering of cell dimensions.

6.6 Front Porch

It follows from all that has been said in the preceding sections that, for a given r.f. power, the ratio between the available accelerating voltage at injection and the voltage for a given beam load during maximum rise of the guiding field will be given by appropriate choice of the length of one structure and the group velocity (see Equations 6.7, 6.11 and 6.16a). If full use is made of the available r.f. power, the voltage follows a certain function during the part of the magnet cycle which is called "front porch". Now, one must avoid loss of particles due to spillout later on after injection, which means that a bucket area of minimum size must be maintained at least all over the cycle. This condition leaves the moving bucket factor $\alpha(\phi_s)$ as the only free parameter for Equation 6.1

during the front porch until the limit corresponding to a $\phi_s = \pi/4$ is reached. From there on the bucket area will grow, a fact which marks the end of the front porch. The parameter $\alpha(\phi_s)$ is adjusted by shaping the magnet current rise as a function of γ:

$$\dot{B} \propto V \sin \phi_s \ . \tag{6.18}$$

The required time for the front porch is obtained by

$$t_{f.p.} = \int_{B_{inj}}^{B(\gamma)} \frac{dB}{\dot{B}} \ . \tag{6.19}$$

Necessarily the accelerating voltage must be increased a certain amount as soon as acceleration starts in order to achieve a finite time. As already mentioned, this will be done, to a certain extent, by the beam itself because beam load is negative during the early part of the front porch. However, for negligible beam load either the r.f. power must be increased or the bucket area must be reduced. In the latter case the voltage margin of Table 6.3 is wide enough to shrink a bucket area of 0.28 down to 0.24 which corresponds to an initial $|\phi_s| \approx 4°$. In Table 4 (next section) we list a most economic version of r.f. plant which is able to handle bunch sizes of 0.22 for vanishing beam load and nearly 0.24 for a beam intensity of 10^{13} ppp during a front porch time of 150 ms.

Other conditions for the front porch are given by aperture limitations and eddy current effects in the vacuum chamber.

6.7 Details of Construction

The accelerating structure is a circular guide loaded with transverse bars and with drift tubes; it is a backward wave structure. All bars are in a horizontal position and will be watercooled. On either end of the tank there is a coupler of coaxial construction for the transmission lines (rigid coaxial lines or waveguides) going up to the equipment room at surface level. Only the accelerating guides themselves are placed in the machine tunnel. The power amplifiers and terminating loads are accessible when the machine is running. One long straight section accommodates the three structures with couplers and flanges. The distance between power amplifiers and structures is at least 60 m and one has to take into account a power attenuation of 5% for coaxials of this length. It is planned to use two power amplifiers via a differential transformer to drive one structure so that it will be terminated properly for radio-frequency at both ends. More and/or bigger power amplifiers can be added later, without major difficulties, if higher accelerating rates and higher beam intensities are desired, as the structures represent matched loads, and cooling and sparking problems leave a wide margin. Table 6.4 lists the most important r.f. parameters.

Table 6.4

Number of cavities	3
Length of a cavity (without couplers), m	20.45
Diameter of cavity, m	0.9
Mode	$\pi/2$
Number of cells per cavity	50
Frequency at transition energy, MHz	183.068
R/Q, Ω/m	600
Effective shunt impedance per cavity, MΩ	11
Peak r.f. voltage at injection MV	3.7
Peak r.f. voltage per turn at 10^{13} p.p.p., MV	5.4
Maximum rate of increase of momentum, GeV/cs	165
Maximum beam power, MW	0.265
Average r.f. power per cavity, MW	0.5
Number of power amplifiers per cavity	2
Front porch time, ms	150
Momentum at end of front porch, GeV/c	$\sim$ 20
Phase slip between bunches and r.f., degrees	
at injection	- 181
at end of front porch	- 15
at $\beta = 1$	+ 42.27
Phase angle, ϕ_s, degrees	
at start of front porch	2
maximum	45

6.8 Low Level System

The r.f. system will be equipped with a phase-lock beam-control system which will be similar, in principle, to that of existing strong focusing machines. In such a system the frequency and phase of the accelerating voltage is derived from the bunched beam itself by means of an induction electrode.

The phase lock system must be supplemented by a radial control system in order to keep the beam at the desired orbit. In this system a voltage derived from a radial displacement electrode (an induction electrode with split electrodes) controls the average energy gain per turn (by controlling the stable phase angle) so as to maintain the particles at the correct radius.

The electronic circuitry for these systems tends to become rather simple because of the small frequency swing. It is possible to isolate the fundamental component of the bunch frequency from the signal induced in the beam induction electrode by means of a fixed-tuned filter. Furthermore, the absolute frequency variation of about 1 MHz is much smaller than in the CPS for example, in spite of the higher harmonic number, so that narrow-band amplifiers can be employed. Variations of phase and amplitude due to beam-loading are corrected by servo-systems.

6.9 Total Cost Estimate for r.f. System

		KFS
(a)	Accelerating structure (TWS) 3 × 20 m, couplers, cooling, supports	3500
(b)	Feeder lines 6 × 60 m + 3 bybrids	800
(c)	Terminating loads, including water system	600
(d)	6 Power amplifiers 250 kW each, including cooling systems	3000
(e)	3 Power supplies 1 MW each, filters, switchgears etc. included	1000
(f)	6 Driver amplifiers, including power supplies	1200
(g)	Low power system, monitoring, controls	5000
(h)	Design cost (model work)	2500
(i)	Spare parts	800
	Total	18,400

Vacuum system included elsewhere.

References

(6.1) K.R. Symon, J.D. Steben and L.J. Laslett, Proc. 5th Int. Conf. on High-Energy Accelerators, Frascati, 1965 (Comitato Nazionale per l'Energia Nucleare, Rome, 1966), Session VI, p. 296.

(6.2) CERN AR/Int. SG/64-15, November 1964.

(6.3) W. Schnell, Proc. 5th Int. Conf. on High-Energy Accelerators, Frascati, 1965 (Comitato Nazionale Energie Nucleare, Rome, 1966), Session I, p. 38.

(6.4) W. Schnell, private communication.

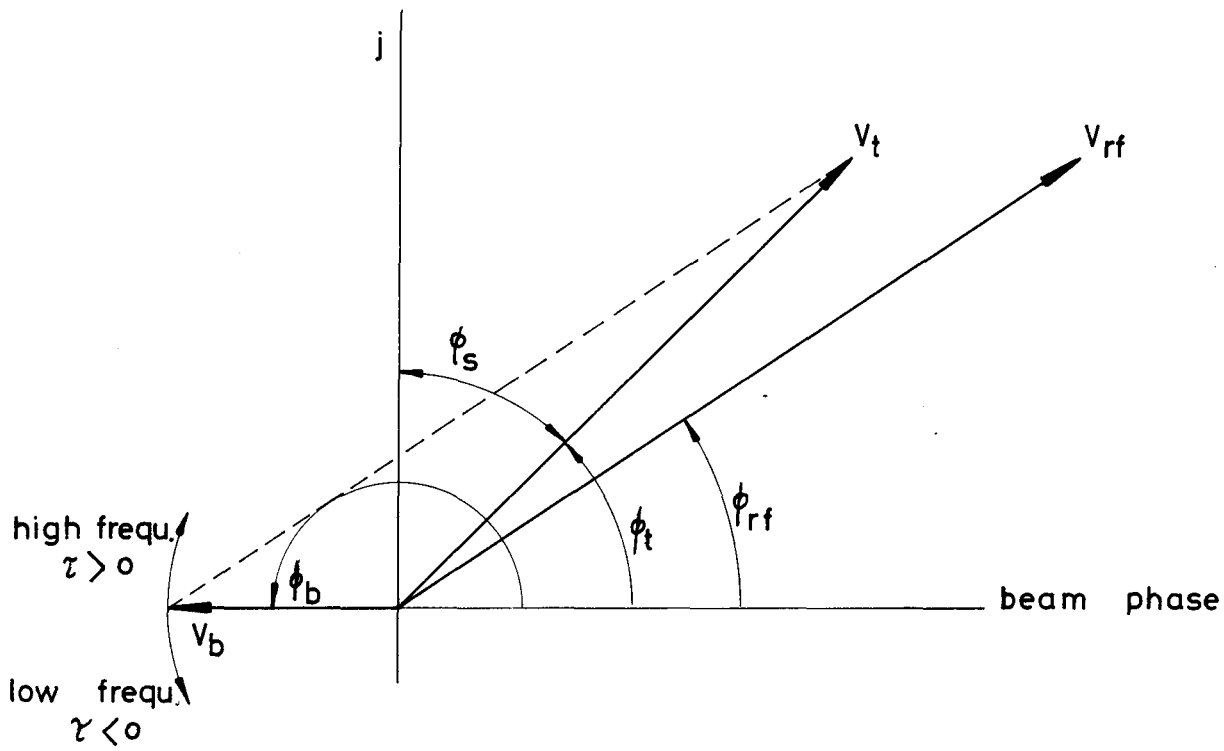

Fig. 6.1 Vector diagram just above transition (τ = 0)

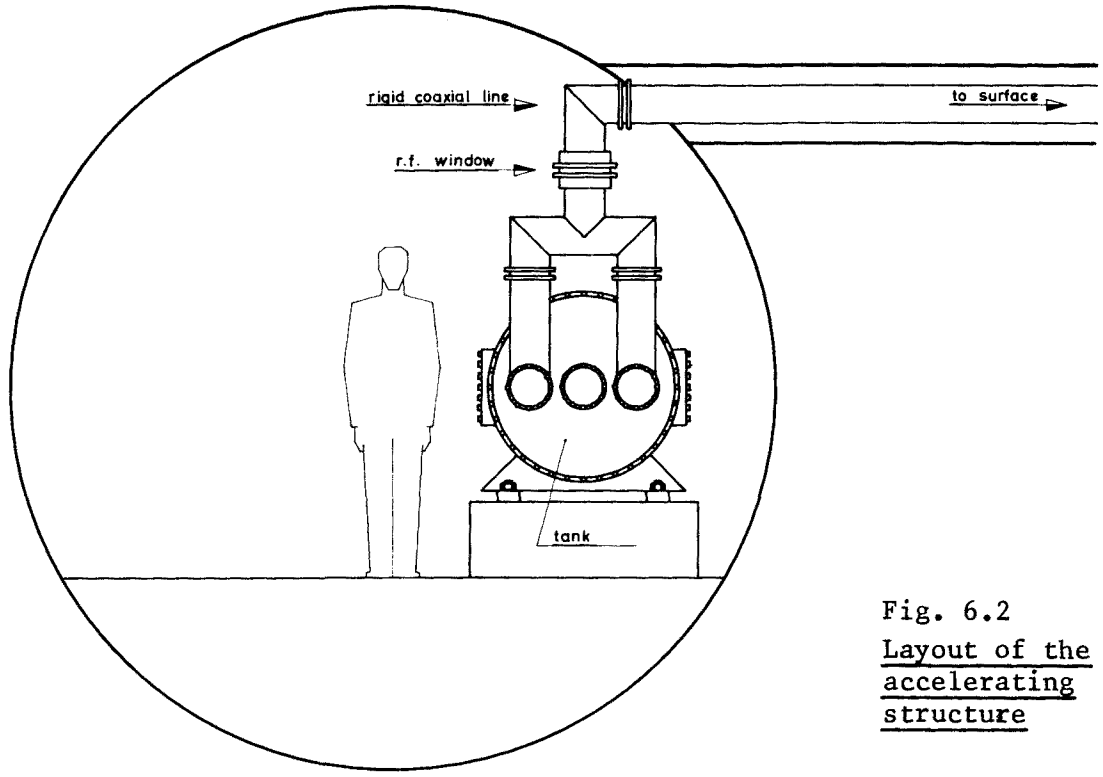

Fig. 6.2
Layout of the accelerating structure

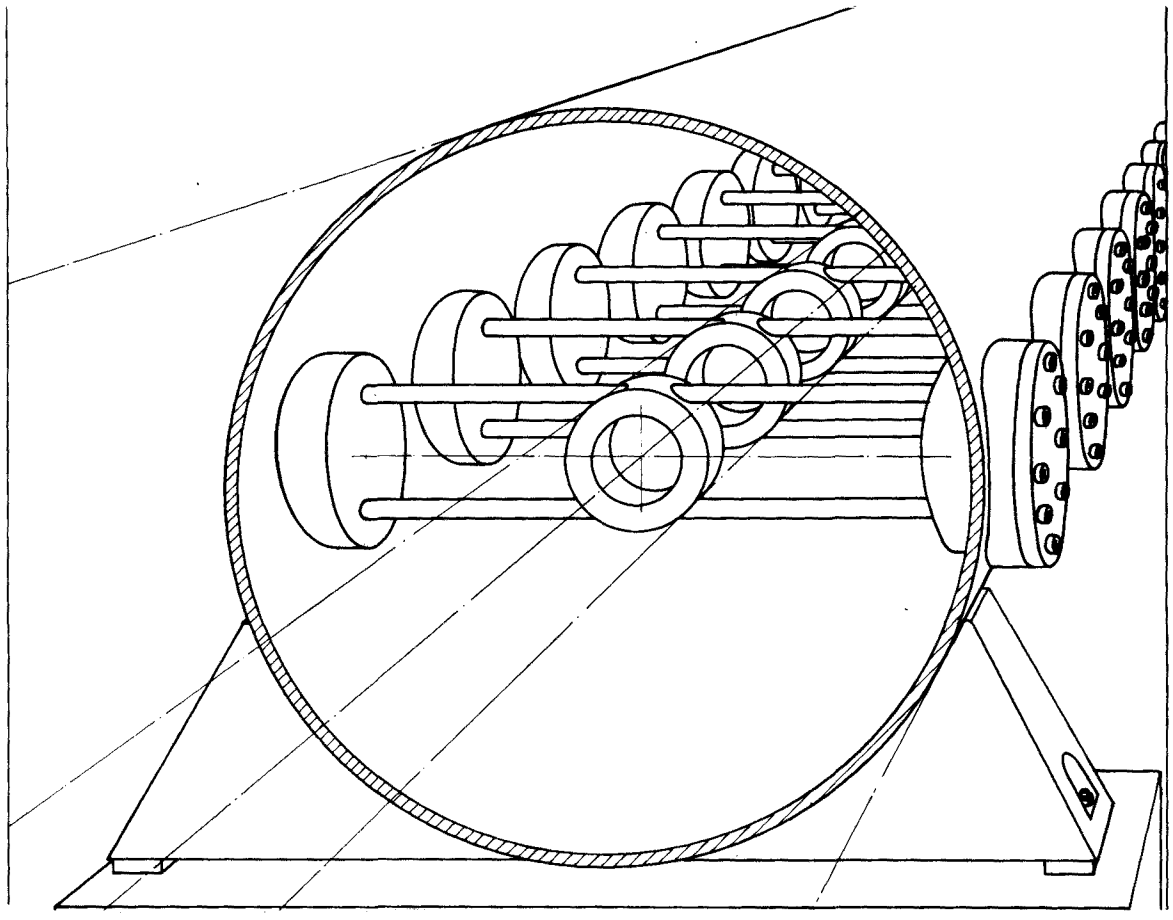

Fig. 6.3 Cut through the structure

Chapter 7

THE VACUUM SYSTEM

7.1 Introduction

This Chapter covers vacuum systems for the main ring, injection and inflection, ejection, transfer lines and accelerating structures.

The system is considered on a modular basis so that where magnets are missing the vacuum system follows a basic pattern which could be replaced by magnets complete with vacuum system.

To minimize gas scattering effects, the pressure should be below 10^{-6} torr[7.1,2]. However, since ion pumps are proposed, a working pressure of 10^{-7} torr is technically attractive (see Section 7.3) and should also allow sufficient margin for effects such as ion induced instabilities[7.3] which may appear later if higher intensities are accelerated.

7.2 Vacuum Chambers

The vacuum chamber in the magnet sections will be quasi-elliptical and will be manufactured from low permeability (< 1.005) stainless steel. The steel must have good welding characteristics with a low outgassing rate. The chambers will be manufactured by seam welding and forming to the appropriate cross-section. A rigorous process of chemical cleaning and degreasing will be necessary. Each magnet chamber will include in its length an integral isolating section of ceramic to prevent circulating currents and will be insulated from the magnet by a layer of insulating material to prevent shorting of the magnet laminations. Wherever possible the chambers will be connected by welding or quick release vacuum couplings (see Section 7.4). A flexible bellows will be included in each unit for installation and alignment purposes. It will not be necessary to have bake-out facilities.

7.2.1 Aperture considerations

The shape of the vacuum chamber in the various magnet gaps is determined by the good field region required.

The magnet aperture must be sufficient to allow for the good field region and for the vacuum chamber thickness, tolerance and deflection under vacuum load. In general, for a given shape of chamber and permitted maximum stress level there is an optimum thickness of chamber which gives the minimum aperture loss, i.e. thickness + deflection. Values of vertical

aperture loss have been calculated for elliptic chambers of different width and major to minor axis ratio[7.4]. The calculations give good agreement with measured deflections on the quasi-elliptical ISR vacuum chamber.

To determine the thickness of the bending magnet vacuum chambers, the inside width of the chambers has been assumed to be the width of the beam plus the sagitta with an extra 10 mm total allowance which is both necessary and sufficient to avoid serious perturbation of the good field by eddy currents.

Table 7.1 gives the thickness of the walls of the different chambers for the 'minimum aperture loss' condition except in the case of Q_D where a nominal 2 mm is used.

Cold stretching or rolling of the chambers will be required to maintain a safety factor of 2.5 in the areas of maximum stress.

Table 7.1

	B1	B2 & B4	B3	Q_F	Q_D
Magnet aperture vertical	36.6	54.9	50.3		
Chamber width (inside)	142.7	89.0	119.6	127.2	54
Chamber height (outside)				29.2	58
Thickness of wall	2.3	1.4	2.0	2.0	2.0
Thickness + deflection	3.0	1.9	2.5	2.6	2.0
Total vertical aperture available for tolerance and insulation	4.0	3.5	5.3	-	-

The aperture available, therefore, for tolerance and insulation is more than adequate and should permit some reduction in the vertical dimension of the magnets at the next stage of optimization.

The deflection and tolerance allowance may be reduced to zero where the vacuum chamber can be pre-stressed by, for example, making it oversize and compressing it between the magnet gap. This has already been assumed for the quadrupoles. It could also be done if the bending magnets were of the window-frame type. There would be a significant saving in ampereturns and stored energy in the magnet. The vacuum chamber allowance in the window-frame magnets discussed in Chapter 4 is 3.0 mm. From Table 7.1 it can be seen that further aperture reductions may be made at the next stage of design.

For a window-frame magnet pre-tested chambers would be assembled into the magnet gap during assembly of the two magnet half yokes. For the H-magnet, one end flange would normally have to be welded on after pushing the chamber through the magnet gap. However, the premium on stored energy makes it imperative to devise economic methods of forming the vacuum chambers into the H-magnet aperture to save the tolerance and deflection allowance.

7.2.2 Eddy currents

Eddy current heating for the worst case, i.e. for the widest, thickest chamber, is estimated at less than 20 W/m. This should be satisfactory.

Measurements of sextupole magnetic field distortion made by NAL agree with the theoretical predictions. Scaling the distortions to our worst case gives $\Delta B/B$ at 6×10^{-3} at the edge of the good field at our maximum value of $\dot{B}/B$. Some time dependent low field sextupole correction will therefore be required (see Chapter 8).

7.3 Vacuum Pumps

The continuous pumping of the system will be by a large number of small sputter-ion pumps. This type of pump has been selected because it is simple, clean, has no access to atmosphere, can act as a convenient pressure gauge as the current is proportional to pressure and could be used for leak detection.

The conductance of the chambers limits the useful size and spacing of the pumps and as all pumps must be outside magnet units their size and spacing is governed by the magnet lattice, the gas desorption rate of the chamber and its cross-section. For the apertures given in Table 7.1, the conductance per magnet unit varies from 1.5 to 7 ℓ/s. With the optimum arrangement, 4 ion pumps with pumping speed 50 ℓ/s each per lattice period (about 64 m) will be adequate to keep the pressure at 10^{-7} torr assuming the gas desorption rate of 10^{-10} torr/ℓ/s/cm^2 which could be expected from well-cleaned unbaked stainless steel. If alternate pumps became usable in limited regions of the machine the pressure rise between pumps would be acceptable.

The total number of pumps for the main ring system apart from the r.f. system is 432.

It will be necessary to ensure that the effect of the stray magnetic field from the pump is negligible at the orbit by connecting the pump through a tee piece approximately 300 mm long.

The estimated life of an ion pump is 40'000 hours at 10^{-6} torr and 400'000 hours at 10^{-7} torr. A working pressure of 10^{-7} torr will thus give extended life to the ion pumps and with an all metal system is reasonably easy to achieve. However, starting and pump-down working will reduce the expected life to nearer the 40'000 hour figure.

The initial pumping for starting the ion pumps will be achieved by a number of installed 2-stage mechanical rotary pumps; 1 per period, pumping through activated alumina traps capable of reaching 10^{-4} torr and isolated by a solenoid valve when not required. These pumps will be sited so that they are shielded from radiation by the magnet blocks, and connected by quick release couplings and plugs and sockets to allow for remote servicing. Each pump with trap will have a pumping speed of 40 m^3/h and be spaced approximately 64 m apart.

Extra turbo-molecular pumps have been allowed for sections where letting up the vacuum system to air is frequent.

7.4 r.f. Cavities

The vacuum in the r.f. cavities must be better than 10^{-7}. The cavities with their drift tubes are essentially 3 cylinders each 20 m long and 900 mm internal diameter. The suggested system is three 500 ℓ/s ion pumps connected below each cavity through 150 mm diameter holes. The cavities will be interconnected by 150 mm diameter connections one of which would contain a T-piece to a turbo-molecular pump set (240 ℓ/s) suitably valved for initial pump down. Each cavity is driven by two co-axial feeds at each end which are in vacuum up to an alumina window. These will require a 15 ℓ/s ion pump per connection (4/cavity) mounted near the input window.

There will be suitable pressure interlock with the r.f. system.

Pumps required for the r.f. system:

500 ℓ/s ion pumps	- 9
15 ℓ/s ion pumps	- 12
240 ℓ/s turbo pump set	- 1

As there will be a 'clean up' time after loss of vacuum, it is recommended that the r.f. section is capable of being isolated by all metal valves from the main ring.

7.5 Injection System to the Main Ring

The transfer line length is 800 m including bends and the expected aperture requirement is 41 × 48 mm. The pressure requirement in the injection (and ejection) transfer line is not so stringent, 10^{-4} would be satisfactory. However, ion pumps again provide the best solution because of simplicity and reliability. A 50 ℓ/s pump every 50 m will give better than 10^{-4} torr; this gives 16 pumps for the line. Initial pump down is achieved by one trapped mechanical pump for each 100 m. The whole line will be isolated from the main ring and the PS by all-metal valves.

Additional pumps will be required for the septum and kicker magnets. Two pumps of 500 ℓ/s each are allowed.

7.6 Extraction from the Main Ring

The initial extraction line to the West Hall will be 800 m long and later the line to the North Hall will be about 2'500 m long.

The transfer line will be about 60 mm diameter and the pump requirements will be similar to that for the injection line.

7.7 Components

All organic seals will be avoided to obviate radiation damage.

Flanges will be of the weldable type wherever possible[7.5], but in regions where space will not allow, quick release clamp type all-metal gaskets will be used.

For convenience of maintenance it will be necessary to divide the ring into suitable sectors by valves. These should be of the all metal gate valve type remotely controlled. These could also be automatically operated in case of a large leak developing.

Each superperiod will have 3 valves, one isolating the long straight, the other two dividing the 15 normal periods.

Additional valves will be required as already stated for the r.f. system, injection and ejection. This brings the total to approximately 24.

7.8 Controls

The control and monitoring of pressure will take place primarily in the six auxiliary buildings which will house the ion pump power units. These units will provide pressure indication around the ring which will be computer monitored with display devices to give indication of pressure in various degrees of detail. A number of hours memory could be included to permit history investigations.

For interlock and safety, pressure gauges of the Penning type will be used to operate pre-set level relays. These will be mounted near the roughing stations.

A computer-controlled ion pump start-up is recommended for such a large number of pumps.

Remote indication by audio tone should be available in the ring through UHF radio or telephone link to allow leak detection by special ion pump power units with the operator in a shielded cab if the radiation conditions require.

7.9 Cost Estimate

Cost estimates have been based on the experience of purchasing the 1.5 km long system for the transfer from the PS to the ISR. This system operates under conditions which are more relevant to the 300 GeV design than the main ISR vacuum vessel.

7.9.1 Main Ring

Pumping equipment

	Quantity	kSF	
50 ℓ/s ion pumps	432	650	
50 ℓ/s ion pump power units	432	750	
500 ℓ/s ion pumps	9	50	
500 ℓ/s ion pump power units	9	30	
15 ℓ/s ion pumps	12	15	
15 ℓ/s ion pump power units	12	15	
Leak detection power units	12	40	
40 m^3/hr mechanical roughing units	108	690	
240 ℓ/s turbo-pump sets	3	70	
75 ℓ/s turbo-pump sets	6	100	
Penning gauge leads (all metal)	108	90	
Penning gauge relay units	108	110	
Cabling		1'000	
Racks and local controls		600	
			4'210

Vacuum chamber

Vacuum pipes	1'520	
Flanges	550	
Bellows	830	
Fabrication	1'030	
Isolation pieces (ceramic)	800	
Straight section and 'missing-magnet' supports	170	
Sundries (leak detection, etc.)	500	
Sector valves	390	
Prototypes	200	
	5'990	
Straight pieces and ancillaries at Stage A	1'120	
		7'110

Installation	1'840
Total for Main Ring	13'160

7.9.2 Injection transfer line (800 m)

Pipe and fitting including installation	800	
50 ℓ/s ion pumps	30	
Power units	30	
Mechanical pumps and fittings	50	
Cabling and local controls	150	
		1'060

7.9.3 Ejection (West Hall 800 m)

Vacuum system	910	
Cabling, etc.	150	
		1'060

7.9.4 Ejection (North Hall 2.5 km)

Vacuum system	2'900	
Cabling, etc.	540	
		3'440

7.9.5 Grand Totals

Main Ring	13'160
Injection Transfer	1'060
Ejection (West Hall)	1'060
Ejection (North Hall)	3'440
	18'720

References

(7.1) Design Study of 300 GeV Proton Synchrotron, Vol. I, p. 137, Nov. 1964.

(7.2) W. Hardt, ISR-300/GS/68-11.

(7.3) H.G. Hereward, P.L. Morton and K.H. Schindl, MPS-SI/Int. DL/68-4.

(7.4) D.R. Moore, Nimrod NDG 70/33.

(7.5) J.M. Voss, ISR-VAC/67-23.

Chapter 8

THE CORRECTING LENS SYSTEM

8.1 Purpose of Correcting Lenses

In earlier designs of A.G. synchrotrons it has been the practice to provide sets of correcting lenses; in general quadrupoles, sextupoles and octupoles. The main purpose foreseen for these lenses (sometimes used in conjunction with poleface windings), was the compensation of machine imperfections. These could occur particularly at injection, due to remanent effects, and at high energies, due to saturation effects in the magnets.

In practice it has often turned out that correcting lenses have been important for a number of purposes that could not originally be foreseen. In particular, the higher intensities reached by accelerators, such as the CPS and the AGS, have required the use of lens corrections to tune out stop bands and to provide Landau damping of certain transverse instabilities. The present tendency at high intensities is for these requirements to be more determinant in the design of correcting lens systems than is the straightforward correction of saturation effects.

For the present machine design, the choice of the correcting lens system is based partly on the future operation at high intensity rather than simply on the compensation of errors in the guiding and focusing fields. Of course such field error compensation will still be available to some degree, but the present approach tends to increase the ratio of octupole strengths to sextupole strengths that will be provided, since it is believed that the octupoles are more effective for Landau damping of bunched beams.

We do not propose to provide correcting quadrupoles in this machine. Tuning of the radial and vertical betatron frequencies will be adjusted by control of the power supplies feeding the main quadrupole lens system, as discussed in Chapter 5.

Skew quadrupole fields may be required in order to reduce coupling between radial and vertical motion, since the beam from the improved CPS may have different vertical and radial emittances. Such fields could probably be provided by means of special windings on the octupoles. A few special quadrupoles may be required for a fast passage through transition energy.

Sextupole and octupole lenses will be provided for a number of purposes. The sextupoles will be required for compensating the momentum-dependence of betatron frequency, reducing gradient errors at and just above injection due to vacuum-chamber eddy currents, tuning out 3rd-order resonances and possibly for some correction of the bending magnet saturation effects at high fields. Octupoles are foreseen for Landau damping, tuning out of 4th-order resonances (including possible non-linear coupling resonances induced by space charge), and the compensation of octupole-type errors which might arise at high field levels in the "elliptical" aperture F quadrupoles, as discussed in Chapter 4. Both sextupoles and octupoles are expected to be useful for general beam diagnostic and "gymnastic" purposes.

8.2 Superperiodicity Constraints

Correcting lenses are normally distributed uniformly around the circumference of the accelerator with a superperiodicity C which is smaller than the main lattice periodicity N for economic reasons. The superperiodicity C must be suitably chosen to avoid the excitation of linear and non-linear resonances. The general numerology of the lattice is discussed in Chapter 2, but it is convenient here to recall certain specific points in this connection.

The increase in particle oscillation amplitude in the neighbourhood of a resonance is governed by the amplitude of the corresponding Fourier component of the perturbation, the order of the resonance and the proximity of the oscillation frequency to the resonance. In general, the machine is most sensitive to resonances of low order, that is of closed-orbit and envelope-oscillation type, corresponding to dipole and quadrupole perturbations respectively. In addition to their nominal fields, sextupole and octupole lenses also generate quadrupole and dipole components for off-axis particles, and can therefore excite low-order resonances. An essential constraint therefore is that integral multiples of C be remote from 2Q. Weaker constraints are that integral multiples of C be not too close to 3Q and 4Q, in order to avoid undue excitation of the 3rd and 4th order resonances respectively.

With the chosen lattice design, short straight sections for correcting elements are foreseen adjacent to each F and D main quadrupole. To permit independent correction of radial and vertical motion two groups each of sextupoles and octupoles will be provided, one group in F and one group in D straight sections; the large ratio (> 5) of β_{max}/β_{min} is advantageous in this respect. Thus the superperiodicity must be a submultiple of the lattice period $N = 108$.

For a nominal Q of 27.75 two values of C, namely 12 and 36, satisfy the above conditions and lie inside a practical range. Then the only superperiod resonances up to 4th order that lie significantly close to the working point are of 3rd order type $3Q = 84$; these coincide with the integer resonances $Q = 28$ and arise from $C = 12$ only. Preliminary calculations indicate that, with the maximum sextupole strength envisaged for $C = 12$, the beating resulting from the proximity of these resonances is acceptably small.

The choice of C = 12 initially, with the possibility of a later increase to 36, fits in well with the "missing-magnet" philosophy. It will be shown in Section 8.3 that sufficient correction strength for early operation can be obtained with 12 lenses of each type in F and D. Any later increase in correction required could be accompanied by a better distribution with C = 36, which would avoid undue increases in beating factors.

8.3 Strengths of Correcting Lenses

At this stage of the studies it is not possible to make very accurate predictions of the amount of sextupole and octupole correction that will be required through the various stages of development of the accelerator. We therefore make approximate estimates, based on simplifying assumptions, for an initial installation of correcting elements on a rather modest scale, which should nevertheless be sufficient for the earlier years of machine exploitation. The possibility of later increasing the number of elements by a factor 3 will then leave a comfortable margin for any further correction required for exploitation at high intensity.

During the final design studies it will be possible to determine more precisely the parameters of the correction lens system, but this would not appreciably affect the cost estimates derived from our present assumptions.

To make an approximate estimate of the sextupole strength we consider first the requirement for compensation of the momentum-dependence of betatron frequency. With sextupoles located close to F quadrupoles a total strength of about 10^3 T m^{-1} just neutralises this dependence at 300 GeV/c. Alternatively, the same strength would compensate a sextupole-type saturation error in the Stage B magnet arrangement corresponding to a $(\Delta B/B)$ of somewhat less than 10^{-3} at the edge of the useful aperture, still at 300 GeV/c. Both effects are equivalent to a reduction of radial betatron frequency with increasing radius. Thus, in terms of the sextupole strength for compensation, the requirements are additive. It is therefore proposed to provide a minimum of 2×10^3 T m^{-1} for an initial installation. Divided amongst a group of 12 sextupoles, of nominal length 1 metre, this would require a B" of 167 Tm^{-2} in each lens, which is a comfortable figure for the required aperture and could be increased somewhat without difficulty.

The estimation of octupole strength is necessarily more vague, since the requirements are at present numerically ill-defined. However, if we were to assume for an initial installation 12 octupoles per group, each octupole having a strength of $B''' = 4 \times 10^3$ Tm^{-3} with 1 metre nominal length, the total octupole correction strength per group would be 4.8×10^4 Tm^{-2}. This would cause an average detuning of $\overline{\Delta Q} \sim 0.01$ for a particle with about 5.3 mm amplitude or a frequency shift of about 0.2 in a beam displaced by $\sim$ 20 mm. This is already a reasonable amount of octupole dispersion for many of the purposes foreseen, though comparisons with the requirements predicted by Gareyte[8.1] for the future CPS suggest that somewhat more octupole strength may later be required for exploitation of the highest intensities.

8.4 Correcting Lens Design

The lens yokes will be laminated both to permit pulsed operation and because this construction is advantageous economically. The estimates in this report are based on a useful aperture of circular shape, but, as with the F quadrupoles of Chapter 3, it may be desirable to consider "elliptical" type apertures for economic reasons. Experience which has been obtained with the "asymmetric" sextupole design of the Intersecting Storage Ring project[8.2], will be useful in this connection.

8.5 Layout, Power Supplies and Cabling

The requirements discussed in the preceding sections lead to a choice of 4 groups, each of 12 correcting lenses, for an initial installation. There will thus be a total of 48 lenses distributed amongst the 216 short straight sections. These straight sections, each of 2.3 m nominal length, also have to accommodate other equipment. In particular, the closed-orbit correction system (Chapter 9) will require some space for dipole magnets and beam sensors in each of the 216 sections. Our assumption of 1 metre nominal length for each correcting lens leaves adequate space in the same straight section for closed-orbit correction elements, coil overhangs etc.

The complexity of power supplies and cabling depends on the degree of flexibility required in the harmonic pattern of the lens excitation. The most basic mode, in which all lenses of one group are series-connected, requires only 4 power supplies and cable circuits, one for each group. Such a system is adequate for many of the purposes foreseen, and at the present time appears to be the most appropriate choice. If during the final design studies, or at a later date, it turned out that a more flexible arrangement were necessary, extra circuits could be installed to meet specific requirements.

The power supply rating for each group is closely related to the design of the correction lenses, which has not yet been studied in detail. We therefore base our estimates on previous designs[8.3], since the small differences in parameters will not have a strong influence on the total cost of an optimised system. On this basis a total peak power of approximately 1.2 MW is required at full excitation to all 4 groups. There would be advantages of flexibility in trying to optimise the complete system so that sextupole and octupole groups have about the same power requirements at full excitation. We have assumed for the purpose of cost estimates that this will be done, and that there will be 4 similar power supplies initially, each of 300 kW, though the assumption is not a critical one.

8.6 Cost Estimates for Initial Installation

24 sextupoles at ∿ 40 kSF	0.96 MSF
24 octupoles at ∿ 40 kSF	0.96 MSF
4 power supplies, each of 300 kW	0.75 MSF
Cabling, 4 circuits each of 14 km at 5 kSF/km, including installation	0.28 MSF
Total	2.95 MSF

This figure does not include development and measurement equipment costs, which are assumed to be covered under personnel and laboratory equipment headings.

References

(8.1) Gareyte, J., Report CERN/MPS/DL 70-5 (1970).

(8.2) Caeymaex, S., Proc. IIrd Int. Conf. on Magnet Technology, Hamburg (May 1970), and Report CERN ISR-MA/70-18.

(8.3) Design Study of a 300 GeV Proton Synchrotron, Report AR/Int. SG/64-15 (1964).

Chapter 9

THE CONTROL SYSTEM

9.1 Introduction

The control system for an accelerator of this size has to be more than just a collection of controls transferred from the various subsections to a main control room. It is desirable that the whole accelerator should be operated from a single point by a small operating crew. For this to be possible, means must be found to analyse the vast amount of data available, and present it to the crew in a suitable form for easy assimilation, and to carry out routine settings and measurements. Both these functions can be provided by a suitable computer-based control system.

If computers are considered as integral parts of the control system from the start, rather than something added to a conventional control system, as has usually happened in the past, many additional benefits can be obtained. The additional benefits come mainly from the flexibility of such a system, and the ability to process the data and present it in a form most convenient for the operator, or to initiate control functions without the intervention of the operator. In order to achieve this, it is essential that all subsystems should be designed to make the maximum use of the control system.

The reliability of computers today minimises the risk taken in relying on their use for the operation of the accelerator. However, provision will be made for the operation of most of the subsystem with the control computer out of action, although it will not be possible operate the complete accelerator under these conditions. In addition, it will also be possible to operate individual items, using a plug-in control box, for commissioning and test, even when the satellite computers and controllers are out of action.

To provide separate cables for each control and indication function, as in a conventional system, would be very expensive, due to the large size of the ring and the wide distribution of the component parts, and so extensive use of multiplexing must be made.

It has been assumed that, as the CPS will be used for physics up to 28 GeV in the existing experimental halls in the forseeable future, as well as supplying the ISR, the CPS will continue to be run from its own control room. As a result, it will not be necessary to transfer any controls from the CPS to the new control centre, although some status information will be required.

9.2 Overall System Layout

At first sight, it would seem that the best way to achieve the stand-alone operation of the various subsystems is to have a satellite computer for each subsystem, under the overall control of a main computer associated with the control centre. This could be satisfactory for subsystems which are well defined and geographically discrete, but some of the subsystems have elements distributed widely around the ring tunnel, and for these such a system would lead to wasteful multiplication of equipment. A combination of separate satellite computers for some subsections, together with a ring tunnel multiplex data acquisition and control system, with its own satellite computer, has been chosen as a good compromise, and a schematic diagram of the system is shown in Fig. 9.1 and the physical layout in Fig. 9.2. Separate data lonks have been provided between the main computer and the satellites, and between the satellites and the controllers. The possibility of using a common data highway calling in at each point was investigated, and it seemed that the resultant complication of the organization of the data transfer would outweigh the cost of the extra data links, However, this choice would require further consideration at the detail design stage.

It will be seen from Fig. 9.1 that where a subsystem is sufficiently compact, as for the r.f. system in building C, a computer is provided with direct links to the various parts of the system. Where the system is divided into separate discrete parts, the computer will be placed near one part, with direct links to that part, and data links will go to the other parts, with a local controller to marshal the data acquisition and control commands. An example of this arrangement is the injection system, which has a computer in building A connected directly to the inflector and associated equipment, with data links to the building housing the transfer equipment supplies and to the CPS control room. The multiplex for systems distributed round the ring, such as vacuum, will be divided into 6 sectors, each under the command of a local controller situated in the appropriate auxiliary building. Data links from these controllers go to the computer MPX which controls the complete system.

9.3 Control Computers

Due to the rapid developments in this field, it would be premature to specify the computers required in any detail, but it is known that computers and associated equipment are available today, from more than one manufacturer, which would fulfil all the requirements.

The main computer associated with the control centre will be of medium size, and will be equipped with a full range of peripheral apparatus, including graphics terminals. The satellite computers will all be of the same type, and may be a smaller model of the main computer, with a minimum of peripheral equipment. The controllers will be miniature computers of the process control type, with stored programmes and no permanent peripherals. They will be able to control the data acquisition process and carry out simple operations, such as checking values against limits. This tree structure, with some processing at each stage, means that it is only necessary to pass information higher up the tree when significant

changes occur. This, together with the ability to schedule parts of the machine cycle for data transfer, can simplify the interrupt system, and allow the use of simple modular software systems.

In the past, a shortage of good real-time executive software has involved many users in a large amount of computer system analysis before work could start on applications programs. Fully adequate executives are now available from several computer manufacturers. These improved systems and the introduction of interpreter languages have simplified the writing of the special application programs very significantly.

9.4 Data Links

The data links between computers, and between computers and controllers, could take many forms, and the relative merits of parallel or serial transmission need to be assessed. However, there should be no difficulty in providing suitable links, since experience shows that data links involving parallel transmission of digital information on multiway twisted pair cables at rates of above a hundred thousand words per second can operate without difficulty over at least 1.6 km. The cables for the links will run round the tunnel, so that the maximum distance between link points, where pulse reshaping circuits can be provided if necessary, is about 1.3 km.

9.5 Interface

In the past, many of the difficulties in applying computers to control applications have been due to the lack of a simple but versatile method of connecting the various data and control points, through multiplexers and converters where necessary, into the computer. Standard systems such as CAMAC are now evolving which should simplify this problem in the future, and one such system will be chosen for use at the main subcentres.

A standard format will be laid down for signals to and from equipment to be connected to the system, and local controls for equipment should be designed to conform with the standard, and to make the maximum use of the control system.

9.6 Multiplex

The multiplex system, for data acquisition and control round the ring tunnel, will be divided into six sectors, with a controller in each of the auxiliary buildings. A multiway twisted-pair cable round the sector will provide a data highway, connected to the large number of multiplex terminals. The controller will interrogate the terminals in sequence and pass the information gathered to the MPX computer, in blocks. Commands flowing the opposite way will fit into programmed gaps in the interrogation sequence. The cycle time, and time constants of most of the apparatus, are sufficiently long to allow this method of operation, which reduces the need for sophisticated programming of the controllers.

A number of coaxial cables will run round the ring tunnel system, calling in at the auxiliary buildings, and terminating at the control centre. These will be used for the transmission of analogue waveform signals, up to about 100 kHz, and the multiplex system will be used to connect signals to these highways as required by the operators.

9.7 Beam Monitors

Beam intensity and position monitors are required for the transfer path, the main ring, and the extracted proton beam lines. In the transfer path, the problems are similar to those for the ISR, and similar monitors can be used. Two types are required for the main ring, relatively narrow band monitors for the closed orbit control, and wide band monitors for commissioning and diagnostic purposes. The monitors for closed orbit control can be similar to the electrostatic position monitors developed for the CPS and ISR, and their use is described in the section on closed orbit control. The wide band monitors are required to study detailed beam behaviour, and it is thought that it will be necessary to have these at a number of points round the ring. A band width of up to one gigaherz is required, and while this can easily be achieved for the pick-up unit itself, the connection of the long length of cable required to reach the control centre would seriously degrade the performance. Therefore these monitors will be located close to the shafts leading up to the auxiliary buildings, so that they can be linked by short lengths of high grade coaxial line to oscilloscopes for local observation. Equipment can also be provided to modulate a high frequency carrier with these signals, for transmission to the control centre. Alternatively, it may be sufficient to use television links for this purpose, transmitting the image of the trace on a local oscilloscope.

Beam profile monitors will be required in the main ring, to observe beam envelope oscillations, and in the transfer path and the extracted beam paths, for emittance measurements. Interception monitors of the luminescent screen and secondary emission types and non-interception monitors of the ionisation beam scanner type have been developed for the PS and ISR and modifications of these can be used. Fork targets will also be required for checking the calibration of the profile monitors.

9.8 Closed Orbit Control

It has been shown, in Chapter 2, that the closed orbit distortion amplitude resulting from the tolerances assumed could be over 32 mm in the horizontal direction and nearly 20 mm in the vertical. In order to reduce the magnet aperture required, it is assumed that this distortion amplitude is reduced to a maximum of 10 mm in the horizontal plane and 5 mm in the vertical. It is expected that the beam size will be a maximum in the vertical direction at injection and in the horizontal direction at transition, and so the closed orbit correction will be most critical at these times.

To assist alignment, and provide some redundancy, pick-up plates will be fitted either side of a quadrupole, in extensions to the quadrupole vacuum chamber. The signals from the units will be integrated over several turns, to reduce the effects of coherent betatron oscillations. The relatively slow signals can then be transmitted by the ring multiplex system, but since the information from all 108 monitors in one plane will be required for the same point in the time cycle, it will be necessary to store the information at the monitor point until interrogated.

The closed orbit will be corrected at injection by means of small dipoles in the short straight sections. The dipoles will have individual power units, controlled through the multiplex system. After measurement of the position of the closed orbit, the corrections will be computed and the dipole currents adjusted to the corrected values. The dipole excitation will be d.c. and so their effect at high energy will be small. Correction at high energy will be by movement of the quadrupoles, so that when the high energy closed orbit has been determined, the corrections to the quadrupole positions will be computed, the machine shut down and the positions of the quadrupoles adjusted. Since the stability of the tunnel in the molasse rock is expected to be very good, it should not be necessary to make this adjustment very often.

The closed orbit amplitude after correction depends on the number and location of beam position monitors and correcting elements and the accuracy of measurement and correction. Simulation studies have shown that if at least four sensors and correctors are provided per betatron wavelength, the most dangerous harmonics of the closed orbit distortion can be made small, although zero reading on the sensors does not mean that the amplitude disappears everywhere. The correctors and sensors should be located close to each other, and maximum sensitivity is achieved if they are positioned close to the point where the amplitude function is a maximum. Thus the monitors and correctors for the horizontal plane should be placed near a horizontally focusing quadrupole and those for the vertical plane near a horizontally defocusing quadrupole. The requirement for at least 4 units per betatron wavelength results in a unit at every quadrupole, giving a total of 216 monitors and 216 correcting dipoles.

Several procedures can lead to the reduction of the closed orbit amplitude, and simulation studies for two of these were made as part of the earlier ECFA Study. In one case, all measurements were made and the best possible correction that could be made by the use of a single corrector element was computed by a least squares fit. This procedure has to be repeated a large number of times to reduce the distortion to an acceptable level. The influence of observational errors and errors in the correction are very small, but the amount of computation for each correction is rather large. In the other case, corrections to the closed orbit are made locally, using three adjacent corrections to form a "half wave" beam bump, adjusted to reduce the error signal at the centre point to zero. This method requires a trivial amount of computation, but the result is strongly dependent on errors in observation and correction. It has been shown that for the tolerances given in Table 9.1, the beam bump

method would enable the closed orbit distortion to be kept within the required 10 mm in the horizontal plane, but the tighter tolerance in the vertical plane would require the beam bump correction to be followed by a few iterations of the first method.

In addition to these simulation studies, practical applications of closed orbit control on the CPS, and at DESY and NINA, have shown that there should be no difficulty in achieving the required control.

Table 9.1

Beam Position Indicators	
Length of pick-up plates	200 mm
Tolerance of centre line position	1 mm rms
Observation error	0.5 mm
Dipole Magnets	
Horizontal correctors:	
Length	250 mm
Aperture	130 mm × 25 mm
Maximum field	0.08 T
Vertical correctors:	
Length	250 mm
Aperture	60 mm × 60 mm
Maximum field	0.036 T

9.9 Timing System

Since the CPS will be supplying beams to experimental targets as well as acting as injector for the main ring, many modes of operation must be catered for. As the time cycles will not synchronize exactly, in some modes the CPS will have to wait until the main ring is ready to accept a pulse, and in others the main ring will have to wait until the CPS is ready. In either case, the CPS ejection prepulse will be used to start the main ring time cycle.

Timing signals to be distributed round the machine and supplied to the experimental areas could include a series of pulses at equal flux increments (the B-train), a series of pulses generated at the beam orbital frequency, a sequence of trigger pulses generated at significant points in the machine cycle, and real time clock pulses.

9.10 Radiation Monitoring

Radiation monitoring requirements are divided into two categories, (a) recording of levels round the machine and experimental areas under normal operation, and (b) alarms or prevention of operation of the machine under abnormal conditions, when dose rates may become excessive in some areas.

The first category usually comes within the sphere of Health Physics, but it may be advantageous to use the multiplex data acquisition system, in areas where it is available, to avoid an excessive number of additional cables.

It will also be necessary to have radiation monitors round the site and surrounding countryside to ensure compliance with the statutary requirements for limitations of dose received by the general public. To connect these monitors into the control data acquisition system would be very costly, and it should be adequate to use battery-operated monitors fitted with recorders for this purpose. It is then only necessary to collect the records periodically.

For the second category, the only danger points for personnel are around the extracted beam lines and at the shafts from the ring tunnel up to the auxiliary buildings, since the ring tunnel will be so far below ground.

Radiation monitors will be placed at such danger points as part of the control system, to give alarms or to switch off the beam if dose rates become excessive. Similar monitors will also be placed in positions where mis-steering of the beam could cause damage to machine components.

Simple beam loss monitors will be distributed at frequent intervals round the tunnel system, so that the pattern of beam loss can be observed. The output from these monitors will be integrated and recorded. From these records, and operating experience, it may be possible to predict the end of life of radiation-sensitive components, to allow planned replacement before breakdown.

9.11 Communications

Because of the great length of the tunnel system it would be expensive to provide permanently-installed telephones at frequent intervals, and the main method of communication, both round the tunnel and about the site generally, will be by radiotelephone. A multichannel main station will be associated with the control centre, and a large number of small portable transceivers will be provided. For maintenance in the tunnels, the small vehicles which will be used to carry tools and spare parts will each be fitted with a multichannel station. A common trunk line will be provided round the tunnel, into which can be plugged normal handsets, mainly for installation and commissioning. Loudspeaking telephones will be provided between the auxiliary buildings and the control centre, and between any local control room and the

main concentration of apparatus in the tunnel. For safety reasons, amongst others, it is essential to install a public address system covering the whole tunnel complex.

Television equipment will be provided for surveillance of the personnel access system, and for beam monitor viewing. In addition, each maintenance vehicle will be fitted with a camera which can be plugged into a trunk line running round the tunnels to allow personnel at the control centre to inspect the progress of the work.

9.12 Personnel Protection

The tunnel will be divided into nine areas, six sectors and three beam tunnels, so that the search can be carried out in each independently and breaking the interlocks in one section does not require the whole tunnel system to be searched again. To give the maximum security, two independent "hard wire" circuits will be completed by door interlocks at the access points connected in series, so that opening either circuit will prevent injection from the CPS, except under special test conditions. Additional contacts will transmit the information on the location of the open circuit to the control centre. The access procedure, which will allow identified personnel into the ring without requiring a search after they have left, can also be monitored by the multiplex system. Consideration is being given to the use of small personal magnetic cards for identification, to enable the computer system to keep track of personnel entering the ring under these conditions. A selective system of emergency stop buttons will be included in the Personnel Protection system.

9.13 Diagnostic Apparatus

Apart from the beam monitors, other diagnostic equipment will be installed. This will include apparatus for measuring the vertical and radial Q during the cycle. Apparatus developed for the ISR, using a short pulse to excite coherent betatron oscillations and a pick-up electrode system with filters, could be used for this purpose. Other diagnostic apparatus is likely to be required to investigate effects resulting from the high beam intensity that may be possible eventually, but this cannot be specified at present.

9.14 The Control Centre

With the involvement of the computer in the control system, it is possible to make all controls and indications available to a single operator. This may well be suitable for the final stage when the accelerator is working routinely, but it is likely to lead to congestion and frustration during commissioning and in the development phase. The best solution seems to be to have a small group of control areas, specialising in particular aspects of the machine operation, one of these dealing with the system as a whole. It is expected that, as experience is gained, it will be possible to concentrate the whole of the control at this one position, where one or two oscilloscopes, a graphics display terminal, one or two storage display units for alarms, etc., and one or two keyboards will be all the equipment required. Multicolour display systems are now becoming available and these may be used to show the relative importance of information displayed.

In such a control system, the control desk is not much more than a computer peripheral, and therefore the exact location is not important. It would be possible to have the control in one position for the initial running, and move it to another for subsequent operation.

The smaller the central control room becomes, the greater the difficulties caused by visitors, guided tours, etc., and provision for these must certainly be made in an International machine of this size. It seems desirable to provide a visitors gallery or exhibition room adjacent to the control room, to allow observation without interfering with the operators. This would be a suitable place for models and other demonstration equipment, and display units, under the control of a keyboard, could show the current operating parameters.

9.15 Cable Administration

Although the extensive use of multiplexing will reduce the number of cables required, it still adds up to an impressive total. Computer-aided design, involving the listing of requirements, choice of route, and the production of cable schedules has been successfully used for the ISR, and it is planned to use a similar system for this project.

9.16 Cost Summary

	MSF
Central computer	1.90
Control centre	0.75
Satellite computers (5)	1.90
Controllers (12)	0.84
Data links (17 links, 30 km)	0.58
Interface (16 sets)	1.12
Sub group multiplex	1.99
Sector multiplex	2.40
Personnel safety	0.80
Radiation protection and loss monitoring	1.48
Communications	1.14
Beam sensing	5.90
Timing system	0.41
Diagnostic equipment	1.60
Cables and terminations not included above	0.75
Total excluding orbit correction magnets and power supplies	23.56
Installation (excluding cable) 10%	2.36
Total with installation	25.92
Orbit correction magnets and power supplies	1.19
GRAND TOTAL	27.11

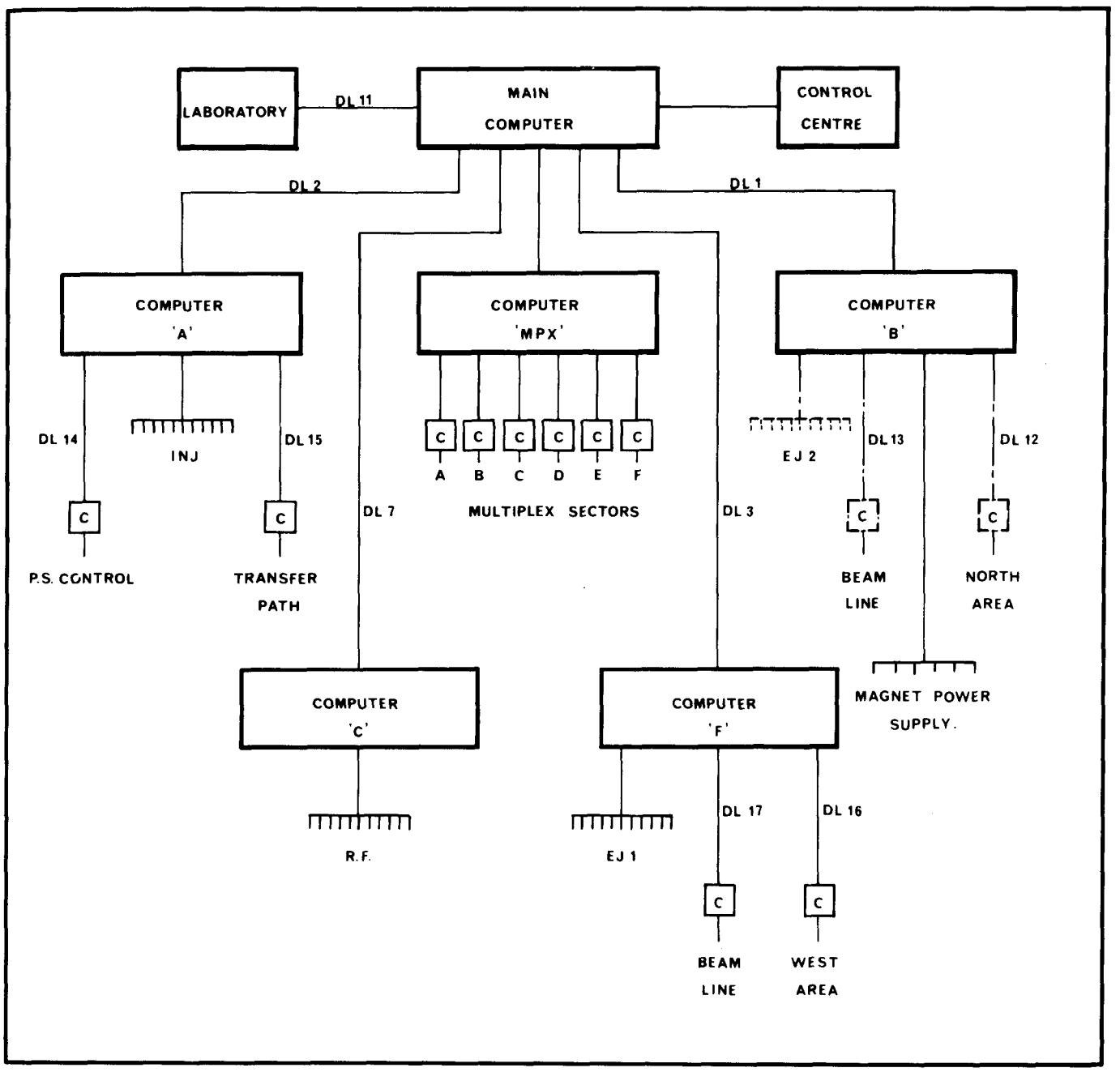

Fig. 9.1 Control schematic diagram

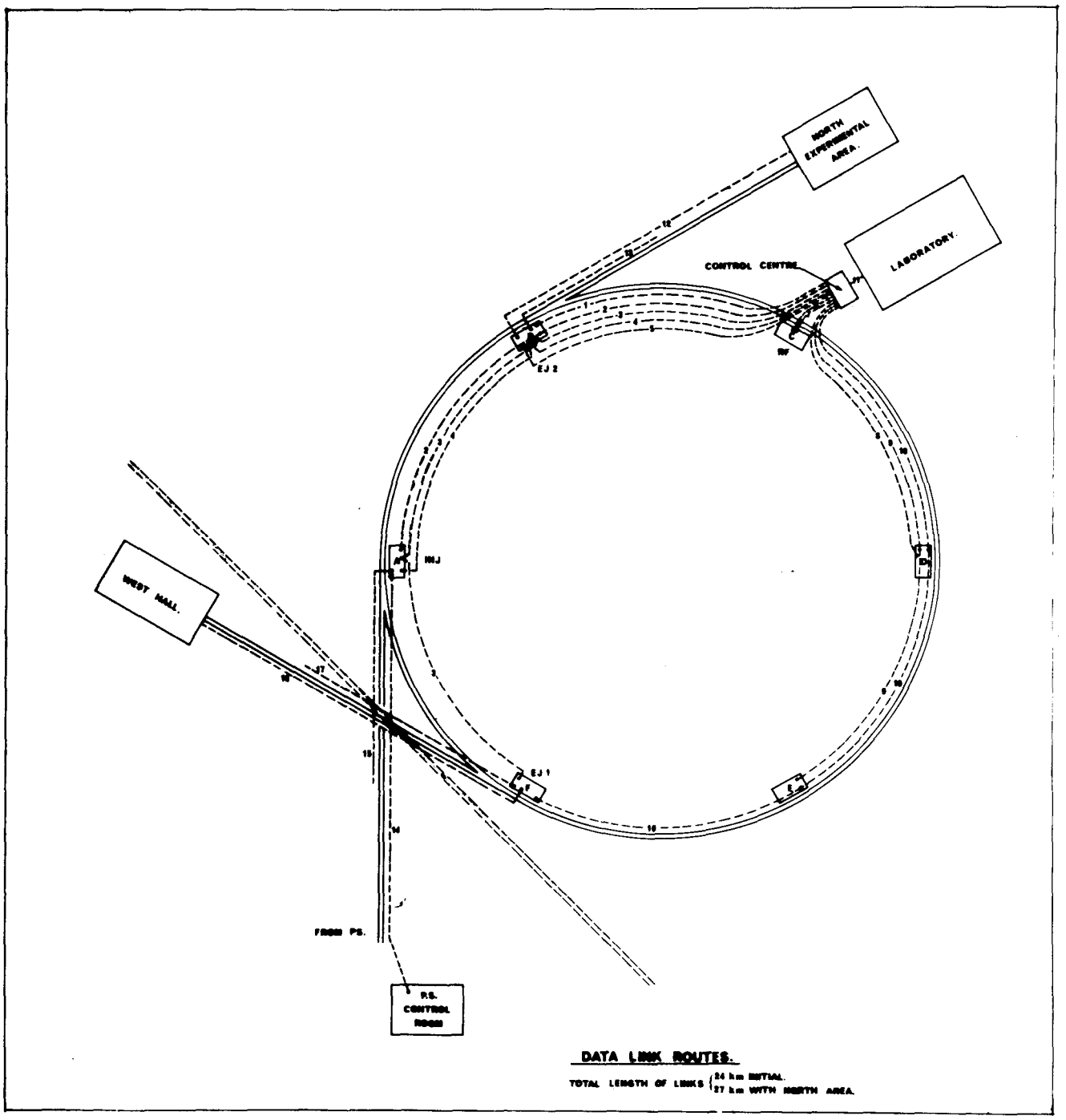

Fig. 9.2 Data link routes

Total length of links {24 km initial
27 km with north area

Chapter 10

THE SURVEY SYSTEM

10.1 Introduction

Altogether, the 800 MeV booster, the 28 GeV PS, the transfer tunnels and the two rings of the ISR comprise about 4 km of tunnelling in which some two thousand components had to be positioned in relation to each other with an accuracy of a tenth of a millimetre.

From the survey point of view, the 300 GeV accelerator represents a two-fold increase in scale compared with the above complex, but the tolerances necessary to enable correct accelerator operation remain the same as for the ISR.

The evolution of survey techniques and the constant improvement in the instruments developed at CERN specifically to meet the particular requirements involved in the construction of large machines will provide a potential solution to the metrological problems encountered with the new accelerator.

10.2 Siting the Tunnel - Connection to the 28 GeV Synchrotron and West Hall

Like the ISR, the 300 GeV accelerator will be an extension to an already existing machine. The precise location of the new accelerator is determined by the actual position of the 28 GeV PS in the latter's system of reference coordinates.

The survey measurements for siting the tunnel will be made in two stages.

The first will be an external trilateration, based on the survey network of CERN I, using electromagnetic distance-measurement instruments e.g. geodimeter, tellurometer, distomat and CERN mekometer. This will be a general-purpose trilateration but will at the same time be designed specifically to fix the coordinates of the survey points at the shafts. The self-consistency of these points will be to within ± 5 mm in relation to each other and to the survey network of CERN I.

The second will be an underground traverse, the bearing being obtained by a Wild GAK 1 gyroscopic theodolite (bearing accuracy: 60 centesimal seconds); the distance will be measured with an MA 100 tellurometer (accuracy over these distances: ± 1.5 mm). The boring machine will be guided around the 6911-metre ring by a theodolite-mounted laser.

As the shafts will be located close to the long insertions which separate the superperiods, the survey system will have to be suited to this periodicity. These six shafts will, in fact, be the only possible means of connecting the trilateration on the surface with the underground traverse before the injection and ejection tunnels are bored; the traverse will start from the first shaft to be dug and will be used to guide the boring machine around the first sixth of the circumference until it reaches the second shaft, and so on. It is an absolute prerequisite of the survey system that the second shaft be already dug, to enable the 1152-metre traverse to be closed on a reference point, the coordinates of which have been determined from the surface trilateration and transferred down to the bottom of the shaft. In this way the transverse deviation of the first sixth of the circumference can be ascertained and adjusted to avoid any cumulative errors over the following sections. The precision obtained on one sixth sector is given by the standard deviation of a gyroscopic traverse:

$$\frac{L.d\alpha \ . \ \sin 1''}{\sqrt{n}}$$

where: L, the length of the traverse between two shafts = 1152 m

$d\alpha$, the standard deviation on a bearing in one station = 60 centesimal seconds

n, the chosen number of stations = 9

$$\sin 1'' = \frac{1}{636.619,772}$$

From this we obtain:

(a) transverse standard deviation = 36 mm

(b) transverse probable error (50% chance of not being exceeded, 2/3 of the standard deviation) = 24 mm

(c) transverse maximum error (99% chance of not being exceeded, 2.5 standard deviations) = 90 mm.

Levelling will be carried out by means of an automatic level; the accuracy achieved will be ± 2 mm per km.

10.3 300 GeV Accelerator Metrology

The "missing-magnet" concept affords a very considerable degree of flexibility when constructing a synchrotron of which the energy is increased in successive stages. A complete metrological scheme must therefore be devised that enables the magnets to be correctly repositioned as each energy stage is reached, since the orbit will be different in each case.

This concept calls for much more than a geometrical survey for the purpose of making measurements to determine a closed orbit, after which it may be possible for the protons to optimise their own trajectory; it requires a permanent geometrical structure so that the

accelerator components can be re-positioned prior to reaching the next energy stage. The reference marks of this structure will be located on wall-brackets (Fig. 10.1) away from the magnets and must remain fully accessible at all times. Moreover, as the synchrotron tunnel will be bored, on the average, 40 m below ground level and, at the most unfavourable point, will be at least 11 metres below the surface of the molasse, we may, on the basis of past experience with the ISR transfer tunnels, be confident of the stability of the brackets. The advantage of this system is that further surveys around the full circle of the accelerator will be needed only at the start of each new stage, prior to the installation of new magnets and realignment of those already installed. In the meantime, local alignments will be made by reference to the nearby brackets.

The 300 GeV lattice is of separated-function type and FODO configuration (Fig. 10.2). The overall circumference will be divided into six sectors, each composed of fifteen normal periods within a tunnel having a radius of 985.4 m, and a long insertion within a tunnel with a radius of 3,350 m. The latter radius was calculated to minimise the radial deviation between each component of the insertion and the chosen line of curvature (Fig. 10.3). The maximum deviation will be ± 0.30 m, which should not lead to any difficulties during the installation period.

The curved sections of the transfer tunnels TT1 and TT2 between the 28 GeV PS and the ISR were used as a model for developing the 300 GeV metrology. In the ISR, the reference figure was a chain of braced quadrilaterals. In the 300 GeV PS, however, the curvature radius prevents direct measurement of the side of the quadrilateral close to the inner wall. Consequently this quadrilateral will have only five sides; hence the term '<u>pseudo-quadrilateral</u>'. The reference figure (Fig. 10.4) will consist of a double chain of these pseudo-quadrilaterals, but for redundancy reasons three sockets belonging to two adjacent pseudo-quadrilaterals have to be aligned. The two outside sockets will be fixed to the outer wall and the middle one to the inner wall. All the distances will be measured with invar wire standardised on CERN's calibration bench (standard deviation: 0.02 mm for a distance of 64 metres) and the deviation of the middle point from the alignment will be measured against a nylon wire stretched between the two outer sockets (standard deviation: 0.03 mm).

To match the geometry to the dimensions of the superperiod, and to the cross-section of the tunnel (4 m), the 1152 m superperiod was broken down into <u>14 equal figures</u> each subtending 82.28 m of the orbit. The total circumference will thus consist of 84 figures. The starting point of the geometry of a superperiod will be the centre of the insertion, in order to ensure a good connection between the 15-period figure and the insertion (Fig. 10.5).

The geodetic adjustment methods, as developed for the ISR reference figure, provided a great degree of flexibility in meeting a schedule which was not particularly favourable for the survey; at the same time, they enabled accuracy to be improved. In the least squares method of adjustment using the coordinate variation method, the contribution made by the Metrology Group was to adopt, as the coordinates for the approximate positions, the

theoretical positions computed from the machine's parameters. The result of the adjustment gives directly the deviations for which the sockets must be corrected to bring them into their theoretical position, thus enabling the "theoretical figure" to be constructed,

The 84 figures of the 300 GeV PS will require 168 reference sockets, hence 336 unknowns, for 504 observation equations. The least squares solution is obtained by seeking to minimise the expression:

$$\sum_{1}^{420} \left[d\ell_{1.2} - \left[(dx_2 - dx_1) \sin G_{(1.2)} + (dy_2 - dy_1) \cos G_{(1.2)} \right] \right]^2$$

$$+ \sum_{1}^{84} \left[da_2 - \left[dx_1 - dx_2 + (dx_3 - dx_1)k \right] \cos G_{(1.3)} \right.$$

$$\left. - \left[dy_1 - dy_2 + (dy_3 - dy_1)k \right] \sin G_{(1.3)} \right]^2$$

where: $k = \ell_{1.2} / \ell_{1.3}$

$\ell_{1.2}$ = length between 1 and 2

$d\ell_{1.2}$ = measured length minus theoretical length between 1 and 2

$G_{1.2}$ = theoretical bearing between 1 and 2

da_2 = alingment offset of point 2 in relation to the straight line 1.3

dx_1, dy_1 = unknowns.

By using the theoretical network as an approximate network, any reference figure can be positioned before the entire circumference of the 84 pseudo-quadrilaterals has been measured. This figural adjustment based on points originating from the external trilateration enables each sixth sector to be given its precise shape, but its position is within the accuracy of the trilateration points, transferred down into the tunnel.

As soon as one of the sixth sectors has been built, the reference-sockets can be positioned on the brackets and each magnet can be aligned as it arrives in the tunnel. Once the injection and ejection tunnels have been completed, thus providing a link with the 28 GeV PS, a complete measurement of the 84 pseudo-quadrilateral figure and of the transfer tunnels will enable the six mutually-independent sectors to be converted into the geometrical structure, the position of which is dictated by the 28 GeV PS and the West Hall. Inside each pseudo-quadrilateral the magnets will be located in their theoretical position.

In the ISR, the theoretical network was used as the approximate one for the adjustments; this meant that the magnets could be installed in octants which were independently positioned in relation to each other. When the final alignment was made from the results of the last adjustment, the magnets did not need to be moved more than 8 mm.

To quote an example, the accuracy with which the sockets of the ISR reference figure were positioned was ± 13 μ for the measurements on 13 May and 25 September, and ± 24 μ for those on 30 September 1970. These results are to a large extent due to the favourable shape of the reference figure. Moreover, before any adjustment, the distance measurements were checked by solving, for each braced quadrilateral, the condition equation for obtaining a geometrical structure: the mean closure values obtained for the three sets of measurements quoted above were 23 μ, 37 μ, and 25 μ respectively.

Measurements of the radial deviation, dr, namely the deviation perpendicular to the orbit between the measured position and the calculated theoretical position, were completed on 23 October 1970 for the 132 magnets in ring I of the ISR. The dr measurement accuracy fluctuated between ± 0.02 for the magnets close to a pair of monuments and ± 0.06 mm for the magnets in the centre of the reference figure.

Inside a pseudo-quadrilateral of the 300 GeV PS, the accelerator components, either a dipole or a quadrupole located close to the brackets, will be positioned by means of invar wires. They will be used as the starting point for positioning the intermediate components housed in the 82.28 metre section of orbit separating the reference sockets. The distance between each component will be measured with an invar wire and the radial position will be determined by measuring the offset between the reference sockets on each magnet and a straight line provided by a nylon wire stretched between the two reference marks of the magnets located near the brackets, as was done for the curved sections of the transfer tunnels.

Attempts were made to check, in the ISR, the reliability of a closed-circuit hydrostatic level. Although the results were sufficiently encouraging to justify the continuation of research in this direction, we had no choice but to use a spirit-level for the actual survey. Spirit-levellings, starting from a PS bench-mark, were carried out through transfer tunnels TT1 and TT2. The results of these levellings indicate the stability of pillars 22 and 77 located at the junctions between the tunnels and the ISR. The sockets on these pillars were used as the reference bench marks for the spirit-levelling of the complete ring. The mean levelling closure error is ± 0.5 mm for the 1 km circumference. The heights of the sockets on the pillars deduced from the least square adjustment of the circuit closing errors are used for levelling each individual magnet. The standard deviation of the dz - vertical deviation between the measured value and the theoretical value - given by a check on ring I undertaken on 20 October 1970, was 0.07 mm.

For the 300 GeV PS, it is expected that, over the 1152 metres of a superperiod, the same accuracy will be achieved in determining the height of the reference sockets. Inside a pseudo-quadrilateral, the accuracy will be the same as for the ISR magnets.

The mean dt value - radial tilt of the magnets - should be less than ± 0.02 mr, as achieved in the ISR.

Although the overall geometry is less favourable than in the ISR, it is expected that the r.m.s. error in position of magnet centres will be at least as good as 0.15 mm in both vertical and horizontal planes (Chapter 2).

10.4 Conclusion

Ground movements, consequent displacement of the sockets of the reference figure, magnet misalignments and inhomogeneities in the magnetic field, all have practically the same effect on the orbit of the accelerated protons.

The rate at which measurements were completed on the ISR represented an improvement on that previously achieved on the 28 GeV PS. The way in which the computations were carried out, and the large number of redundant observations make it possible to define the accuracy with which the accelerator components had been positioned. A comparison of successive sets of measurements will, therefore, enable slight movements of the sockets to be distinguished from position errors due to measurement uncertainties which cannot be overcome with the methods used.

In spite of the fact that the shapes of the reference figures in the 300 GeV PS are much less amenable than in the case of the ISR, it should be possible to achieve the required accuracy; either by conventional methods such as invar wires with CERN distinvars or revolutionary ones such as nylon fishing lines for alignments over distances greater than 100 m. If new instruments based on electromagnetic distance-measurement achieve an accuracy equal to or better than that of the invar they would naturally be tested, built and used for metrological work on the 300 GeV PS.

As the new accelerator will be sited next to CERN I, the ISR calibration bench, whose microscope and 4-metre standard rule have already served for the survey of the 28 GeV PS, can be used for all tests on the new equipment as well as for calibration of lengths shorter than 64 metres; it will be necessary to lengthen this base to 83 metres to meet the needs of the new project. An annual budget of 200'000 SF should prove sufficient, provided the present situation is not disturbed by the advent of new electronic equipment.

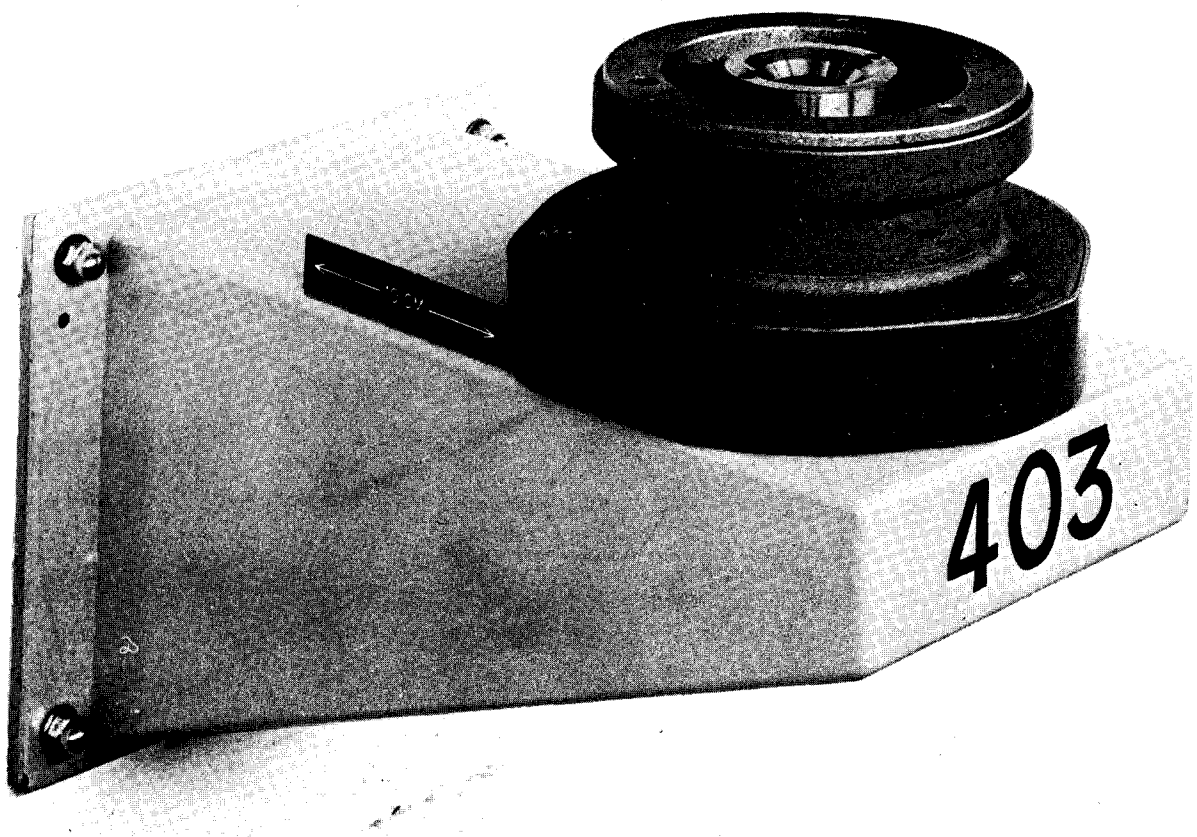

Fig. 10.1 Bracket or Cantilever fixed to the tunnel wall with adjustable socket carrying the precision hole

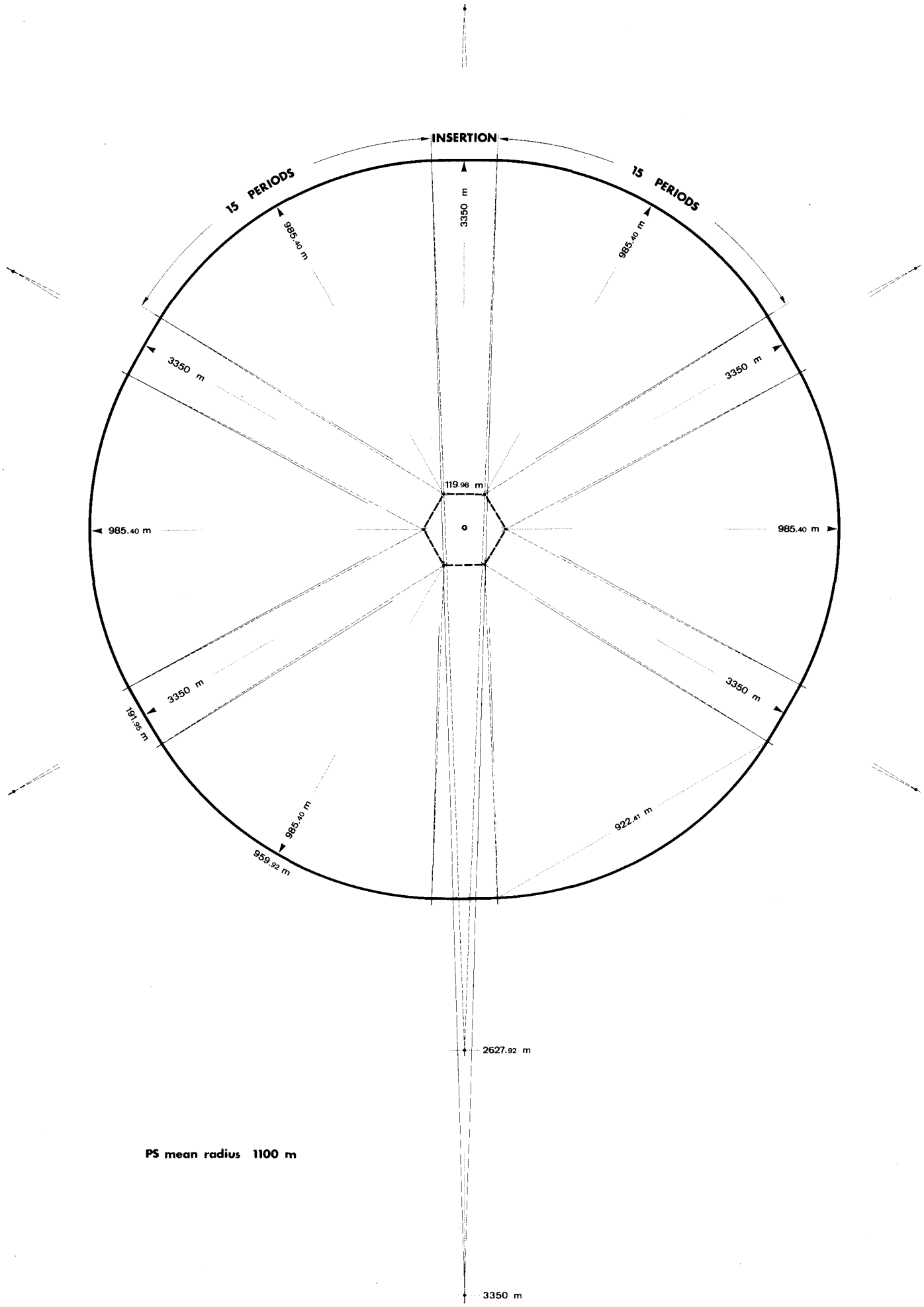

Fig. 10.2 300 GeV PS Geometry

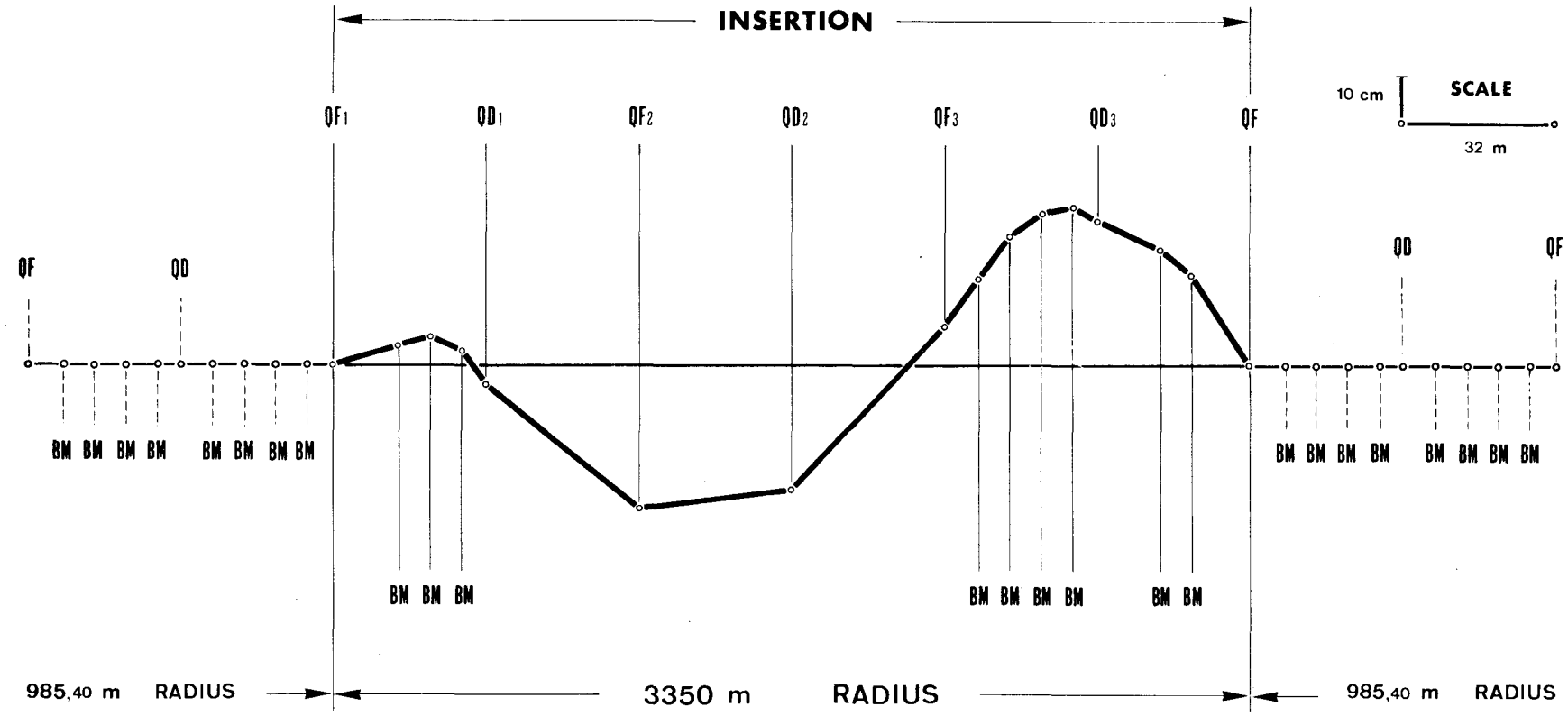

Fig. 10.3 Location of the theoretical orbit in relation to the 3350 m radius arc used for positioning the tunnel

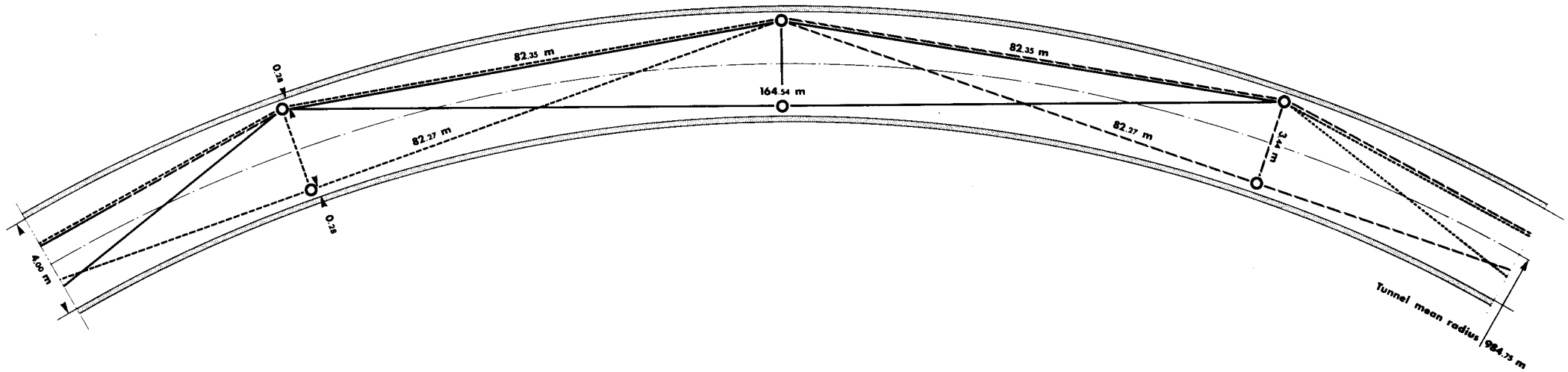

Fig. 10.4 Basic metrological scheme for the 300 GeV Synchrotron

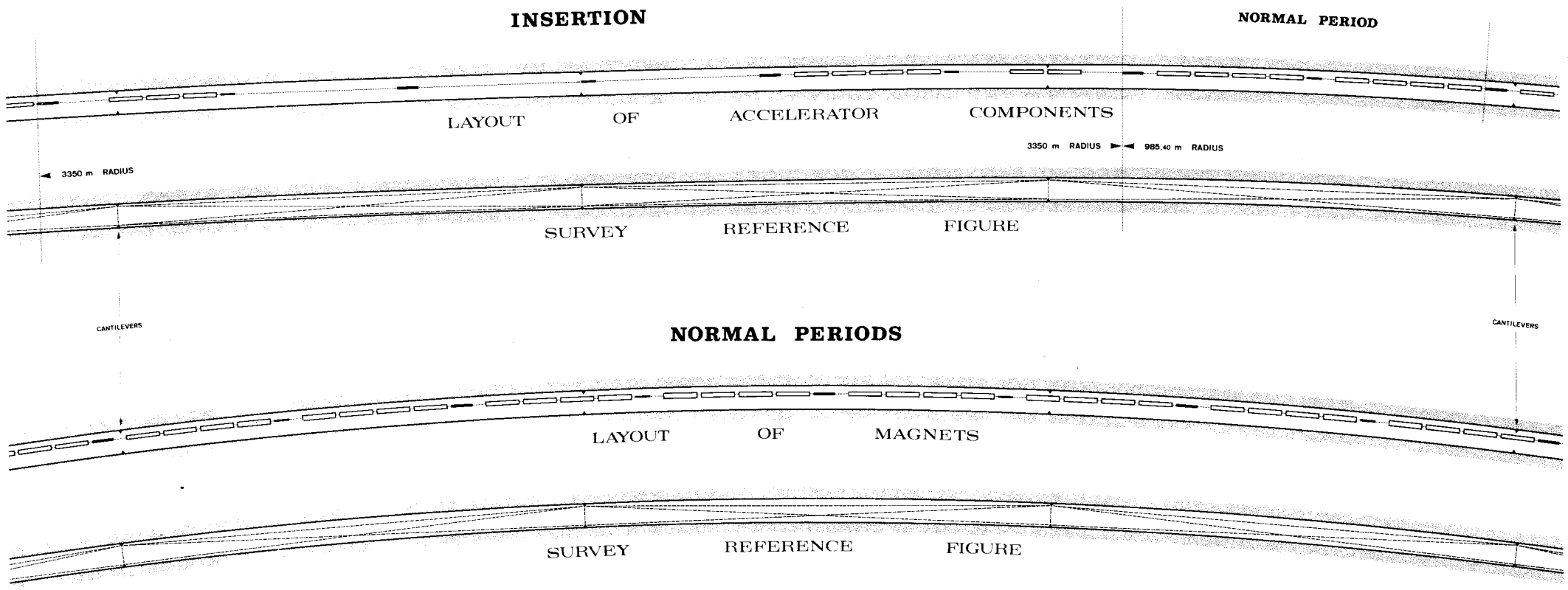
INSERTION
NORMAL PERIOD
LAYOUT OF ACCELERATOR COMPONENTS
3350 m RADIUS
985.40 m RADIUS
3350 m RADIUS
SURVEY REFERENCE FIGURE
CANTILEVERS
NORMAL PERIODS
CANTILEVERS
LAYOUT OF MAGNETS
SURVEY REFERENCE FIGURE

Fig. 10.5

Chapter 11

THE RADIATION PROTECTION SYSTEM

11.1 Introduction

Radiation problems are mainly concerned with the radiation hazard to personnel due to operation of the accelerator and the effects of radiation on the different materials used. In this Chapter we have summarized these problems as far as they affect the design of the main synchrotron ring and experimental areas.

For a general discussion of many of the radiation problems we refer to the Design Report of the CERN Study Group on New Accelerators, to the ECFA Reports, and to the CPS improvement study, which give some of the basic information. In addition to these, we base this Chapter on the increased operational experience with ejected beams and on new Monte Carlo calculations for shielding and induced activity estimates which have been shown to agree well with available experimental data. A detailed list of references complementing the few given in this Chapter can be found in Machine Committee Report MC/50.

The proposed location and level of the main ring tunnel provides sufficient natural shielding to cope with the low dose rate requirements for the population at large and to allow the present use of the countryside above the accelerator to be continued without disturbance.

The proton losses envisaged in the main ring will keep dose rates from induced radioactivity and radiation damage to acceptable levels.

The proposed use of the West Experimental Area with reduced intensity will not create important radiation problems. The North area can be designed to accept the full proton beam at a comparatively low cost. The radiation problems there do not present insuperable technical difficulties.

11.2 Biological Requirements

11.2.1 Population at large and individual members of the public

The recommendations of the International Commission on Radiological Protection (ICRP), which have been accepted by France and Switzerland, give acceptable limits for radiation exposure for different groups of persons. The limit for the population at large is 5 rem/30 y and for individual members of the public is 0.5 rem/y. CERN has adopted the Swiss inter-

pretation of these general rules so that the dose in an unsurveyed area must not exceed 5 rem/30 years. The yearly average derived from this limit is 170 mrem.

As to date it is not very probable that ICRP will change their recommendations, the presently adopted regulations in France and Switzerland are a safe base for the design of such a long-term project as the 300 GeV accelerator. Interpretation of these regulations in special cases would be subject to agreement with the authorities concerned.

11.2.2 Radiation workers

The limits of exposure of radiation workers recommended by ICRP have been adopted by all CERN Member States. The whole body exposure* is limited to 5 rem/y for adults over the age of 18 years. For 2000 working hours per year this gives an average dose rate of 2.5 mrem/h. The whole-body exposure is restricted to 3 rem in any 13 consecutive weeks but there are no limitations on the rate of accumulation within this period.

11.2.3 Radiation protection policy and adopted levels of acceptable exposure

Radiation protection for the 300 GeV project has to comply with the national regulations in France and Switzerland as well as with those in all the other CERN Member States, however, since all the countries have based their national regulations on the recommendations of the ICRP there are practically no differences in the acceptable limits of exposure.

For the 300 GeV Design we assume that everywhere outside the CERN site the radiation levels should be below 5 rem/30 y = 170 mrem/y. This means in practice that the average dose rate at the CERN fences should be $\leq$ 30 µrem/h. For non-restricted radiation areas inside the CERN site the limits are 2.5 mrem/h; for areas with higher dose rates access and work in the area has to be restricted.

Access to radiation areas should be regulated such that undue exposure of persons is avoided. It is a good practice to limit the exposure of each radiation worker who is regularly performing work in areas of high dose rates to one-half of the permissible average dose rate. In areas where dose rates are above 6 rem/h work should be performed by remote manipulation.

---

* Different limits are given for the exposure of the different parts of the body, for instance, 75 rem/y for the fore-arms, hands, feet and ankles, and 30 rem/y for the skin, thyroid and bones.

11.3 The Interaction of Primary Protons and the Nuclear and Electromagnetic Cascades

11.3.1 Primary proton interactions

The interaction of protons in machine components is the starting point of all radiation problems. In routine machine operation practically the total beam interacts in external targets and beam dumps. In ejection septa or beam scrapers in the main ring not more than 2% of the total beam is expected to interact. In quiet regions of the main ring no single magnet will receive more than 0.01% of all accelerated protons. The following table gives the number of interacting protons at some typical locations.

Table 11.1

Elements	Proton Momentum P_o (GeV/c)	Number of interacting protons per pulse
External target { North area	400	10^{13}
External target { West area	200	10^{12}
Beam dump { North area	400	10^{13}
Beam dump { West area	200	3.10^{12}
Ejection septum	200-400	10^{11} compare with description of the ejection system
Beam scraper	200-400	2.10^{11} (see Chapter 12)
Random loss point in main ring { average	400	10^{8}
Random loss point in main ring { maximum	400	10^{9}
Loss point in EPB	200-400	10^{11} (3.10^{10} towards West area)
Injection in main ring	10	3.10^{12}

To allow for adequate shielding of the main ring we assume a maximum intensity of 10^{13}/protons per second at a top energy of 1000 GeV. For all other radiation problems we consider only a maximum intensity of 10^{13} p/pulse at 400 GeV with 6.10^{6} pulses/year: for dose rate calculations we assume a pulse repetition frequency of one per 3 seconds. As discussed in the section describing the ejection system, scattering of protons in septa or scattering in targets leads to an effective line source downstream of these elements in the main ring. Similar loss distributions occur along the external proton beam lines and along secondary beam lines. Such beam losses have been observed in present accelerators.

In addition to the protons interacting at or near full energy one expects losses of 10 GeV/c protons at injection in the main ring; this represents a radiation problem similar to the operation of an internal target at the CPS[11.1,2].

11.3.2 The nuclear and electromagnetic cascades

The primary proton interactions induce the development of hadronic and electromagnetic cascades which transport and deposit the energy of the interacting protons in matter. The development of these cascades especially in the energy region of interest here is not completely understood. The main features of the cascades which are relevant for assessing the radiation problems are, however, now sufficiently well known. The transport and spatial distribution of the cascade in shielding materials and in the material of accelerator components is determined by the cascade of hadronic particles with energies above 100 MeV. The dominant mechanism of energy disposition at the envisaged energies is, however, the electromagnetic cascade induced by the decay of π^{o}-mesons into gammas. The radiation transport in transverse direction with respect to the primary beam is determined by the hadronic cascade. The shielding in forward direction is, however, determined by penetrating muons from the decay of charged π and K mesons. The radiation transport in ducts and tunnels is dominated by fast neutrons.

The three-dimensional development of the hadronic-electromagnetic cascade in the proton energy region of interest can be described by Monte Carlo calculations[11.3]. The transverse development of the nuclear cascade can also be described by approximate analytical techniques starting from the diffusion equation[11.4]. The results of the two approaches are in mutual agreement and in addition are consistent with the experimental results obtained at present accelerators.

The essential physical assumptions which enter into the cascade calculations at several hundred GeV are:

(i) The absorption cross-sections of hadrons on nuclei are assumed to remain constant above 20 GeV. This assumption is in agreement with most of the current theoretical models and with cosmic ray experiments.

(ii) The momentum spectra of hadronic secondaries created in hadron nucleus collisions are described in the calculation by empirical extrapolation formulae, which were fitted at present accelerator energies to experimental data. Extrapolations with these empirical formulae agree rather well with the predictions of models like the thermodynamical model or the multi-Regge model, with the scaling behaviour as predicted by Feyman and with the hypothesis of limiting fragmentation.

The energy deposition by the electromagnetic cascade is now well understood theoretically and experimentally (see for example Ref.(11.5)).

Monte Carlo cascade calculations have been performed for a variety of geometrical arrangements which resemble closely to situations around an accelerator, for example:

(i) A massive cylinder which represents either an end-stop or a target,

(ii) a target in front of or inside a hollow cylinder, representing a target in front of a magnet unit or a target or beam stopper inside an empty tunnel,

(iii) a target in front of a sandwich magnet,

(iv) a line source, representing the target, vacuum tube and some magnet units inside a cylindrical tunnel.

The most useful results of cascade calculations relevant to radiation problems are the following:

(i) The flux density of particles, used to determine the necessary shielding.

(ii) The density of hadronic interactions (hadronic cascade star density) which is closely related to the induced radioactivity.

(iii) The energy deposition density in the material which is equivalent to the direct radiation dose or the heat deposited in the material[11.3,6].

In Fig. 11.1 we give as an example of such a calculation the star density and dose per proton interacting in a target as a function of radius in an iron cylinder 10 m downstream. The star density is given for the front face of this cylinder but the dose is that applicable to the maximum of the build up curve.

11.4 Shielding

11.4.1 General method of shielding estimates

a) Shielding against strongly interacting particles

Estimates of the attenuation of hadron flux densities are based on experience at 25 GeV extrapolated to 300 GeV and on Monte Carlo cascade calculations. Flux densities obtained outside the shield, and consequently the attenuation requirements, are assumed to be correct within a factor of 3. The stray flux outside the shield is assumed to scale with energy as $E^{0.7}$, and for calculating the attenuation in earth or rock at places where the radiation is in equilibrium we use an attenuation length of 115 g/cm^2. For an equilibrium spectrum we assume 1 mrem/h = 3 part ($\geq$ 20 MeV)/cm^2 s and = 1 part ($\geq$ 100 MeV)/cm^2 s.

b) Shielding against muons

The estimates for the muon shielding are derived from the calculations of Kuhlmann and Wüster[11.7] and those of Keefe and Noble[11.8]. In addition to the angular distribution of pion production the deviation of pions and of muons by magnetic fields and the effects of collimators are also to be considered. We use simplified calculations to obtain an overall estimation of muon fluxes and shielding required. More detailed work is in progress to arrive at a refined shielding layout. The character of these estimates impose a more conservative attitude for the width of the muon back-stop than for any other shielding requirements. At the energies considered 10 muons/(s cm^2) are equivalent to 1 mrem/h.

11.4.2 Shielding of the main ring

A 5% local beam loss was assumed. For dose rates $\leq$ 5 µrem/h on the shielding surface due to hadrons (this factor of 6 allows for contributions from other sources of radiation or contamination) the transverse shielding required is as follows:

Table 11.2

GeV	p/sec	g/cm^2	$\rho = 1.8$ m	$\rho = 2.2$ m
300	$3 \cdot 10^{11}$	2400	13.5	11
300	$3 \cdot 10^{12}$	2650	15.0	12
1000	10^{13}	2900	16.0	13

From this table we see that to obtain sufficient attenuation for the assumed conditions we need 16 m of earth (ρ = 1.8) or 13 m of rock (ρ = 2.2). Estimates show that the dose rate from muons is lower than from hadrons at the surface. The lowest surface level on top of the main ring periphery occurs near bore hole S1/S2 (about 422 m above sea level). The top layer of the molasse rock occurs at 415 m above sea level. In order to provide a total of about 2900 g/cm^2 we would need about 8 m of molasse rock shielding (1700 g/cm^2) in addition to the 7 m of earth and gravel (= 1250 g/cm^2). From the radiation protection point of view the floor level of the ring should therefore not be higher than 403 m above sea level. With the ring tunnel bored at 400 m above sea level (lowest point of the circular tunnel) a comfortable safety margin is provided. With this shielding, nowhere on top of the ring will the stray radiation field impose restrictions on the use of the area.

Around the circumference of the main ring there will be 6 access shafts; two of them are at the ejection straight sections and one at the injection region. The shafts are 20 to 70 m long and are connected with the ring by horizontal access tunnels. It is the dose rate due to the escape of fast neutrons which determines the design of the access tunnels. The attenuation required is $4 \cdot 10^5$ for a 1% beam loss distributed over the whole ring allowing for random fluctuations of an order of magnitude in the loss at any given position. Access tunnels to the long straight sections are to be > 20 m upstream of the position of the first septum in the ejection straight sections.

In order to calculate the neutron attenuation through such access tunnels, the computer programme ZEUS ALB[11.9], a three-dimensional monokinetic Monte Carlo calculation, was used. This programme was successfully checked by comparing flux density measurements in the CERN PS access tunnels with the computed attenuations[11.10]. Examples of access tunnels are given in Fig. 11.2 and the three cases are compared in the following table.

Table 11.3

Position	Attenuation		
	15 m straight (i)	40 m straight (ii)	25 m curved (iii)
Mouth	1	1	1
Entry into chamber	40	10^3	$2 \cdot 10^3$
Roof of chamber	$8 \cdot 10^2$	$2 \cdot 10^4$	$4 \cdot 10^4$*
18 m shaft	$5 \cdot 10^4$	$1.5 \cdot 10^6$	$3 \cdot 10^6$
30 m shaft	$2 \cdot 10^5$	$5 \cdot 10^6$	$1 \cdot 10^7$
50 m shaft	$8 \cdot 10^5$	$2 \cdot 10^7$	$4 \cdot 10^7$
70 m shaft	$1.6 \cdot 10^6$	$4 \cdot 10^7$	$8 \cdot 10^7$

*This is the same attenuation ($4 \cdot 10^4$) as for a 50 m straight tunnel.

The three solutions require a strict beam loss control in the ring sections near the access shafts; they are adequate if for solution (i) a concrete cover of 60 cm is provided on the top; the same is needed for a magnet shaft located 15 m from the ring tunnel. The curved tunnel solution is the most convenient as it does not require additional shielding or very long tunnel sections.

We have assumed that there is a connection chamber at the bottom of the shaft of about $8 \times 8 \times 8$ m^3. Reflection of neutrons from the walls of this chamber into the vertical shaft is small.

11.4.3 Shielding of ejection tunnels

The transfer tunnel to the West Experimental Area will pass underneath Route Nationale 84 (RN 84). Assuming losses of the order of $3 \cdot 10^{10}$ p/(pulse . 100 m) as described above, the transverse shielding required is 1500 g/cm^2, or about 8 m of earth. In order to control the dose rate at RN 84 external monitors are necessary to stop the EPB if dose rates become unacceptably high. These external monitors are needed in addition to beam loss monitors inside the tunnel (see Chapter 9).

The muon flux density will be small at RN 84 ($\approx$ 0.01 μ/cm^2 s). Beam losses in the rising section of the EPB will create muon flux densities of $2 \cdot 10^3$ cm^2 s in front of the rising section of the tunnel on the shielding surface above transfer tunnel 4 (TT4). The transverse shielding on TT4 upstream of the neutrino target will be provided by 1500 g/cm^2 of earth. Ejection beam dumps will be located in the first section of the transfer tunnels.

The transfer tunnel to the North Experimental Area will reach the EPB level (6 m below ground) at a point 170 m from the fences of the new site. Hadrons and muons will not create dose rates greater than 30 μrem/h at the CERN fences as this beam will remain underground up to the target stations. Upstream of the targets a minimum of 6 m of earth transverse shielding ($\sim$ 1200 g/cm^2) or the equivalent in concrete must be provided for a beam loss of $\leq 10^{11}$ p/pulse.

11.4.4 Shielding of the West Experimental Area

The hadron shielding required near the targets for 10^{12} p/pulse interacting in each target is of the order of 1900-2000 g/cm^2; 2400 g/cm^2 is needed for the transverse shielding of the hadron back-stop and 1700 g/cm^2 for the transverse shielding of the decay tunnel of the neutrino experiment. The difference in shielding for hadrons between 200 GeV and 300 GeV primary proton energy is less than 50 g/cm^2 transversally. The transverse hadron shielding provides an effective attenuation also for sideways scattered or deflected muons. In the forward direction for 200 GeV, a muon back-stop consisting of a 90 m long 4.80 m wide 3.60 m high steel plug is required. This includes the effect of deflections by a magnetic field of 7.5 T x m at a distance of 15 m upstream of the back-stop. For a different target layout the shielding will need to be re-evaluated. For 300 GeV the length of the back-stop is 140 m whereas the transverse dimensions remain the same. The following table summarizes the transverse shielding requirements for the West Area.

Table 11.4

	p/pulse interacting	dose rate (in µrem/h) at fences	dose rate (in µrem/h) at shielding surface	transverse shielding g/cm^2
Target T_ν	10^{12}	20	40	1950
Decay tunnel	10^{12}	10	40	1700
Target T1	10^{12}	15	150	1900
Target T2	$2 \cdot 10^{12}$	15	400	1850
Back-stop	$2 \cdot 10^{12}$	15	400	2400

11.4.5 Shielding of the North Experimental Area

The EPB and secondary beam lines will normally be below ground level. The EPB will supply different experimental areas; all targets could be installed at the EPB level underground at $\sim$ 445 m above sea level. With such layout advantage can be taken of the rising site around the experimental strip for muon shielding. The muons from an experimental area will not affect the background of the next downstream area, the areas can be well enough separated in angle and/or distance. The underground EPB and the natural muons shielding imply important savings in shielding material.

The shielding requirements in this area are determined by the dose rate limits for radiation areas and the background requirements for experiments. For 10^{13} protons/pulse interacting in a target, the lateral shielding needed is 1700 g/cm^2 around the target. For the undisturbed EPB (losses $\lesssim 10^{10}$ p/pulse) the lateral shielding required is about 1000 g/cm^2. Dose rates will be less than 30 µrem/h outside the fences of the new CERN site at $\sim$ 200 m from the target.

11.4.6 Skyshine

The roof shielding of the accelerator and experimental areas has been designed to give dose rates at the perimeters of the site lower than those permissible for the population at large on the assumption that the fence is in full view of the part of the shield where the dose rate is highest. Air and roof scattering considerations can only reduce the estimated dose rates at the perimeter.

11.5 Induced Radioactivity

11.5.1 General method for estimating induced activity dose rates from remanent activity

An accurate prediction of the dose rates to be expected due to remanent activity in the 300 GeV accelerator would involve (i) a knowledge of the fate of every proton accelerated, i.e. where it interacts, and (ii) a knowledge of the development of the hadron cascade in the different materials and complex constructional geometry of the components used in the accelerator. We use hadronic cascade star densities, obtained by Monte Carlo calculations in different idealized geometries to estimate the induced activities and gamma dose rates from the radioactive isotopes produced[11.11]. The calculations have been compared with measurements at the CPS. The calculations of remanent dose rate are standardized for a 30-day irradiation period and a 1-day cool down time; dose rates one hour after shutdown can be expected to be 3-4 times higher than those quoted. Similarly, the dose rates quoted are those in contact with the active materials. For very large components the dose rate at 40 cm from the surface could be about a factor of 2 lower than this, but when the activity is concentrated in a small volume the reduction will be about a factor of 10, and a factor of 100 for very small items. However, the surface dose rate, which includes the contribution from soft β and X-rays, could be up to a factor of 10 times higher than the dose rate quoted.

11.5.2 Radioactivity in the 300 GeV ring

a) Radioactivity in the accelerator structure

The radioactivity in the accelerator structure is mainly confined to regions of large beam losses close to septa and scrapers. Some typical values estimated for the 300 GeV components and dose rates measured at the CPS normalized to the beam losses stated in Section 11.3 are given in the following table.

Table 11.5

Contact Dose Rates for a 10^{11} p/pulse Loss
24 h after end of a 30-day operation

	300 GeV machine	CERN-PS
Magnet surface (quiet region)	20 mrem/h	1 mrem/h
First magnet following septum/ target	40 rem/h (5 cm from orbit)	0.2 rem/h (50 cm from orbit)
Beam scraper	20 rem/h	-
Septum	500 rem/h (surface dose rate)	-
Septum tank contact	2-10 rem/h (10 cm from orbit)	3-10 rem/h (7 cm from orbit)

b) Radioactivity in the tunnel walls

The remanent dose rate due to induced activity in the tunnel walls depends mainly on thermal neutron capture by the sodium content of the concrete. Near the wall the contributions to the dose rate from the magnets and the wall (1% Na) are approximately equal. In quiet areas of the machine this dose rate will be < 1 mrem/h, but in the regions of the ring containing septa and scrapers the dose rate from activity in the concrete near the tunnel walls will be $\sim$ 100 mrem/h.

11.5.3 Radioactivity in the transfer tunnel

With an assumed loss of $3 \cdot 10^{10}$ ppp due to ejection in the transfer tunnel from the 300 GeV PS ring to the West Experimental Area, we could expect dose rates at the most exposed surface of beam transport elements to be $\sim$ 6000 mrem/h; the dose rate near the tunnel wall will be $\sim$ 30 mrem/h. These figures are based on a loss occurring at a single point: the average dose rates in this region will be at least a factor of 10 lower.

Dumps for 1% of the beam* are to be installed at the upstream end of the transfer tunnel, and in these regions the dose rates will be high. At the entrance face of a 40 cm diameter steel dump up to 10^3 rem/h can be expected locally; at the outer surface of the dump the contact dose rate could be up to 10 rem/h. These dumps will need to be installed in a specially constructed tunnel section; the dump could itself be a short 'stub' tunnel.

---

* Resulting from the test and setting up periods integrated over the year.

11.5.4 Radioactivity in target stations

The radioactivity induced in external targets and in downstream beam transport elements as well as in the shielding around the target is, together with the activity induced in the dumps, the most important radiation hazard when the accelerator is shut down. Even though one particular target station may not be in use continuously, at the end of a period of one month's operation the dose rate from induced activity will be close to the saturation dose rate. The following table gives estimated dose rates for the most active components in an achromatic target station (see Chapter 13).

Table 11.6

Dose Rates in Target Stations
(beam intensity $3 \cdot 10^{12}$ protons/pulse at 200 GeV/c)

Component	Dose rate (rem/h) (contact)
Target (2x2 mm^2)	$6 \cdot 10^6$
M1 magnet, pole face - front	$4 \cdot 10^3$
- most active part	10^4
M1 magnet, outer surface	40
SM1 sandwich magnet - front face	10^3
- outer face	10
SM4 sandwich magnet - front face	$2 \cdot 10^2$
- outer face	2
Collimator front	10^5

The steel walls of the target station will also become radioactive; under the above beam conditions dose rates $\sim$ 10 rem/h can be expected close to the inner surface of the target station from the walls alone. Dose rates on the outer surface of the 1 m steel shielding around target station 1 will be $\leq$ 50 mrem/h.

11.5.5 Radioactivity in cooling water

Cooling water for the r.f. cavities, magnets and quadrupoles of the main ring will be contained in a closed circuit. The majority of the long-lived activity in demineralized water will be removed in an ion-exchange column. Water from such cooling circuits should not be discharged into the normal drainage system. Pipes from the ring and primary beam lines carrying radioactive water must not pass through occupied areas or unshielded areas outside the fences where the required dose rate levels are low. The highly radioactive cooling water from target stations must be kept separate from the other circuits. Most of the induced radioactivity in water has short half-life; it therefore decays quickly when the accelerator is off.

11.5.6 Radioactivity in ground water

Surface water will not be able to penetrate the dry molasse rock through which the accelerator ring tunnel is bored, apart from a small amount of seepage down the vertical shafts drilled into the molasse. Measurements of ground water activity at the CERN-PS have shown that this activity is insignificant[11.12]; most of the activity is retained in the earth by ion exchange processes. It would be prudent to arrange for water draining past the ejection tunnels and North Area (target stations) to be collected and not released into the normal drainage system without first checking its activity.

11.5.7 Radioactivity in air, ventilation system

a) Production of gas and radioactive aerosols

The most frequent isotopes in air activation are ^{13}N, ^{15}O, ^{11}C, ^{41}A and ^{7}Be. Some of the gaseous products may form aerosols; these can also be formed by activation of dust when suspended in the air or deposited on highly irradiated surfaces. Aerosols may be a product of erosion of radioactive walls or corrosion of active machine parts. Generally aerosols and dust have a much lower specific activity than activity in a gaseous form.

Exposure to air activity is dominated by the external radiation rather than by the hazard due to internal radiation.

b) Ring tunnel

The saturation concentration of gaseous activity in the ring at machine stop is about $3 \cdot 10^{-5}$ $\mu Ci/cm^3$ assuming a loss of $6 \cdot 10^{11}$ p/pulse. After 15 minutes the activity of the isotope mixture has decayed to less than 1/10th of its initial value or to about the same order of magnitude as the maximum permissible concentrations. Therefore access to the ring tunnel is not restricted by air activation. A ventilation rate of the ring of 10%/h (see Chapter 15) implies an evacuation velocity of about 4 linear metre/min in the three exhaust shafts. Thus radioactive air from the tunnel will arrive at the tunnel's exit after about 10 minutes and due to decay the radioactivity will not exceed permissible limits for radiation workers. The maximum permissible concentration for the population at large is 1/100th of that for radiation workers. The hazard from radioactive gases should be 1/10th of that from other radiation sources and consequently a dilution factor of about 1000 is required. The predominant meteorological conditions in the valley (only two-wind direction and frequent inversions) are conducive to the deposition of any airborne activity in localized regions. Thus in addition to providing a means for suitable dilution, filters to trap suspended activities (e.g. ^{7}Be) will also have to be installed.

c) Target stations*

We expect that the specific air activity in the target station of the West Hall will be

---

* This estimation assumes that no vacuum can be provided in the target station. With an evacuation box containing all the elements of the target station no air activation problem would occur.

$2 \cdot 10^{-2}$ $\mu Ci/cm^3$. In the North Hall the concentration could be as high as 10^{-1} $\mu Ci/cm^3$. It follows that air from target stations must not be released to experimental areas but must be filtered and scrubbed before recycling ($\sim$ 10 times/h) or exhausting (dilution $1/10^4$ - $1/10^5$).

11.6 Radiation Damage and Radiation Heating

11.6.1 General aspects

Materials and components subject to radiation damage and hence limited life, are used in the construction of particle accelerators and auxiliary equipment. In order of importance these are:

(i) Magnet coil insulation and adhesives used for laminations,

(ii) cable insulation, hoses, vacuum seals, lubricants, etc.,

(iii) special electronic components, for example, transistor and other semi-conductor devices and optical components,

(iv) magnet steel and ferrites.

In addition to the foregoing, attention is given to the acceleration of metallic corrosion by the products of radiolysis of air and water.

11.6.2 Radiation dose levels

The doses mentioned in the following table refer to maximum yearly dose rates obtained by Monte Carlo calculations compared with measurements performed at the CPS and at NIMROD[11.1,13].

Table 11.7

Maximum Yearly Dose Rates to Components in rad

($6 \cdot 10^6$ pulses/year)

Components	Quiet regions		Eject. reg.*	Target stations* (maximum values)	
	max.	average		10^{12} p/p 200 GeV	10^{13} p/p 400 GeV
Magnet coils	5.10^7	5.10^6	5.10^9	10^{11}**	2.10^{12}**
Magnet steel	10^8	10^7	1.10^{10}	2.10^{11}***	5.10^{12}***
Control boxes on top of magnets (semi-conductors etc.)	10^4	10^3	-	-	-

* Hot regions: only a small area of the accelerator will be highly exposed.

** 7 cm from beam, maximum build-up.

*** 2.5 cm from beam, maximum build-up.

11.6.3 Control of radiation damage by selection of materials

a) Organic materials

A wide range of plastic materials and components are available which are capable of withstanding radiation doses of 10^9 to 2.10^{10} rad[11.14]. An important class of organic materials is the epoxy group. These materials are used for fabricating the magnet coil insulation. The radiation resistance* of unfilled and unreinforced epoxy resin systems currently available for use as impregnation materials in the coil making industry in Europe is limited to 5.10^9 rad. However, various epoxy resin pre-impregnated glass mica tapes used as insulation for magnet windings are available up to 1.10^{10} rad. Newly developed glass reinforced resin systems, tested as sample, are practically not attacked at 1.10^{10} rad and some are reported to withstand 2.10^{10} rad[11.15].

The radiation resistance of elastomeric components is limited to 2.10^9 rad[11.14]. A number of oils and greases tested to levels of 2.10^9 rad are available[11.14].

b) Concrete and ceramics

These materials withstand irradiation better than organic materials. Low power bending and quadrupole magnets have been made with concrete insulation. Ceramics have also been used for magnet construction. A variety of inorganic materials are also being used for cable insulation[11.16].

c) Electronic components

Semi-conductors are the most radiation sensitive electronic components. Changes have been observed in some components at doses of 10^4 rad equivalent. If, therefore, they must be used in radiation environments, they should be carefully selected and installed as far as possible away from the radiation source. Other electronic components such as capacitors, etc. must also be carefully selected. Radiation sensitive organics must be avoided in these components[11.14].

d) Metals

Permeability changes in magnetic materials can be expected to occur at doses of 10^9 rad (soft magnetic materials) and 10^{12} rad (permanent magnetic materials). These changes in μ saturate at about the 20% level, leading to only small changes in the magnetic field properties.

e) Effects on corrosion

Although corrosion of metals in aqueous media has been observed to increase under radiation, it is estimated that this problem can be kept in hand by taking adequate precautions, i.e. water purification, resistivity and pH control, use of appropriate inhibitors, etc.

---

* Radiation dose (rad) to reduce the mechanical properties (flexural, tensile or shear strength) to 50% of its initial value.

Agressive chemicals produced by the irradiation of moist air in the tunnel consists of ozone and a mixture of nitrogen oxides. These chemicals might introduce corrosion problems to exposed surfaces. The ventilation rate in the ring tunnel also determines the concentration of corrosive gases. For an average of 6.10^{11} p/pulse lost in the ring we would have a concentration of about 0.1 ppm of noxious gases within 10 hours corresponding to the maximum permissible concentration in air. With an air exchange of 10%/h the concentration of these gases is also acceptable.

Much of the problem associated with radiation damage effects can be limited by adopting, where possible, one or more of the following procedures:

(i) use of radiation resistant materials where possible, for example, the use of inorganic insulation instead of plastic materials. The use of metallic vacuum seals, aluminium extensions on the water cooling hoses, etc.,

(ii) the placing of many essential components outside the radiation environment,

(iii) local shielding of vital components, for example, electronic components in control boxes on top of magnets,

(iv) replacement of components has to be considered for equipment which will inevitably be subject to high radiation levels.

11.6.4 Radiation heating

Cascade calculations of the energy deposition in targets[11.6] are in good agreement with experiments at 12 and 24 GeV/c. The calculations at 300 GeV/c are expected to have errors of up to 30% due to the somewhat arbitrary assumptions on π^o production in inelastic events. The following table gives instantaneous temperature rises during one short burst, without considering heat dissipation.

Table 11.8

	P_o(GeV/c)	Number of incident protons	ΔT (^oC)
Cu target 2×2 mm^2	300	10^{13}	1000
Al target 2×2 mm^2	300	10^{13}	350
W target 2×2 mm^2	300	10^{13}	3700
Pole face of sandwich magnet with 2 cm gap	300	10^{13}	10
Fe beam dump, beam 2 mm Ø (maximum)	300	10^{13}	1000

At intensities of about 10^{13} protons it is proposed to use rotating thin discs as targets; this reduces for long bursts easily the heat density by a factor 50 to 100. The construction of collimators and beam dumps has to allow the dissipation of up to 500 kW of power. Solutions similar to the ones applied at the ISR are envisaged.

11.7 Recommendations and Particular Protection Measures

11.7.1 Control of intensity of stray radiation

The stray radiation outside the shielding enclosure and induced activity in the accelerator can most efficiently be controlled by reducing unwanted interactions of the accelerated protons. Beam losses inside the ring and the ejection tunnels will be controlled with respect to both magnitude and location to comply with the conditions for which the shielding has been specified. Radiation monitors are needed in areas where the dose rate has to be controlled within close limits; these will be interlocked with the acceleration or ejection systems. Besides these reactive monitors, area surveillance is provided by recording monitor stations and survey measurements.

11.7.2 Control of induced activity by material selection

The production of induced activity can only to a limited extent be controlled by selecting material in which the primary protons interact. For example Cobalt and Nickel steel should be used as little as possible. For compact beam dumps light elements are not efficient. The use of depleted Uranium in beam dumps and collimators should be limited because of the high levels of induced radioactivity produced. Heavy-alloy (90% W, 7.5% Ni, 2.5% Cu) is expensive. A reasonable compromise is steel lined with marble. Lining the interior surface of a target station with 25 cm of marble, limestone or selected mortar can reduce the dose rate from the walls by a factor of 10. Concrete should be made from aggregates which contain little sodium and manganese. It is proposed to use a similar aggregate to that used for the PS ring tunnel (0.3% Na). At present we do not recommend either adding a boron compound to the mix or lining the wall with cadmium or coating the walls with a boron loaded paint in order to reduce the remanent activity.

11.7.3 Control of exposure from induced activity

At the 300 GeV accelerator control of exposure from induced radioactivity will be the most important way of controlling the overall exposure to personnel. Dose accumulated by working in a radioactive area can be reduced by (i) local shielding, (ii) remote handling, and (iii) waiting for the decay of activity. The two first methods can effectively be applied only if components have been designed with this in mind (see Sections 11.7.4 and 11.7.5), while the third method implies an efficient scheduling of the work. The gain factor as function of irradiation, cooling and working times is well understood[11.17]. Approximate average decay values from the CERN-PS are given as an example in the following table.

Table 11.9

Time from end of irradiation	Relative dose rates
5 min	6
30 min	3.8
4 hours	2.0
1 day	1.0
3 days	0.7
1 month	0.3
3 months	0.18

It is intended to place beam loss monitors all around the ring. In addition to providing valuable information on the dose to machine components, the history of losses at the measuring positions, stored in a computer, can be used to predict the magnitude and the decay rate of remanent activity at each place. After a few hours of cooling time the average gamma energy of activation products is around 1 MeV. Thus temporary local shielding by about 5 cm of lead, giving an attenuation factor of about 20, will allow access to many hot regions.

The exhaust gases from target stations where large amounts of active air and aerosols are produced can only be rejected after suitable filtration and suitable dilution. When working in active areas inhalation of dust can be avoided by suitable filtration of the air, by the painting of exposed surfaces as well as by vacuum cleaning.

11.7.4 Quick-Disconnects

Probably the most efficient method to reduce exposure is to shorten the time needed for a given job. This can be achieved by using 'quick-disconnects' which can equally well be operated by man or manipulator. We therefore suggest that the whole of the machine, i.e. the main ring, transfer tunnels, target stations and experimental areas, be designed on the philosophy of quick-disconnects. The main advantage of such standard connections is the ease with which elements can be interchanged or removed from active areas for exchange or repair. Acceptance of a quick-disconnects policy means that every connection and mechanical assembly is designed with speedy operational maintenance in mind. By this approach the use of manipulators (which always takes much more time than human intervention) can be kept to a minimum, i.e. to where dose rates forbid personal occupancy.

11.7.5 Criteria for remote handling

Remote handling, mechanical handling and transport are considered together here because within the accelerator environment they share similar spatial and operational limitations.

As a general rule it is advisable to design remote handling devices for all those areas where the dose rate at the working distance (40 cm) is estimated to be greater than 1 rem/h; remote handling is essential at dose rates above 6 rem/h. Personal occupancy of such areas will have to be restricted to periods of less than 6 minutes: 30 minutes occupancy of such

an area would mean the accumulation of the maximum allowable dose for a 3-month period. Small, highly active components, e.g. targets, should always be handled remotely.

Successive phases in the development of the 300 GeV accelerator, viz. installation, testing, start-up, operation, maintenance, etc. will make different demands on the handling and transport systems. Great advantages are to be gained during all these phases by planning at the outset to use general purpose equipment, often available commercially, and designing the machine elements to suit.

For the new ring a ground vehicle handling system will be most effective. In the ejection areas, where high dose rates are anticipated, the same vehicles will be used in conjunction with manipulators and local shielding to reduce the dose to personnel.

Tests of all remote handling devices should be carried out in replicate inactive areas before installation in the accelerator.

a) Requirements for the 300 GeV PS ring tunnel

The estimates of dose rate from remanent activity in Section 11.5 are based on a design intensity of 10^{13} protons/pulse. According to these remote handling facilities will be required, e.g. for septa and main ring magnets and quadrupoles in the ejection regions and for beam scrapers. In most cases components can be removed as whole units; specialized handling facilities for stripping these units will be outside the ring.

b) Requirements for the external target stations

The confined space within the shielding of target stations will eliminate the use of general purpose manipulations, but specialized remote handling devices are essential for the installation and removal of all components.

Access to the target station is envisaged by removing part of the roof shielding. Removal and installation of components will be done using a crane, the operator working in a shielded cabin.

Each element of the target station will be designed on the plug-in principle, so that, as it is installed, it is lowered on to pre-aligned modular plates which are supplied with electrical power, water and controls.

By providing special removable shields which are normally kept outside the target station and which can be inserted remotely after the removal of nearby active components, it should be possible to allow limited access of personnel into the target station in order to perform occasional, essential maintenance to the modular plates.

c) Storage and hot-cell facilities

A central storage facility in which highly active equipment can be allowed to cool down

must be foreseen. This will also help to keep the accelerator tunnels free of components which are redundant or temporarily out of use. In this facility an overhead crane will be needed to take active components directly from the transporter and to stack them according to their radioactivity. Special handling facilities must be provided within the same building for stripping, investigation and minor repairs.

11.7.6 Personnel monitoring and access control

Exposure from prompt leakage radiation and from remanent activity will be controlled by personnel and area monitoring. Personal dosimeters will be necessary in those areas where the dose rate cannot be controlled to levels below 1.5 rem/y. These will need to be sensitive to neutrons, charged particles and photons. This applies equally well to area monitors.

Access to radiation restricted areas (ring, ejection and EPB tunnels) will be remotely controlled from the Main Control Centre (magnetic cards, TV, intercom). In all areas of high dose rate, work has to be supervised continuously. An interlock system will ensure that after access has been authorized the accessible area is protected against possible penetration by particle beams (see Chapter 9).

Access to the main ring, the ejection tunnels and the experimental areas depends on beam handling and sharing:

(i) During setting up of the PS the beam is dumped in the PS dump D_1 (in SS 16),
(ii) initial tests of injection and acceleration must be done at low intensities. A beam disposal system using the ejection system to the West with beam dump in the upstream part of the transfer tunnel or a separate beam dump must be available,
(iii) stop of filling of the 300 GeV machine is done by reprogramming the PS for 28 GeV physics and closing a beam dump in the injection tunnel,
(iv) access to the primary beam areas requires suppression of ejection and switching off the first bending system into the transfer tunnel to the appropriate areas. If the ejection system is operating one has to operate the beam dump in the transfer tunnel. For a number of secondary beam areas the same procedure will be necessary as beam stoppers cannot suppress the muon flux in the high energy secondary beam lines.

11.8 Cost Estimates

Only the extra investment costs for radiation protection are given. These are typically for shielding, remote handling facilities, etc. Some of the radiation protection expenses not given here will be contained within the budget of the other Chapters. We indicate in the last column those expenses which are common to radiation protection and experimental areas. Shielding costs of the West Experimental Area are given for the case of all primary and secondary beams being above ground level. In the North Area beams and targets are 6 m underground. Lateral shielding is part of civil engineering.

Costs Estimated According to 1970 Prices

(MSF)

	Cost	In Radiation Budget	Included elsewhere
Shielding			
West Area - 200 GeV			
a) two targets T1 + T2	5.3		5.3
b) muons	8.4		8.4
c) neutrino experiment + neutrino target	14.1		14.1
d) secondary beams	0.8		0.8
North Area			
a) two targets	2.0		2.0
b) extra tunnel shielding	4.0		4.0
Recording monitors			
a) stray radiation	1.0	1.0	
b) air + water	0.5	0.5	
Remote handling and special mechanical arrangements			
a) first ejection area	1.0	1.0	
b) additional ejection area	0.6	0.6	
c) extra costs for target stations, West and North Areas	5.0		5.0
d) local shielding	0.3	0.3	
e) shielded vehicle and cranes (extra costs)	0.2		0.2
f) remote handling area	0.9	0.9	
g) storage area	0.3	0.3	
Treatment of radioactive air and water			
a) main ring	0.1		0.1
b) target stations	0.2	0.2	
c) ground water, drainage in target areas and back-stops	0.3		0.3
	45.0	4.8	40.2

11.9 Conclusion

The radiation protection system as described in this Chapter is able to provide a well-balanced safety standard with respect to health hazard from ionizing radiation and contamination risks, and an acceptable lifetime for machine components. In particular the shielding of the ring tunnel will attenuate the penetrating radiation to levels of a few per cent of the natural background under the most unfavourable conditions. The radiation and activity escaping through the accesses can be controlled without difficulties. Safe working conditions can be achieved in both the West and North Experimental Areas. The shielding costs are significant for the West Area but moderate for the North Area. Extra costs due to induced activity and radiation damage are of the order of a few percent of the cost of the accelerator.

The members of the public living nearby and also the area outside the fences of the project will not be affected by the operation of the accelerator and no restrictions to the use of the countryside will be imposed. Practically everywhere outside the fences the radiation and contamination levels will be so insignificant that only refined measuring methods will be able to detect them.

References

(11.1) G.S. Levine, Mrs. D.M. Squier, G.B. Stapleton and G.R. Stevenson, 300 GeV/Rad. Note/70-22 (1970).

(11.2) 1966 CERN-LRL-RHEL Shielding experiment at the CERN Proton Synchrotron, UCRL 17941, Sept. 1968.

(11.3) J. Ranft, Nucl. Instr. & Meth., 81, 29 (1970).

(11.4) K. O'Brien, HASL-203 (1968).

(11.5) G. Bathow, E. Freytag, K. Tesch, R. Kajika and M. Köbberling, Proc. II Int. Conf. on Accelerator Dosimetry, Stanford, p. 222 (1969).

(11.6) J. Ranft, TUL 38 (1970).

(11.7) P.E. Kuhlmann, H.O. Wüster, CERN/ECFA 66/WGZ/US-S65/peh-jow-1 (1966).

(11.8) D. Keefe and C.M. Noble, Nucl. Instr. & Meth., 64, 173 (1968).

(11.9) F. Gervaise and M.M. d'Hombres, Note CEA (1968).

(11.10) M.M. d'Hombres, C. Devillers, F. Gervaise, B. de Séréville et P. Tardy-Joubert, CEA R-3491 (1968).

(11.11) J. Ranft and K. Goebel, 300 GeV/Rad. Note 70-24 (1970).

(11.12) F.E. Hoyer, CERN 68-42 HP (1968).

(11.13) C.D. Johnsen, R. Sheldon and G.B. Stapleton, RHEL/M 175 (1969).

(11.14) M.H. Van de Voorde, CERN 70-5 (1970).

(11.15) D. Evans, J.T. Morgan, R. Sheldon and G.B. Stapleton, RHEL/R 200 (1970).

(11.16) D. Neet, SLAC public. 134 (1965).

(11.17) M. Barbier, Induced Radioactivity, North Holland (1969).

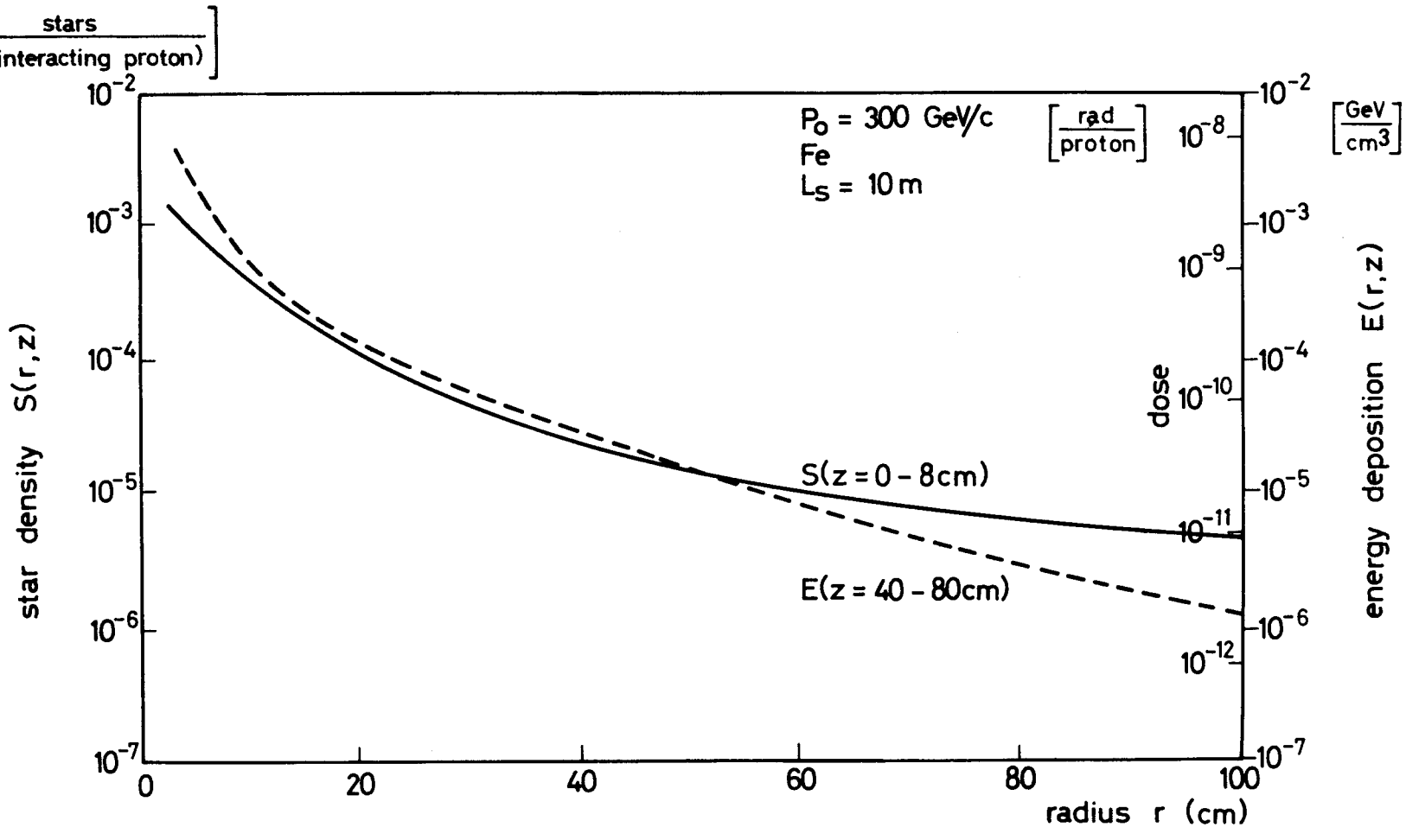

Fig. 11.1 Star density and energy deposition inside an iron cylinder with inner radius r = 4 cm located 10 m downstream a target or septum

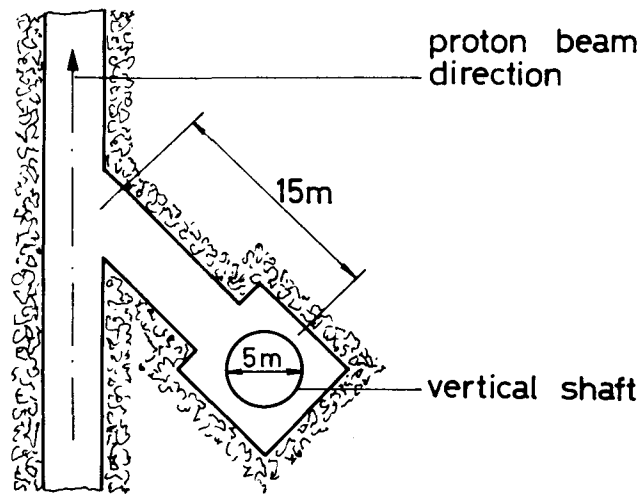

(i)

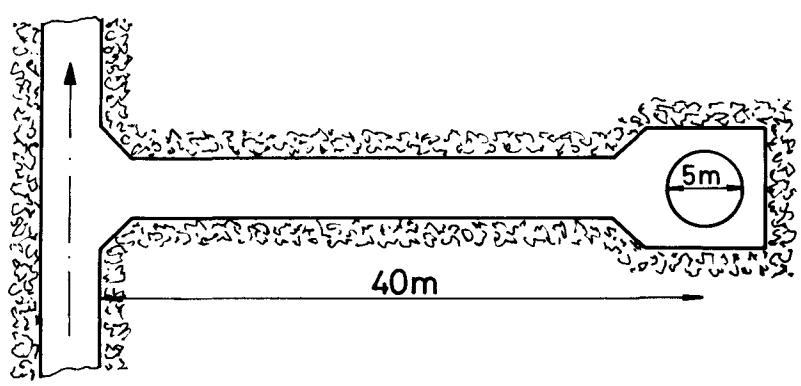

(ii)

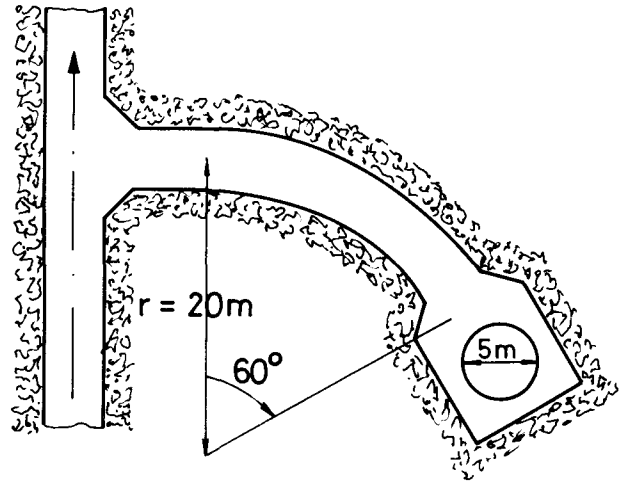

(iii)

Fig. 11.2 Examples of access tunnels

Chapter 12

THE EJECTION SYSTEM

12.1 Introduction

This report describes extraction systems for the 300 GeV accelerator. It was found possible to place all the extraction elements in the lattice without introducing a special insertion. These elements allow extraction up to the highest energy envisaged for the conventional stage of the machine. For the superconducting stage some of these elements will obviously have to be redesigned.

The extraction channel elements used for both fast and slow extractions are described. Several schemes of fast and slow extraction are discussed. The ejection losses are evaluated and their spatial distribution analysed.

Indications of the required magnetic field and ripple tolerances are given. Beam sharing between different channels is briefly discussed and cost estimates given.

12.2 The Lattice from the Extraction Point of View

The use of separated functions, focusing quadrupoles and bending magnets, allows one to conceive the extraction in a new perspective. The study is then conducted in the following way:

(i) selection of a period number and quadrupole lay-out,

(ii) localisation of the extraction elements in the superperiod,

(iii) lay-out of the bending magnets.

This process allows the machine to be as compact as desired (with the restriction that 3 consecutive long straight sections are required for the r.f.); it is also possible to envisage numerous solutions for the extraction system.

The superperiodicity is not imposed by the extraction; the number of beam outlets must be as small as possible (1 for Project A, 2 for Project B).

Three types of straight sections are used for extraction.

12.2.1 Long straight sections

In this project without special focusing insertions, the length of the long straight section is determined by the distance between two quadrupoles. In this straight section is placed the longest element of the system, the extractor magnet. The extractor magnet makes the beam go from an orbit near the edge of the vacuum chamber to the outside of the quadrupoles and bending magnets.

The displacement which must be produced by this magnet is a function of the outer dimensions of the quadrupoles and bending magnets. For a given angular deflection a long available free space makes it easier to achieve the required displacement. Hence it is better for extraction to have a small number of periods if one wants to avoid special insertions.

In the first proposal of this type of lattice the number of periods was 84. This number has been increased in this project for considerations linked to the use of the CPS as an injector. Nevertheless the length of the long straight section is quite adequate for the envisaged extraction elements.

12.2.2 Medium straight sections

These sections are obtained by removing one or two of the four magnets in a half period. These straight sections are used to place the full aperture fast kicker (see Section 12.6.1) and the beam scraper (see Section 12.7.3). The medium straight sections have the periodicity of the superperiod.

12.2.3 Short straight sections

There are two straight sections of this type per period. A few sections will be used to place dipoles, quadrupoles and sextupoles.

12.3 Expected Beam Properties

Observations at the CPS show that already in the 10^{12} p/p range there are considerable transverse and longitudinal blow-ups which cannot be neglected in the design of the extraction of a high intensity machine. The beam does become smaller as it is accelerated but not as rapidly as single particle theory would suggest.

The underlying mechanism of these phenomena is still very obscure and it would not be realistic to attempt any sort of scaling of the PS data to another machine.

We have therefore taken a somewhat arbitrary blow-up factor of about 2 which we apply to the normalised emittance between injection and utilization energy. It is expected that if higher values did occur and were found intolerable, suitable compensation methods would be developed.

One gets the following set of expected values (a = half diameter):

Table 12.1

Beam Dimensions at Ejection

	200 GeV/c	300 GeV/c	400 GeV/c
E_H ($\pi 10^{-6}$ rad m)	0.6	0.45	0.30
a_H (mm) at $\hat{\beta}_H$ = 110 m	8.1	7.0	6.2
E_V ($\pi 10^{-6}$ rad m)	0.35	0.23	0.18
a_V (mm) at $\hat{\beta}_V$ = 110 m	6.2	5.0	4.5
$\Delta p/p$	$\pm 5.10^{-4}$	$\pm 3.5.10^{-4}$	$\pm 3.10^{-4}$
ΔR (mm) at $\hat{\alpha}_p$ = 4.9 m	± 2.5	± 2.0	± 1.5

The expected radial beam size is critical for fast extraction with a fast kicker at 50 GeV. If this operation is required it would be necessary to decrease the intensity down to a level where the emittance and the blow-up are sufficiently reduced.

If debunching of the slowly extracted beam is necessary for counter experiments it could easily be achieved using well proven r.f. gymnastics techniques developed at the CPS. However, it is necessary to have in the coasting beam a high enough momentum spread to ensure its stability against rebunching under the effect of the coupling impedance created by the r.f. structure.

This problem was studied for the previous 300 GeV machine; there an energy spread blow-up would have been necessary. However, the parameters of this machine are from this respect more favourable and no blow-up seems to be needed.

12.4 The Extraction Channel

The extraction channel is composed of 3 elements:

S_1 - an electrostatic septum (Fig. 12.1)
S_2 - a copper septum magnet (Fig. 12.2)
S_3 - an iron septum extractor magnet (Fig. 12.3)

S_1 and S_2 produce a horizontal deflection. S_3 gives an upward vertical deflection. This was chosen on the basis of the following estimate of the main quadrupoles and bending magnet outer dimensions (half horizontal × half vertical).

F quadrupole : 270 × 190 mm
BI bending magnet : 419 × 246.5 mm

One clearly sees that the required vertical displacement to avoid the first downstream magnet is half of the necessary horizontal one.

This vertical deflection is a sizeable fraction of what is needed in the external transport line to bring the beam back to ground level.

The lay-out of the channel is based on the following assumptions:

(i) the same channel is used for both the slow and the fast ejections,
(ii) all the elements stay at a fixed position (no displacement during the accelerating cycle),
(iii) the elements are designed for 400 GeV but the channel could be extended up to a higher energy,
(iv) at the present time no magnetic element of the main ring has been modified, such as magnets with holes in the yoke, etc.,
(v) the radial position of the three elements is set near the beam envelope at injection which is at 44 mm in the focusing quadrupole between S_1 and S_2.

The selection of the lay-out of the 3 septa was done by optimization of the deflections and apertures required for the elements. The parameters of the septa are;

Table 12.2

Ejection Channel Parameters

	S_1	S_2	S_3
Position in lattice (Fig. 12.4)	19	25	33 to 35
Septum thickness (mm)	0.15	2	10
Length (m)	6	6	13
Field strength	100 kV/cm	0.123 T	1.5 T
Vertical aperture (mm)	12	12	200
Horizontal aperture (mm)	18	20	30
Deflection (mrad)	0.15	0.55	14.6

These elements are more fully described below.

12.4.1 Main ring apertures

The aperture requirements for ejection were calculated for the lowest design energy of 200 GeV. However, it is possible to extract down to about 50 GeV but with a beam of reduced emittance.

The apertures in the quadrupoles located between S_1 and S_3 on one side, and all around the machine on the other side, are sufficient as explained below. In the ejection region α_p is small and the full nominal aperture of quadrupoles is not occupied by the injected beam. The septum can therefore be closer to the centre of the vacuum chamber without interfering with the injected beam.

In the slow ejection situation the F quadrupole after S_1 must accommodate beyond the septum position (44 mm), 15 mm corresponding to the jump (see Section 12.5) and 3 mm for the exit angle of the beam. The extreme beam position is 62 mm which is also the nominal value of the F quadrupole half-aperture.

In the fast extraction case one must add to the same 44 mm the beam diameter at 200 GeV (16.2 mm).

In the D quadrupole following S_2, the beam envelope is at 17.5 mm. Here in addition to the jump and the exit angle taking into account the β-function, it is necessary to add the 10 mm "hole" created by S_2. This gives a total of 34.2 mm to be compared with the 27 mm half aperture of the D quadrupole.

For fast extraction, using the same reasoning as for the F quadrupole,one finds 33.9 mm. This additional aperture of 7 mm is quite compatible with the quadrupole design provided that one builds an enlarged vacuum chamber (which could be made with a stressed foil; the field quality in this enlarged aperture region is not critical. As shown in Section 12.5, an extra aperture all around the machine is not needed. This is made possible at the cost of somewhat more sophisticated schemes.

12.4.2 The electrostatic deflector S_1

The 6 m long electrostatic deflector S_1 (Fig. 12.1) will provide a working field of 100 kV/cm in order to achieve a deflection angle $\theta = 0.15$ mrad at the nominal momentum $p = 400$ GeV/c. This gap will be adjustable and set at 18 mm to accommodate the jump for the slow ejection, with a corresponding voltage of - 180 kV applied to the cathode.

The anode, at ground potential, will constitute the septum of the deflector, hence it has to be as thin as possible and yet meet stringent geometrical and electrical requirements. A possible compromise is to use a metal foil of thickness ≤ 0.1 mm, which will give an apparent septum thickness of about 0.15 mm over the total length of S_1. The sagitta d of the trajectories in the electrostatic field of S_1 will be $d = 0.11$ mm. It is possible that an array of wires could be made thinner than a foil septum but it is not yet clear that it could stand such a high electric field.

The position and angle of both electrodes will be remotely adjustable under vacuum for setting up the optimum ejection conditions. S_1 may thus be run at a larger gap for ejection at smaller momentum values (say 3 to 4 cm at 50 GeV/c), especially for fast ejection when the beam dimensions have not yet shrunk below the nominal value of 18 mm which is considered for the slow ejection jump at S_1. The electrostatic field will then be smaller since the total voltage is not to exceed 250 kV but will always be more than sufficient to provide the required deflection angle.

For operation at higher momentum values, the same value θ = 0.15 mrad could be obtained by increasing the length of S_1 to 7.5 m at the same field level since enough space is available, but one hopes from the progress of the CPS septum prototype that the required field of 125 kV/cm will be attainable.

In order to reduce the proton losses on S_1 and therefore to improve the high voltage behaviour and ease the maintenance problems, an array of thin wires will be used upstream and aligned with S_1 to Coulomb scatter most of the protons away from S_1.

12.4.3 The copper septum magnet S_2

The 6 m long copper septum deflector S_2 (Fig. 12.2) will have to provide at 400 GeV a deflection of .55 mrad. The needed field strength is 0.123 T. In a 12 mm wide gap with the allowed 2 mm thickness the current density is 48 A/mm^2, which is a conservative figure chosen in order to allow operation over flat-tops longer than the nominal 700 ms.

This magnet has characteristics comparable to a device under development at the CPS. The septum is made of directly cooled tubes. The cooling channels are of necessity very narrow and the small water flow would mean that the magnet would have to be made in sections of about 1 m long.

This magnet is pulsed and is in series with S_3.

12.4.4 The iron septum extractor magnet S_3

In addition to the reason given at the beginning of the Chapter, power consumption and reliability make us prefer to use an iron septum (Fig. 12.3). This magnet is similar in principle to a device used for the ISR injection. The beam has to be raised to a height of 280 mm above the median plane, by the end of the 28 m straight section.

With an effective iron septum thickness of 10 mm, one might expect to achieve 1.5 T with a tolerable fringe field.

The horizontal aperture must be 30 mm is one takes the 200 GeV beam emittance and the deflection given by S_2.

The vertical aperture of 200 mm makes allowance for the beam displacement inside the magnet. The length of 13 m could be made with 2 sections of about the same length as the main ring bending magnet.

If we assume a current density of 25 A/mm^2 in the conductors the power is about 200 kW, assuming a 50% duty cycle. Pulsed operation seems necessary in view of the fringe field to be expected. However, the extra voltage required for pulsing would not be large, if the rise time is of the order of 1 second.

If one chooses a suitable number of turns S_2 and S_3 can be powered in series.

12.5 Slow Extraction

Slow extraction has been the subject of a considerable amount of theoretical and experimental study in the last year. Efficiencies of 95% have been achieved at the CPS and further improvements are under way.

Two main types of resonant extraction have been developed. Integer at CERN, 1/3 integer at BNL. A non-resonant scheme using a target has been proposed for the NAL accelerator in addition to their 1/3 integer scheme.

In order to limit radiation damage, a high extraction efficiency is obviously needed. The loss on the septum is given by the ratio of its thickness to the "jump". The jump is the increase of betatron amplitude per turn. For a 1% loss on a .15 mm thick septum (S_1) it is necessary to take a 15 mm jump. This coarse estimate does not take into account the particle distribution on the septum which decrease the efficiency. But we have not included the positive effect of the scattering wires placed in front of S_1 (see Section 12.7).

In the resonant extraction, particles leave the stable area along a well defined trajectory, the separatrix. Its angle and position are determined by the elements (quadrupoles and sextupoles) creating the resonance. The extraction channel requires a well defined orientation of the separatrix at its entrance.

The particles of different momenta are driven into the resonance by a slope in the main magnetic field flat-top. This ensures that the extracted particles have always the same radial position in spite of the beam momentum spread.

12.5.1 Integer resonance

The integer resonance is excited by a quadrupolar field which moves Q_H to the nearest integer value. A system of two special quadrupoles placed one period apart (position 2082 and 2102*, Fig. 12.5) tunes Q_H on the resonance. The orientation of the separatrix can be adjusted by a suitable choice of the quadrupole strength ratio. A third quadrupole is added (position 2112) in order to allow variation of the chromaticity of the extraction system.

These 3 quadrupoles must be able to produce strength of 30 T (1.2 m × 25 T/m). The non-linearity needed is produced by one sextupole (in 2082) of 120 T/m strength (0.8 m × 150 T/m^2).

---

* The lattice is divided into 2160 sections, 20 to a period. The lengths of the sections and their positions correspond to the quadrupoles, bending magnets and drift lengths of a normal period.

If it were felt necessary to avoid filling up completely the short straight section 2082 one could decrease the needed quadrupole strength by using the main machine quadrupole to produce part of the needed Q shift.

This lay-out allows one to make a closed orbit bump (produced by the same dipole magnets as used in the fast extraction, see Section 12.6) to adjust the orbit position near the electrostatic septum S_1. The bump does not interact with the extraction quadrupoles and the sextupole, hence does not affect the resonance process. The particles reach their largest excursion at the level of the S_1 septum. At the cost of this complication, no extra aperture is needed.

12.5.2 Third integer resonance

To produce this resonance it is necessary to move the Q_H value to the nearest 2/3 integer value. In order to produce the separatrix orientation two special quadrupoles located symmetrically with respect to S_1 are needed. The phase advance between the quadrupoles and S_1 must be close to π. With such a scheme one can adjust the slope of the separatrix within a range of $\pm 25^{\circ}$. The perturbation outside the extraction region produced by these quadrupoles can be made negligible.

The quadrupoles of strength 9 T (1 m × 9 T/m) must be located symmetrically with respect to S_1. The resonance is excited by a pair of sextupoles placed at the opposite ends of a diameter of the machine. The necessary strength is 100 T/m (1 m × 100 T/m^2; 0.4 T on the pole tip).

The septum radial position is 44 mm. To avoid losses around the ring and to avoid increasing the aperture, it is necessary to produce a 10 mm orbit bump near S_1. (This can again be produced by the set of dipoles used for fast extraction.) This orbit bump leads to an apparent radial position of 34 mm for S_1. It avoids the beam losses due to particles leaving the admittance on the other separatrices.

12.5.3 Slow extraction with target

An extraction scheme proposed by NAL using a scattering target has been considered for this project. A simple and efficient lay-out would consist of a tungsten target located about $\lambda/8$ upstream of the electrostatic septum S_1. This choice takes into account the values of the phase advance and of the β function. A long burst would be created on this target and dipoles excited so that the target shadow be cast just inside S_1. (Again the same set of dipoles foreseen for fast extraction can be used.)

With the pessimistic assumption that all the protons hitting the .15 mm thick septum are lost, the calculated efficiency is about 90% for a 2 mm long tungsten target. With a first stage wire septum the multiple Coulomb scattering in the wires would increase this efficiency to approximately 95% for a .5 mm long target.

However, the target action produces a slight blow-up of the vertical beam emittance.

12.5.4 Comparison of slow extraction schemes

Extraction with target requires a minimum number of elements (no special quadrupoles nor sextupoles). The rather low efficiency given by the first studies might be tolerable for operation in the low intensity range. But this scheme has not been sufficiently studied to assess its value for higher intensities.

Integer and 1/3 integer resonances have been compared from many points of view. One of them is beam survival. For the 1/3 integer it is proportional to spill speed. It was found both by analytical and numerical computation that 2% of the beam survives a 500 ms spill and must subsequently be extracted from the machine. On the other hand no beam survival arises in the integer extraction driven by a dipole.

The ripple requirements for the bending magnets (see Section 12.8) are stricter for the integer; on the other hand the 1/3 integer resonance imposes stronger tolerances for the quadrupole ripple. From the power supply point of view it is maybe easier to achieve a smaller ripple in the quadrupole supply but dipolar defects on the closed orbit in the extraction region are easier to correct.

The integer resonance is, in principle, more sensitive to the beam momentum spread but the adopted scheme avoids this drawback.

Both types of resonances lead to radial extracted beam emittances smaller than the one of the circulating beam. This emittance reduction is larger for the integer resonance.

The two resonance schemes use similar elements, quadrupoles and sextupoles, with a different lay-out. From this point of view no immediate choice would be necessary.

However, for the purpose of the adopted lay-out and the cost estimates we have selected the integer resonance which on the balance of available evidence seems somewhat preferable.

12.6 Fast Extraction

The fast extraction scheme envisaged uses the same extraction channel as the slowly extracted beam. It consists of a beam dump system, that brings the closed orbit parallel to the three septa and a device which shifts the beam over the first septum. The latter may be either a full aperture kicker magnet or a fast bump system as envisaged at BNL.

12.6.1 Fast extraction with a full aperture kicker

In the lattice, the positions of the fast kicker (F.K.) and of the electrostatic septum (S_1) are foreseen to be at the locations 3 and 19 (Fig. 12.4) respectively. The phase shift between the two elements then is $\Delta\phi = 82.4^{\circ}$, which results in a kick-to-jump ratio of

$1.32 \cdot 10^{-2}$ mrad/mm. Taking into account a suitable safety clearance on both sides of the septum the required jump is 15 mm at 400 GeV. This corresponds to a maximum field strength for the kicker magnet of 0.260 T.m.

A rough estimate of a suitable full aperture kicker magnet gives the following parameters:

Table 12.3

Full Aperture Kicker Parameters

Magnetic strength (at 400 GeV)	0.260 T.m
Aperture	120 mm (radial) × 30 mm (vertical)
Rise time	100 ns
Line voltage	80 kV
Impedance	20 Ω
Modules	9 × 400 mm
Total length	4.6 m

The theoretical efficiency for full beam extraction is $\eta > 99\%$ when the ring is completely filled. To achieve the rather wide gap of the electrostatic septum required at low extraction energies (50 GeV) the cathode is movable (Section 12.4). The possibility of using a single fast kicker for the two fast extraction channels (West and North) deserves further study.

12.6.2 Fast extraction by beam shaving

With this scheme "fast bumps" are used instead of a full aperture kicker. For full beam extraction during one machine revolution, the bump rise time will be around the machine revolution time ($\sim$ 20 μs) rather than the 100 ns for the fast kicker.

With the apparent septum thickness of 0.15 mm, in the above case, the theoretical efficiency is 98%, not taking into account the fraction of protons outscattered after hitting the wire septum.

By reducing the fast bump amplitude it is possible to shave only a fraction of the beam emittance and therefore extract a small fraction (a few percent of the beam).

The favourable positions of the fast dipole magnets, giving an adequate phase shift, are the locations 3 and 42 (Fig. 12.4). At 400 GeV the required magnetic strength is of the order of 0.25 T.m.

From the point of view of cost estimates this solution is by far the most favourable one, but has not yet been sufficiently studied.

12.6.3 Closed orbit bumps

For the fast extraction a set of 6 dipoles are necessary to bring the closed orbit parallel to the septa. They are positioned (Fig. 12.5) at locations 2, 12, 22, 29, 42 and 62. At 400 GeV the required strengths are less than 1 T with 1 m magnets. The residual closed orbit distortion outside the extraction region is less than 2%.

The same set of dipoles is adequate for the various slow extraction schemes.

12.7 Ejection Losses and Scrapers

12.7.1 Absorption and Coulomb scattering of protons in septa, scattering targets and scrapers

The interaction of primary protons with the ejection system elements is inevitable. The most important of these elements are the following: the (wire and foil) first septa used for slow and fast ejection, scattering targets which can be used for slow ejection (Section 12.5.3) or halo removal and beam scrapers used to collect protons scattered in septa or scattering targets. The fractions of primary protons interacting inelastically in these devices and scattered out can be calculated with Monte Carlo techniques, taking into account the phase space distribution of the circulating beam and reasonable misalignments of the elements considered for a variety of situations.

Less than 20% of the protons hitting a wire septum are absorbed. In a corresponding foil system, absorption amounts to more than 60%.

If scattered protons hit the edge of a scraper, less than 10% are scattered out again. Outscattering can reach, however, up to 70% with grazing incidence of the protons, the alignment of the scraper is therefore important.

12.7.2 The beam loss distribution in the main ring

There are two contributions to the loss distribution in the main ring, (i) secondary particles created by protons interacting in ejection elements hit the vacuum chamber or other machine components downstream, (ii) a large fraction of the Coulomb scattered protons may reach the wall downstream of the scattering point or at any position around the ring depending on particularities of the closed orbit (random losses). The two types of loss distribution can be calculated with the Monte Carlo method. Corresponding calculations agree with loss distributions measured at the CPS downstream of targets and ejection septa.

Secondary beam losses are in practice concentrated on the first 25 m downstream the loss point if there are machine elements in this region. About 50% of the protons scattered from a foil septum are expected to be lost on the wall in the first $\lambda/2$ downstream the septum, the other 50% must be expected to lead to random losses somewhere around the ring if no scraper is used.

12.7.3 Scrapers to remove scattered protons

A large fraction of the protons scattered in the septum can be expected to lead to random losses. A scraper should concentrate these losses as soon as possible after the septum. Two mechanisms can be used to drive the scattered protons onto the scraper, ionization energy loss and Coulomb scattering. The system using Coulomb scattering is more efficient in the lattice proposed. A scraper positioned about 0.4 λ downstream the ejection septum is expected to remove all protons which could lead to random losses with an efficiency of about 90% or better.

The scraper position is indicated in Fig. 12.4 (lay-out of ejection components). The scraper should be at least 3 m long out of a heavy material like Fe, vertically and radially adjustable and faced (about 0.1 mm) with a light material.

12.7.4 Halo scraper

Halo trimming might be necessary before the beam ejection. It is proposed that this is also done in the ejection straight section to localize the radiation problem. Halo protons are Coulomb scattered in the horizontal and vertical scattering targets located near the first septum. The scattered protons are scraped by the scraper 0.4 λ downstream the septum. This scheme avoids positioning scrapers in other superperiods correct with respect to the phase of the resonant orbit. The same scraper positions should, however, be reserved in all superperiods. The scraper could also be used for low intensity or low energy beam dump.

12.7.5 Beam dump

Scrapers cannot be used for internal beam dumping at intensities much larger than a few times 10^{12} protons. At higher intensities a set of fast bumps sweeping the beam into a simplified but obviously less efficient extractor channel seems presently the most favourable system. The beam could, if necessary, be directed away from the tunnel by additional magnets. The conditions under which a full intensity beam has to be dumped are not yet well understood and a detailed investigation of such a system has still to be done after having gained experience at lower intensities. The necessary space in a long straight section has to be reversed.

12.7.6 Beam loss estimate

One should take slightly pessimistic beam loss figures in assessing the radiation problems.

Table 12.5

Expected Losses

Loss on the electrostatic septum	1%
Halo removed by the scraper	1%
Random losses around the ring resulting from the test and setting up periods integrated over the year	1%

(The percentages are relative to the circulating beam.)

12.8 Tolerances

12.8.1 Field tolerances

The influence of magnetic field errors has been studied using a particle tracking computer programme. The principal effect of the field error is to curve the separatrix. The jump width over the septum decreases together with the efficiency and the apparent emittance increases.

The criterion taken for an acceptable non-linearity amount is to limit the jump reduction to about 10% compared to the ideal linear case.

For the third integral slow resonant extraction, taking the non-linearities individually, acceptable values for $\Delta B/B$ at $x = 40$ mm are:

Table 12.6

Acceptable Non-linearities (1/3 Integer Ejection)

Sextupole errors	$S < 1.5 \times 10^{-3}$	for bending magnets
Decapole errors	$D < 3.5 \times 10^{-3}$	
14-pole errors	$V < 4.5 \times 10^{-3}$	
Octupole errors	$OK < 2 \times 10^{-3}$	for the quadrupoles

This last value has also been confirmed by analytical calculations.

For the integer resonance the allowed tolerances are larger by a factor 2.

Higher values lead to insufficient jump widths and even to complete stability.

The main conclusions are:

(i) The limits given above are really sharp limits. So, for instance, for $S = 1.5 \times 10^{-3}$ a still very good situation was found, while for $S = 2 \times 10^{-3}$ the particle motion has become completely stable.

(ii) It seems that mainly the value of the field error $\Delta B/B$ at the limit of the aperture is relevant, and that the analytic form taken for $\Delta B/B$ as a function of x changes the results only within a factor 2.

(iii) Computations up to now allow the preliminary conclusion that for reasonable strengths of the extraction lenses and a reasonably small number of correcting elements the maximum tolerable field error $\Delta B/B$ at $x = 40$ mm is about 3×10^{-3}.

12.8.2 Effect of ripple on the slowly ejected beam

During the beam extraction the rate of variation of the stable area must remain constant during the spill time in order to get a uniform intensity beam.

Numerical and analytical evaluations are in good agreement. Numerical calculations assume f = 80 Hz as ripple frequency; the sensitivity to ripple varies as 1/f. According to these calculations, the ripple tolerances on the sextupoles are not very severe. The extracted beam will be 100% modulated with a relative ripple of 10% in the 1/3 integer resonance and 3% in the integer resonance.

The ripple distributed over all the machine quadrupole corresponds to $\Delta I/I = 3 \cdot 10^{-6}$ for 100% modulation.

Theoretical study of the bending magnet ripple suggests a ripple tolerance of the same order. But exact calculations which take into account non-uniform distribution of the ripple around the ring await final design of the power supply.

In any case it is necessary to plan for correction at the beam level with a suitable servo-system. However, one must not forget that a servo-system cannot properly compensate the ripple if it is already initially too strong.

12.9 Beam Sharing

The presence of two experimental areas (North and West) and the existence of two main modes of beam utilization (fast extraction for feeding bubble chambers and slow extraction for counter experiments) has led us to consider briefly various beam sharing schemes.

12.9.1 Sharing between one fast and one slow ejection or two fast extraction into two different channels can be consecutive or simultaneous.

a) Consecutive sharing does not create any fundamental problem and can be easily done at two different energies but does not lead to the optimum beam duty cycle.

b) Producing a fast ejection burst during a slow spill when the beam is debunched appears feasible with fast extraction by beam shaving (see Section 12.6.2). An unacceptable intensity modulation of the slowly ejected beam would result if fast kickers were used.

12.9.2 Sharing between two slow extraction channels

a) Consecutive sharing at the same energy with the debunched beam appears possible but results in a lower beam duty cycle per channel.

b) Consecutive sharing at different energies during the same pulse (say 200 GeV in the West Hall and 400 GeV in the North Area) requires that one works with a bunched beam in the first extraction; since the rest of the beam must be accelerated further this may be quite acceptable for many experiments, bearing in mind that the r.f. structure will be at 180 MHz. One might also envisage either partial or full debunching followed by adiabatic retrapping at the end of the first spill, but there is no operational experience of the efficiency which could then be expected.

c) Simultaneous slow extraction at the same energy into the West and North Area channels asks for an additional phase shift between the outgoing separatrices corresponding to the two areas. This comes about because the lattice superperiodicity of 6 is chosen to be not commensurate with the betatron wave number, therefore the separatrix has a different angle in similar positions of the two different extraction sections.

To bring the separatrix at the same favourable angle with respect to the two extraction channels, two solutions have been studied:

- The two channels are geometrically shifted, but this would require to remove more bending magnets and lead to a lower top energy and is therefore not acceptable.
- The separatrix at the level of S_1 of the second channel is shifted by a pair of quadrupoles. However, the possible shift is only of about 30° it is quite suitable for the 1/3 integer resonance where one has 3 separatrices but is not sufficient in the integer resonance.

12.10 Instrumentation

Experience at the CPS has shown that a considerable amount of instrumentation is required to achieve a high efficiency operational extraction.

In addition to the general purpose instrumentation of the main ring such as current transformer, pick-up electrodes, beam probe scanners, ionic beam scanner, Q-measuring device, magnetic field peaking strips, wide-band pick-up station, air ionization chambers for loss measurements, etc. for our purpose, one should have the equipment listed below.

Table 12.7

Instrumentation for Ejection

Main Ring	
Position and profile detectors	
1. Miniscanner	controlled by computer, scanning of the beam with an insulated target placed in front of each septa and linked mechanically to them.
2. Beam position pick-up	in front of the fast kicker.
Losses	
1. Ionization chambers	placed near septa; measurement of loss used for efficiency calculations.
2. Cerenkov counter	directive counter useful for better localisation of losses.
Ripple compensation	magnetic element chosen according to type of extraction - closed loop compensation with detector in external beam can servo the shape of slow extraction as well.
External Beam	
Beam intensity	
1. Transformers	toroidal transformer placed around the beam; working well for fast extraction; will probably work for slow extraction.
2. SEC	Secondary Emission Chamber.
3. Telescope	2 or 3 scintillators aligned to look at target.
4. Charge of insulated target	measured by electrometer + A/D conversion.
Position and profile detectors	
1. Screens + TV	remote-controlled, 1 per focus + 1 per splitting.
2. SEC with strips	also used for emittance measurements (choice of place accordingly), 1 per branch.
3. SEPD	Slow Extraction Position Detector, 1 per movement correcting element.
Movement compensation	one of the beam transport elements must have additional windings for this purpose.
Debunching	
1. Telescope with scintillators	delayed coincidences and/or time between pulses measurement devices could give information to obtain effective length (computer treatment).
2. Remote-controlled counter movable in the beam	sapphire could be used, enough light to deduce the time structure.

12.11 Cost Estimates

This estimation is based as much as possible on the extrapolation of corresponding elements ordered for the CPS.

Although in this report the elements are all calculated at the nominal energy of 400 GeV, it was assumed for the cost calculation that at lower energy stages, smaller less expensive elements would be installed.

Table 12.8

Ejection System Costs (KSF)

	200 GeV	300 GeV	400 GeV
Extraction channel (including power supplies)			
Electrostatic septum S_1	500	500	500
Copper septum magnet S_2	300	400	550
Iron septum magnet S_3	300	900	1450
	1300	1600	2500
Lenses (including power supplies			
Dipoles (6)	500	650	800
Quadrupoles and sextupoles (4)	500	650	800
	1000	1300	1600
Fast Kickers* (including electronics)	5000	6250	7500
Scraper and Target	300	400	500
Development	1500	2000	2500
Electronics and controls	1000	1250	1500
Instrumentation	500	600	700
	10600	13400	16800
Installation	4000	4500	5000
	14600	17900	21800

Installation costs are only a very rough estimate, they cover water, cables, bus bars, electricity mains, cable ducts, etc., bearing in mind that the ring tunnel is 40 m below ground level. Buildings for power supplies are not included, neither is the beam dump whose cost we estimate to be about 5000 KSF.

---

* In the case of the use of fast bump (12.6.2) for fast extraction by beam shaving the cost would be considerably reduced but this scheme has not been studied far enough to make cost estimates possible.

References

The many references which support this work have been omitted for the purposes of this publication. They may be found in CERN Int./MPS/DL 70-11.

Bibliography

O. Barbalat, Price Estimates of the Ejection System for the 200/500 GeV MR 29 Synchrotron, EJ/16, MPS/DL Note 70-11.

D. Dekkers, List of Apparatus needed for the Tuning of Extraction, EJ/30, Oct. 1970.

J. Erb and G. Merle, Influences of Higher Multipoles in Bending Magnets and Quadrupoles on Resonant Extraction (in preparation, summary in EJ/33).

J. Faure, A. Hilaire, A. Laisné and J. Parain, Main Magnet Bending Field Tolerances for Extraction, SEFS TD 69/43, ER 24.

M.R. Harold, Some Notes on the Practical Difficulties of Slow Ejection at High Energies, EJ/29, Nimrod (ABT) 70-31.

A. Hilaire, Influence de défauts de champ magnétique, forces quadrupolaire et sextupolaire sur l'aire stable en éjection résonnante, SEFS TD 69/39 ER 23 and SEFS TD 69/68 ER 29.

G. von Holtey, Note on Closed Orbit Bumps for the MR 29 Lattice, EJ/4.

K.H. Kissler, Slow Ejection Sharing Schemes for the "Project B" Machine, EJ/25, MPS/SR - Note 70-37.

A. Laisné and J. Parain, Extraction Channel at 500 GeV without Special Insertion, EJ/9, DSS/SOC UTI/17.

A. Laisné, Integral Resonant Extraction from the MR 29 Lattice, EJ/12, Feb. 1970.

J. Ranft, How to Scrape Multiple Scattered Protons from the Septum, EJ/7, TUL 26.

J. Ranft, Scattering of 250/c Protons in a Wire Septum and in a Scraper, EJ/10, TUL 27.

Ch. Steinbach, Slow Extraction by Target Scattering, EJ/27, CERN/MPS-CO/70-7.

E.J.N. Wilson, A Simple Adiabatic Model to Calculate Current Ripple Tolerances during Slow Ejection, EJ/3.

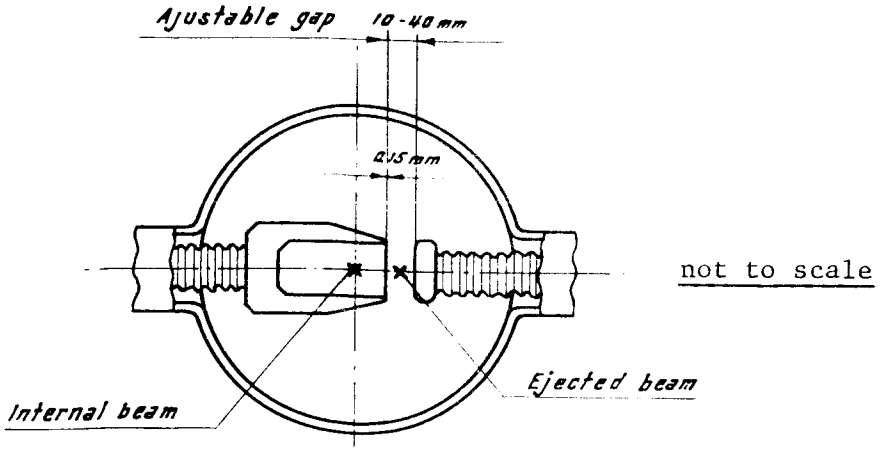

Fig. 12.1 Electrostatic septum S_1

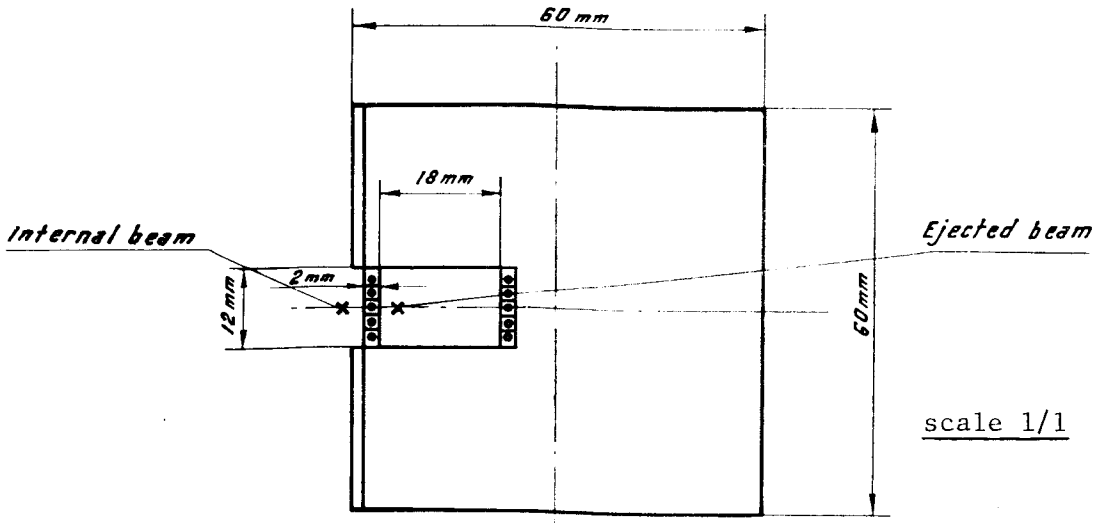

Fig. 12.2 Copper septum magnet S_2

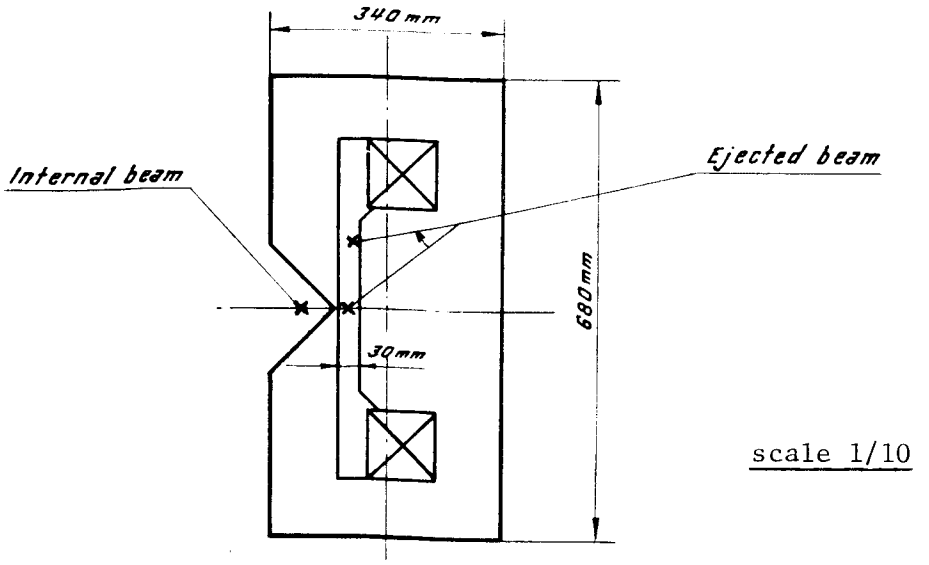

Fig. 12.3 Iron septum extractor magnet S_3

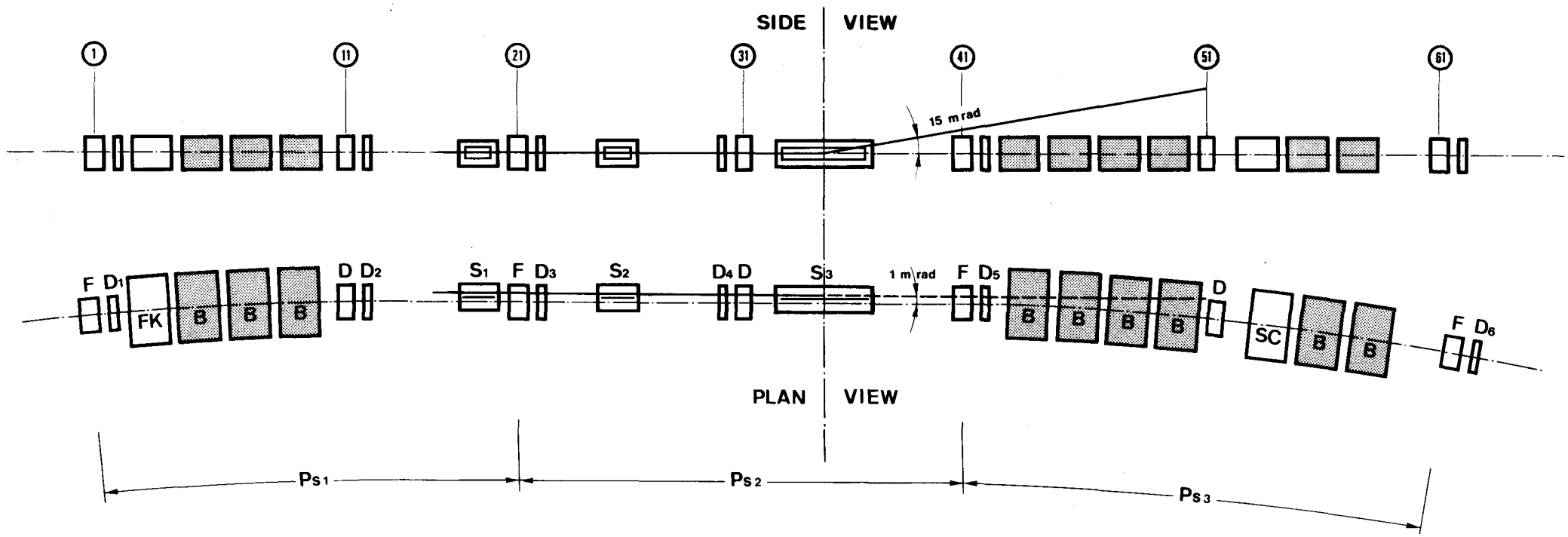

				position
D_1	Dipole for extraction	1.0 m	1 T	2
D_2	" " "	"	"	12
D_3	" " "	"	"	22
D_4	" " "	"	"	29
D_5	" " "	"	"	42
D_6	" " "	"	"	62
FK	Fast kicker	4.6 m	0.260 T.m	3
S_1	Electrostatic septum	6.0 m	100 kV/cm	19
S_2	Copper septum magnet	6.0 m	0.12 T	25
S_3	Iron septum extractor magnet	13.0 m	1.5 T	33-35
SC	Scraper	3.0 m	-	53
F	Main focusing quadrupole			
D	Main defocusing quadrupole			
B	Main bending magnets			

Fig. 12.4 Extraction channel

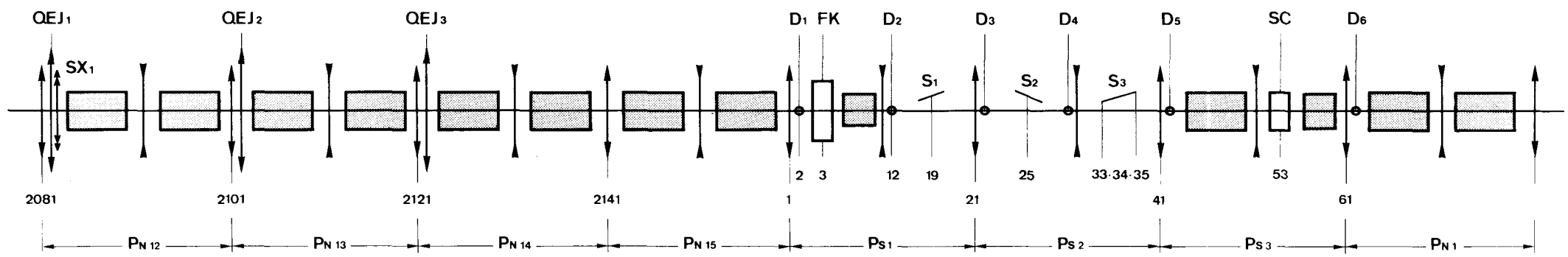

Fig. 12.5 Location of extraction elements

QEJ1	Integer resonance quadrupole	1.2 m	25 T/m	2082*
QEJ2	" " "	"	"	2102
QEJ3	" " "	"	"	2122
SX1	" " sextupole	0.8 m	150 T/m^2	2082
FK	Fast kicker	4.6 m	0.260 T.m	3
S_1	Electrostatic septum	6.0 m	100 kV/cm	19
S_2	Copper septum magnet	6.0 m	0.12 T	25
S_3	Iron septum extractor magnet	13.0 m	1.5 T	33-34-35
SC	Scraper	3.0 m	-	53
D1	Dipole for extraction	1.0 m	1 T	2
D2	" " "	"	"	12
D3	" " "	"	"	22
D4	" " "	"	"	29
D5	" " "	"	"	42
D6	" " "	"	"	62

*Position number refer to the computer programme listing corresponding to the lattice.

Chapter 13

THE EXPERIMENTAL AREAS

13.1 Introduction

The planned exploitation of the 300 GeV accelerator[13.1] is based on the utilization of two experimental areas. The first is the West Hall, a facility already existing on the CERN site, which would be the first area to be available for physics experiments. The second is the North Area which would become available at the completion of the 8-year construction programme.

The principle behind the incorporation of the West Hall into the 300 GeV machine programme was based on two factors[13.2]. The first is the possibility to start experimental physics in the high-energy range at the earliest possible date. The second is the opportunity to profit from the considerable capital investment contained in the West Hall and the possibility to have available for use from the start of the accelerator, two sophisticated pieces of experimental equipment, the Omega magnet and spark chamber system and the large hydrogen bubble chamber (BEBC).

In this Chapter details will be presented on a possible utilization of the West Hall as an area fed by 200 GeV protons, starting during the sixth year of the programme. It is assumed that the West Hall will be the only experimental area available until the completion of the programme, when the North Area will become available. The possible modifications one could make if the first operation of the accelerator were to be at 300 GeV are also considered. It should be stressed that the beam designs and layout in this report are not by any means intended as a definite plan for utilization, but more as an exercise to see where the problems lie and to get some reasonable feeling for the costs involved in exploiting the West Hall. One will clearly pay close attention to the experience to be obtained at the NAL accelerator before finally fixing the layout.

Regarding the possibilities of the North Area, one will have even more time to benefit not only from the early operational experience of the NAL accelerator, but also of the West Hall utilization at 200 GeV in making the final decisions on the best layout. Thus only very preliminary ideas and cost estimates are presented at this time.

13.2 West Hall

13.2.1 Existing facilities

The West Hall complex includes a main experimental area which is 160 × 64 m^2 and several subsidiary covered areas, fully equipped for experimental utilization. The total area involved is ≈ 14,000 m^2. In addition, there is space for expansion beyond the present limits of the Hall, but for the purposes of this report no modifications of the Hall are considered.

The West Experimental Area will contain two major items of experimental equipment which will have already been exploited during the period 1972-1975, using the 25 GeV/c proton beams available from the CPS. These are the large European bubble chamber (BEBC) and the Omega magnet and spark chamber system which can be thought of as an electronic equivalent of a large bubble chamber. These two major items will represent not only a considerable capital investment but also a large amount of experience already gained at the lower energies available from the present beams. In addition, the West Hall will contain the beam transport, shielding, water and power necessary to operate the West Hall at the 25 GeV/c level for these two instruments. Lists of the equipment already existing or on order are given in Tables 13.1 to 13.3.

Table 13.1

Existing Beam Elements

Quantity	Designation	Gap (cm)	Length (m)	Resistance (Ω)	Type, remarks
11	M 2 m	11, 14, 17, 20	2	0.195	PS
5	HB 2	8	2.5	0.184	ISR
29	Q 200	20	2	0.2	PS
7	Q 100	20	1	0.2	PS
6	QFS	10	0.8	0.067	ISR
7	QDS	9.1	0.82	0.066	ISR
3	QFL	10	1.2	0.108	ISR
2	SM	6	1	pulsed magnet: 12 ms base, sinusoidal pulse.	
6 - 10	CM	20	0.5	0.1	PS correction magnets, not yet ordered.

Table 13.2

Existing Power Supplies

Quantity	Max. Current (A)	Max. Voltage (V)	Type, Remarks
2	470	200	ISR
1	490	148	ISR
2	430	230	ISR
3	530	70	ISR
1	530	115	ISR
1	power supply for pulsed magnet		
30	1000	230	R2B
15	600	130	R1B
10	250	25	T1B
10	1000	150	D
5	1000	-	Filter
5	1000	-	Series regulator

Table 13.3

Existing Shielding

Blocks	Total approx. weight (tons)
A. Concrete	
Blocks	29'000
Beams	2'140
Total	31'140
B. Iron	
Blocks	3'300
Beams	500
Total	3'800

The total amount of money invested in the West Hall, including BEBC and the Omega system is in the region of 180 MSF. The major part of this investment would be of immediate value to the 300 GeV Programme. A detailed study of the possible utilization of the existing elements and power supplies has not yet been made, and so no reduction in costs had been assumed so far for these elements.

13.2.2 Beam layout

A layout of beams in the West Hall to cover a wide range of secondary particles and momenta and making full use of BEBC, Omega and the length of the hall is shown in Fig. 13.1. For clarity the positions of beam transport elements and shielding have been omitted. The proton beam enters the hall approximately along the present 25 GeV proton line to BEBC (i.e. parallel to the North wall). The beam is shared between three target stations in the hall, namely T_1, T_2 and T_ν. Target station T_1 is an achromatic station (beams at zero degree production angle and the EPB returned to its original direction). The continuing proton beam is refocused on to T_2 which, for a 200 GeV/c EPB, is situated 80 m downstream from T_1. T_2 is an end target station with several finite production angle beams. T_ν is a target station for a neutrino or r.f. beam for BEBC and is fed with a fast spill from a beam switch upstream of T_1.

Target stations T_1 and T_2 have been intentionally designed to be dissimilar so that one may keep the possibilities in target stations and beam layouts as flexible as possible at this early stage. Other designs, no doubt, will appear with further study and with experience at NAL. The fixed positions of BEBC and Omega and the limited length of the hall are the important constraints on the present layout.

Figure 13.2 shows the shielding required for the above scheme with a 200 GeV/c extracted proton beam and with the assumption of $\sim 10^{12}$ interacting protons/s at each of the target regions: T_ν (averaged over a full year), T_1, T_2 and the EPB back stop. The secondary beams provided in the layout are:

1. Neutrino beam to BEBC
2. r.f. separated beam to BEBC (p_{max} = 150 GeV/c).
3. High energy beam for electronic experiments (p_{max} = 150 GeV/c).
4. } Two medium energy beams (p_{max} = 75 GeV/c).
5. }
6. Medium energy beam to Omega (p_{max} = 50 GeV/c).
7. Low energy beam (p_{max} = 25 GeV/c).

The need for the provision of a neutral beam is recognized but not shown on the layout because of the lack of detailed information on components and shielding in the median plane in the forward direction. In the NAL designs, the beams are generally three stage beams with fine momentum resolution determined by collimators. In contrast, our beams have large momentum bite $\Delta p/p \simeq (1 - 2\%)$ with the fine resolution determined by a spectrometer in the final arm. The final fluxes on the experiments' targets are quite adequate as can be seen

from Table 13.4. These estimates are based on the thermodynamical model of Hagedorn and Ranft[13.3] for protons on a Beryllium target. The yields are, of course, higher at less than the maximum momenta, for π^+ rather than π^-, and for K^+ rather than K^-. Up to 100 GeV/c the antiproton fluxes in the beams are about 10^5 per 10^{12} interacting protons.

Table 13.4

Yields for 10^{12} Interacting Protons on Be Target at 200 GeV

Target	Beam	Production Angle	Solid Angle	Nominal $\Delta p/p$	π^- Yield	K^- Yields
T_1	North, 150 GeV/c	0 mrad	2.4×10^{-6} ster	1%	1.0×10^{7} at 100 1.0×10^{6} at 150	1.5×10^{5} 0.6×10^{4}
	South, 50 GeV/c	0 mrad	2.4×10^{-6} ster	1%	2.0×10^{7}	1.2×10^{6}
T_2	North, 75 GeV/c	5 mrad	5×10^{-6} ster	1%	2.0×10^{7}	0.8×10^{6}
	South, 75 GeV/c	5 mrad	5×10^{-6} ster	1%	3.5×10^{7} at 50	1.8×10^{6}
	South, 25 GeV/c	10 mrad	3×10^{-6} ster	1%	1.3×10^{7}	1.5×10^{6}
T_ν	Neutrino	0 mrad	1.5×10^{-2} ster	wide band	10^{8} neutrinos/m^2	at BEBC
	r.f. to BEBC	0 mrad	1×10^{-6} ster	0.4%	2.0×10^{5} (at 150 GeV/c)	3×10^{4} (separated at 50 GeV/c)

13.2.3 Neutrino experiments

Neutrino experiments will certainly be among the most important experiments to be performed at the 300 GeV accelerator at CERN. In this Section two alternative ways of providing a neutrino beam in the CERN West Hall are described[13.4].

The first (a horizontal beam) uses the ejected proton beam (EPB) arriving parallel to the North Wall of the West Hall and a target station 400 m upstream of BEBC. The muons are absorbed by a steel shield in the West Hall. Such a neutrino beam would be effectively limited to operation with 200 GeV/c protons because of the geometrical restrictions and the high cost of the steel shielding. The shielding is included in Fig. 13.2.

The second (an inclined beam) uses the proton beam soon after ejection and a target station underground in a tunnel rising towards BEBC. The shielding would be provided by the natural molasse and earth between the end of a decay tunnel and BEBC. Such a neutrino beam would be about three times less efficient than the first version at 200 GeV/c because of the reduced solid angle. However, it could be optimized for 300 GeV/c and be operated effectively for 200 GeV/c or even 400 GeV/c protons in addition. Radiation, cost, and operation problems are considerably less for this inclined beam than for the horizontal beam in the West Hall. The lower neutrino fluxes could be compensated by additional running time.

The cost estimates for the above options are compared in Table 13.5. These are additional costs assuming existing equipment is fully used. The solution using an inclined decay tunnel appears to have considerable economic advantages, as well as leaving more space available in the West Hall. Thus this could be considered as an alternative to the beam (1) indicated in Figs. 13.1 and 13.2.

Although this Section has been oriented towards a neutrino beam into BEBC, counter neutrino experiments could also be mounted in front or behind BEBC in either solution.

Table 13.5

Cost Estimates (in MSF) for 200 and 300 GeV/c Operation of Two Possible Neutrino Beams

		Beam Line			
		Horizontal		Inclined	
	Momentum (GeV/c)	200	300	200	300
1.	Focusing elements R1 (horn), R2, (R3)	0.20	0.20	0.20	0.20
	Modification and conditioning of existing elements				
2.	Power Supplies	0.25	0.25	0.25	0.25
	(additional costs assuming existing equipment is modified and used)				
3.	Controls etc.	0.10	0.10	0.20	0.20
4.	Buildings for power supplies, etc.	0.05	0.05	0.60	0.60
5.	Shielding: 14'000 ton (200 GeV/c) Fe	10.00	13.60	-	-
	19'000 ton (300 GeV/c) Fe				
6.	Proton Beam Transport	-	-	1.75	2.75
7.	Tunnel Costs (additional for ν beam) (460 m decay tunnel and branch)	-	-	1.00	1.00
	Totals (MSF)	10.6	14.20	4.00	5.00

13.2.4 r.f. Separated Beam for BEBC

An r.f. separated beam can be built, using a target located at the place of the neutrino target, about 400 m in front of the chamber. As an unseparated beam, it can transport particles up to 150 GeV/c.

In order to separate particles up to the highest possible momentum within the available length, it is foreseen to modulate the primary proton beam on the target with a first r.f. cavity. The second is located as far as possible from the target ($\sim$ 320 m). This should allow the separation of K's up to 55 GeV/c with the present cavities (f = 2855 MHz). This method of separation needs a very small target and a very small spot size for the primary proton beam, but these requirements seem compatible with the possibilities of the accelerator.

A dump of the primary beam has to be installed about 70 m after the target.

Such a beam would use 25 quadrupoles of 10 cm aperture, 2 m long and would require a total bending power of 53 Tesla metres for a top momentum of 150 GeV/c. Typically a gap of 5 cm is required for the bending magnets.

The cost of the beam handling elements is given elsewhere. For the r.f. separator, collimators, electronics, cables, the cost would be 1.8 MSF, without the shielding and proton dump. Existing equipment which would be used accounts for 1.5 MSF so the additional cost for high energy operation would be 0.3 MSF.

In order to separate K's at higher momenta, it is necessary to use higher frequencies, up to 10,000 MHz. This requires study and developments whose cost is difficult to estimate, but which should not exceed 3 MSF. With such separators, the maximum momentum for K's should be around 85 GeV/c.

13.2.5 Beams for electronics experiments

The layout shown in Fig. 13.1 provides 5 charged particle beams for electronics experiments. It is hoped to add a neutron or K_L^o beam at a small production angle when more details are available on the physical arrangements inside the target stations. The charged particle beams are unseparated and provide of the order of 10^7 particles per pulse, which for most experiments is close to the maximum that can be handled electronically. The momentum acceptance in the beams has been taken to be 1%. It is envisaged that those experiments needing one pion mass resolution would use multiwire proportional chamber spectrometers in the final stage of the beam. Particle identification can be achieved by gas DISC counters and long threshold Cerenkov counters.

a) High energy, high resolution beam (beam 3)

This beam is produced at zero production angle from the achromatic target station T1. Three stages are foreseen: the first one will provide the momentum selection, the second one, with a 12 m long parallel section satisfying the DISC requirements of low divergency, will be used for mass determination; finally, the third stage is foreseen for accurate momentum measurement on individual particles. In this stage, detectors with 0.3 mm resolution should permit momentum measurement with error smaller than 100 MeV/c.

The total length of the beam is 215 m. Its maximum energy is 150 GeV/c.

b) Medium energy beam to Omega (beam 6)

This beam will also be produced from the achromatic station T1 at zero production angle. r.f. superconducting cavities are foreseen for this beam with a drift space of about 100 m between them. With S-band working cavities, separation of K from π will be possible up to 22 GeV/c and that of $\bar{p}$ from π up to 40 GeV/c. With X-band cavities separation will be possible up to 40 GeV/c for K and 50 GeV/c for $\bar{p}$.

The beam is designed with the many stages required for the best use of the r.f. separators, that is, momentum selection stage, momentum recombination and focusing on the first cavity, focusing on the second cavity, focusing on the beam blocker, momentum measurement and matching to the experiment.

The maximum angular acceptance foreseen is $4 \cdot 10^{-6}$ sterad but it will depend on the performance of the cavities and from the actual running energy of the beam.

The total length of the beam is 240 m. Its maximum foreseen energy is 50 GeV/c.

c) Medium and low energy beams (beams 4, 5 and 7)

Two 75 GeV/c and one 25 GeV/c beams are produced from target T2. These are classical two stage beams. The 25 GeV/c beam (beam 7) is in fact almost identical with the s_5 spectrometer used in the East Hall during 1970. The 75 GeV/c beams are two stage beams of length 160 m with dispersion at the first focus of 2 cm for $\Delta p/p = 1\%$. The 25 GeV/c beam is also two stage, of length 88 m and with dispersion of 1.5 cm for $\Delta p/p = 1\%$.

13.2.6 Special beams

The beams discussed in Section 13.2.2 fall in the category of standard beams continuously available for many experiments. In addition other types of beams can be considered. Four possible beams of special type have received attention.

a) Long-lived neutral beam

This can be considered as almost a standard beam and it is intended to incorporate a neutral beam into the layout when the shielding studies have advanced sufficiently to allow one to make a reasonable design. Not only high energy neutrons would be available but also K_L^o mesons which allow very interesting experimental possibilities.

b) Muon beam

A possible way of modifying an existing beam to produce muons is to utilize the first stage of, for example, beam (3) in Fig. 13.1 as the decay path for muons from the pions and kaons in the beam. The residual hadrons would then be absorbed in a steel block and the subsequent stages of the beam would be used to focus and transport the muons to a target. Preliminary calculations indicate that $\sim 10^6$ muons per pulse could be obtained in this way in a momentum band of $\pm$ 3%.

c) Electron or photon beam

This could be regarded as already included in (a) since it is initially a neutral beam, however, for reasonable intensities of photons, a much larger acceptance would be necessary. A second target of heavy material would be used to convert the γ-rays to electrons. After momentum analysis and focusing the electrons would be available for an experimenters target or could be reconverted into γ-rays, whose energy could be measured by the tagging technique, using a third target.

Because of the multiple stages, such a beam would require high intensities and large acceptance magnets.

d) Hyperon beam (or K^{o}_{S} beam)

The provision of a hyperon beam is almost an experiment in itself rather than a facility. Special magnets, shielding, and beam transport are needed because of the short life of the hyperon. Such a beam is currently under construction at the CERN PS and the results could lead to a desire to make a similar beam from 200 GeV/c incident protons. A K^{o}_{S} beam could also be considered in the same category as a hyperon beam.

Any of the above beams could be installed in the West Hall, probably with the effect of removing one of the standard beams. It is one of the virtues of the West Hall that changes in beam layout can be considered especially if only 200 GeV protons are used. It might well be that after the completion of the North Area the West Hall will become an area of predominantly special beams because of this flexibility, since the problems of shielding around beams of momenta $\geq$ 300 GeV/c are such that the probable installation in the North Area will be mainly earth shielded and thus rather inflexible towards changes in beams.

13.2.7 Standardization of beam elements; costs

a) Standardization

The secondary beams listed in Table 13.6 can be constructed with the following beam elements:

Bending Magnets

gap : 5 cm
width : 6.5 - 10 cm
lengths: 3 m, 5 m
field : 1.8 T

A possible economic way of producing such magnets would be to use the same laminated iron core as the machine magnets (4.8 cm gap). The coil configuration would be different and a current density of 500 A/cm^2 is suggested as an optimum.

Quadrupoles

1) aperture: 5 cm
gradient: 20 T/m
lengths : 2 m, 3 m.

A possible economy again might occur if the core shape of the machine quadrupoles (Q_D) were to be used, modified in length and coil configuration, giving a quadrupole of aperture 6 cm.

A second quadrupole type with aperture 10 cm is also needed, with the following parameters:

2) aperture: 10 cm
gradient: 24 T/m
lengths : 2-3 m.

This would be a new design. A current density of ≈ 1000 A/cm^2 is suggested.

All these beam elements could be built with laminated cores since this is cheaper for large series production. Additional magnets with larger apertures and gaps will be available from the stock existing in the West Hall and from other CERN areas if necessary. These would be useful for the 25 GeV/c beam, producing an even larger acceptance than quoted. They could also be used for the beam transport $T_1 - T_2$ where 15 cm quadrupoles are desirable. For the high energy beams, the gaps and apertures of the CERN standard elements are not well matched to the needs. However, they could well be useful in the experiments themselves, as large acceptance spectrometer magnets.

Table 13.6

Cost Estimate for 200 GeV/c Layout in the West Area

(1970 Prices - excluding special elements in target stations)

Beam		Total length (m)	Aperture gap (cm)	Gradient (T/m) Field (T)	Magnet Costs, incl. power supply + cooling (kSF)		Power consumption (kW)	
RF								
(2)	BM	37	5	1.8	1250-1390		600	
	QP	50	10	15	1950-2100	3200-3490	850	1450
150 GeV/c								
(3)	BM	28	5	1.8	910-1050		450	
	QP	36	10	24	1480-1590	2390-2640	610	1060
75 GeV/c								
(4)(5)	BM	16	5	1.8	520- 620		260	
	QP	14	5	17	290- 320	× 2	60	× 2
	QP	4	10	15	160- 170	1940-2220	70	780
50 GeV/c to Ω (6)	BM	15	5	1.8	490- 560		250	
	QP	32	10	24	1260-1340	1750-1900	540	790
25 GeV/c								
(7)	BM	12	5	1.8	390- 450		200	
	QP	14	10	24	550- 590	940-1040	240	440
Between tgts								
T_1-T_2	QP	18	15	20		950-1050		450
					Totals	11170-12340		4970

For the purpose of the present study, superconducting beam elements have not been considered since present indications are that they are not an economical solution except in special cases where extremely short beams are needed. This will clearly need reconsideration, if superconducting elements become less expensive in the future.

b) Cost estimate for the beam elements

For the beams indicated in Fig. 13.1, a cost estimate for magnets, power supplies and cooling is listed in Table 13.6. Since it is difficult to predict the mean power consumption of experimental magnets, no running costs are included. The cost optimum for bending magnets is shifted to a higher current density (500 A/cm^2, compared with 300 A/cm^2) when running costs at a continuous level are included in the optimisation. For quadrupoles, a very flat optimum exists around a current density of 1000 A/cm^2, with or without running costs included in the optimisation[13.5]. An upper and lower limit of costs is given according to specific costs of power supplies (0.15 - 0.3 kSF/kW) and different mean flux in the return yokes. The cooling costs are assumed to be 0.2 kSF/kW including cooling towers, etc.[13.6].

13.2.8 Beam switch and target stations

a) Beam switch

The fast ejected beam is deflected onto a target T_ν to provide BEBC with either a neutrino beam or an r.f. separated beam.

As illustrated in Fig. 13.3, switching is controlled by the vertical fast kicker magnet K, which is powered during fast spill. In conjunction with the series of septum magnets D_1, D_2, D_3, and the vertical benders VM_1 and VM_2, it creates a 60 cm separation between the fast-spill and slow-spill branches.

The layout of the fast and slow spill branches of the proton beam in the vicinity of T_ν and T_1 is shown in Fig. 13.4.

Suitable parameters for the various elements are summarized in Table 13.7.

b) Achromatic target station, T_1

In the slow ejected branch, the beam is first focused onto an achromatic target station T_1, illustrated in Fig. 13.5. This provides two high-quality secondary beams S_1 and S_2 at zero production angle; and permits the continuing proton beam to follow its original path, independently of the momenta chosen for S_1, S_2.

The S_1 momentum is changed by varying the fields in the bending magnets M_1, M_2 and the special "sandwich" septum magnets SM_1 - SM_4: the S_2 momentum may then be chosen independently, in the approximate range 0.17 - 0.33 $p(S_1)$, by varying the fields in the septum and bending magnets M_3, M_4 and M_5.

Suitable parameters for the different magnets are quoted in Table 13.8.

Table 13.7

Magnets for Beam Switch

Kicker Magnet, K

Length	5 m
Field	0.47 T
Deflection	2.8 mrad
Rise Time	∿ 50 us
Cost of Magnet and Power Supply	150 kSF

Beam Dividing Magnets	D_1	D_2	D_3
Septum thickness (mm)	16	30	60
Magnet aperture (mm)	15	15	15
Length (m)	2.0	2.0	2.0
Field (T)	0.9	1.5	1.8
Deflection (mrad)	2.6	4.4	5.4
Mean current density in Septum (A/mm^2)	90.0	80.0	48.0
Cost of Magnet (kSF)	14	17	24
Cost of Power Supply (kSF)	------300---------		

Matching and Transport Quadrupoles	L_1-L_5	Q_1-Q_8
Length (m)	2	3
Aperture (mm)	60	30
Gradient (T/m)	25	35
Cost incl. power supply (kSF)	5×56	8×60

Bending Magnets

	M_1-M_6 VM_1, VM_2	M_7-M_9
Length (m)	6	2
Gap (mm)	60	60
Field (T)	1.8	1.8
Cost incl. power supply (kSF)	8×210	3×70

Table 13.8

Magnets for Target Station T_1

Sandwich Magnets		SM_1	SM_2	SM_3	SM_4
Length	(m)	1.0	2.0	2.5	5.0
Horizontal Aperture (front)	(mm)	300	340	390	420
Horizontal Aperture (back)	(mm)	320	390	420	420
Vertical Aperture in Field Region	(mm)	28	32	37	50
Vertical Aperture in Field Free Region	(mm)	58	68	80	100
Horizontal Aperture at end of Field Free Region	(mm)	45	60	80	150
Field	(T)	1.6	1.7	1.8	1.7
Conductor Thickness	(mm)	11	17	35	75
Average Current Density	(A/mm^2)	116	80	41	18
Cost of Magnet	(kSF)	50	100	160	360
Cost of Power Supply	(kSF)	---------300---------			

H Type Magnets		M_1	M_2	M_5
Length	(m)	5.0	5.65	3.0
Field	(T)	1.8	1.8	1.8
Vertical Aperture	(mm)	50	100	100
Horizontal Aperture	(mm)	500	230	150
Cost of Magnet	(kSF)	400	450	100
Cost of Power Supply	(kSF)	70	70	70

Septum Magnets M_3 and M_4		
Length	(m)	2
Septum Width	(mm)	50
Vertical Aperture	(mm)	40
Horizontal Aperture	(mm)	300
Max. Field	(A/mm^2)	29
Current Density in Septum	(T)	1.8
Cost of Magnet	(kSF)	2×100
Cost of Power Supply	(kSF)	300

c) Finite production angle station, T_2

Protons which have not interacted in T_1 are refocused at T_2. There, secondary beams at different finite production angles are selected by a suitable arrangement of septum magnets; nine of these are involved in the scheme, illustrated in Fig. 13.6 to provide two 75 GeV/c beams at ± 5 mrad, and a 25 GeV/c beam at 10 mrad.

Typical septum magnet parameters are given in Table 13.9.

Table 13.9

Septum Magnets for Target Station T_2

		S_1	S_2	S_3
Length	(m)	1.5	1.75	1.75
Septum Width	(mm)	6	24	50
Vertical Aperture	(mm)	45	50	60
Horizontal Aperture	(mm)	50	100	150
Current Density in Septum	(A/mm^2)	100	44	27
Cost of Magnet	(kSF)	3×28	3×35	3×52
Cost of Power Supply	(kSF)	----------300----------		

13.2.9 Radiation problems in the West Experimental Area

The West Experimental Area is situated close to the Route Nationale 84. The radiation field outside CERN must not produce a dose rate higher than 170 mrem/y (= average dose rate of 30 μrem/h with 6000 hr of operation/year). These low dose rate levels at the fences determine the shielding requirements in most places of the West Area rather than the limits for unrestricted radiation areas inside the hall (≤ 2.5 mrem/h).

Shielding thicknesses required for hadron attenuation around the three targets are typically 1900 g/cm^2, for the EPB about 1500 g/cm^2 and for the decay tunnel for the neutrino experiment about 1700 g/cm^2. These numbers are given for earth or concrete and are 25% higher for steel. The amount of hadron shielding needed will not depend much on the final energy chosen. Raising the energy from 200 GeV to 300 GeV requires about 50 g/cm^2 more transverse shielding thickness. A possible shielding layout for the West Hall based on the preliminary design discussed in Section 13.2.2 is given in Fig. 13.2.

For the muon backstop it is proposed to use a 4.8 m wide and 3.6 m high steel beam dump, the length of which is a nearly linear function of the primary proton energy. For 200 GeV, 90 m are proposed. Behind this muon backstop the dose rate due to muons is below 1 mrem/h for $2 \cdot 10^{12}$ p/s interacting in the second target station. Along the side of this muon dump the dose rate due to multiple scattered and deflected muons is estimated to be below 10 mrem/h, taking into account the deflection of pions and muons in the magnets of the target

stations. An external earth shielding of 1500 g/cm^2 around the transfer tunnel 4, 1300 g/cm^2 at transfer tunnel 5 and 1300 g/cm^2 on the north side of halls E3 and E1, can be provided. Most of the costs are already included in the building cost.

Shielding costs:	Target T_1 + T_2	5.3 MSF
	μ backstop	8.4 "
	Target T_ν , + secondary beams	5.1 "
	Neutrino shielding	10.0 "

13.2.10 Beam transport to the West Hall

The transport system proposed consists of a periodic lattice 780 m long whose construction is similar to that of the accelerator itself. The lattice will be preceded by a matching section 54 m long from the ejection point and will be followed by focusing sections to the targets (see Section 13.2.8).

In order to transport the ejected beam from the machine to the West Hall, with the present position of the accelerator and beam layout as indicated in Section 13.2.2, both vertical and horizontal bending is needed. The vertical displacement from the accelerator level (402 m) to the nominal beam height in the West Hall (448 m) can be achieved using two vertical bends. In between these a horizontal bend of 118 mrad is necessary to bring the beam into the West Hall parallel to the North wall.

The transport elements proposed are essentially identical with the elements of the accelerator, although one might wish to choose a different coil configuration to optimise running costs. The parameters are:

a) Quadrupole

Aperture Ø = 60 mm
Length = 2.65 m
Max. gradient = 22 T/m

b) Bending magnets

Aperture = 60 × 40 mm^2
Length = 6.0 m
Max. field = 1.8 T.

The lattice consists of 12 periods each 67.8 m long, with $\mu = \pi/2$, $\beta_{max} = 114.66$, $B_{min} = 20.04$. The acceptance is compatible with the emittance of the ejection system. The disposition of the elements is shown in Fig. 13.7. The horizontal bending of 118 mrad is achieved with 8 magnets (at 200 GeV/c) in an achromatic structure. 300 GeV/c or 400 GeV/c protons could be transported by increasing the number of horizontal bending magnets to 12 and 16, respectively. The vertical bending is composed of an initial bend of 62 mrad (from the ejection line which is 15 mrad from the horizontal) and a final bend of 77 mrad to return

the beam to the horizontal plane. This can be achieved (at 200 GeV/c) by two vertical bend periods each containing 6 magnets. Again 300 or 400 GeV/c protons could be transported by increasing the number of bending magnets. At 300 GeV/c 2 × 8 magnets are needed and for 400 GeV/c an additional 4×3 m long magnets would be added. The quadrupoles are designed to operate up to 400 GeV/c.

The beam transport costs, estimated including power supplies and cooling are:

Max. Momentum	No. of Bending Magnets	No. of Quadrupoles	Estimated Costs (Quadrupoles + Magnets)
200 GeV/c	20	24	1.8 + 4.2 = 6.0 MSF
300 GeV/c	28	24	1.8 + 5.9 = 7.7 MSF
400 GeV/c	32 + (4 × $\frac{1}{2}$)	24	1.8 + 7.2 = 9.0 MSF

13.2.11 Possibility of 300 GeV/c protons in the West Hall

One of the possible options of the 300 GeV Programme would be to put all the effort in providing 300 GeV/c protons as soon as possible, which is estimated to be during the sixth year of the Programme. The North Area would not, however, be completed until the end of the eight year programme. The question which must be answered is whether the West Hall could benefit from the additional energy.

The problem of increased energy protons in the West Hall is two-fold. The production of higher energy muons means that shielding must either be increased in length, resulting in higher costs, and reduced space in the Hall, or some other technique must be used to eliminate the problem of the muon radiation. The second problem is the limited length of the West Hall. Since secondary beams tend to grow in length in proportion to the maximum momentum for which they are designed, it is not obvious whether a higher momentum beam could be placed in the West Hall to make maximum use of the higher energy protons.

These problems have been studied by a grup in the NP Division of CERN[13.7] and the following sections summarize the result of this exercise, which is limited to consideration of the counter beams. The utilization of 300 GeV protons for neutrino physics has already been discussed in Section 13.2.3, and it is assumed here that the inclined beam solution would be chosen. It is also assumed that the r.f. separated beam for BEBC would remain essentially unchanged.

a) Muon shielding

The design of the shielding downstream of the production target for a 300 GeV EPB must take into account the flux of muons resulting from the decay of pions and kaons between the production target and the beginning of the shielding. In particular, the average muon flux at the CERN fence behind the West Area ($\sim$ 540 m from the production target) must be kept below the value of 1 $\mu/cm^2 \times s$, which corresponds to a radiation level of $\sim$ 0.1 mrem/h.

The flux of muons emerging from an iron shielding has been calculated as a function of the shielding thickness, for various values of the angle between the muon and the EPB directions. These calculations require a reasonable extrapolation from 25 GeV to 300 GeV of π and K production cross-sections vs. the momentum and angle of the secondary particle, and the knowledge of the muon energy losses. Energy losses due to bremsstrahlung and pair production become comparable to the ionization losses above 150 GeV. Multiple scattering of the muons in the shielding is also taken into account.

For an average rate of $2 \cdot 10^{11}$ interacting protons/s, and assuming a decay path of 10 m between the production target and the shielding which is probably a minimum possible value, it is found that the muon flux becomes less than 1 $\mu/cm^2 \times s$ at a distance of 540 m from the target only for iron shieldings more than 120 m long.

Multiple Coulomb scattering requires the shielding to be approximately 3 m wide by 3 m high, corresponding to a total weight of $\sim$ 8000 ton.

Doubling the total number of muons produced (e.g. by doubling the average rate of interacting protons), would require increasing the shielding by $\sim$ 8 m of iron to keep the muon flux to the above-mentioned maximum level.

We believe that this solution for the shielding problem is unrealistic, because of the very high cost involved for the total amount of iron needed ($\gtrsim$ 6 MSF). As a solution, we propose a shielding whose main component is a magnetized iron block[13.8], 6 m long × 2 m wide × 2 m high, located as close as possible (a few metres) to the production target, and containing appropriate holes for the passage of the secondary beams. This block contains coils producing a horizontal magnetic field B = 18 kGauss, perpendicular to the EPB direction, which deflects positive particles downwards and negative particles upwards. Muons with momentum p_μ going through this block are deflected by an angle $\alpha = 3250/p_\mu$ mrad (p_μ in GeV/c), corresponding to a variation of the muon transverse momentum $|\Delta p_t| = 3.25$ GeV/c. Since the muons produced with such a large transverse momentum are expected to be $\sim 10^{-4}$ of those produced at 0°, such a shielding device is very effective in removing the muons from the forward direction and dispersing them in the vertical plane according to their momentum. The minimum deflection angle, corresponding to $p_\mu = 300$ GeV/c, is $\alpha_{min} \sim 11$ mr. Since the beam height in the West Area is 206 cm, all the positive muons (deflected downwards) will penetrate into the ground well before reaching the back wall of the area. The negative muons being deflected upwards, no radiation level will be detected at the CERN fence (540 m from the production target) before reaching a height of $\sim$ 10 m above the ground (the ground level at the CERN fence is 3 m below the West Area floor). The bulk of the muons will obviously be found at heights of 30-40 m above the ground level, since their average momentum is $\sim$ 50 GeV/c.

Finally, it may turn out to be necessary to use magnetized iron blocks as beam dumps for all the secondary beams exceeding an average intensity of $\sim 10^6$/s, to eliminate the muons produced in the decay of the beam particles.

b) A possible beam layout

A possible layout of secondary beams is shown in Fig. 13.8. One production target (T1) is located inside the TT5 building on the same position as for the 200 GeV scheme. The proton beam line is supposed to be oriented at 100 mrad with respect to the longitudinal walls of the hall.

The layout of beams is conditioned by the need to reduce as much as possible the muon background on the experimental area and on the fence of the site, as said before.

The secondary beams are emitted at finite production angle and are independent one from the other for polarity and energy. The magnetized iron shielding, 6 m long, is located starting 3 m after the target. The beams traverse this shielding through narrow channels where no field is present. The overall background in the hall is strongly reduced by this method but on the other hand, this strong collimation very close to the source can produce an unwanted halo that must be cut to provide a reasonable momentum selection. This can be achieved with a preliminary stage to redefine the source by means of narrow slits. The momentum selection stage will then follow.

From the target three secondary beams are foreseen. Furthermore a very reduced intensity full energy proton beam (1) is allowed to continue across the hall down to a second target T2, which might be used for special, not yet defined purposes (hyperon beam for instance). It will be also possible in an easy way to sweep the protons out of this line and get along it a neutral beam produced in T1 at nearly 0^{o} production angle.

The three suggested beams are, in addition to the proton beam:

2. A 250 GeV/c maximum energy beam emitted at 2 mrad production angle. This beam is shown on the north side of the EPB line, it has a length of 240 m and an angular acceptance of $1.5 \cdot 10^{-6}$ sterad. It consists of a "preliminary" stage, a momentum selection stage, which can be used also for mass determination, and a momentum selection stage, which can be used also for mass determination, and a momentum measuring stage. The experimental set-up on this beam might extend inside building E2 (70 m length available).

3. A 150 GeV/c maximum energy, high resolution beam, emitted at 3.5 mrad production angle. This beam, shown on the south side of the EPB line, is 210 m long and has an angular acceptance of $2.5 \cdot 10^{-6}$ sterad. Its structure is similar to that of beam 2. The space available between the experimental target of this beam and the end of the hall is 60 m, but might be increased rather easily outside the hall.

4. An r.f. separated, 50 GeV/c maximum momentum beam for the Omega experiment. This beam will be 240 m long, will have an angular acceptance of $2.5 \cdot 10^{-6}$ sterad and will have approximately similar performance as described previously for the 200 GeV/c

scheme. Also in this beam, however, a preliminary stage, not indicated in the figure, will be necessary to redefine the source.

For all these beams, quadrupoles of 60 mm aperture and g = 33 T/m and bending magnets of 5 cm gap and 1.7 T have been assumed. Furthermore, 4 septum magnets, 4 m long each but of different field and septum thickness, are mounted immediately after the magnetized iron shielding: two of them on beam 2; and one each on beam 3 and 4, to separate the beams.

13.3 North Experimental Area (300 - 400 GeV/c)

The North Experimental Area will be designed with the aim of providing beams up to the highest energies available from the new accelerator. As indicated in the Introduction, only preliminary ideas on how to achieve this aim will be presented.

13.3.1 Shielding at high energies

As can be clearly seen from Section 13.2, shielding becomes a major problem at higher energies, and the economy of using earth shielding becomes very attractive.

A possible way to achieve this situation is to keep the EPB below the surface level all the time. In this way the muon problem disappears since these are just stopped in the earth. Because one must derive secondary beams from targets in the EPB, a level not too far below the surface is preferred, and from a study of the ground profile it seems that a possible solution would be to raise the EPB from machine level up to an altitude of $\sim$ 445 m and let it continue horizontally. Such a rising section would be rather similar to that discussed for the West Hall in Section 13.2.10 of this Chapter. The beam would be horizontal at the new level 600 m after ejection if a vertical bending angle of 130 mr is assumed. At this point the ground level is 450 m and beyond it rises to a maximum of 473 at a distance of 2.7 km from ejection.

The EPB tunnel would be located in the topsoil and so a cut-and-fill construction seems indicated. The secondary beam lines could be accommodated in similar cut-and-fill tunnels, thus using the surrounding earth as a natural shield.

13.3.2 Secondary beams

It is not very useful at this stage to make, as an exercise, a layout drawing of beams, as has been done in this Chapter for the West Hall. However, one can consider the general question of possible ways of deriving high energy secondary beams from the targets in the EPB.

A possible way of separating the secondary beams from the EPB which is under study at present consists of using a small horizontal bend in the EPB, which then is pointing somewhat away from its nominal line. A target located at this point could be used to derive beams (of order three in number), which would be transported in tunnels to the location of the experiments. A typical distance needed to provide a high resolution, 400 GeV/c, secondary beam is of the

order of 600 m. Thus some 600 m beyond the target the beams would emerge into an experimental zone, which would house the various experiments.

After traversing the first target, which could be thin, the protons would be refocused and deviated to the other side of the nominal EPB line to interact with a second target, which would feed high energy beams to a second Experimental Zone. Such a scheme is indicated in Fig. 13.9.

13.3.3 Experimental zones

Such experimental zones, with a floor level 2 m below the beam height (i.e. 443 m) could be covered by a roof of very light construction. If the roof could be made to slide open, major experimental installation changes could be affected using a gantry crane operating through the roof. Thus the top of such zones need not project above surface level. Since the ground level at this stage is at $\geq$ 451 m, one has already $\geq$ 8 m vertical height up to surface level. The area needed for such experimental zones could be relatively small, probably $\sim$ 30 m wide and $\sim$ 250 m long.

13.3.4 Further possibilities, Neutrino physics

Finally the EPB could be brought back to its nominal line. A final target, which could be on the EPB line, might be a valuable possibility for producing a neutrino beam for counter physics experiments. The natural earth would be used as a muon filter and proton backstop so the experiment would be located a long way beyond the end of the EPB tunnel, in a small underground vault. The value of such a final target is that whatever protons are unused by the first two targets would interact in the (thick) final target. A neutrino experiment would thus be able to run parasitically for long periods, which is desirable when studying such small cross-section processes. Since the inclined beam solution for neutrinos in the West Hall could operate up to 400 GeV/c (see Section 13.2.3), it does not seem necessary to consider moving BEBC to the North Area, or provide for a bubble chamber installation there, at the present time.

13.4 Summary of Costs

The costs estimated will be presented in two parts: the West Hall which should operate early in the sixth year of the Programme and the North Area which will only be ready at the end of the 8-year Programme. It is assumed that the West Hall operates only up to 200 GeV/c for this estimate. Furthermore, the layout indicated in Section 13.2.2 has been adhered to, including the horizontal neutrino beam.

13.4.1 West Hall (200 GeV/c)

a) Proton Beam Transport to West Hall; Targets; Shielding

Beam transport elements	6.0
Beam switch magnets and matching elements	2.7
Shielding around Targets: T1, T2	5.3
μ-backstop	8.4
Special costs to cope with high radiation levels in target stations	2.0
	24.4 MSF

Not included: Tunnel costs, Running costs, EPB Transport Controls

b) Secondary Beams

Beam transport elements	12.0
Neutrino beam (mainly shielding costs)	10.6
Target stations T1, T2 (Special magnetic elements)	4.0
Shielding for T_ν and secondary beams	4.3
Beam stoppers, local interlocks, collimators	3.0
Vacuum chambers (secondary beams), pumps	1.0
	34.9 MSF

Not included: r.f. separators, Cerenkov counters, Detectors in secondary beams, experimental magnets, etc.

13.4.2 North Area (300 - 400 GeV/c)

This estimate must be considered as an order of magnitude calculation rather than a reliable number since no detailed studies have yet been made of the North Area. The beam transport is estimated for 400 GeV/c maximum momentum.

a) Proton Beam Transport; Targets; Shielding

Beam transport elements	14.0
Special elements for focusing on targets	1.5
Special costs to cope with high radiation levels in target stations	3.0
Local shielding around targets	2.0*
	20.5 MSF

Not included: Tunnel costs, Running costs, EPB Transport controls.

* Included in Chapter 15 costs.

b) Secondary Beams (6 have been assumed)

Beam transport elements	∿35.0
Target stations (special magnetic elements)	∿10.0
Beam stoppers, local interlocks, collimators	∿ 3.0
Vacuum chambers (secondary beams), pumps	∿ 3.0
	∿51.0 MSF

Not included: Tunnel costs for secondary beams, Costs of Experimental Zones, r.f. separators, Cerenkov counters, detectors in secondary beams, experimental magnets, etc.

13.5 Conclusions

This Chapter has summarized the results of the first stage of a study of the utilization of the experimental areas of the 300 GeV accelerator. Most of the work has been devoted to the West Hall and in order to start, certain assumptions have been made. These were based essentially on an extrapolation of the planned operation of the West Hall at 25 GeV/c to an energy of 200 GeV/c with the minimum changes possible. For example, the height of the ejected proton beam in the West Hall was chosen to be the same as that to be used at 25 GeV/c; conventional shielding methods were used in the design; a neutrino experiment was planned using an extension of the present technique with iron shielding to stop the muons. With these assumptions it has been shown that the West Hall can be used effectively as an experimental area for physics with 200 GeV protons, and the costs of the proton beam transport and secondary beams have been estimated (Section 13.4.1). This was the main aim of the study.

However, as might be expected, during the course of this study alternative possibilities involving different assumptions have become clearly preferable. This is well illustrated in Section 13.2.3 where a study of the possibilities for neutrino experiments in the West Hall has shown the advantages of abandoning the conventional approach used at lower energies involving a steel muon filter in favour of a design using the natural rock and earth to stop the muons. This has been shown not only to be economic at 200 GeV/c but to allow neutrino experiments up to 400 GeV/c with the existing bubble chamber (BEBC).

Having shown that the natural earth shielding is an economic solution for the neutrino beam, one can investigate how the high cost of shielding for the other targets could be reduced if the earth could be used as a shield there also, as has been discussed for the North Area. This has not yet been studied in detail but a possible way would be to abandon the assumption that the EPB comes into the West Hall, as is the case for 25 GeV/c, at a height of 448 m. If the EPB were to become horizontal at a height of ∿ 440 m, the targets could be located underground and the secondary beams brought up to the surface in the tunnels TT4 and TT5. Not only would this arrangement eliminate the need for a steel muon backstop,

but also it would allow the targets for secondary beams to be moved further upstream thus giving much more space in the West Hall to the experiments, as well as allowing even longer beams which would certainly benefit, for example, the r.f. separated beams.

If such a solution does turn out to be attractive, further economies could be made on the proton beam transport to the West Hall by moving the centre of the accelerator about 50 m to the north. The EPB could then be transported to the West Hall with virtually no horizontal bend from the ejection point to target T_1, whereas the preliminary design in Section 13.2 has a total bend of 230 mrad between ejection and T_1. This is not possible when the EPB is brought up to 448 m because of the proximity of RN 84 and the need to keep within the tolerance of radioactive levels on this highway. The additional 8 m of depth would remove to a large extent the problem of radiation on RN 84. It is also clear that the difficulties of operating the West Hall at energies greater than 200 GeV would be reduced if such an alternative is possible, since the shielding would still be provided by the natural earth and rock, at no extra cost.

The philosophy of this study has been to design a possible layout for the West Hall at 200 GeV, with some consideration of what might be possible at 300 GeV, with the implicit assumption that the higher energies would be used in the North Area. This does not mean that the West Hall would become obsolete when the North Area and higher energies are available. The accelerator could be operated with two magnetic flat-tops and the two areas could be operated simultaneously, for example with the West Hall ejection at 200 GeV/c and the North ejection at 300 or 400 GeV/c (or even higher eventually). Thus the existence of the West Hall to cover the lower energy range enables the North Area to be very specifically designed for the utilization of the highest energy secondary beams.

No detailed design of such high energy secondary beams has been made, but some preliminary ideas on the possible ways of deriving such beams from targets in the EPB have been presented, with the emphasis on using the natural earth shielding. It seems quite possible to locate two experimental zones, each to accommodate 3-4 experiments, fed by secondary beams up to 400 GeV/c, within the first 1.5 km of the strip to be available from the North Experimental Area. In addition to the possibility of neutrino experiments using the earth shielding beyond, the additional 2.5 km would be available for later development, especially if the accelerator goes to even higher energies by utilizing superconducting magnets.

In summary it might be said that this study has shown that even using extrapolation of present techniques, the West Hall can be used effectively at 200 GeV/c and even possibly up to 300 GeV/c. More importantly, the study has shown where different approaches should be tried in the next stage of the planning process, which could yield important advantages both in the optimization of the space available for physics experiments and in the cost of shielding and beam transport.

References

(13.1) J.B. Adams, "An Alternative 300 GeV Programme", CERN/943 (24 May, 1970).

(13.2) J.V. Allaby and C. Rubbia, "Comments on the Potentialities of Meyrin as a Site for the 300 GeV Accelerator", NP Internal Report 70-14, (4 May, 1970).

(13.3) a) H. Grote, R. Hagedorn and J. Ranft, "Particle Spectra" (private communication - to be published).

b) M. Awschalom and T. White, "Secondary Particle Production at 200 GeV", NAL/FN-191.

(13.4) H. Wachsmuth, "Neutrino Experiments in the West Hall", 300 GeV Beams Group Note (22 October, 1970).

(13.5) G. Hartwig, "Cost Calculation and Optimisation of Bending Magnets and Quadrupoles", GFK-IEKP, BSG-Notiz 70/5 (June 1970).

(13.6) W. Rudloff, J.V. Schaewen and E.J.N. Wilson, "Some Guidelines for Cost Comparison", CERN-MC/4 (27 August, 1969).

(13.7) CERN NP Beam Committee. The people who have participated in this work are: J.V. Allaby, L. Di Lella, A. Lundby, R. Meunier, A. Michelini, G. Petrucci, E. Picasso and J. Steinberger.

(13.8) Such a magnetized iron shielding has also been considered by NAL. See R.H. March, NAL Summer Study 1969, Vol. 1, Section 8, p. 8 and 27.

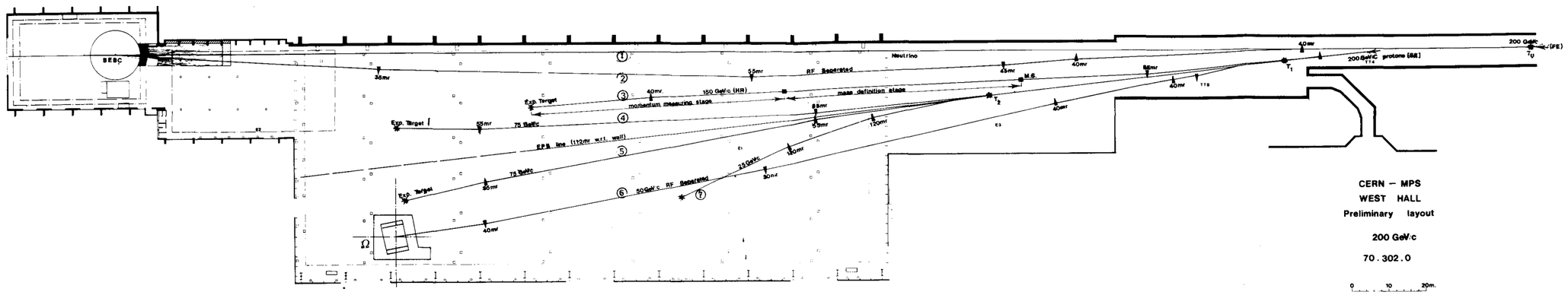

Fig. 13.1 West Hall - Preliminary layout for 200 GeV

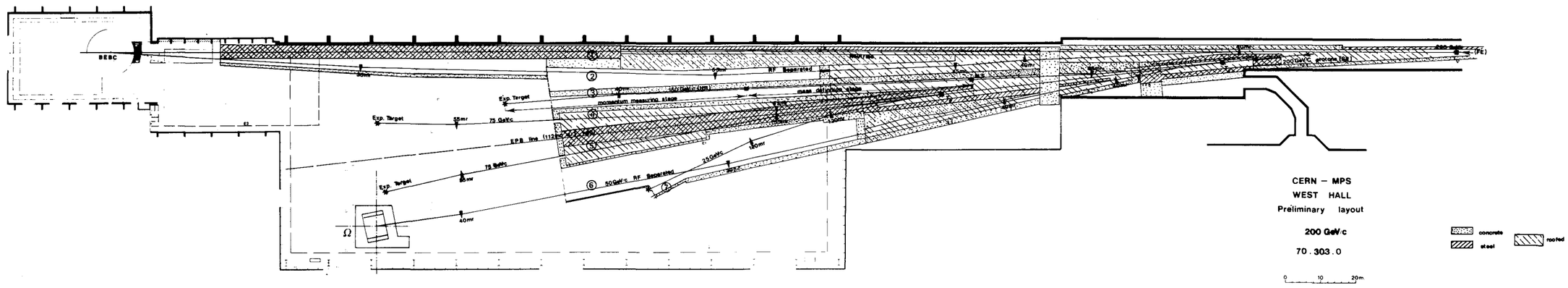

Fig. 13.2 West Hall - Preliminary layout for 200 GeV with shielding

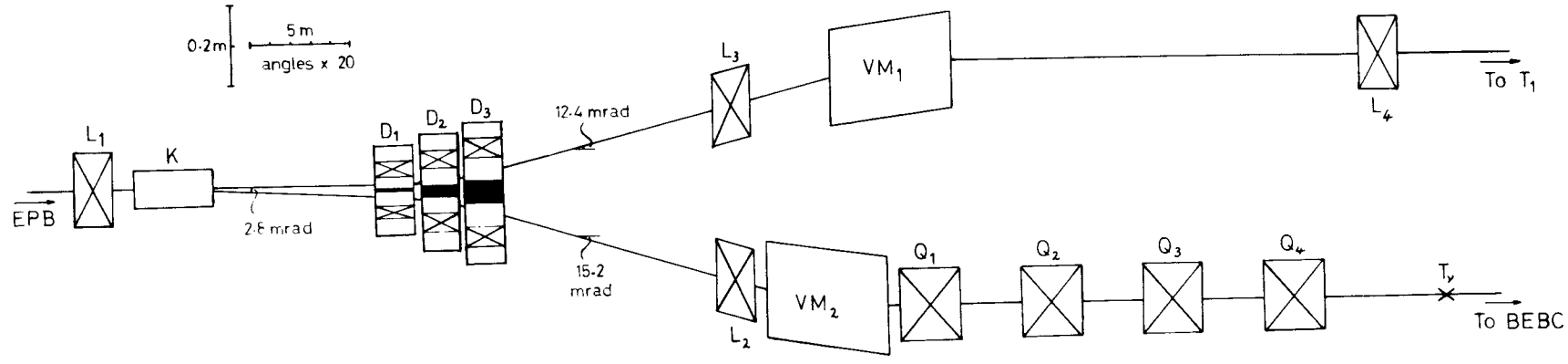

Fig. 13.3 Beam switch (side elevation)

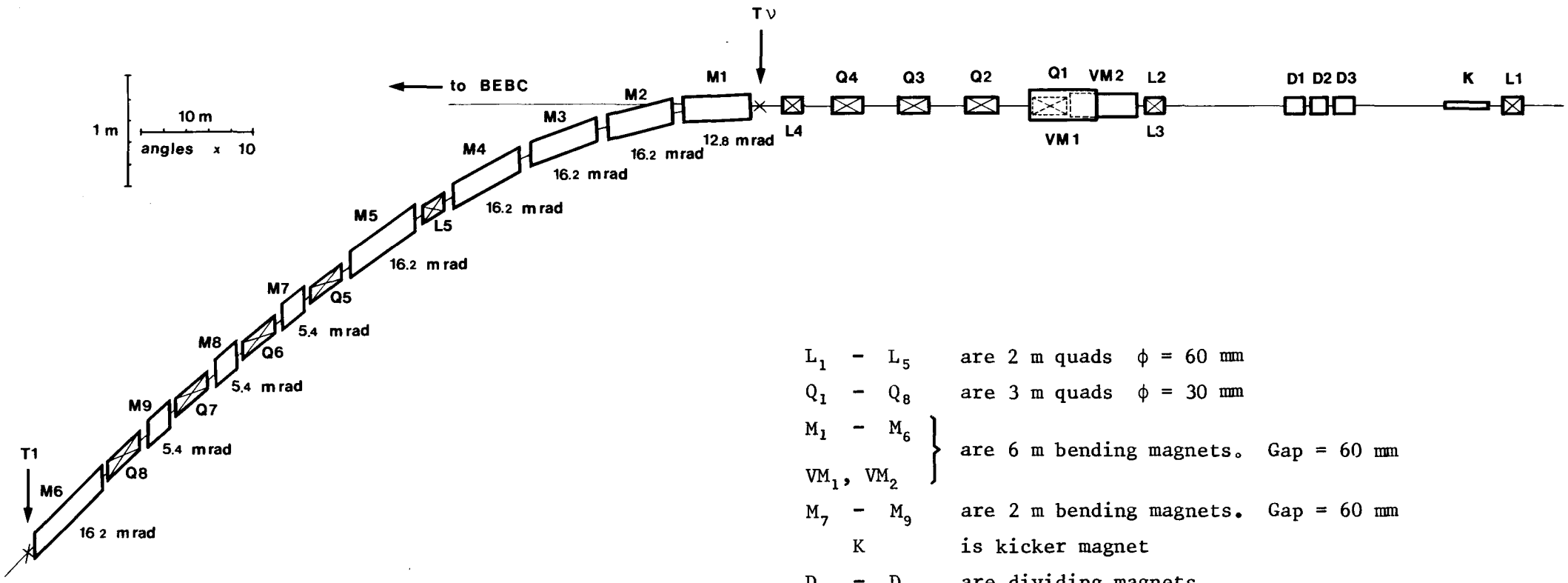

L_1 - L_5 are 2 m quads ϕ = 60 mm

Q_1 - Q_8 are 3 m quads ϕ = 30 mm

M_1 - M_6, VM_1, VM_2 } are 6 m bending magnets. Gap = 60 mm

M_7 - M_9 are 2 m bending magnets. Gap = 60 mm

K is kicker magnet

D_1 - D_1 are dividing magnets

Fig. 13.4 Plan view of layout for TT4

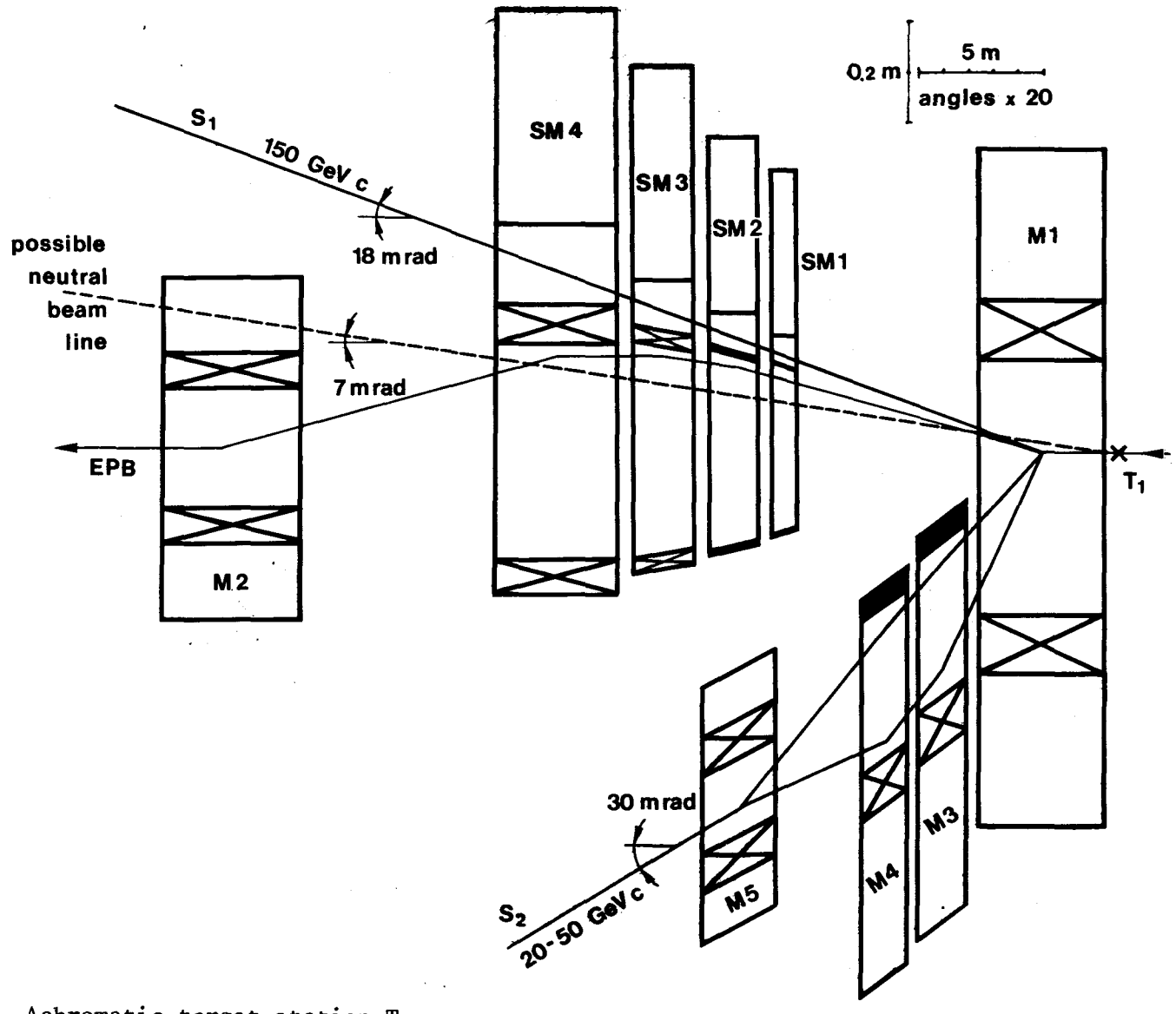

Fig. 13.5 Achromatic target station T_1

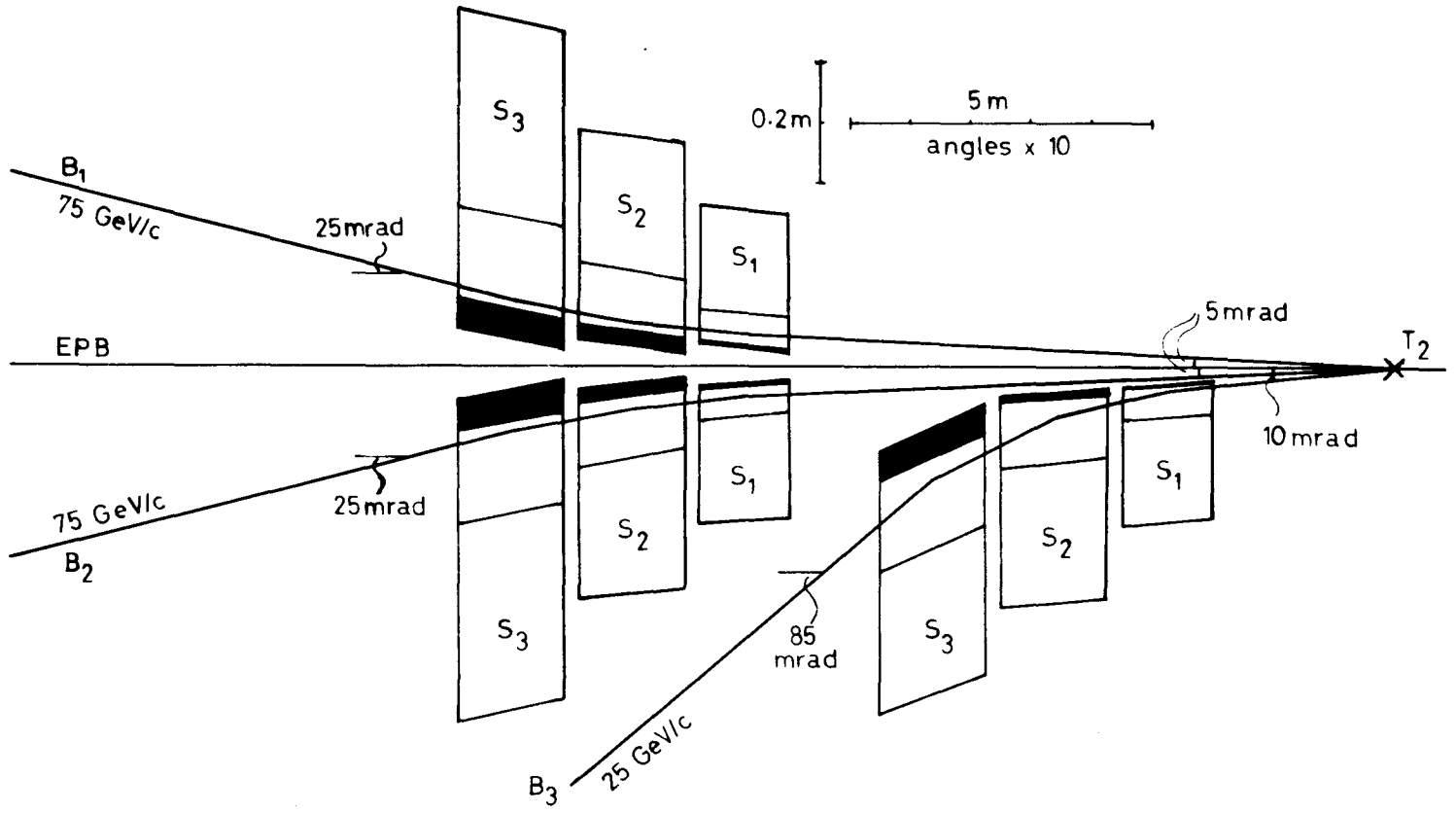

Fig. 13.6 Target station T_2

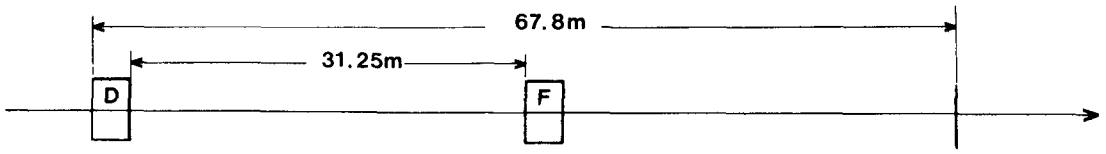

Straight Period, Type S

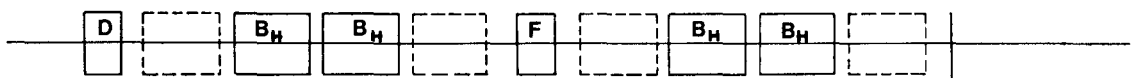

Horizontal Bend Period, Type H*

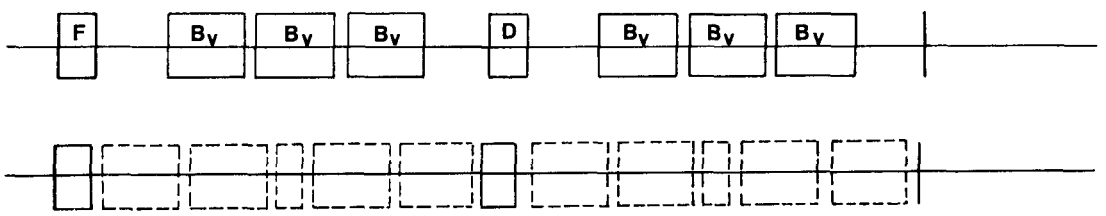

Vertical Bend Period, Type V*

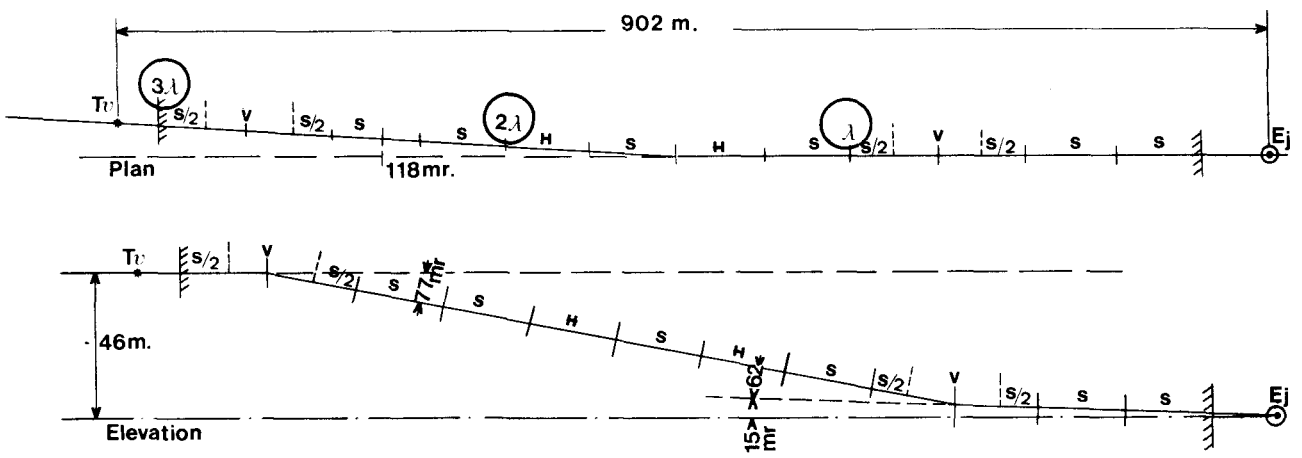

* In dotted Lines, possible configuration for 400 Gev/c

Fig. 13.7 Beam transport system - LSS 6 to west area

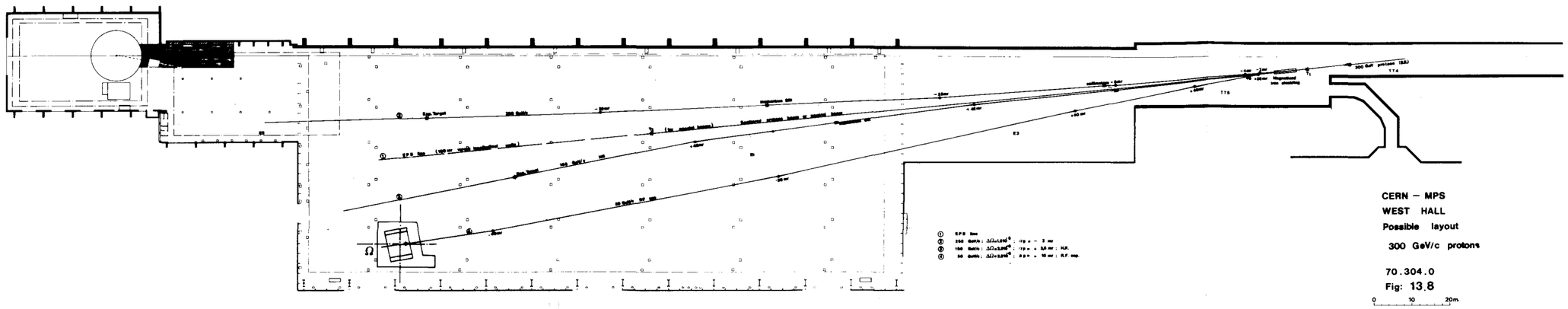

Fig. 13.8 West Hall - Possible layout at 300 GeV

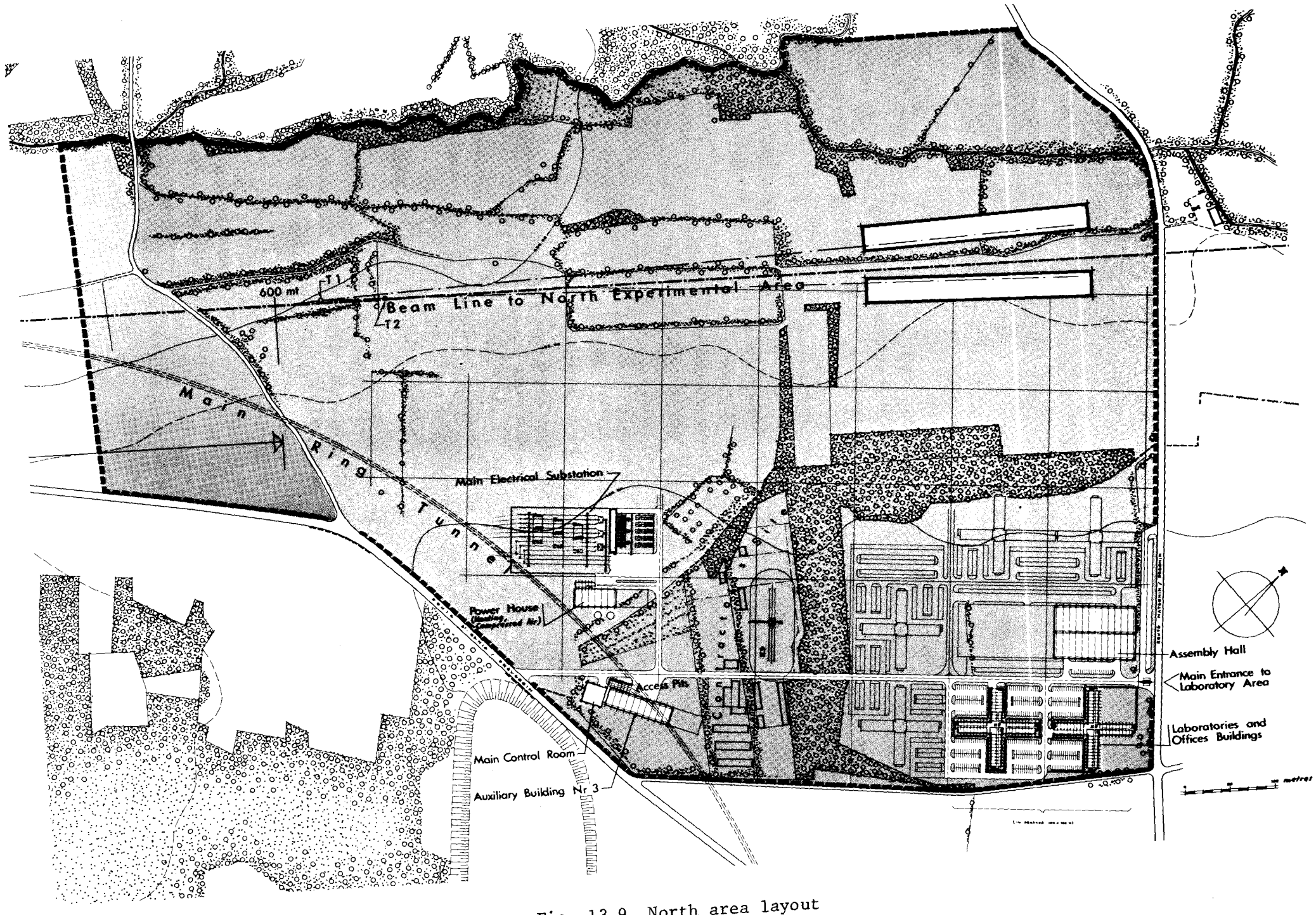

Fig. 13.9 North area layout

Chapter 14

THE SITE

14.1 Introduction

In June 1970, the CERN Council approved expenditure to enable studies to proceed on a site for the 300 GeV accelerator, located in France and Switzerland, next to the existing laboratory. In July, borings and in situ tests were under way.

These studies, of a geotechnical nature, were undertaken principally to determine the width of the molasse plateau on which the new accelerator would be built, so that its diameter could be defined, and to check that the ground north of the St. Genis-Geneva road was of identical quality to that of the CERN I site, if not slightly better. The level at which the new synchrotron will be built is some 40 metres below the 28 GeV PS and ISR, and it is expected that the quality of the molasse will improve with depth.

It should not be forgotten that accelerator builders are familiar with the properties of this molasse as a foundation rock. It was on the basis of these very properties, well-known as a result of more than 10 years' measurements on the PS and ISR, that the technical specification for the 300 GeV site was drawn up, and the stability tolerances determined. Not one of the 300 GeV accelerator sites hitherto examined provides such a mass of information and experience as the Meyrin site; it is sufficient to quote as an example the 1200 m of tunnelling which have already been blasted in the molasse.

14.2 Geology and Structure of the Geneva Basin

The Geneva basin is essentially a synclinorium which extends from the first chain of the Jura to the Salève anticline; it is occupied by the southern extremity of the perialpine molasse basin. Its structure is gently folded and part of it is isoclinal. This structure is revealed by three alignments of molasse hills running from SW to NE. The first alignment passes through the villages of Challex, Dardagny, Peissy, Choully, Bourdigny, Prévessin, Moëns, Ornex and Bossy; CERN I is situated on this alignment and so is the projected laboratory. The second starts at the Fort-Sainte-Catherine hill (to the east of Viry) and passes through the villages of Bernex, Pregny and Chambésy; the third can be seen only in the hill at Cologny. Some twenty million years elapsed between the formation of the oligocene molasse and the Ice-Age pleistocene deposits without leaving any trace in this basin.

The molasse in the area is normally of two types: a variegated molasse at the bottom, resting on Mesozoic formations, in particular on a Cretaceous foundation (Barrémian) and, at the top, a gypsum molasse. The latter formation is not encountered on the proposed site.

Traces of only two glaciations, the Riss and the Würm, are found on these molasse areas. The basic Würmian moraine is generally a clay of a yellowish colour at the surface, changing to blue-grey and steel-grey at depth; it may contain striated pebbles of alpine material and also change into a sandy or gravel moraine. The moraine, which is evenly spread over the whole basin, overlies the "ancient" alluvium in those regions where it had been deposited; elsewhere, the moraine lies directly on the molasse.

The 4 m diameter accelerator tunnel, whose floor will be 22 metres below the lowest point in the topography, will be bored solely in the molasse of the Choully-Moëns-Ornex isoclinal structure. In no case will the moraine deposits overlying the molasse be used as a foundation for the machine.

The molasse of this structure belongs to the "Upper Stampian" or "Chattian" (O_3. Geographical Atlas of Switzerland, sheet 12). The dating is confirmed by several Helix (Plebecula) ramondi Brongniart found in the boring samples.

The thickness of this molasse was determined at the SW end of the Choully-Prévessin-Ornex structure, by means of a borehole drilled near the village of Peissy in 1944 and 1945. The first calcareous horizon at the bottom of the molasse was not encountered until the boring had penetrated to a depth of 293 m.

14.3 Location of the 300 GeV Accelerator on the Molasse Structure of Choully, Prévessin and Moëns

As the accelerator will be housed in a circular tunnel bored in the molasse, practically all harmful effects on vegetation will be avoided. Even in the most unfavourable conditions, the intensity of radiation at ground-level will be well below permitted levels. As the accelerator will, on the average, be at a depth of about 40 m below the surface, the transfer tunnels for the injected and ejected beams will also be bored in the molasse. Consequently, major changes in the loading of the ground, due to the installation of the experimental apparatus and shielding in both the West and North Areas, will in no way affect the operation of the synchrotron, since its physical stability will depend solely on the natural stability of the molasse hill in which the tunnel will be bored.

Borings F1, F2 and F3, and S1, S2 and S3 (see Fig. 14.1) served to determine the width of the molasse hill in a direction perpendicular to its axis running through Choully, Moëns and Ornex, since the centre of the synchrotron is located exactly on this alignment (see cross-sectional view A in Fig. 14.2). From the results of these borings the radius of the accelerator can be defined as 1'100 m.

A detailed examination of the core drillings already obtained confirmed that the underlying molasse was quite suitable. The sandstones and sandstone marls offer an overall homogeneity and compactness which increase with depth. Located beneath the normal Ice-Age overburden, the molasse in the area where the accelerator will be sited is composed mainly of compact and homogeneous marls, for the most part sandy and micaceous, alternating with very homogeneous sandstones generally of fine or medium coarseness, of uniform size, marly with a marlaceous or marly calcareous cement. Occasional layers of variegated marls, soft and brittle, are intermingled with these formations.

At the level where the ring will be located, i.e. 400 m, the formations found after boring were shown to be an increasingly sandy marl and a sandstone, with small layers of variegated softer marls, generally much less than a metre thick. As for fractures, only a few very small quasi-vertical or oblique fissures were found in the core drillings. Piezometers were inserted in certain boreholes, and, as in the ISR, results showed the whole area to be perfectly dry.

The number of experimental areas having now been reduced to one, the area required for the latter is only about 2 km^2. It can be located on a plateau limited by two brooks, the Petit-Journans at the west and the Lion at the east.

As for the topography of the site (Fig. 14.2), the levels are, for the most part, somewhere between 440 m and 460 m: the proposed site thus meets the requirements set out in CERN/485/Rev. The difference between the lowest and highest points on the profile of the ground immediately above the ring is 46 m. These two points are 1530 m apart. In the region of the North Experimental Area, the difference between the highest and lowest points is less than 20 m and the topography is such that the area can be drained naturally.

14.4 Seismology

On page 21 of document CERN/644/Rev. Vol. 1, details will be found of the seismic activity in the Geneva area. It is, however, doubtful that the intensity of the strongest earthquake felt on the Meyrin site was VII, γ between 100 and 250 mm/s^2, on the modified Mercalli scale. On April 17, 1936, the epicentre of the Frangy-Chaumont earthquake - one of the strongest felt in France in 1936 - was at a point mid-way between these two villages. The intensity fell sharply, however, around the epicentral area and, for an intensity of VII to VIII at the epicentre, the total macro-seismic area was only 1900 km^2 (see Fig. 14.3). The area of intensity V is longer in the N-S direction, 35 km as opposed to only 20 km in the E-W direction. Generally, it includes the whole plateau of molasse from the Vuache to the first chain of the Jura. On the eastern side, the isoseists do not coincide with the limits of any geological units; a sharp damping of the movements was, however, observed on the molasse plateau. This was so marked that, at the site of the proposed laboratory, the earthquake was recorded as having an intensity of only III, although the epicentre was no further away than 25 km. The molasse plateau also serves to damp the microseismic waves which affect

the ground in this region. These are natural waves caused by the ocean lapping against the continental shelf with a frequency of between 3 and 7 seconds, and industrial microseismic waves having a frequency of the order of a tenth of a second. The plateau also serves to damp the effects of intercontinental earthquakes.

14.5 Hydrology

When the ISR were constructed, only a limited water table was found in the moraine. It was not, in fact, located at the moraine/molasse interface; in the alluvial deposits there are discontinuous clayey layers which prevent the water from reaching the molasse. This was confirmed by the existing borings on the new site.

The molasse encountered during excavation of the ISR and transfer tunnels was found to be dry. The permeability values recorded by oedometer are extremely low, of the order of 10^{-10} to 10^{-11} m/s, sometimes less than 10^{-11} m/s, after which they become impossible to measure. The average permeability values of the molasse in this area were calculated from the rate at which the water rose in the boring tubes or the piezometers: this is of the order of 10^{-9} m/s. This average value assumes that the molasse in which the boring was made, or in which the piezometers were inserted, was homogeneous as far as permeability was concerned. This is clearly not the case, but whenever water did penetrate the molasse it was through fissures; the permeability values in this area are low, since the amount of water passing through the fissures is not great. The "cut and fill" method was used when building the 15 m wide tunnel. In the whole length of the 1 km-long excavation, which in some points was 22 m deep, only a few fissures were discovered, and the amount of water passing through was very small.

The majority of the transfer tunnels between the 28 GeV PS and the ISR were blasted out of the molasse. At only four points in the 600 m of tunnelling was water seen to enter, and only then at a low flow-rate; it was not a source of serious difficulty when the tunnel was being lined. A service tunnel 1.60 m in diameter and 600 m long was also blasted in the molasse; there was no inflow of water whatsoever.

14.6 Rock Mechanics

Although samples show the molasse to be heterogeneous, it is, when considered on a large scale, relatively homogeneous as far as its overall geotechnical characteristics are concerned. The sedimentary formations of this molasse are of continental and detrital origin, and they possess all of the characteristics of this type of material. The values obtained for the modulus of deformability measured in the laboratory vary according to the sample, but the values obtained for layers of a given thickness show less scatter. Tests carried out during the construction of the ISR showed the average value of the modulus of deformability to be 14.5 kbar for the marl samples and 21.5 kbar for the sandstone samples.

In the ISR, the deformability of the molasse was measured in the region of the supports of the concrete beams on which the magnets were to be installed. The jack-test measurements were made with a 0.30 m diameter plate on a molasse which was decompressed due to the fact that the width of the tunnel foundations was about 20 metres. The modulus of deformability for the 162 tests made proved to be 12.3 kbar.

No special problems were encountered during the boring of the transfer tunnels, and it was not felt necessary in the constructional stage to make any jack tests.

The samples from the borings on the new site fell into four main categories: variegated marls, non-sandy marls or partly sandy marls, sandstone marls and sandstones. Borings S1 and S2 revealed a layer of fine to medium sandstone, which was marly, soft, slightly and partly impregnated with hydrocarbons (with a porosity of about 30%). Samples of all the above materials have been examined in the laboratory.

The following table gives the wet density, unconfined compression strength and modulus of deformability for the various samples:

Table 14.1

Samples of molasse	Wet density	Rc (bar)	E (kbar)
variegated marls	2.25	33	5.7
non-sandy or partly sandy marls	2.30	62	8.8
sandstone marls	2.33	109	16.7
sandstones	2.40	230	43.3
soft sandstones with hydrocarbons	2.20	50	8.5

From the appearance of the boring samples when arranged in a continuous line it was possible to determine the percentage of material in each category, and calculate moduli of deformability, representative of a 10 m band around the 400 m level, for each of the borings. These values showed much less scatter than those obtained for each category of sample obtained, and varied from 11.2 kbar (S2) to 21.2 kbar (F5).

There is no doubt that the molasse on each side of the road forms a single unit, for the following two reasons. Firstly, the modulus values measured on samples obtained at the time of studies on the ISR foundation rock matched those of the samples from the new site. Secondly, the latter also are in good agreement with the results of jack tests made around the ISR. In fact, the quality of the molasse slightly improves with depth.

14.7 Stability

In addition, it should not be forgotten that for the last fifteen years measurements have been carried out on the molasse supporting the CERN I laboratory with a view to determining its stability and deformation under load.

Figure 14.5 shows the vertical movement of the pillars of the 28 GeV PS over a period of ten years. The pillars are anchored into the molasse, which remains absolutely stable as long as it is not deformed by a change in the loading, such as: removal or addition of earth above the accelerator tunnel, constructional work on the experimental areas near the synchrotron, experiments, such as those on the neutrinos, which require considerable alterations in the amount of shielding. Results of measurements on pillars 3, 4 and 5 show a vertical stability of ± 0.2 mm. The graphs for pillars 3 and 4 show that the deformations are elastic.

The reference figure for the metrology of the 28 GeV PS was a regular octagon with a central point. Repeated measurements showed the horizontal stability to be 0.1 mm per 100 m per year.

A measurement carried out independently of any triangulation confirmed these figures. From 24 August 1965 to 13 February 1968 a pair of Marussi horizontal pendulums were mounted on the centre pillar of the synchrotron. These instruments measure the variation in the inclination of the vertical, and therefore that of the support on which the instrument is mounted. It will be seen from Fig. 14.6 that the movement of the molasse and of the pillar itself has not exceeded 0.2 mm in two and a half years.

It is too early to predict the stability of the molasse and of the foundations of the ISR magnets, since the components have only just been installed. Nevertheless, measurements have been carried out repeatedly since May 1970 in transfer tunnels TT1 and TT2, which were bored through the rock, and results have shown the stability to be identical to that of the pillars of the 28 GeV PS. The measurements were made on pillars erected on the floor of the tunnel and on brackets set into the walls. The pillar/bracket combination showed that, over the last five months, both the horizontal and vertical stability was ± 0.1 mm over distances of the order of 100 m.

14.8 Conclusion

The results obtained from measurements in the 28 GeV PS were, in fact, used as a basis for drawing up the technical requirements for the 300 GeV project; in particular, the specification stated that a rock with a modulus of deformability greater than 10 kbar would offer the two-fold advantage of reducing construction costs and improving operational reliability. With the experience gained in constructing the transfer tunnels of the PS/ISR complex we may be certain of the natural stability of the molasse, in which, some 40 metres

below ground-level, the 300 GeV accelerator tunnel will be bored. Firstly, the tunnel will be bored with a machine; the molasse will therefore not be disturbed to the same extent as it would have been had a "cut and fill" method or blasting been used, and the modulus of deformability in situ may be expected to exceed the 12.3 kbar value obtained in the ISR tunnel. Secondly, as the experimental areas are located at a considerable distance from the 300 GeV PS, the tunnel will not be subjected to extraneous loads which might affect its behaviour.

The West Experimental Area, which will be used in the first stage of the project has already been built. The North Area, which will be the next step of the Programme, is now in course of study.

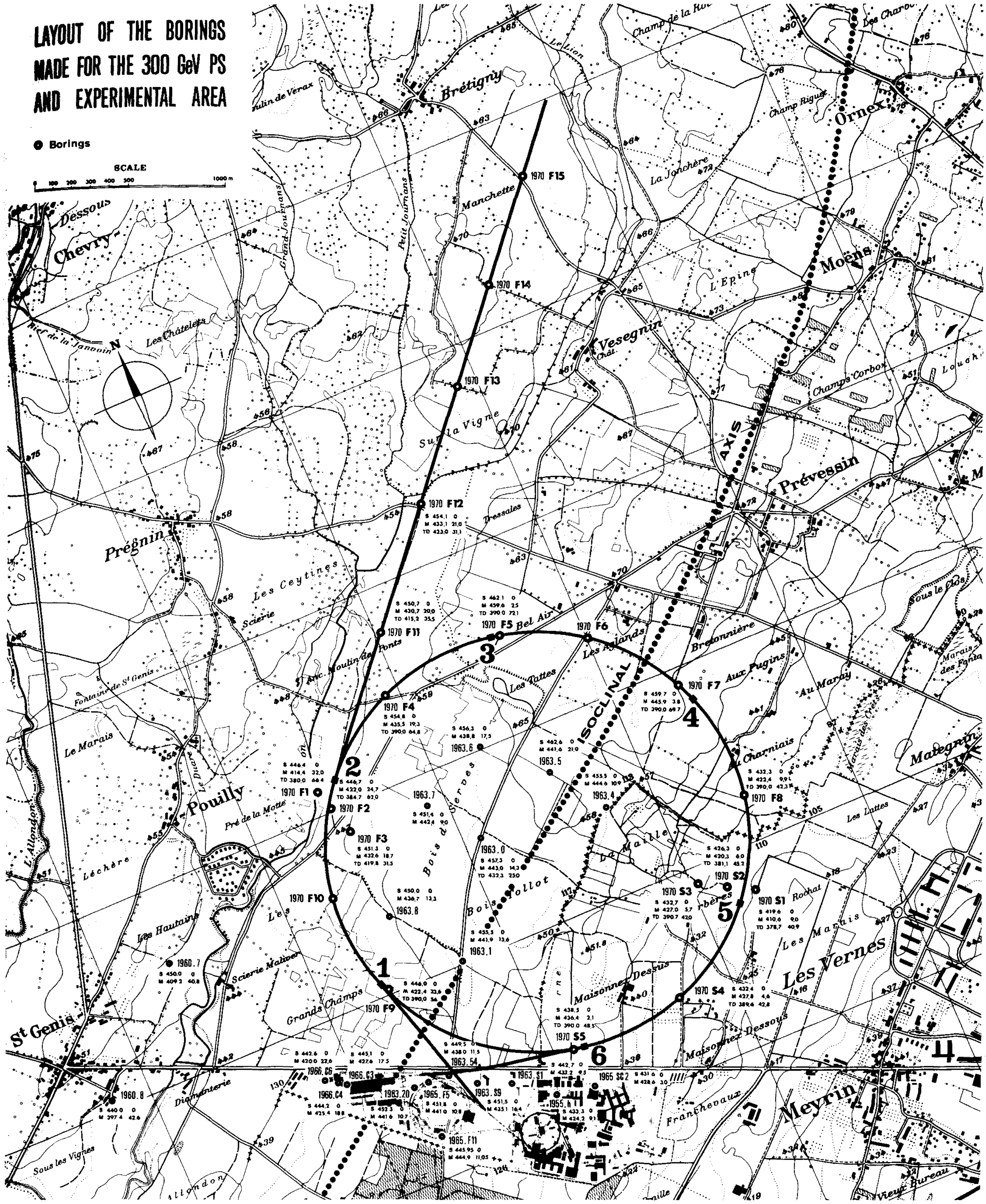
LAYOUT OF THE BORINGS
MADE FOR THE 300 GeV PS
AND EXPERIMENTAL AREA
Borings
SCALE
0 100 200 300 400 500 1000 m
N
AXIS
ISOCLINAL
1
2
3
4
5
6
1970 F1
1970 F2
1970 F3
1970 F4
1970 F5
1970 F6
1970 F7
1970 F8
1970 F9
1970 F10
1970 F11
1970 F12
1970 F13
1970 F14
1970 F15
1970 S1
1970 S2
1970 S3
1970 S4
1970 S5
1963.0
1963.1
1963.4
1963.5
1963.6
1963.7
1963.8
1963.54
1963.20
1963.S1
1963.S9
1965.F5
1965.F11
1965 SC2
1966.C3
1966.C4
1966.C6
1955.h
1960.7
1960.8
Brétigny
Chevry
Dessous
Ornex
Moëns
Vesegnin
Prévessin
Prégnin
Pouilly
St Genis
Meyrin
Les Vernes
Les Châtelets
Les Ceytines
Le Marais
Léchère
Les Hautains
Grands Champs
Sous les Vignes
Diamanterie
Scierie
La Jonchère
L'Epine
Champs Corbox
Champ Riguet
Manchette
Petit Journans
Grand Journans
Sur la Vigne
Tressales
Bel Air
Les Tattes
Bois de Serves
Bois Tollot
La Maille
Aux Pugins
Au Maray
Bretonnière
Les Lattes
Maisonnex Dessus
Maisonnex Dessous
Franchevaux
Vieux Bureau
L'Allondon
Le Lion
Sous le Clos
Matégnin
Rochat
Les Marais

Fig. 14.1

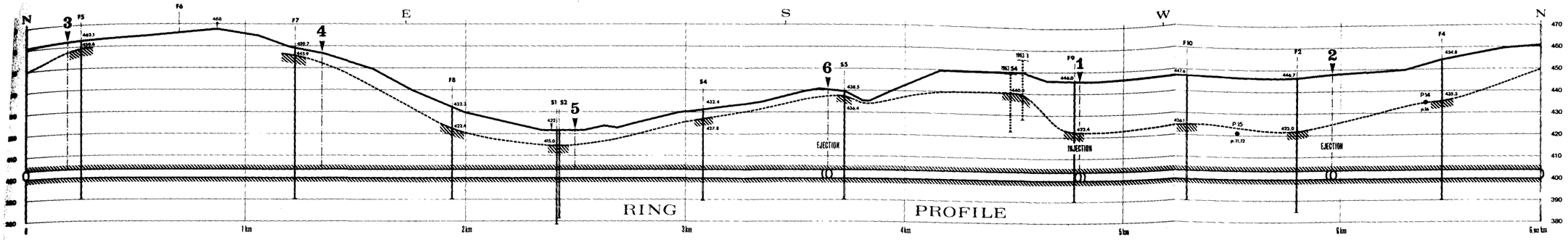

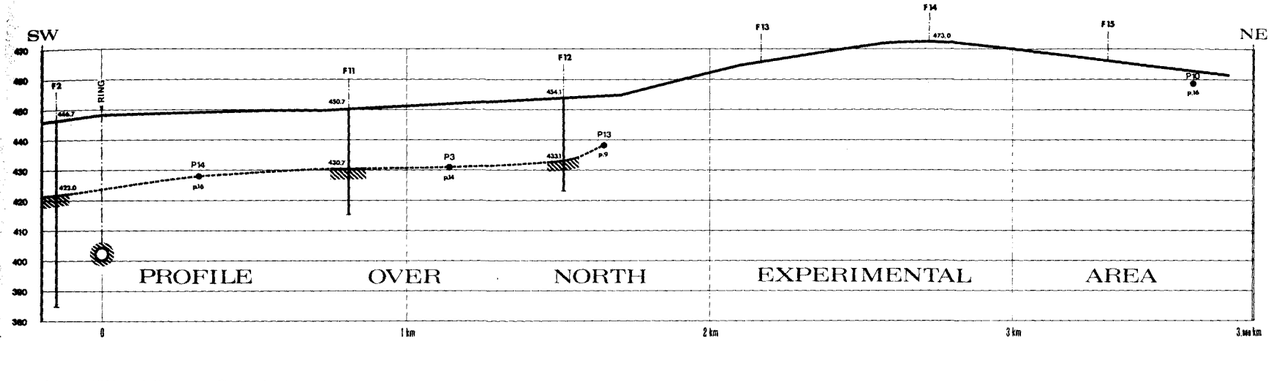

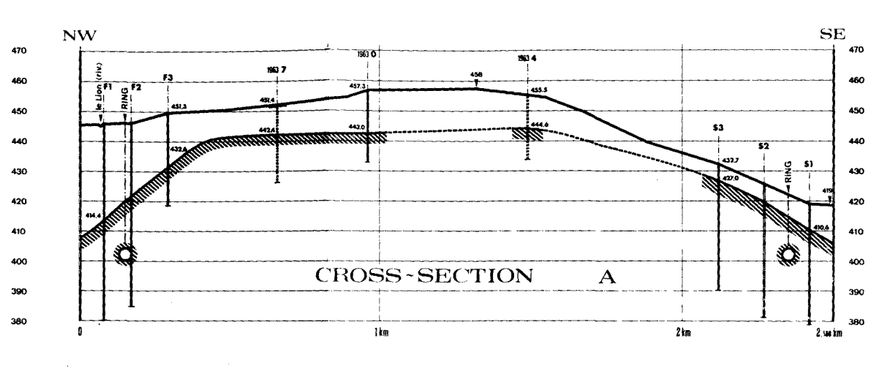

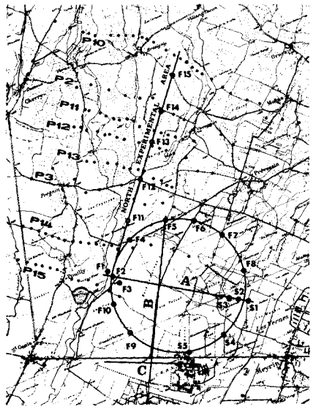

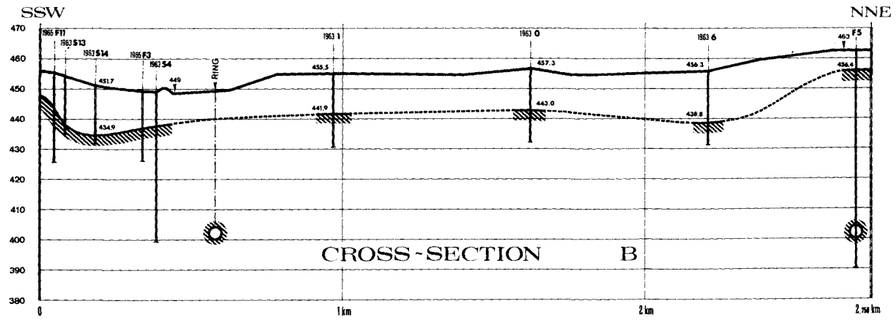

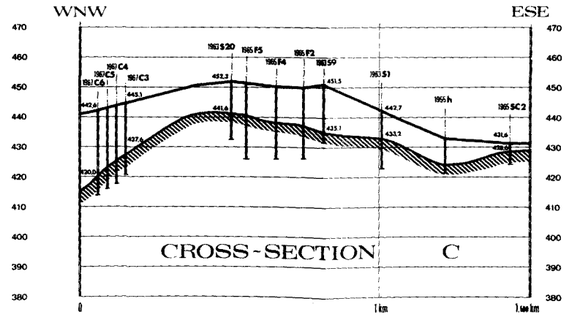

GROUND PROFILE and MOLASSE LEVELS

FIRST LAYER OF MOLASSE

P10 Resistivity measurement made in 1965 when prospecting for cooling water for CERN I

Fig. 14.2

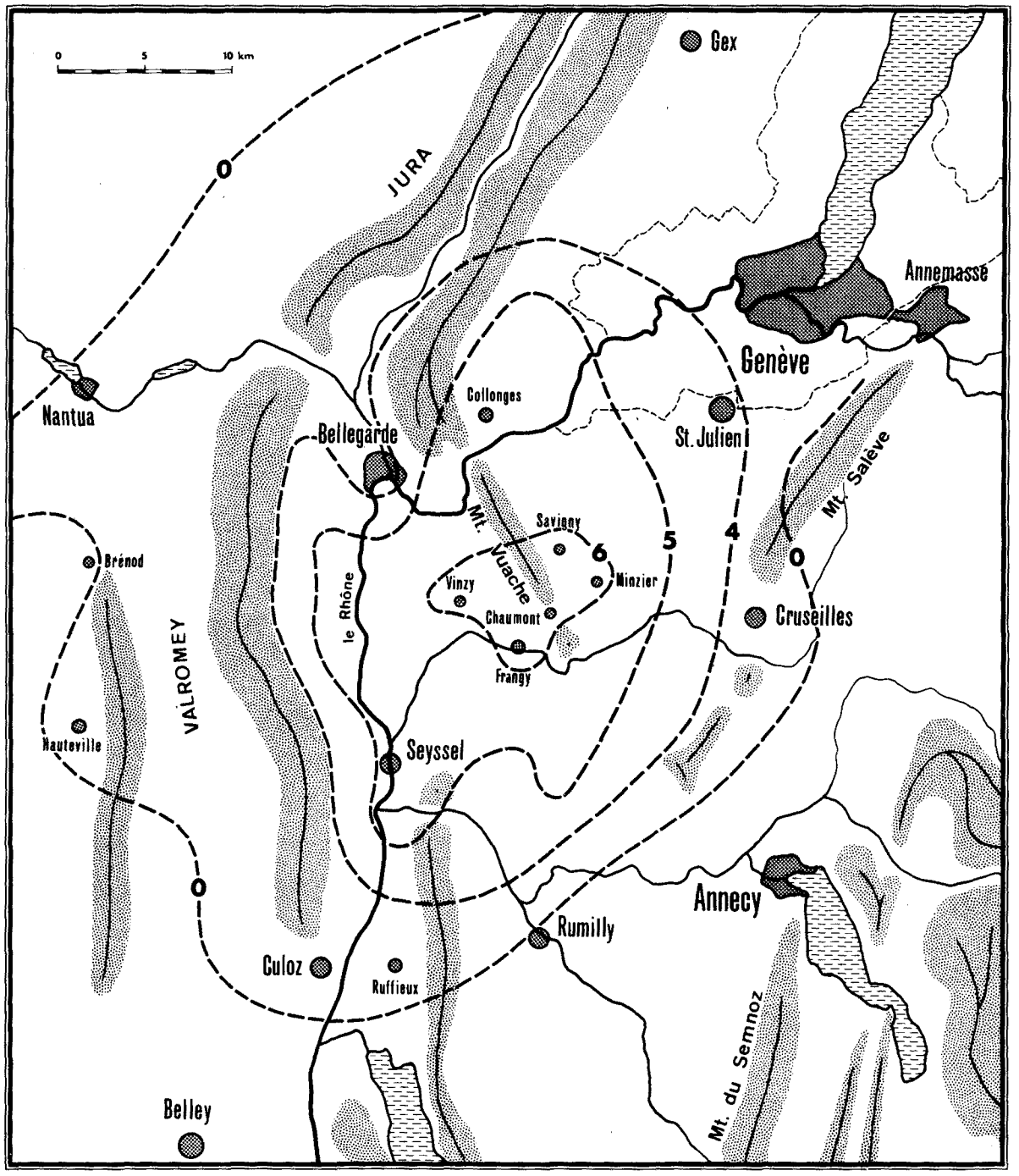

Fig. 14.3 Isoseists of Haute-Savoie earthquake which occurred on 17 April 1936 (after E. Rothé, 1942)

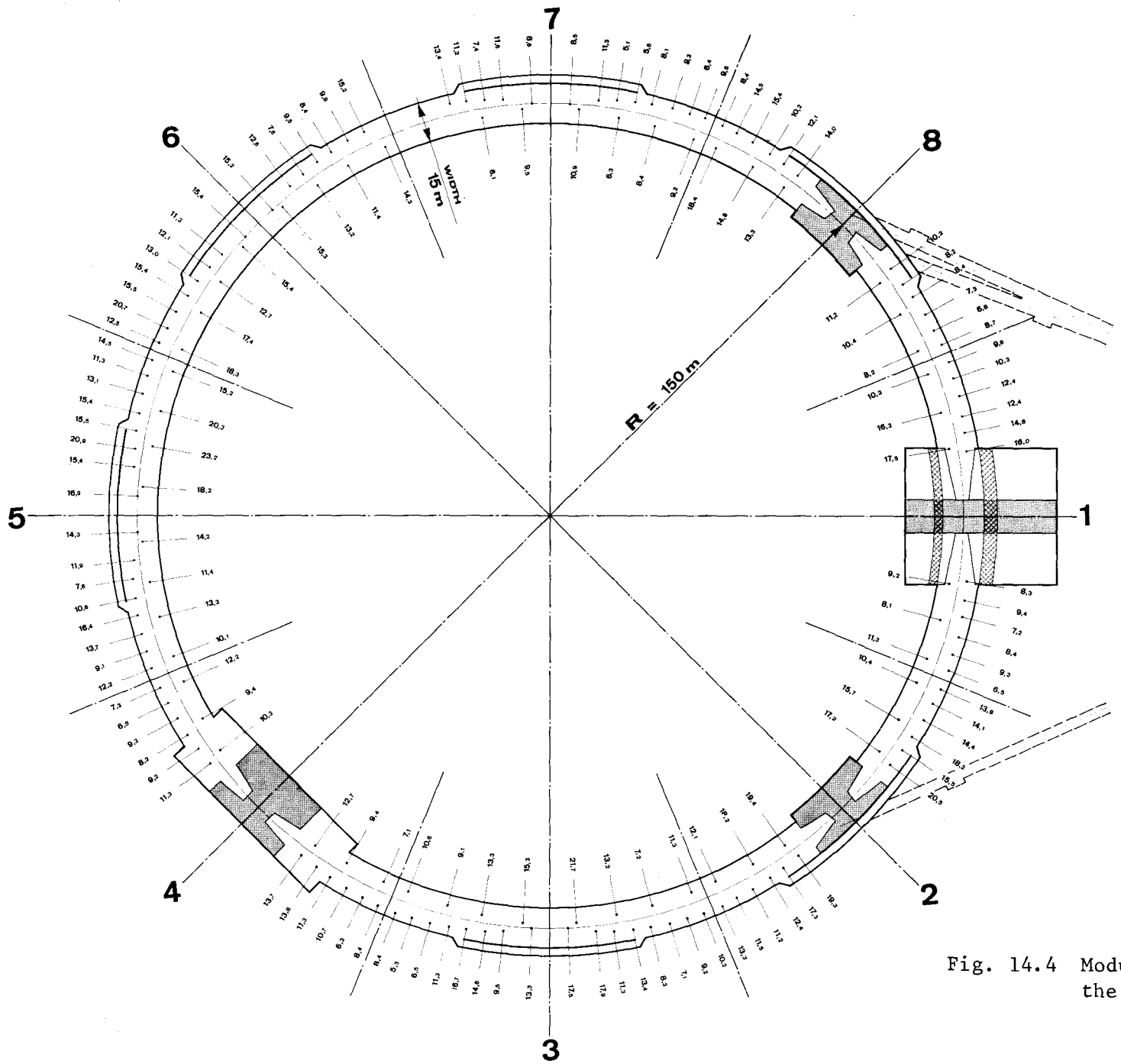

E values given in Kbar
Average value of E = 12,3 Kbar
Jack-tests with a 30 cm dia. plate

Fig. 14.4 Moduli of deformability of the Molasse under the ISR

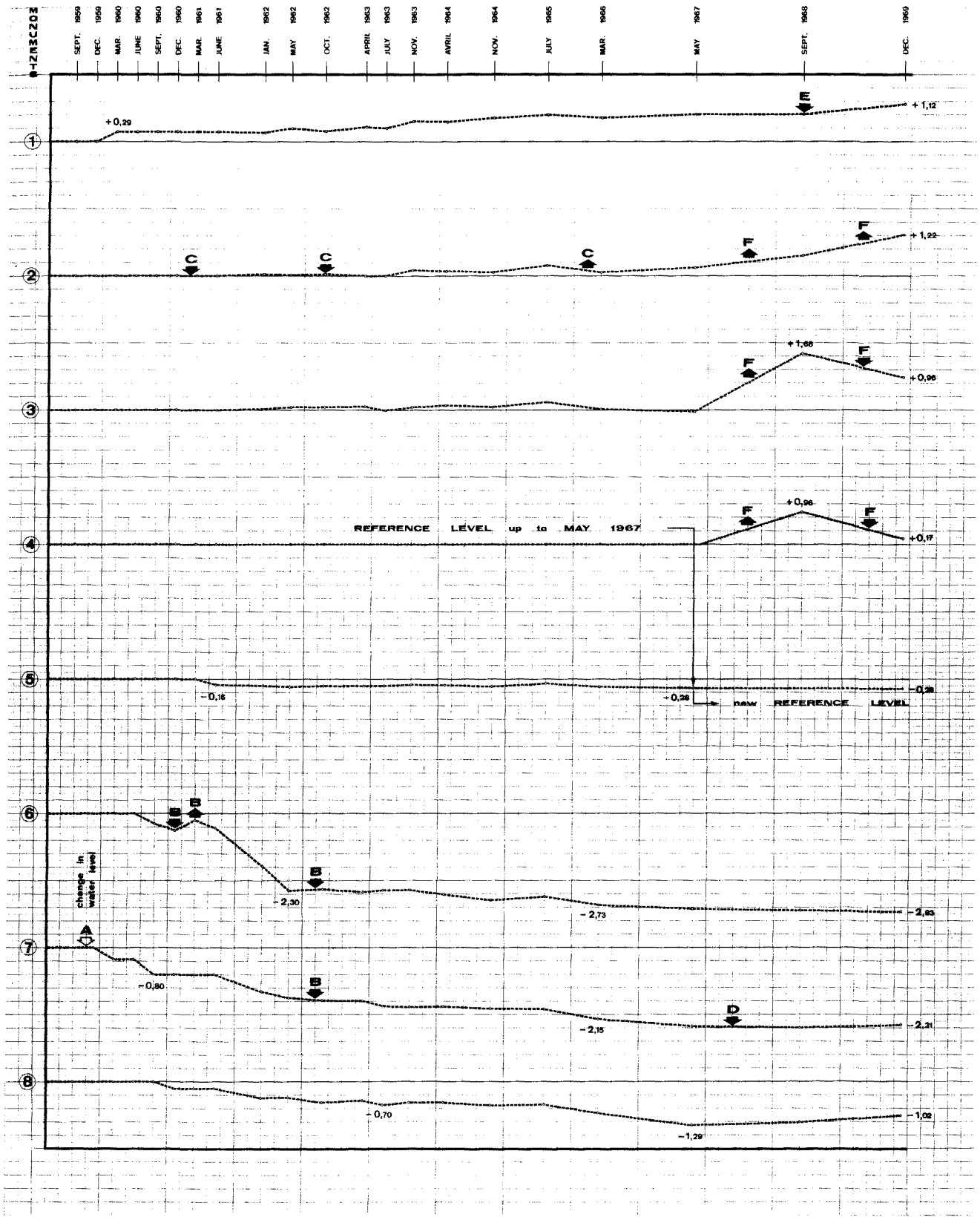

1959 . 1969

Fig. 14.5 Vertical movement of the PS survey monuments in relation to their theoretical level

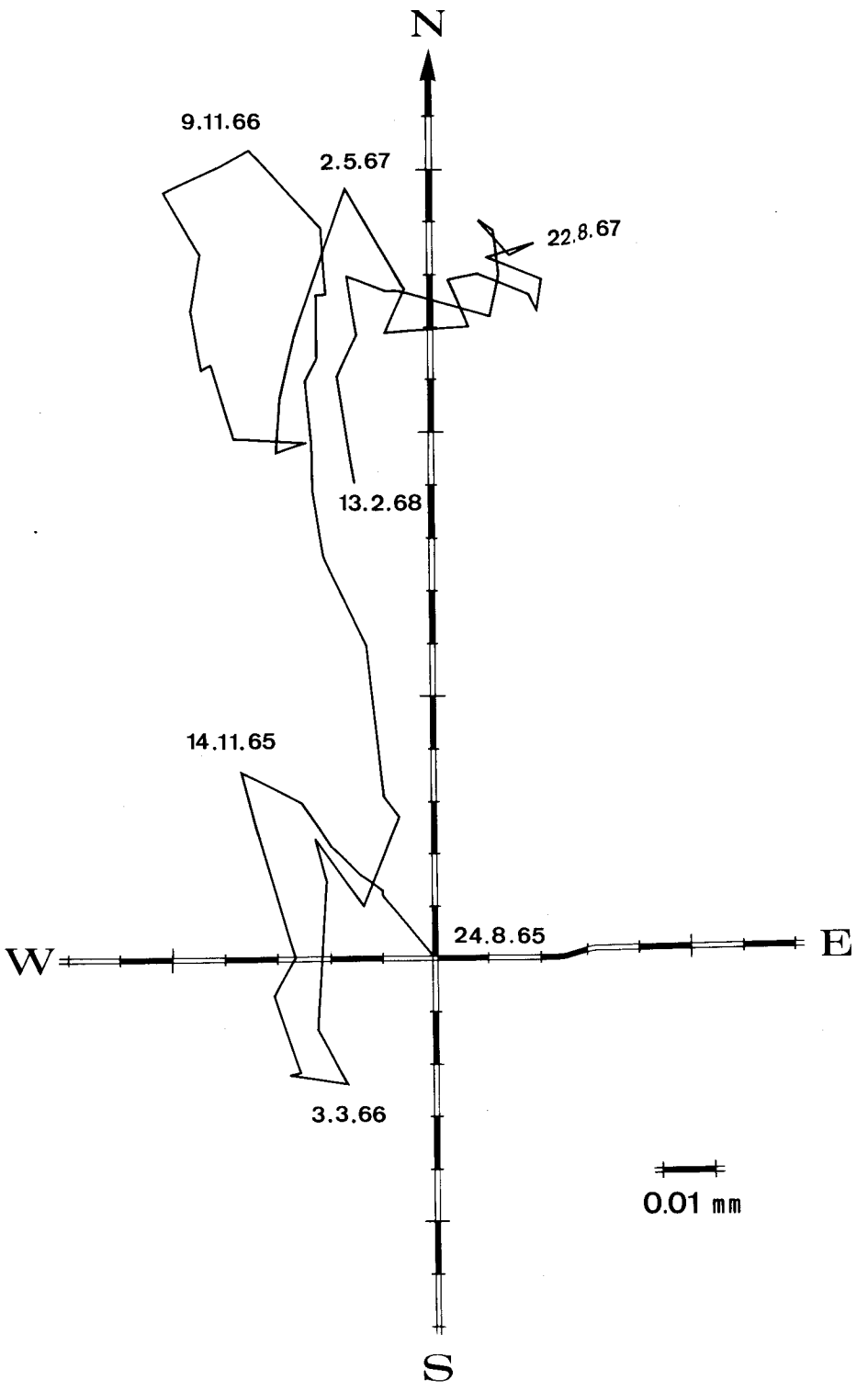

Fig. 14.6 Movement detected in the monument at the centre of the PS according to measurements with horizontal pendulums over the period 24 August 1965 to 13 February 1968

Chapter 15

GENERAL EQUIPMENT AND BUILDINGS

15.1 General

The layout of the synchrotron is dictated by the injection and ejection beam lines, the ring diameter and depth being determined by the useful extent of the site and of the underlying molasse.

An overriding consideration for the design is to avoid any spoiling of the rural setting on the site: this will imply, among other things, limiting the use of and careful siting of overhead electric lines, making maximum use of existing roads together with careful design and landscaping of buildings.

A rational, economic routing of the external supplies required (electricity, water) is also essential; good road connections with CERN I and with the main road network are of course also needed for the staff and for the delivery of goods and supplies. The present site is in fact well equipped with roads; it does not seem necessary to ask for new public road work, apart from improvement, widening and development of cross-roads on the existing network. Some new secondary roads are of course needed to serve some of the buildings of the project (see Fig. 15.1). The central laboratory complex will be conveniently close to the existing highways and traffic centres:

6.7 km from the Geneva Airport and Autoroute Geneva-Lausanne
3.4 km from the Geneva-Lyon highway
9.7 km from the Geneva main railway station.

The siting of the building contractors and the likely development of the various phases of work as a function of time have also been considered in arriving at the overall plan proposed here. The locations of the main parts of the project are shown in Fig. 15.1.

It is envisaged to launch as soon as possible the construction of the main laboratory centre: located at the north of the ring, close to the future North Experimental Area, this will include several multi-purpose cross-shaped buildings containing offices, laboratories, shops etc. and one large assembly hall (about 10,000 m^2). The construction of this centre will extend over several years: in the first phase (second year of the project) there will be enough space to accommodate about 250 people.

The underground ring tunnel (at an average depth of 40 m below the surface) will have six access points: four of these will be equipped as cable and pipe penetrations, plus personnel and light equipment access, while two will also permit the handling of the heaviest machine components. At the top of every access shaft there will exist an auxiliary equipment building, containing power distribution, rectifier banks, local controls, water pumps and heat exchangers etc. Where appropriate, these buildings will also house the injection and ejection power supplies and the radio-frequency equipment. The auxiliary building closest to the main laboratory centre will include the main control room.

Two beam transfer tunnels will link the ring to CERN I: one is a branch of the existing ISR and West Area beam line, and will be used for injection, while the other will return the high energy protons to the West Area. The boring of these and of the North ejection tunnel, together with the main ring tunnel, will present some interesting problems.

A detailed description of the main ring tunnel and of the various other parts of the project is given below.

15.2 Main Ring

The work described in this Section includes the main ring tunnel, together with its access pits and auxiliary buildings, and also the injection tunnel from PS and ejection tunnels to West and North Experimental Areas (see Fig. 15.1).

15.2.1 Main ring tunnel

Of an average diameter of 2.2 km, the main ring will have a developed length of 6'912 m consisting of:

6'582 m of normal cross-section (see Fig. 15.2)
330 m of "variable" cross-section where the injection and ejection tunnels join the main ring (see Fig. 15.4).

The bottom level of the main ring tunnel has been fixed at an elevation of 400 m above sea level, corresponding to a depth which varies between 23 m and 65 m with respect to the surface. The main ring tunnel will be entirely built in the molasse rock, with a minimum of 11 m of molasse cover on top, plus the layer of moraine up to the surface.

The normal cross-section will have a net internal diameter of 4 m corresponding to a diameter of 4.40 m for the boring allowing a concrete lining thickness of about 20 cm. This lining could be foreseen as pre-fabricated elements of waterproof concrete fixed to the rock by means of cement injections or by some other procedure to be suggested by the consulted firms. The joints between elements would be made in such a way as to ensure the water-tightness of the tunnel. The supports of the magnets, as well as the roadway for the magnets installation trolleys, will consist of a platform of reinforced concrete fixed to the tunnel, in order to guarantee a perfect stability.

The excavation procedure must avoid disturbing the molasse layers near the working area. Therefore, the excavation of the tunnel will be executed by means of a boring machine of a type to be suggested by the consulted firms. These machines have existed for several years and have been operated successfully in similar rocks.

The regions of the main ring tunnel which correspond to the three variable cross-sections joining to the injection and ejection tunnels (see Fig. 15.4) will be bored in a first phase by the same machine used for the normal cross-section. In a second phase the tunnel will be enlarged to its final profile, by means of a second boring machine with an adjustable head or by some other procedure.

15.2.2 Access pits (see Fig. 15.3)

The main ring tunnel will have six access points designed similarly to each other. At each of the six points a 5 m wide pit will connect the auxiliary building on the surface to the machine level. This pit will be equipped with a 1-ton lift, emergency ladders and working platforms and will allow both personnel access and cable and pipe penetrations.

The pit will also serve as air-conditioning duct, for either air inlet or outlet. Moreover, two pits will be equipped with a shaft permitting the transport of the machine magnets by means of a crane (or a mobile gantry crane) and special lifting devices guided by means of rails fixed to the walls of the shaft. The bottom of the pits will be connected to the main ring tunnel by a short tunnel of horse-shoe section (about 15 m long) to be constructed in a conventional way.

15.2.3 Auxiliary buildings

Six such buildings will be constructed on the access pits in order to house the rectifiers, power supplies, power sub-stations, beam controls and other control equipment, air-conditioning and ventilation equipment, heat exchangers etc. In principle these buildings would not be identical, their dimensions will vary according to the equipment necessary at each point. The average dimension of the auxiliary buildings will be about 1000 m^2. The construction type is assumed to be light, with steel structure and metal cladding. A double floor is planned, to allow the laying of cables and pipes connecting the equipment to the main ring tunnel. One of the six auxiliary buildings, the one nearest to the main laboratory complex, will be combined with the Main Control Room.

The supply of water and electric power to these buildings will be provided by pipes and cables buried in the ground. Heating and air-conditioning will be independent for each building.

15.2.4 Injection and ejection tunnels (see Fig. 15.4)

There will be three tunnels:

(i) one 700 m long injection tunnel connecting the transfer tunnel TT2 of the ISR to the main ring tunnel;

(ii) one 700 m long ejection tunnel connecting the main ring tunnel to tunnel TT3 of the ISR towards the West Area,

(iii) one 600 m long ejection tunnel to the North Experimental Area, having a maximum slope of 12%.

The cross-section of these tunnels has an internal diameter of 4 m and is identical to the one of the main ring tunnel.

The first two tunnels, which are entirely contained in the molasse, would be executed with the boring machine used for the main ring tunnel. For the third tunnel, which has to cross a thick layer of moraine, several methods can be planned for the part in the moraine (e.g. open excavation, protection by sheet piling or by diaphragm walls in the soil). The final solution should be suggested by the consulted firms.

15.3 Experimental Areas

The utilization of the synchrotron will be based on two main experimental areas, which will come into operation at different times.

15.3.1 West Experimental Area

This area is the existing complex of buildings and facilities where 25 GeV physics with the CPS extracted beam will start soon (1972). By the time commissioning of the 300 GeV synchrotron comes, the area will house two large experimental facilities, the 3.5 m hydrogen bubble chamber (BEBC) and the magnetic spark chamber system (Omega), both well run-in and fully operational. The full complement of equipment and supporting facilities in the area (beam transport magnets, power supplies, cooling, shielding, controls, etc.) and the 3 years or so of experience in physics experimentation with 25 GeV protons make this area a very important asset for the immediate utilization of the new accelerator.

It is planned to eject the proton beam (probably at 200 GeV or less) along an ejection tunnel joining the main ring to the upstream end of the area (see Fig. 15.1); from there on, the area will consist of a target station, a chain of three experimental halls (totalling about 15'000 m^2), the two large experimental facilities mentioned above (BEBC and Omega), surrounding apron space, roads, etc. Supporting buildings of various kinds also exist in this region.

The main Experimental Hall (Hall E1) has a floor area of 10,000 m^2, is 65 m wide in a single span and about 150 m long: it is equipped with two large cranes (40 tons and 60 tons) with 9.5 m hook height.

Extensions of the beams beyond the built-up area are in principle also possible.

The construction of the junction between the ejection tunnel and the existing West Area beam tunnels (tunnel TT3 of the ISR) will present some problems but it is thought possible to carry on this work without too much upsetting the operation at 25 GeV.

15.3.2 North Experimental Area

The development of this area is assumed to take place somewhat later, in the seventh and eighth year of the Programme. Therefore, the design of this area is still in a preliminary stage, and only some general ideas can be presented here. It is assumed that the proton beam will be ejected along a tunnel similar to the one used for the West Area, reaching ground surface some 600 m from the ring. From there on the beam will be confined in a shielded duct and will be brought to several target stations. Experimental halls and open apron areas will be located downstream of the targets, in a geometry still under study, the aim being to keep the experimental areas offset from the forward muon flux. A certain use of the natural site levels will also be made, with the aim both of minimizing excavation and backfill work and of reducing muon shielding requirements. The landscaping of the area will also be an important consideration in the design.

15.4 Laboratories, Offices and Other Facilities (see Fig. 15.5)

15.4.1 Laboratory complex

Figure 15.5 indicates general layout of these various buildings which would consist of six buildings of 2 floors above ground floor, totalling 30,000 m^2 gross surface, and an assembly hall of 11,700 m^2.

In the first stage, two buildings and the assembly hall would be built, the remainder of the construction being spread out over the 8 years of the Programme. The buildings would be located according to a square, regular network enabling them to be connected up by a simple network of straight service tunnels and roads.

These buildings (see Fig. 15.6) will be constructed to be adaptable to be used without external modifications, as offices, laboratories, small workshops, computer rooms, small assembly halls, library, conference rooms, canteen, etc. These low buildings (about 10 m high) will ensure harmony with the existing trees in that region, which will be preserved.

Construction methods for these buildings will use prefabrication for the obvious reasons of speed of construction and economy due to standardization. A preliminary enquiry has been sent to specialized firms in the Member States in order to determine the most economical prefabrication procedures.

The assembly hall will be of a conventional construction and will have the same height as the six office-laboratory buildings. It will consist of two bays of 29 metres equipped with two cranes of 30 tons (lifting height 6 m).

15.4.2 Other facilities

Figure 15.5 shows the other constructions assembled in the same area and in particular:

(i) main electrical sub-station
(ii) power house
(iii) contractors' site.

These three facilities are planned to serve the North Experimental Area as well.

In the first stage of the construction, temporary electricity and heating supplies will be provided for the first two office buildings, the assembly hall and the contractors' site installations. The latter have been centralized and grouped together near the laboratory so as to spoil as little as possible the general aspect of the site.

15.5 Supplies and Services

15.5.1 Electricity

Power to the new laboratory will be provided by the production and distribution centre of Génissiat (Electricité de France) about 33 km away, by means of a double 225 kV line.

One of the lines will be used only for the supply of the ring magnets, the other supplying the laboratory and experimental areas.

The sub-station (see Fig. 15.5) will be equipped in the first stage with two transformers of 75 MVA, 225/18 kV either of which can be connected to one or the other of the two incoming lines.

On the 18 kV side, it is foreseen that for normal operation, each transformer will be connected to one separate bus bar system, one supplying the machine magnets and the other the laboratory installations and the experimental halls. While for special operation, in case of a breakdown of one transformer, the whole site, including the machine magnets, will be fed by one transformer at a somewhat reduced rate.

The possibility of installing a third identical transformer remains open for future developments of the laboratory.

An emergency line could connect the present CERN sub-station with the new laboratory's sub-station.

The supply of 18 kV power to the complex of laboratories and experimental halls will include:

(i) Distribution via a circular loop to the 6 sub-stations of the auxiliary buildings so as to feed auxiliary equipment, as well as the lighting and power distribution inside the ring. This same loop will supply, from some of the six sub-stations, the pumping station on the water reservoir, as well as all the ejection and injection equipment of the accelerator.

(ii) Powering of a first distribution sub-station in the office and laboratory area.

(iii) Separate powering of another sub-station in the North Experimental Area, close to the first experimental hall.

15.5.2 Water

A draft design, studied in collaboration with the Services Industriels of Geneva, envisages a supply of water from the Geneva lake with the following characteristics:

(i) The water flow in the first stage would be of 1.000 ℓ/s (700 ℓ/s for the cooling of the magnets, 300 ℓ/s for the rest: laboratories, experimental halls, etc.).

(ii) The water intake would be at 40 m depth in the lake, about 1.5 km off "Le Vengeron" in the Canton of Geneva, where the temperature is 13° C or less for more than 95% of the year.

(iii) The water would be treated with ozone, filtered and sterilized by chlorine bioxyde in a treatment and pumping station built on the shore of the lake at "Le Vengeron", thus becoming of drinking grade.

(iv) The water would be pumped through 9,300 m of cast iron, 1,000 mm diameter, pipeline into an underground reservoir of a volume of 10,000 m^3 situated in Swiss territory near one of the access pits of the ring (see Fig. 15.1).

(v) Another pumping station installed on this reservoir will feed a network which, following just under the surface the lay-out of the ring, will supply each of the 6 auxiliary buildings. The office-laboratory complex and the North Experimental Area will be supplied through a branch close to the access pit nearest to the laboratory area.

(vi) In each of the auxiliary buildings, the primary water will flow through plate heat exchangers to cool the secondary, demineralized water to be circulated in the magnet coils.

(vii) When leaving the heat exchangers, the primary water will be evacuated at a temperature of about 28°, and will flow in a conduit to the Rhône river.

15.5.3 Telephones

The new laboratory will require a telephone system with about 1500 extensions. It will be designed to handle each year:

(i) 400,000 international or interurban calls,

(ii) 300,000 calls to the region of Geneva,

(iii) 1,500,000 internal calls of which 1/3 will be to CERN I.

Two possible solutions are being studied together with the French and Swiss Administrations.

(i) A solution which is similar to that adopted for the Franco-Swiss Airport of Bâle/ Mulhouse. The internal calls of both laboratories would be handled by an enlarged CERN I exchange which would allow connections to be made as directly as possible to the Geneva system. All long distance and international calls from CERN II would pass along a special cable into the French system.

(ii) The installation of a special CERN II exchange connected to the French system but closely linked to CERN I to allow internal calls to be dialled directly and to permit easy access to the telephone system of the Canton of Geneva.

15.5.4 Heating

A central (superheated water) boiler plant near the west end of the office and laboratory area (labelled Power House on Fig. 15.5) will be equipped, in a first phase, with two steam-generators of 6,000,000 Kcal/h each. The superheated water will be distributed to the office and laboratory buildings and to the halls through pipes passing through the service tunnels.

In each of these buildings appropriate heat exchangers, as well as mixing-stations will ensure the supply of the hot water necessary for the different services, namely:

(i) heating of offices and laboratories by hot water radiators,
(ii) heating of halls by superheated water panels and warm air blowers,
(iii) preparation of sanitary hot water.

15.5.5 Air-conditioning of the main ring tunnel

Automatic plants for the air-conditioning in the tunnel will be installed, where appropriate, in the auxiliary buildings. These stations will be equipped with oil-fired heat generators, a refrigerating unit and air fans, as well as the appropriate exchangers in order to ensure the following functions:

(i) heating of fresh air in cold season,
(ii) drying and cooling of fresh air in warm season,
(iii) blowing of such treated air into the main ring tunnel via the access pits.

The characteristics of the equipment of each station will be determined taking the climatic conditions used for other CERN designs, namely:

(i) minimum dry temperature - 12° C
(ii) maximum dry temperature + 32° C
(iii) maximum specific humidity 20 gr/kg of air.

Considering the characteristics of the molasse in which the tunnel will be bored and the average depth at which the tunnel will be constructed, the continuous loss through the wall will be of about 3 Kcal/h/m^2, corresponding to a total loss of about 300 kW.

15.5.6 Compressed air

A compressor will be installed in the power house. The compressed air will be stored in a tank and distributed from there to different users by a piping system passing through the service tunnels which supply the office and laboratory area and the halls.

15.6 Cost Estimates

All figures are in MSF at 1970 costs, contingencies not included.

	Stage A	Stage B (Total)
15.6.1 Main Ring Tunnel		
Including three normal straight sections, three enlarged straight sections for injection and ejection, six access pits (two of which are equipped for transporting heavy loads, and four for personnel and services), six auxiliary buildings located on top of the access pits (7,000 m^2 total area). Basic technical equipment of buildings is included (lighting, local power distribution, cable trays, earthing, telephone, compressed air distribution, air-conditioning of main tunnel, heating of auxiliary buildings, cranes, lifts, drain sumps and pumps, local distribution of primary water in auxiliary buildings)	59.5	59.5
15.6.2 Injection tunnel		
Total length 700 m, same cross-section as main ring tunnel. Including connection to transfer tunnel TT2 of the ISR. Basic technical installations are included, similar to main ring tunnel	5.0	5.0
15.6.3 Ejection tunnels		
To West and North Experimental Areas. Total length 1300 m (700 m for West Area, 600 m for North Area), same cross-section as main ring tunnel. Including connection to the transfer tunnel TT3 of the ISR. Basic technical installations are included, similarly to main ring tunnel; the air-conditioning is included under point 15.6.1	8.3	8.3

15.6.4 Laboratory complex and Main Control Room

Six laboratory buildings, containing offices, laboratories, workshops, etc., each about 21,000 m^3. Parking space around each block (about 200 cars) is included. Basic technical installations are included (lighting, heating, local power distribution, telephones, etc.). Not included are furnishing, special installations for conference rooms or computers, labs for chemical or radioactive work, etc.

Total cost per block: 3.5 MSF

	Stage A	Stage B
Main control room next to auxiliary building No. 3 (2 floors of 700 m^2 each, one of which air-conditioned), including basic technical installations but not including control racks or cable trays		
Cost: 1.5 MSF		
Totals: Stage A, 4 laboratory blocks	15.5	
Stage B, 6 laboratory blocks		22.5

15.6.5 Assembly Hall

Total area 11,700 m^2, equipped with two 30-ton cranes. Including basic technical installations (heating, lighting, local power distribution, cranes, telephones, compressed air, primary water distribution). Not included special installations for magnet measurements, vacuum work, etc.		
Totals:	10.0	10.0

15.6.6 Temporary buildings

Four barracks for a total of 1700 m^2 of floor area. Complete with all technical installation for office and light laboratory use. Furniture not included	1.0	1.0

15.6.7 Main electric sub-station

Comprising switch gear and bus bars systems at 225 kV for two incoming lines, two 75 MVA transformers 225/18 kV, switch gear and bus bars systems at 18 kV. Local controls, interlocks, etc. are included. Including all local civil engineering work required (about 6,000 m^2 of open area, 500 m^2 of equipment building). Not included are the incoming high voltage lines nor the outgoing 18 kV cables	4.3	4.3

15.6.8 North Experimental Area

Tentative estimates only, as a proper design will only be made later. All Stage B only.

70,000 m^2	of reinforced concrete apron	8.5
2,500 m	of service tunnel for cables and pipes	2.5
4,000 m	of service duct	1.0
2,000 m	of beam duct, top removable shielding not included	8.0
10,000 m^2	of experimental hall	11.0
	neutrino facility	15.0

	Stage A	Stage B
Access roads for the North Area are not explicitly budgeted for, the concrete apron being assumed to provide for this. General grading of the area is included within the limit of 100,000 m^3 total excavation volume. Total		46.0
15.6.9 Shielding (movable blocks)		19.0
15.6.10 Roads, parkings, drains, service tunnels, temporary supplies, etc.		
Electricity, water, heating plant for contractors' site and early occupation of laboratory area	0.8	0.8
Service tunnel connecting main electric substation, power house, main control room and laboratory complex (1,000 m total)	1.5	1.5
Access roads to laboratory complex, and to auxiliary buildings (4 km total), parking around auxiliary buildings (180 cars total)	3.0	3.0
For laboratory complex: drainage system for surface water (into the Lion river) and for waste water (into the St. Genis sewers)	1.4	1.4
Geological site investigations	0.8	1.2
Survey monuments for general site work	0.1	0.1
Total	7.6	8.0
15.6.11 General site supplies		
18 kV power distribution cables and secondary substations	2.1	3.0
Primary water distribution, including pumping station, pipes, trenches and civil engineering work. Included: ring drainage system collecting used primary water and building drain water, up to main collecting point close to auxiliary building No. 5. Not included: water reservoir, lake water supply plant and piping, main water evacuation from auxiliary building No. 5 into the Rhône river	8.3	12.0
Power house, comprising final central heating plant, compressed air generating plant. Building and civil engineering included	3.0	3.0
General site distribution in laboratory complex area (heating and compressed air pipes, fire hydrants)	2.0	4.0
Telephone exchange, cables and local distribution boards (assumed to be an extension of CERN I exchange). Some civil engineering work is included	1.5	2.0
Total	16.9	24.0

		Stage A	Stage B
15.6.12	Demineralized water plants and distribution pipes for magnets and lenses	5.7	7.3
	GRAND TOTAL	133.8	214.9

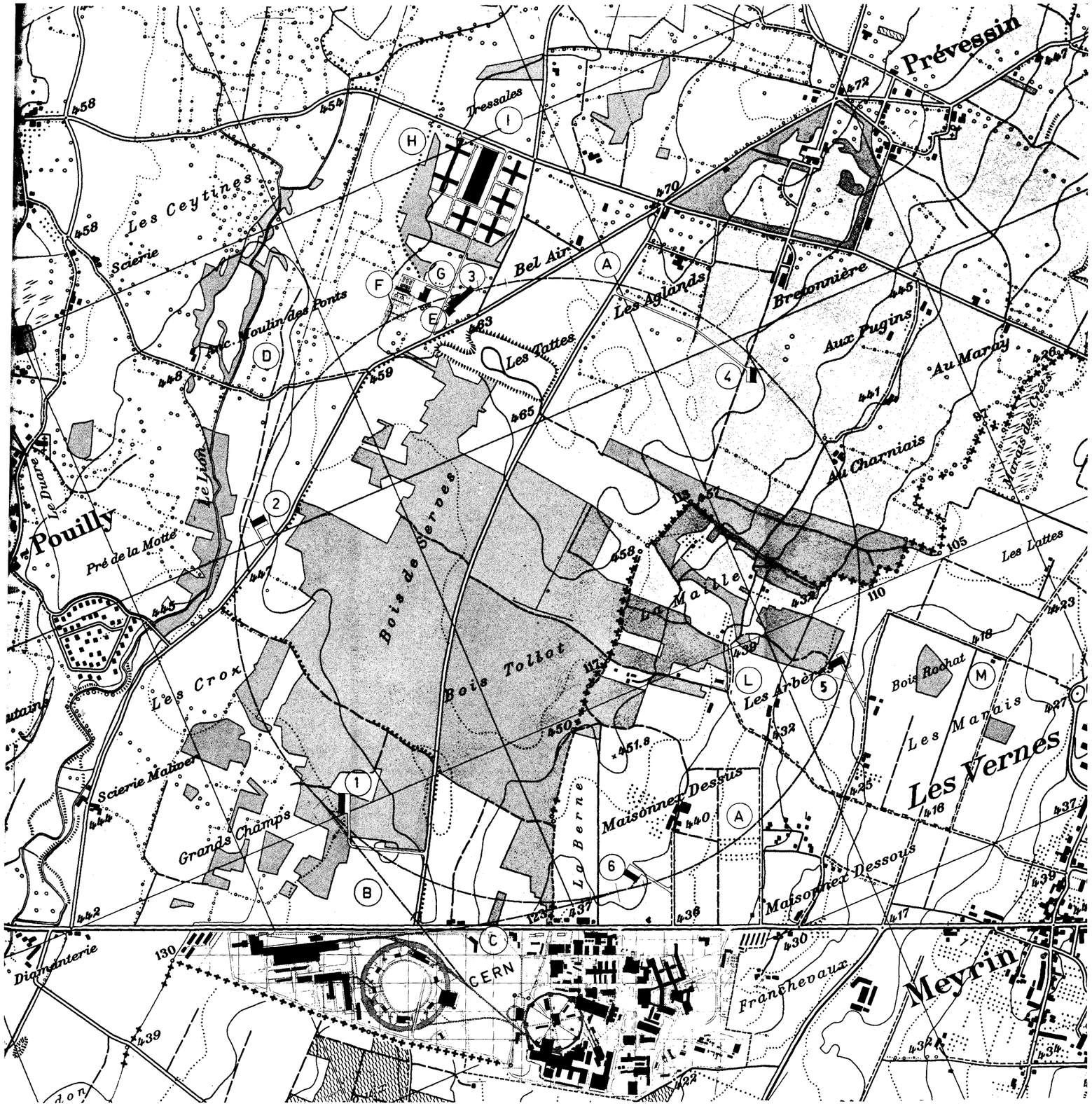

- (A) MAIN RING
- (B) INJECTION TUNNEL
- (C) EJECTION TUNNEL TO WEST EXP. AREA
- (D) EJECTION TUNNEL TO NORTH EXP. AREA
- (E) MAIN CONTROL ROOM
- (F) MAIN ELECTRICAL SUB-STATION
- (G) POWER HOUSE
- (H) LABORATORIES AND OFFICES BUILDINGS
- (I) ASSEMBLY HALL
- (L) WATER RESERVOIR AND PUMPING STATION
- (M) LAKE WATER PIPELINE
- (1) (2) (3) (4) (5) (6) AUXILIARY BUILDINGS AND ACCESS PITS

0 500 M 1 KM

General Site Layout

3.11.70 V.M.

fig. 15.1

SIS/R/16754

MAIN TUNNEL

TYPICAL CROSS SECTION

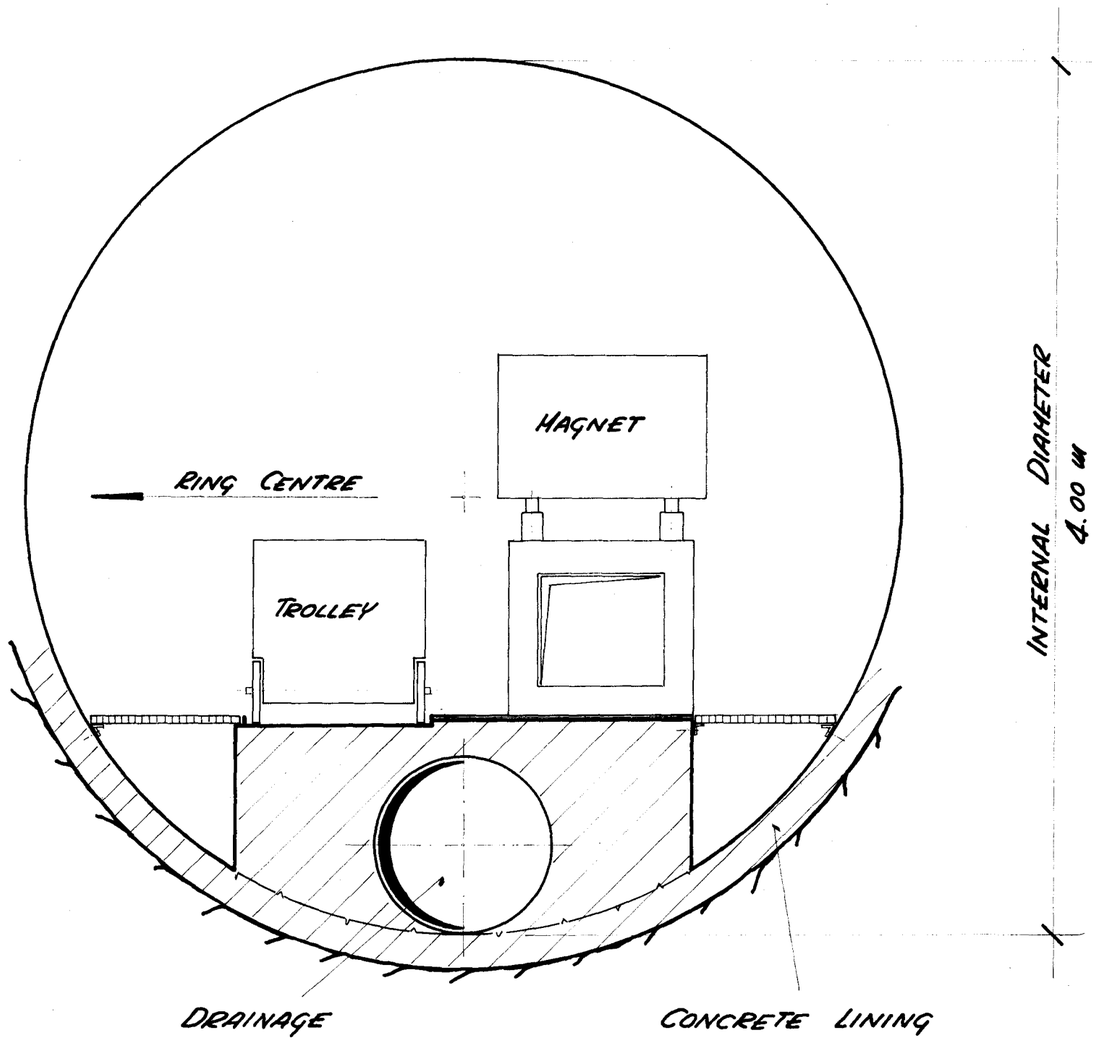

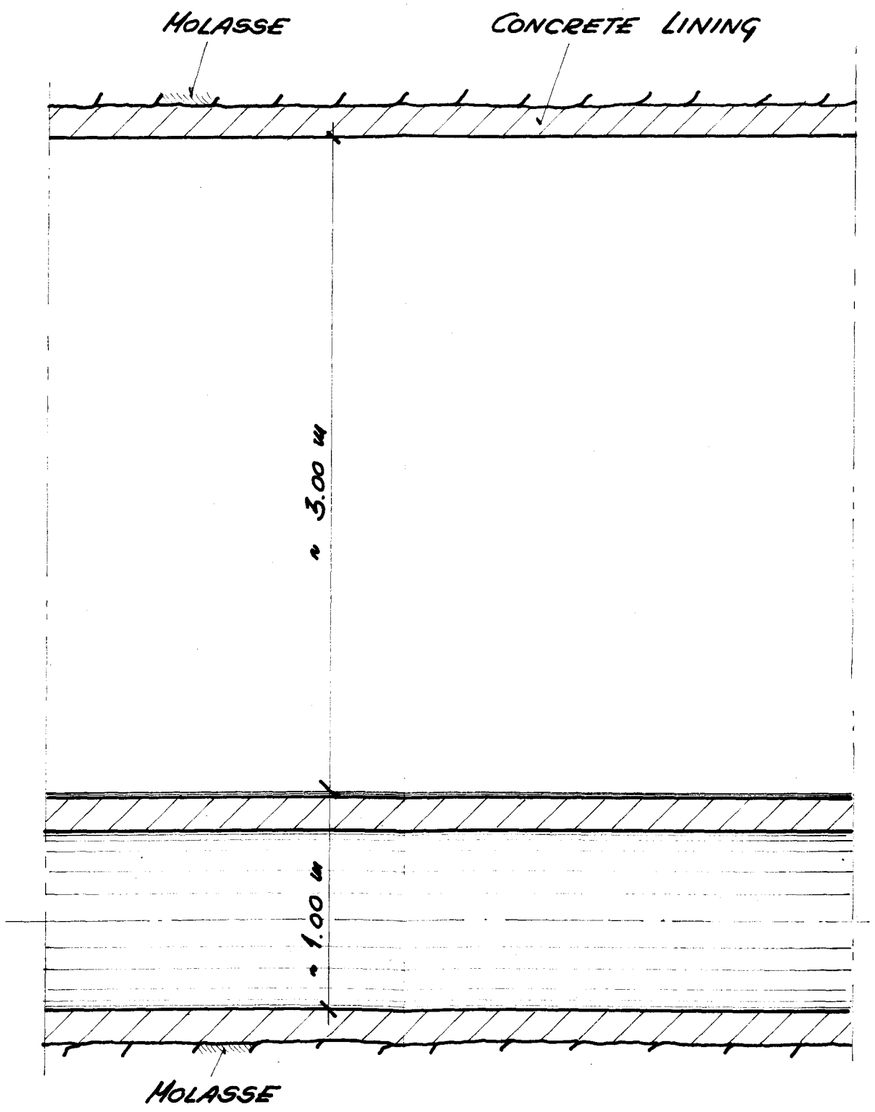

SCALE

0 0.5 1 METRES

SIS/R/16753

DIV. S.B 26.10.70

FIG. 15.2

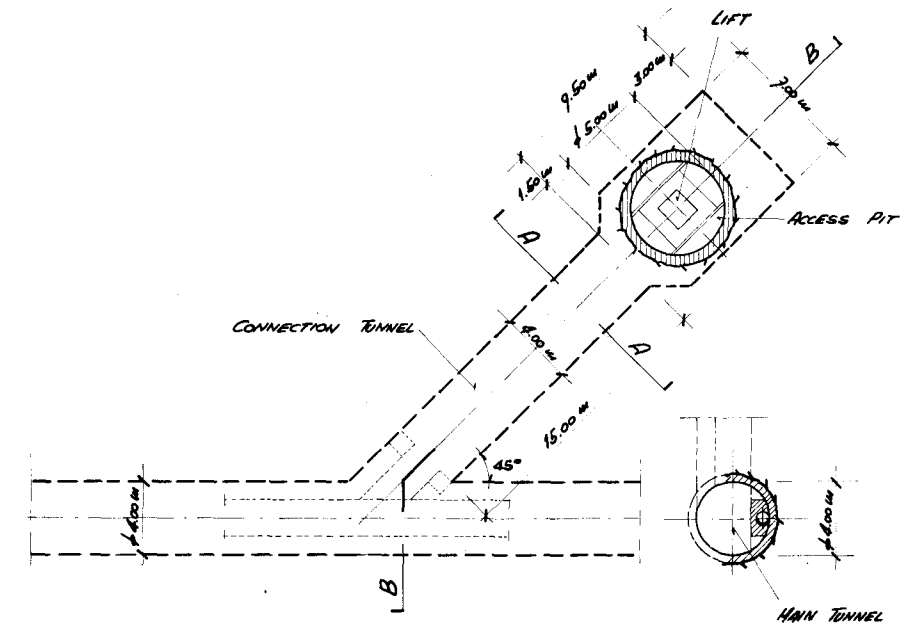

SECTION A-A

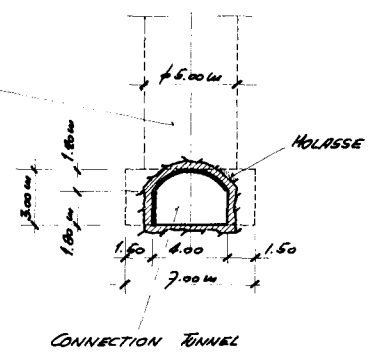

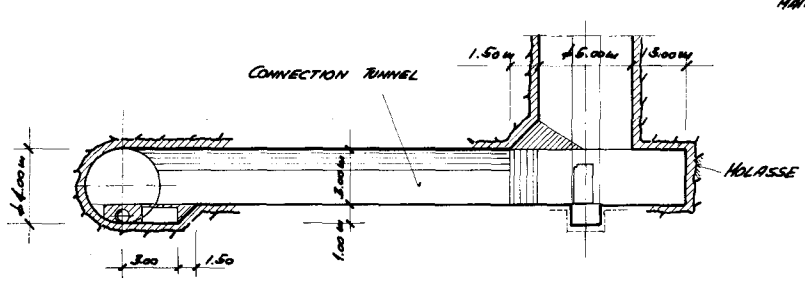

SECTION B-B

ACCESS PIT FOR PERSONNEL

SECTION C-C

scale 1:10

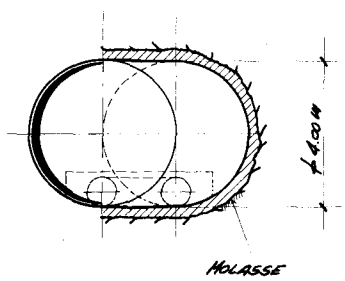

ACCESS PIT FOR DRILLING MACHINE, MAGNETS AND PERSONNEL

SCALE

0 5 10 METERS

DIV. 5B 06 to 70

FIG. 15.3

EJECTION REGION

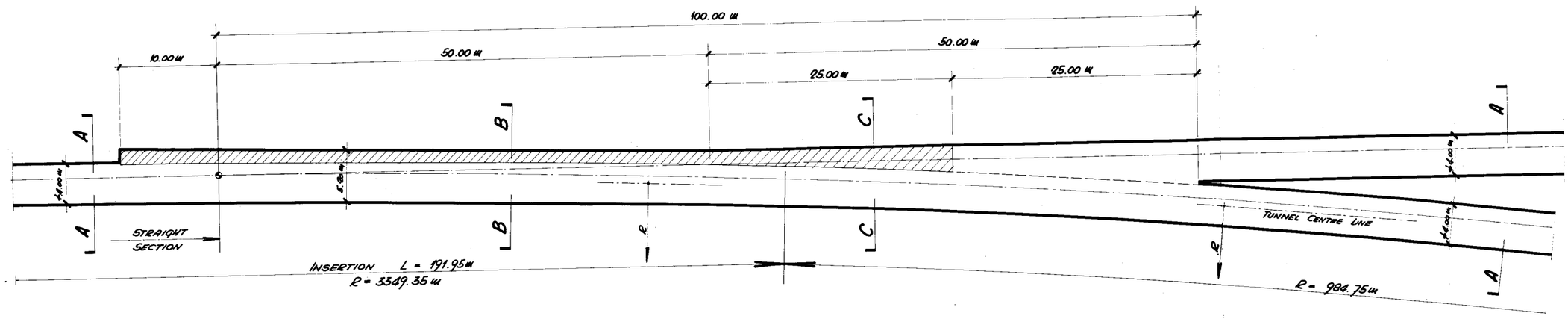

SECTION A-A

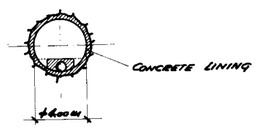

SECTION B-B

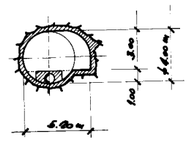

SECTION C-C

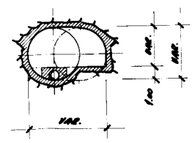

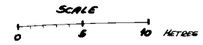

DIV. SB 97 to 70

FIG. 15. 4

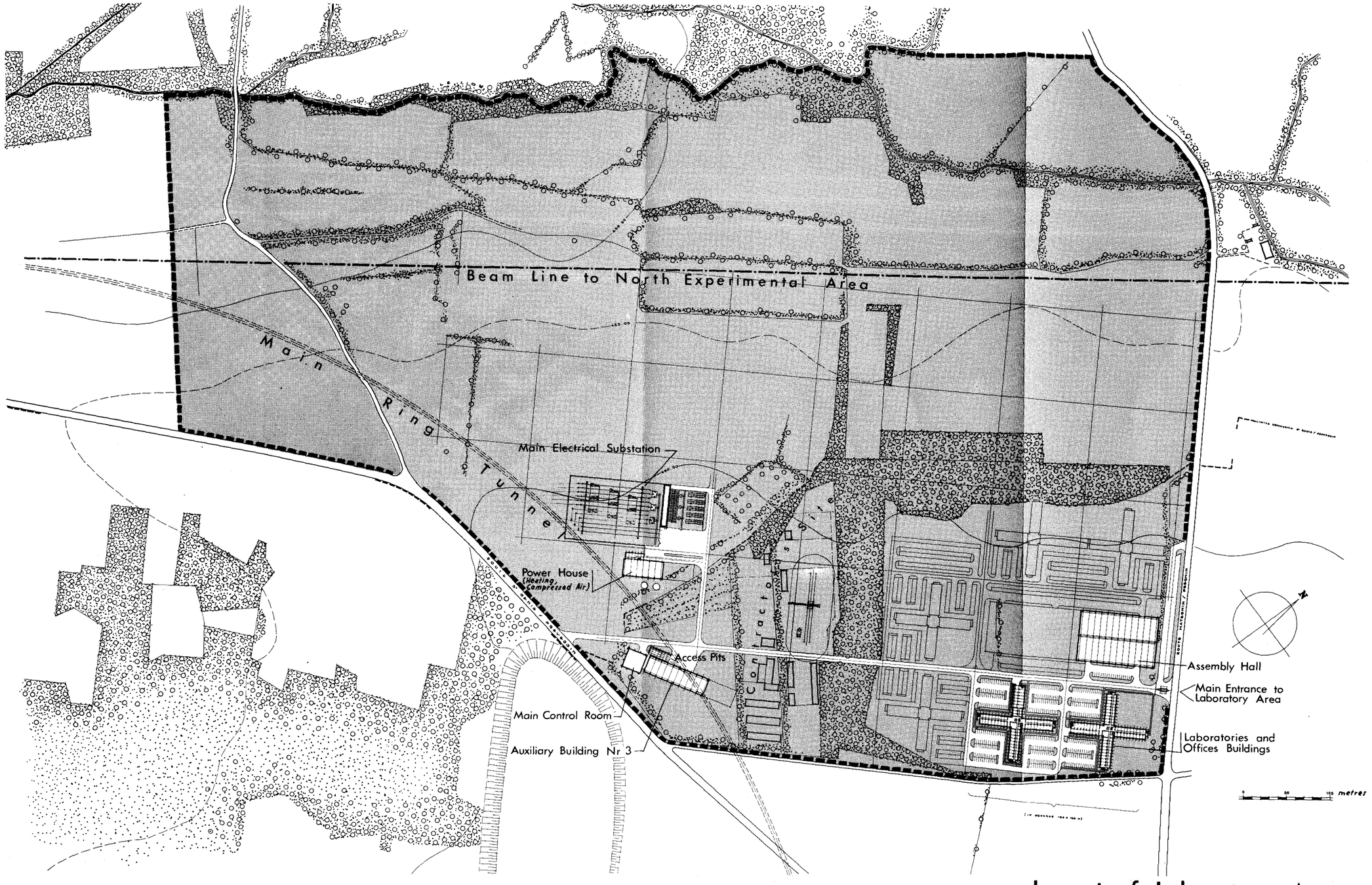

Layout of Laboratory Area

3.11.1970 fm/k.

fig. 15.5

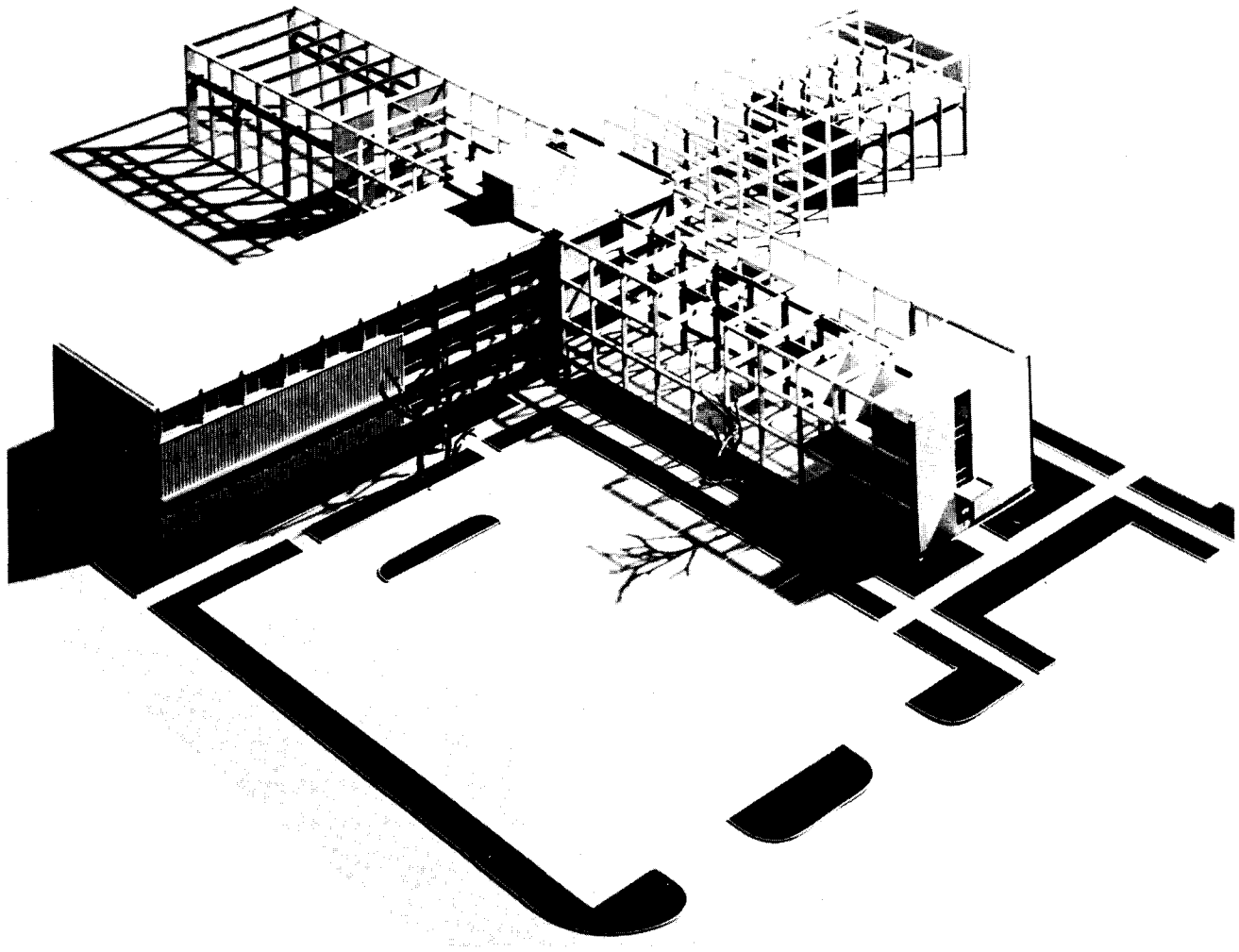

Laboratories and Offices Building

fig. 15.6

Chapter 16

TIME SCHEDULES, MANPOWER REQUIREMENTS AND COST ESTIMATES

16.1 Introduction

There are several ways of compiling the time schedules, manpower requirements and cost estimates for a project such as the European 300 GeV Programme. However, in the course of discussions on this project during the last few years with the nuclear particle physics community in Europe and with the Member States of CERN several boundary conditions have been established which exclude many possible compiling methods.

Essentially the boundary conditions now established are:

(i) The total cost of the Programme cannot exceed 1150 MSF at 1970 costs and constant prices.

(ii) The duration of the Programme is 8 years.

(iii) The annual expenditures in the Programme, assuming it starts on the 1st January 1971, at 1970 costs and constant prices are (MSF);

1971	1972	1973	1974	1975	1976	1977	1978	Total
30	105	165	180	175	165	165	165	1150

(iv) The annual expenditures may exceed the amounts given above by no more than 15% in any year provided the total Programme cost remains always 1150 MSF.

(v) The operating energy of the machine shall be at least 300 GeV and the operating intensity shall be at least 10^{12} protons per second.

(vi) There shall be two experimental areas, one of which will be the existing West Experimental Area on the present site of CERN and the other a North Experimental Area to be built during the course of the Programme.

(vii) The machine shall supply a proton beam to targets feeding the West Experimental Area in the sixth year of the Programme, i.e. in 1976. The energy of this proton beam shall be decided during the course of the Programme, probably in 1973 or 1974. The energy of this beam shall not be less than 150 GeV but it could be 300 GeV depending on the decision taken.

(viii) The energy of the proton beam feeding the North Experimental Area shall be at least 300 GeV and the North Experimental Area shall be ready for starting research work at the end of the Programme, i.e. at the end of 1978.

This rather formidable list of boundary conditions was not arrived at independently of the possibilities of planning and constructing the 300 GeV facilities but, during the course of the discussions, many compromises had to be made so that now it is by no means easy to draw up a design and construction schedule with manpower figures and cost estimates which satisfies all the boundary conditions.

The method which has been used in this Chapter is essentially an iterative process. Starting with the requirements for proton beams at different times during the course of the Programme a time schedule can be established which roughly satisfies the boundary conditions. From this time schedule the critical path for design and construction can then be discovered and the schedule adjusted to satisfy the required dates for the operating energy stages. Using this initial schedule it is then possible to draw up the annual manpower requirements of the Programme and finally to cost the Programme year by year.

On the first iteration, carried out in this manner, it was found that the peak in annual expenditure, normal in a project of this type and occurring in the third and fourth years of the Programme, exceeded the prescribed annual budgets for these years. This situation was foreseeable, since, during the course of the discussions with CERN Member States, it had been found necessary for financial reasons to smooth out this natural expenditure peak.

The aim of the second iteration was therefore to spread the annual expenditure of the peak years into neighbouring years and to reprogramme the construction schedule so that the energy stages of the machine could still be obtained at the required dates.

Several iterations of this type were carried out and what is presented in this Chapter is a practical solution which satisfies the boundary conditions noted above. However, this solution is not unique and may not be the one which will finally be adopted by the team appointed to carry out the Programme. Certainly, it cannot be far away from the final solution and, whatever the outcome, it demonstrates that a satisfactory solution is possible.

Further progress in the iterative process depends on refinements in the costing of individual items in the light of the industrial conditions appertaining in Europe in the next few years and on the delivery dates which can be obtained at that time for components on the critical path. It will also depend on the rapidity with which the project staff can be built up and the times of acquisition of different parts of the new site.

What follows, therefore, is a practical plan for designing and constructing the European 300 GeV facilities which satisfies all the boundary conditions mentioned above and which cannot be very different from the plan which will finally be adopted.

16.2 Time Schedules

Given that the 300 GeV Programme requires that a proton beam be available to feed the West Experimental Area in the sixth year of the Programme, the first five years of the Programme can be divided into time-sequential stages, designed to satisfy this principal requirement, from which the critical path may be discovered.

Roughly speaking, the work during the first year of the Programme will be concerned with the detailed design of the facilities and the individual components and with building up a staff for this purpose. The work of the second year will be mainly concerned with specifying and tendering for the components, with placing orders on European industry and with preparations in industry for manufacture. The third and fourth years of the Programme will be the time during which industry manufactures the components and progressively delivers them to the site for assembly and installation. The first half of the fifth year will be devoted to testing the individual components installed in their operating positions and the remainder of the fifth year to getting the machine to work satisfactorily. In this way a beam of protons could be made available to feed the West Experimental Area in the sixth year of the Programme.

It has been agreed that the work of preparing the West Experimental Area to receive the proton beam in the sixth year of the Programme will be carried out by CERN-Meyrin using the budgets allocated to the Programmes of CERN-Meyrin. The 300 GeV Programme and its budget, therefore, only contain provision for bringing the proton beam to the West Experimental Area and providing targets for that beam.

During the sixth, seventh and eighth years of the 300 GeV Programme the work divides into two parts. Firstly, the machine will be operated at whatever energy level is decided for the proton beam feeding the West Experimental Area. Secondly, the North Experimental Area will be constructed and the machine completed to provide a 300 GeV proton beam to this new Experimental Area.

In order to maintain the maximum flexibility for research, the layout of the North Experimental Area and its equipment will be decided during the course of the Programme in the light of experience with the Intersecting Storage Rings at CERN-Meyrin, the research being carried out with the 400 GeV machine at NAL, Batavia, U.S.A. and the initial experience with the beam layouts in the West Experimental Area. At the present time, it is only possible to make very rough cost estimates for the North Experimental Area and essentially to reserve part of the budget for the 300 GeV Programme for this purpose.

It should be clear from this rough time schedule that the requirement for a proton beam to feed the West Experimental Area in the sixth year of the Programme is the critical one as far as planning is concerned.

Even a superficial examination of the time-sequence for the first five years of the Programme given above reveals that the critical path of the Programme during these years is determined by the time required for the design, manufacture, assembly, installation and testing of the magnets for the machine. It seems clear that all the other machine components can be provided in shorter times than those required for the magnets. It is therefore necessary to examine the provision of the machine magnets in more detail.

The first year of the Programme will be devoted to the detailed design of the bending and focusing magnets required for the machine. This work will involve model tests, at least to establish the manufacturing technology. To carry out this work a team of magnet designers must be built up quickly in the first year and space must be provided for them to work in.

The second year of the Programme will be devoted to tendering for the magnets, placing orders for them with European industry and in preparatory work in industry for their manufacture. Part of this preparatory work involves the selection and ordering of the steel and the copper for the magnets.

The magnet manufacture, assembly and installation must be carried out in the third and fourth years of the Programme. It is unlikely that a single European manufacturer could carry out all this work in two years but fortunately, with the design chosen, the machine magnets divide into five different types; three bending magnet types and two focusing magnet types. It is therefore possible to consider using up to five different manufacturers for the magnet and by that means to keep to two years for the manufacture, assembly and installation of this machine component.

However, the arrival over a period of two years of magnets from several manufacturers requires that assembly halls be ready on the site to receive them. The first hall should be ready at the end of the second year of the Programme and the second hall at the end of the third year. Clearly the magnet group must be installed on the new site before the first magnets arrive which means that laboratories and offices for this group must be ready for occupation by the middle of the second year. To achieve this, the building of these laboratories must begin in the middle of the first year and hence they must be designed and ordered in the first six months of the Programme.

Even if assembly halls are built on the site ready to receive the magnets from industry at the right time it would hardly be economical to provide sufficient assembly halls to store all of them. Therefore the ring tunnel, in which they will finally be installed, must also be ready to receive the assembled magnets in due time. It is planned to bore this tunnel in the rock underlying the site. If construction starts at the beginning of the second year of the Programme and takes two years to complete, sections of the tunnel will be ready to receive the assembled magnets at the correct times.

Thus it can be seen that the critical path of the Programme during the first five years is set by the machine magnets and that this component determines the time schedules for the design and construction of the offices, laboratories, assembly halls and the ring tunnel on the new site. All other components can be fitted into the magnet time schedules and the consequent buildings programme time table.

So far, no reference has been made in this time scheduling to the limitations imposed by the annual expenditures agreed for the Programme. Essentially this is a problem of annual capital expenditures during the first five years since the staff expenditure during this period is relatively small and increasing almost linearly with time. Capital expenditure on the Programme can be broadly divided into two parts; that required for the machine equipment and that required for the buildings, tunnels and services on the site. During the first five years of the Programme the capital cost of the machine equipment is about 300 MSF and it peaks strongly in the fourth year of the Programme. In order to fit expenditures into the agreed profile over the first five years it is essential that the capital expenditure for buildings, tunnels and site services, which amounts to about 200 MSF, reaches its peak about one year before the peak in capital expenditure for machine equipment. This scheduling also agrees with the need to have laboratories, assembly halls and the ring tunnel available before the magnets arrive from industry. However, this schedule is very tight and it means making a very quick start on the design and construction of the site and buildings item of the Programme.

The time schedules, following the Programme planning described above, are summarized in Fig. 16.1. Sufficient detail is given to allow a check to be made on the practicability of the planning, the manpower requirements, and the estimated annual expenditures for the Programme.

16.3 Manpower Requirements

Following the time schedules outlined in Fig. 16.1, the build-up of the manpower required for the Programme has been estimated and is shown in Fig. 16.2.

The important number, on which many other staff numbers depend, is the size of the group required to construct the 300 GeV machine. This has been estimated at 400 total staff. The build-up of this staff in the first years of the Programme is critical to the time schedules outlined above and clearly the quicker it can be built up the better. However, there are at least two limitations on the rate at which machine staff can be built up. The first is the rate at which they can be recruited from CERN-Meyrin, the National European Laboratories, the universities and other employments. The second is the rate at which working accommodation can be provided for them. Initially they will have to be accommodated in barracks at CERN-Meyrin but, as has already been mentioned, laboratory and office accommodation must be rapidly constructed for them on the new site.

The planned built-up of the staff of the Machine Group is 150 by the end of the first year, 300 by the end of the second year and 400 by the end of the third year.

The Services Group, i.e. site services (building design and construction, etc.) and administrative services (personnel and finance), builds up in proportion to the Machine Group during the first three years. The ratio assumed for Services Group staff to Total Laboratory Staff is the ratio currently appertaining at CERN-Meyrin, namely 0.37. It is not necessary that all Services Group staff shown in Fig. 16.2 be recruited for the 300 GeV Programme since many of these services can be supplied by CERN-Meyrin under contract. Thus accommodation for the Services Group on the new site will depend on the extent to which CERN-Meyrin can provide the required services using staff already accommodated on the present site.

In the fourth year of the Programme it is planned to start a group to prepare for research in the North Experimental Area. This group initially will assist with and gain experience from the layouts being prepared by CERN-Meyrin for the West Experimental Area. The extent to which this group later expands and becomes involved in research in the North Experimental Area depends on arrangements to be worked out with CERN-Meyrin and the European nuclear particle physics community during the course of the Programme. The build-up of staff, indicated in Fig. 16.2 towards the end of the Programme is, therefore, only provisional at the present time.

In the fifth year of the Programme part of the Machine Group will prepare themselves to take over the operation of the machine to allow research to be carried out in the West Experimental Area. During the seventh and eighth years of the Programme about half of the Machine Group will be engaged in this task; the remainder will be concerned with completing the machine for use with the North Experimental Area at the end of the Programme.

16.4 Cost Estimates and Annual Expenditures

Until the design of the machine is finally determined during the latter part of the first year of the Programme and more definitive approaches have been made to European industry, the cost estimates for the Programme can only be approximate. However, the design is sufficiently advanced by now to make a provisional estimation and, of course, the total Programme cost is now fixed at 1150 MSF. Such an estimate is given in Fig. 16.3. This estimate is based on the estimates of the Working Groups of the 300 GeV Machine Committee, due allowance being made for the appropriate contingency factors.

The capital costs are based on current prices for the different items of the Programme following the machine and laboratory design established at the present time. Capital costs are divided into the two main categories mentioned above, namely, machine equipment and site equipment and buildings.

Staff costs are based on man-years calculated from the staff requirements for the Programme given above. In translating man-years into financial figures an average cost of 50 kSF per man-year has been assumed. This figure includes salaries and all those costs normally falling in sections 1 and 2 of the CERN financial accounts.

Machine operating costs assume that operation begins during the sixth year of the Programme and reaches an expenditure level of 40 MSF p.a. during the seventh and eighth year of the Programme. Staff costs for machine operation are not included in this item of expenditure but are included in the total staff costs of the Programme.

The annual expenditures on the Programme follow the total estimated costs given in Fig. 16.3, the time schedules given in Fig. 16.1 and the staff build-up given in Fig. 16.2.

Figure 16.4 shows the annual expenditures in the four main categories of Machine Equipment Capital, Site and Buildings Capital, Staff Costs and Machine Operating Costs. The peaks in annual capital expenditures for Machine Equipment and Site and Buildings can clearly be seen as well as the displacements in time between them necessary to fit the agreed annual expenditure profile for the Programme.

It will be observed that the drop in total capital expenditure with respect to the peak years during the last three years of the Programme is offset by the expenditure required for Machine Operation during these years. Consequently, a certain exchange is possible between capital and operating expenditures in this period. This flexibility allows the energy of the proton beam fed by the machine to the West Experimental Area to be either 200 GeV or 300 GeV in the sixth year of the Programme, since the higher energy and the extra capital expenditure required to achieve it can be obtained by delaying the start of research at 300 GeV in the West Area by about six months to one year with respect to a start at the 200 GeV energy level. Thus a 200 GeV energy proton beam could be made available in the first half of the sixth year whereas, if it is decided to start at the 300 GeV energy level, research could begin towards the end of the sixth year.

Finally, in Fig. 16.5, the total annual expenditures for the Programme are compared with the profile already determined and laid down in document CERN/958. Expenditures in the second, third and fourth year of the Programme can be seen to be higher than the agreed profile by 12%, 15% and 13% respectively, but these estimated over-expenditures are recuperated later on in the Programme by under-expenditures so that the total Programme costs remain at 1150 MSF. It has already been mentioned as a boundary condition that yearly expenditures in excess of the agreed profile are permitted during the Programme up to 15% above the agreed figure in any year providing, of course, that the total Programme cost remains unchanged.

16.5 Conclusion

This Chapter is aimed at demonstrating that the many boundary conditions listed at the beginning of the Chapter can be met by reasonable and practical Programme time schedules, manpower requirements and cost estimates. It was mentioned that the process of fitting these parameters to the boundary conditions is an iterative one and the iteration has only been carried far enough at this time to demonstrate a practical solution.

During the first year of the Programme, more exact cost estimates will be made for the many items of the Programme and checked against the industrial prices and delivery dates then appertaining in Europe. Surprises, both pleasant and unpleasant, are only to be expected at that time but it is to be hoped that they balance out on the average to produce overall cost and time estimates not very different from those given in this Chapter. Only then will it be sensible to carry on with the iterative process and to harmonize further the estimated annual expenditures with the agreed profile.

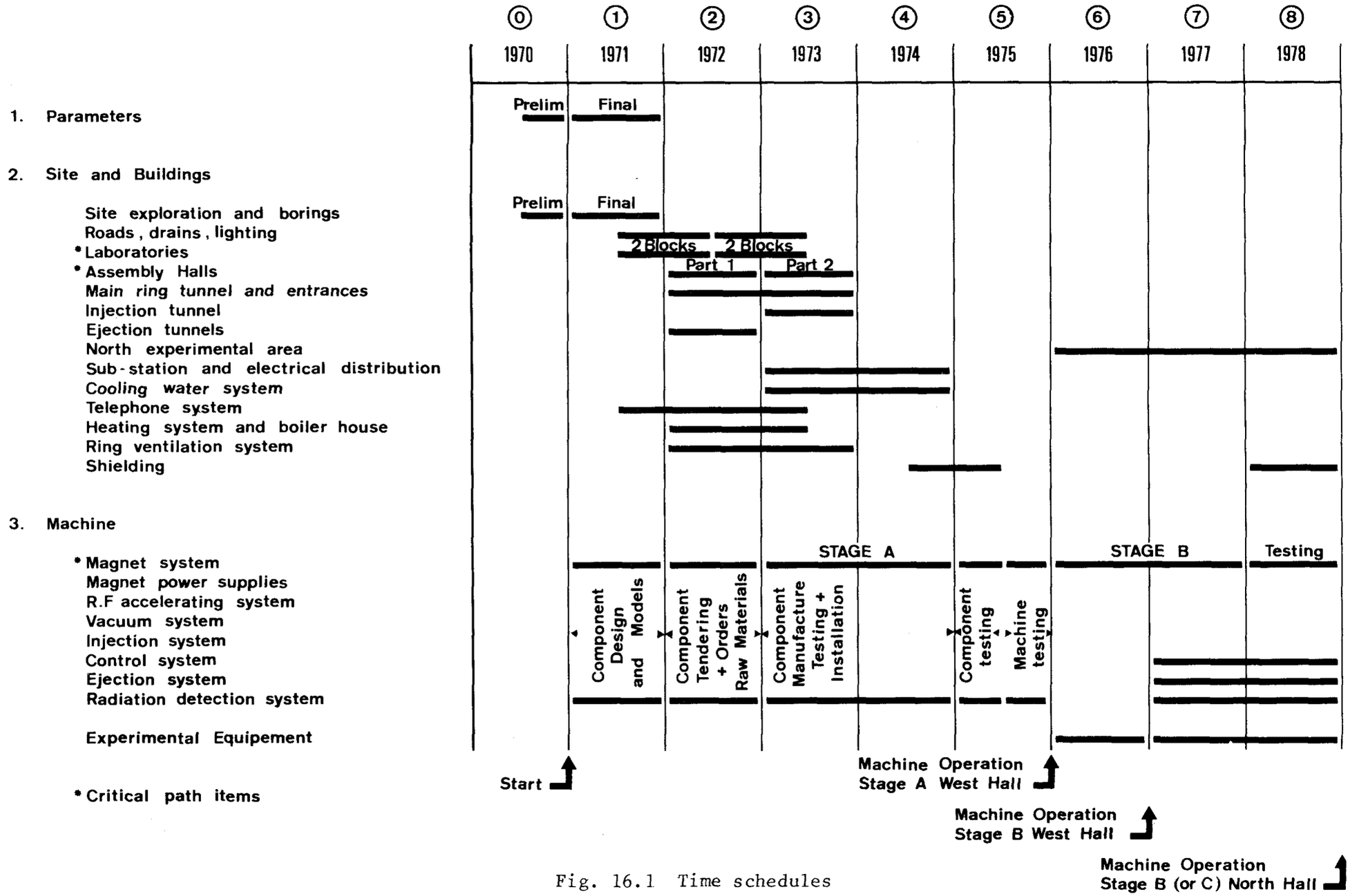

Fig. 16.1 Time schedules

Staff at the end of each year

	1971	1972	1973	1974	1975	1976	1977	1978
Machine Group	150	300	400	400	400	400	400	400
Services Group	90	180	240	255	270	300	335	380
Research Group	-	-	-	25	50	100	175	250
Total	240	480	640	680	720	800	910	1030
Man-years	120	360	560	660	700	760	855	970

Fig. 16.2

Cost Estimates (1970 costs and constant prices)

	Stage A (200 GeV)	Stage B (300 GeV)
1. Machine Equipment		
Injection System	7.4	7.4
Magnet System	58.0	78.5
Magnet Power Supplies	22.0	22.0
Accelerating System	18.4	18.4
Vacuum System	15.3	18.7
Correcting Lenses	3.0	5.0
Control System	30.5	30.5
Survey System	1.0	1.6
Radiation Protection System	4.2	4.8
Ejection System	19.6	37.5
Experimental Areas Equipment	16.0	85.5
Installation Labour	40.0	63.0
Computing	10.0	20.0
Contingency	50.0	80.0
Total Machine Equipment	295.4	472.9
2. Site Equipment and Buildings		
Main ring tunnel complex	59.5	59.5
Injection tunnel	5.0	5.0
Ejection tunnels	8.3	8.3
Laboratory complex and MCR	15.5	22.5
Assembly halls	10.0	10.0
Temporary buildings	1.0	1.0
Main electricity sub-station	4.3	4.3
North Experimental Area (with shielding)	-	65.0
Roads, drains, service tunnels, etc.	6.7	6.7
Electricity distribution system	2.1	3.0
Water distribution system (prim.& sec.)	14.0	19.3
Heating plant and compressed air eqt.	3.0	3.0
Heating and compressed air distr. system	2.0	4.0
Telephone exchange and distr. system	1.5	2.0
Site fencing	0.5	1.0
Site borings and survey monuments	0.9	1.3
Laboratory equipment and tools	24.0	50.0
Furniture	1.1	1.5
Transport equipment	0.5	0.5
Contingency	32.0	53.6
Total Site Equipment and Buildings	191.9	321.5
3. Staff Expenses	120.0	249.2
4. Operating Expenses at Stage A	-	100.0
5. Total Programme Cost	607.3	1143.6

Fig. 16.3

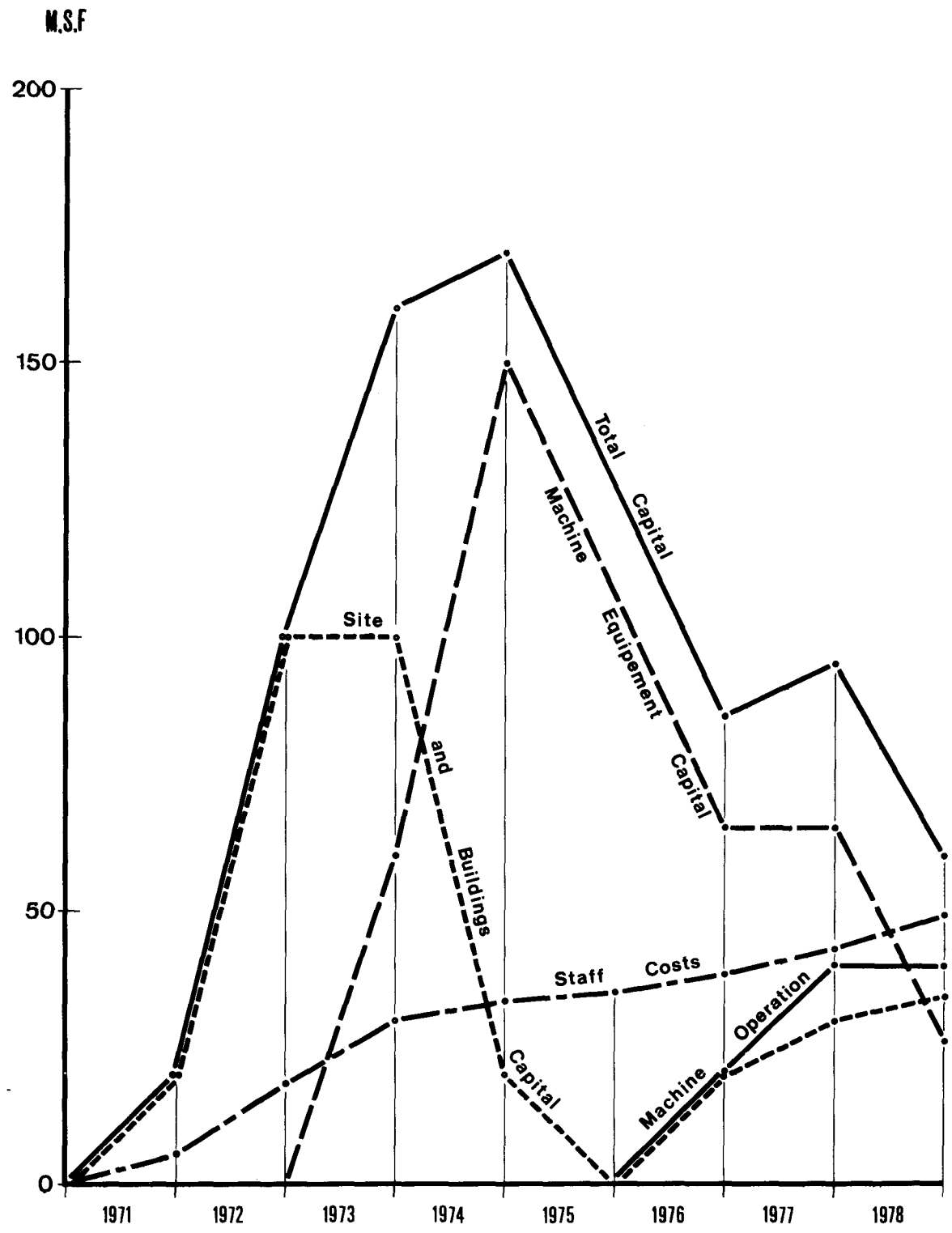

Fig. 16.4 Breakdown of annual expenditure
(1970 costs)

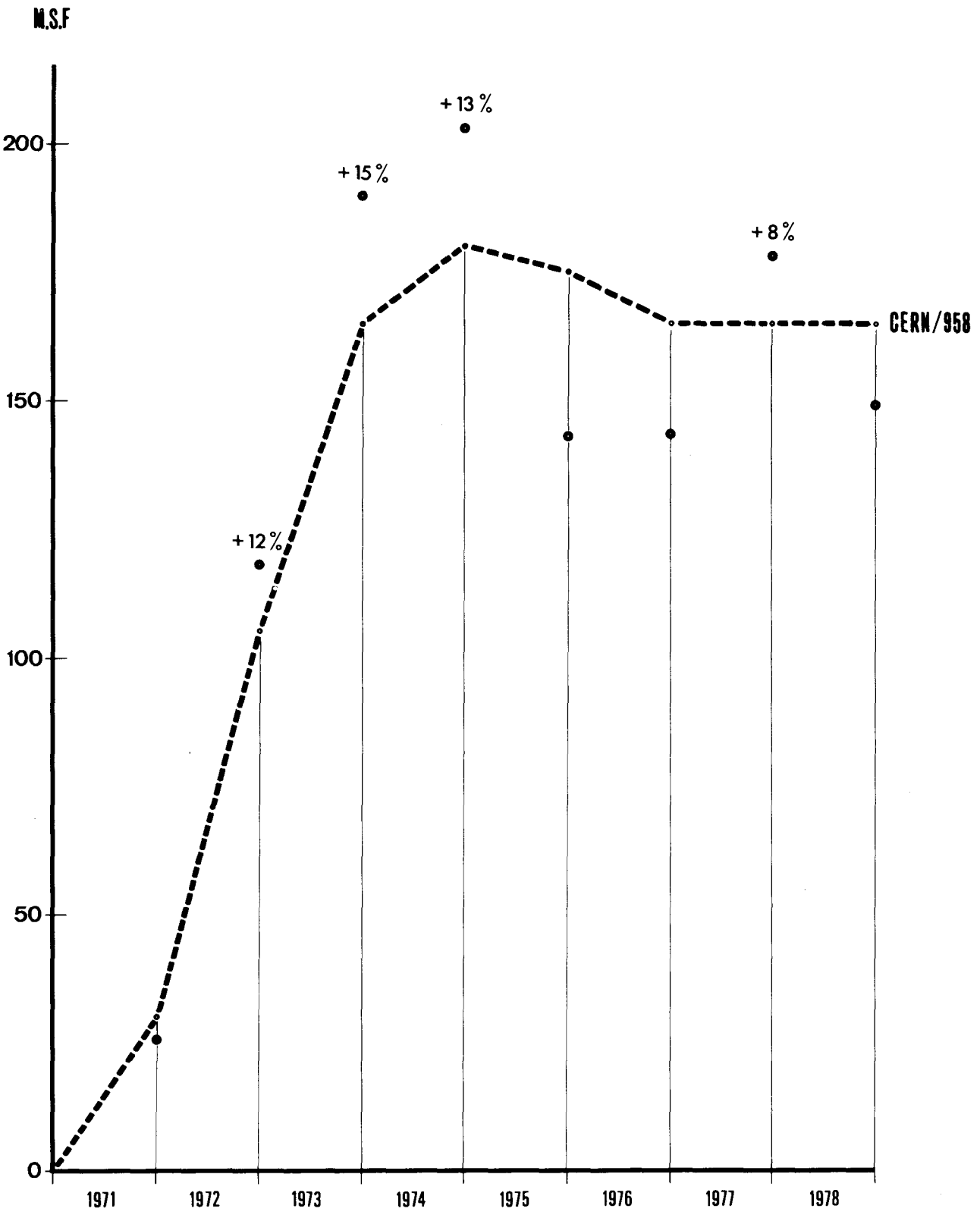

Fig. 16.5 Total annual expenditure
(1970 costs)

ANNEX I - LIST OF PARAMETERS

Main Ring Tunnel

Total length	6912	m
Diameter when lined	4	m
Lining thickness	0.2	m
Centre line of tunnel above sea level	402	m
Tunnel cover at lowest point on surface	11 m rock + 7 m earth	

Lattice and Orbit Parameters

	A	B	C	
Maximum momentum	200	300	400	GeV/c
Maximum bending field	1.8	1.8	1.8	T
Magnetic bending radius	370.6	555.9	741.2	m
Mean radius	1100	1100	1100	m
Injection momentum	10	10	10	GeV/c
Injection field	0.090	0.060	0.045	T
Number of bending magnets per normal period	4	6	8	
Quadrupole gradient for Q = 28.75 F	8.456	12.68	16.91	T/m
D	12.05	18.08	24.10	T/m
Quadrupole gradient for Q = 27.75 F	8.23	12.34	16.45	T/m
D	11.73	17.60	23.46	T/m

Nominal length of F quadrupole		3.799	m
Nominal length of D quadrupole		2.650	m
Nominal length of bending magnet		6.017	m
Length of inter-magnet gap		0.6	m
Length of short straight section		2.304	m
Free length in empty semiperiod		28.782	m
Length of period		63.994	m
Structure of a period		FODO	
Number of periods	(N)	108	
Number of superperiods	(S)	6	
Nominal working point	(Q)	27.75	
Total transition energy/rest energy	(γ_{tr})	24.6	
Phase advance/period	(μ)	92.5	°
Maximum β value in F quadrupole	($\hat{\beta}_H$)	108.4	m
Maximum β value in D quadrupole	($\hat{\beta}_V$)	110.2	m
Minimum β value in D quadrupole	($\check{\beta}_H$)	17.8	m
Minimum β value in F quadrupole	($\check{\beta}_V$)	18.0	m
Maximum of momentum compaction function	($\hat{\alpha}_p$)	4.9	m
Minimum of momentum compaction function	($\check{\alpha}_p$)	-0.2	m

Tolerances (r.m.s.)

Location of magnet centres	0.15	mm
Random error in bending field (ΔB/B)	0.5	‰
Random tilt in median plane of magnets	0.2	mrad
Stray horizontal field (Bx)	0.28	G
Stray vertical field (By)	0.12	G
Uncorrected closed orbit distortion amplitude (horizontal)	32.1	min
(vertical)	18.7	min
Probability of this amplitude being exceeded	2	%
Random error in quadrupole strength (ΔK/K)	2	‰
Increase in beam size due to ΔK/K	6	%
Systematic error in field at edge of nominal bending magnet aperture	1	‰
Systematic error in gradient at edge of nominal quadrupole aperture	2	‰

Aperture Requirements at β max

	Horizontal	Vertical	
Corrected closed orbit amplitude	10.0	5.0	mm
Semi-aperture for betatron oscillations at injection	(27.5)	19.4	mm
Semi-aperture for betatron oscillations at transition	18.1	-	mm
Semi-aperture for a momentum spread of ±3 ‰ after trapping	(14.7)	-	mm
Semi-aperture for a momentum spread of ±7 ‰ at transition	34.4		
Total semi-aperture requirements	62.5	24.3	mm

Injection System*

Transfer momentum	10	GeV/c
CPS bunch frequency	9.5	MHz
CPS momentum spread (Δp/p)	$\pm 1.3 \times 10^{-3}$	
CPS emittance (H × V)	$7 \times 3.4\ \pi$	mm mrad
CPS intensity	10^{13}	p.p.p.
Number of bunches transferred	20	
Kicker firing interval	> 50	us
Total transfer time	< 2	ms
Debunching time	115	ms
Main ring momentum acceptance at transition (Δp/p)	$\pm 7 \times 10^{-3}$	
Corresponding momentum acceptance after capture (Δp/p)	$\pm 3 \times 10^{-3}$	
Corresponding momentum spread of debunched beam before capture (Δp/p)	$\pm 1.5 \times 10^{-3}$	
Corresponding bunch area	0.2	radian
Self-bunching limit at 10^{13} p.p.p.	$A \geqslant 0.13$	radian

*For the purposes of this parameter list, transfer of 20 individual bunches by means of the full aperture kickers using a fast recharging system is assumed.

Magnet System (H Magnets)

	Q_F	Q_D	B1	B2	B3	B4	
Number for Stage A	108	108	186	192	--	12	
Number for Stage B	108	108	186	186	186	30	
Number for Stage C	108	108	186	192	396	--	
Nominal length	3.799	2.650	6.017	6.017	6.017	4.512	m
Field at all stages	--	--	1.8	1.8	1.8	1.8	T
Field gradient at Stage C	16.91	24.10	--	--	--		T/m
Height of momentum aperture (gap)	20.3	49.0	36.6	54.9	50.3	54.9	mm
Width of nominal aperture	125.2	53.5	132.7	79.1	109.7	79.1	mm
Radius of inscribed circle	31.0	29.0	--	--	--	--	mm
Core weight per unit	3.8	2.5	16.6	19.3	20.8	14.1	tons
Copper weight per unit	0.225	0.200	0.99	1.54	1.40	1.23	tons
Number of turns per unit	4 × 4	4 × 5	16	24	22	24	
Peak current at 300 GeV	1210	1210	3410	3410	3410	3410	A
Peak current density at 300 GeV	6.5	6.5	6.65	6.65	6.65	6.65	A/mm^2
Stored energy per unit at 300 GeV	3.8	3.0	83	137	130	102.5	kJ
Maximum inductance per unit	5.2	4.2	15.7	25.9	24.7	19.4	mH
Resistance per unit	12.4	10.9	7.4	11.2	10.2	8.8	mΩ
Conductor height	14.5	14.5	23.9	43.0	40.0	43.0	mm
Conductor width	14.5	14.5	24.5	14.25	15.3	14.25	mm
Cooling channel	Ø = 5	Ø = 5	Ø = 10	25 × 4	20 × 5	25 × 4	mm
Lamination height	380	430	493	489	493	489	mm
Lamination width	540	430	838	988	1016	988	mm

Magnet Power Supply

Bending Magnets	A	B	C	
Voltage	33.7	34.4	35.3	kV
Peak current	3.41	3.41	3.41	kA
r.m.s. current	2.27	2.22	2.26	kA
Peak power	111	113	116	MW
Losses (I^2 r.m.s. × magnet resistance)	19	28	39.3	MW
Reactive compensation	-62	-63	-65	MVAr
Net load (r.m.s.)	54	63	73	MVA
Total magnet inductance	8	12.9	17.7	H
Total magnet resistance	3.65	5.68	7.67	Ω
Cable resistance	0.37	0.37	0.37	Ω

Quadrupoles	A	B	C	
Voltage	3.3	4.7	6.1	kV
Peak current	807	1210	1650	A
r.m.s. current	530	790	1120	A
Peak power	2.7	5.7	10	MW
Reactive compensation	-2	-3	-4	MVAr
Net load (r.m.s.)	1.7	3.7	6.7	MVA
Public Supply Load				
r.m.s. load on EDF	55.7	66.7	79.7	MVA
Mean power from EDF	25	35.5	50	MW
Nominal Excitation Profile				
Injection	0.2	0.2	0.2	s
Front porch	0.15	0.15	0.15	s
Rise with round off	1.18	1.98	3.32	s
Flat top	0.7	0.7	0.7	s
Decay with round off	0.87	1.19	1.44	s
Rest	0.1	0.1	0.1	s
Total cycle time	3.2	4.32	5.91	s
Peak $\dot{B}$	1.6	1.07	0.8	T/s

Pulse to pulse tolerance on current	$(\Delta I/I)$	$\sim 10^{-4}$
Ripple voltage tolerance at injection	$(\Delta V/V)$	< 25%
Ripple voltage tolerance at ejection	$(\Delta V/V)$	< 1%

Acceleration System

Number of cavities	3	
Length of a cavity (without couplers)	20.45	m
Diameter of cavity	0.9	m
Mode	$\pi/2$	
Number of cells per cavity	50	
Frequency at transition energy	183.068	MHz
R/Q	600	Ω/m
Effective shunt impedance per cavity	11	MΩ
Peak r.f. voltage at injection	3.7	MV
Peak r.f. voltage per turn at 10^{13} p.p.p.	5.4	MV
Maximum rate of increase of momentum	165	GeV/cs
Maximum beam power	0.265	MW
Average r.f. power per cavity	0.5	MW
Maximum phase angle	45	°
Front porch time	150	ms
Momentum at end of front porch	~ 20	GeV/s
Harmonic number	4224	
Maximum frequency swing	0.55	%
Frequency swing for injection at 10 GeV/c	0.44	%
Maximum possible bunch area at injection due to bucket size	0.24	rad

Vacuum System

Main ring pressure	10^{-7}	Torr
Number of ion pumps (50 ℓ/s^{-1})	432	
Number of rotary pumps (10^{-4} Torr)	108	
Additional pumps for r.f., transfer line and ejection to experimental areas	57	
Number of gate valves	24	

	Q_F	Q_D	B1	B2+B4	B3	
Wall thickness	2.0	2.0	2.3	1.4	2.6	mm
Chamber width (outside)	131.2	58.0	147.3	91.9	123.7	mm
Chamber height (outside)	29.2	58.0	36.6	54.9	50.3	mm

Correcting Elements

	Number	Length (m)	Strength	
Sextupoles	24 (72)*	1	167 T . m^{-2}	
Octupoles	24 (72)	1	4000 T . m^{-3}	
Power supplies for above	4		300 kW	
Dipoles for horizontal closed orbit	108	0.25	0.08 T	
Dipoles for vertical closed orbit	108	0.25	0.036 T	
Beam position indicators	216	0.2	-	
Pick-up observation error			0.5	mm
Tolerance on central line position (r.m.s.)			1	mm

Ejection System

Beam size before ejection (mm)	200 GeV	300 GeV	400 GeV
Betatron amplitude at β = 110 (H)	8.1	7.0	6.2
Betatron amplitude at β = 110 (V)	6.2	5.0	4.5
Momentum spread ($\Delta p/p$)	$\pm 5 \times 10^{-4}$	$\pm 3.5 \times 10^{-4}$	$\pm 3 \times 10^{-4}$
Semi-aperture for momentum spread at α_p = 4.9 m	2.5	2.0	1.5

*The initial installation will be 24 units but space is reserved for up to 72 units.

Ejection Channel	S1	S2	S3	
Septum type	Electrostatic	Copper	Iron	
Thickness	0.15	2.0	10.0	mm
Length	6	6	13	m
Field strength	100 kV/cm	0.123 T	1.5 T	
Aperture (H × V)	18 × 12	20 × 12	30 × 200	mm
Deflection	0.15	0.55	14.6	mrad

Full Aperture Kicker		
Length	9 × 400	mm
Strength at 400 GeV	0.26	T . m
Aperture (H × V)	120 × 30	mm
Rise time	100	ns
Impedance	20	Ω

Closed Orbit Bump Magnets		
Number of magnets per ejection channel	6	
Strength	1	T . m

Slow Ejection (Integer resonance)		
Efficiency (theoretical)	99	%
Jump at β_{max}	15	mm
Sextupole strength at 400 GeV	150	$T . m^{-2}$
Sextupole length	0.8	m
Quadrupole gradient at 400 GeV	25	$T . m^{-1}$
Quadrupole length	1.2	m
Number of quadrupoles	3	

ANNEX II

LIST OF MEMBERS OF THE 300 GeV MACHINE COMMITTEE AND ITS WORKING GROUPS

(Conveners are underlined)

The 300 GeV Machine Committee

J.B. Adams	CERN
J.V. Allaby	CERN
F. Amman	Frascati
F. Bonaudi	CERN
M.C. Crowley-Milling	Daresbury
J.A. Fox	RHEL
J. Gervaise	CERN
K. Goebel	CERN
D.A. Gray	RHEL
W. Hardt	CERN
W. Heinz	Karlsruhe
L.C.W. Hobbis	RHEL
K. Johnsen	CERN
P.M. Lapostolle	CERN
R. Lévy-Mandel	Saclay
S. van der Meer	CERN
B. Milman	Orsay
D. Möhl	CERN
B.W. Montague	CERN
J. Parain	Saclay
B. de Raad	CERN
L. Resegotti	CERN
W. Schnell	CERN
P.H. Standley	CERN
E.J.N. Wilson	CERN
H.O. Wüster	DESY
C. Zettler	CERN

The Machine Lattice Working Group

F. Arendt	Karlsruhe
E.J.N. Wilson	CERN

The Injection System Working Group

Y. Baconnier	CERN
O. Barbalat	CERN
C. Bovet	CERN
D. Boussard	CERN
A. Brückner	CERN
D. Fiander	CERN
W. Hardt	CERN
H. Hartmann	Bonn
K.H. Kissler	CERN
J.M. Lefèbre	Saclay

D. Möhl	CERN
G. Plass	CERN
K.H. Reich	CERN
F. Schäff	CERN
A. Sørenssen	CERN
E. Weisse	CERN
E.J.N. Wilson	CERN
C. Zettler	CERN

The Magnet System Working Group

A.G.A.M. Armstrong	RHEL
G. Bronca	Saclay
D.A. Gray	RHEL
J. Hamelin	Saclay
V. Jung	Karlsruhe
R. Lévy-Mandel	Saclay
L. Resegotti	CERN
J. van Schaewen	Karlsruhe

The Magnet Power Supplies Working Group

J.A. Fox	RHEL
S. van der Meer	CERN

The Acceleration System Working Group

M.C. Crowley-Milling	Daresbury
D. Möhl	CERN
G. Saxon	Daresbury
W. Schnell	CERN
D.J. Thompson	Daresbury
C. Zettler	CERN

The Vacuum System Working Group

D.A. Gray	RHEL
E. Fischer	CERN
B.S. Halliday	Daresbury
D.R. Moore	RHEL

The Correcting Magnet System

B.W. Montague	CERN

The Control System Working Group

E. Brugia	Saclay
L. Burnod	CERN
M.C. Crowley-Milling	Daresbury
J.T. Hyman	RHEL
J.H.B. Madsen	CERN
G. Schaffer	CERN
R. Segalas	Saclay
J.S. Worgan	Daresbury
H.O. Wüster	DESY

The Survey System Working Group

J. Bruderlein	CERN
J. Gervaise	CERN
M. Menant	CERN

The Radiation Protection System Working Group

M. Barbier	CERN
M. Ellefsplass	CERN
E. Freytag	DESY
K. Goebel	CERN
L.C.W. Hobbis	RHEL (until 1.7.70)
L. Hoffman	CERN
J.H.B. Madsen	CERN
J. Ranft	Leipzig
B. de Séréville	Saclay
G. Stapleton	RHEL
G.R. Stevenson	RHEL
Ph. Tardy-Joubert	Saclay
H. Vialettes	Saclay
M. van de Voorde	CERN

The Ejection System Working Group

Y. Baconnier	CERN
O. Barbalat	CERN
D. Dekkers	CERN
J. Erb	Karlsruhe
J. Faure	Saclay
C. Germain	CERN
M.R. Harold	RHEL
A. Hilaire	Saclay
L.C.W. Hobbis	RHEL (until 1.7.70)
G. von Holtey	Bonn
K.H. Kissler	CERN
A. Laisné	Orsay
G. Merle	Karlsruhe
J. Parain	Saclay
J. Ranft	Leipzig
C. Steinbach	CERN
P. Strolin	CERN
H. Walther	DESY
E.J.N. Wilson	CERN

The Experimental Areas Working Group

J.B. Adams	CERN
J.V. Allaby	CERN
Ph. Bernard	CERN
J. Engler	Karlsruhe
P. Fleury	Ecole Polytechnique
K. Goebel	CERN
R. Gouiran	CERN
G. Hartwig	Karlsruhe
N.M. King	RHEL
P. Lazeyras	CERN
L. di Lella	CERN
H. Lengeler	CERN
D. Maden	RHEL
A. Minten	CERN
J. Parain	Saclay
G. Petrucci	CERN
B. de Raad	CERN
J. Ranft	Leipzig
M. Reinharz	CERN
J. Steinberger	CERN
M. Steuer	Vienna
D. Treille	Orsay
H. Wachsmuth	CERN
T.G. Walker	RHEL
E.J.N. Wilson	CERN (until 1.9.70)

The Site Working Group

J. Gervaise	CERN
E. Lanterno	Genève, Musée d'histoire naturelle
MECASOL (Bureau d'Etudes)	Paris

General Equipment and Buildings Working Group

J.B. Adams	CERN
B. Bianchi	CERN
F. Bonaudi	CERN
H. Laporte	CERN
J. Rouel	CERN
O. Bayard (electricity)	CERN
K. Braun (water cooling)	CERN
J.A. Fox (electricity supply)	RHEL